USING INDUCIBLE DEGRADATION TO CHARACTERISE THE ROLES OF TRIP13 AND CEP57 IN MITOSIS

This dissertation is submitted for the degree of Doctor of Philosophy

Jordan Alexander Holt,
BSc ARCS

Institute of Cancer Research
University of London

UNIVERSITY
OF LONDON

Declaration

This thesis is the result of my own work and includes nothing that is the outcome of work done in collaboration except where declared in the text and specified in figure legends. Neither this thesis nor any significant part of it is substantially the same as any that I have submitted, or, is being concurrently submitted for a degree or diploma or other qualification at the University of London or any other university or similar institution.

Jordan Holt

December 2020

COVID-19: statement of impact

During my final year, the COVID-19 pandemic interrupted my studies. For a period of 2 months, I was unable to perform lab work and subsequently I was awarded a 2-month extension by the Institute of Cancer Research (ICR). In order to follow current government safety guidelines, the ICR limited the number of people allowed into specific work spaces after the interruption. My lab adopted a policy of 2 separate groups that worked 1-week long shifts in order to not come into contact with the other group. The interruption and safety regulations had a significant effect on the progression of my project focused upon the characterisation of CEP57.

When the interruption began, I was still developing cell line tools to study CEP57 in living cells (inserting Centrin-GFP as a fluorescent marker into my CEP57-AID clones). When I returned, I had to optimise these cell lines by controlling for the levels of expression and single cell sorting them before I could use them in any of my assays. The main way I was characterising the role of CEP57 in mitosis was through live cell imaging, often using synchronised cells. These experiments were technically challenging; required several days to set up; required optimisation of filming conditions, and in some cases yielded a very low number of cells and therefore had to be repeated many times. Furthermore, the restrictions made it challenging to pursue multiple avenues of research at once and this hindered my abilities to pursue different hypotheses at the same time.

In summary, due to the nature of my project I believe that the COVID-19 pandemic severely hindered my progress in my final results chapter. This delay limited my ability to build a clear model of CEP57's molecular function.

Approved:

Jonathon Pines 

Jordan Holt 

Abstract

DNA and centrosomes are both semi-conservatively replicated once per cell cycle and it is essential that the DNA and centrosomes are divided equally between daughter cells in mitosis. When this fails, it can lead to aneuploidy, which is a hallmark of cancer. Whilst centrosomes are not essential for mitosis in some organisms, centrosome dysfunction also leads to incorrect cell division and is highly prevalent in some cancers.

Evolutionary conserved checkpoints exist throughout the cell cycle to halt the progression of cells that have undergone damage in the previous cell cycle stage to ensure the fidelity of transmission of DNA. In mitosis, the Spindle Assembly Checkpoint (SAC) ensures that sister chromatid separation does not occur prematurely, which would lead to unequal separation of DNA. The SAC has evolved to arrest cells until all kinetochores have been correctly attached to the mitotic spindle.

The centrosome is the microtubule organising centre (MTOC) and in cycling cells it facilitates the assembly of the bi-polar spindle during mitosis. In mammalian cells, inheritance of an incorrect number of centrosomes arrests cells in G1 through the action of p53.

Over the last few decades, our understanding of signalling pathways, such as the SAC and centrosome cycle, has been greatly expanded by removing specific proteins from a system and examining the consequences. The function of a protein can be targeted directly or indirectly by upstream perturbation at either the DNA or RNA level. This can lead to secondary effects that may complicate the interpretation of phenotypes. Whilst small molecule inhibitors act at the protein level and are often rapid and reversible, they can also have off-target effects, and the design and validation of new inhibitors can take several years. It is also unlikely that a small molecule inhibitor can be designed for every protein, especially non-enzymatic proteins that lack a clearly targetable domain.

More recently, acute degradation techniques have provided an attractive alternative for conditional protein inactivation that mitigate some of the challenges and limitations of previous techniques. The Auxin Inducible

Degron (AID) system was developed in 2007 to target specific proteins for acute and rapid degradation. With the advent of CRISPR/Cas9, AID presents a specific system that, in theory, enables the targeting of any protein at the endogenous level for rapid and complete knock-down. Due to the acute nature, it provides an elegant system to study cell cycle regulators.

In this thesis, I have used AID to characterise the roles of two genes that function in different pathways in mitosis: TRIP13 and CEP57. Mutations in TRIP13 and CEP57 both lead to a rare autosomal recessive disease known as Mosaic Variegated Aneuploidy (MVA) syndrome. Affected individuals suffer from developmental disorders, microcephaly and in some cases a prevalence to cancer from an early age.

With the help of the adaptor protein p31^{comet}, TRIP13 has been shown *in-vitro* to catalyse a conformational change in the mitotic checkpoint complex (MCC) protein Mad2. At the start of my PhD, the *in-vivo* role of TRIP13 in the SAC was partially characterised (unpublished data) in my laboratory: Dr Chiara Marcozzi had generated TRIP13 knock-out (KO) cell lines but had observed clonal variation in mitotic timing and changes to the levels of Mad2 and p31^{comet}. Due to the chronic and irreversible nature of KO cell lines, and potential adaptation to the levels of other SAC proteins, the phenotype of TRIP13 remained unclear. I used TRIP13 as a proof of principle to setup my AID system and to confirm the phenotype observed after removal of TRIP13. Interestingly, I find that TRIP13 is not essential to initially activate the SAC in contrast to previously published literature. My results indicate instead that TRIP13 plays a role in both maintenance and silencing of the SAC as TRIP13-AID cells no longer arrest in response to microtubule depolymerising agents. I also show that depletion of TRIP13 rapidly leads to a change in the levels of Mad2 and p31^{comet}, showing that the changes are not a side effect of CRISPR mediated KO and instead implicating TRIP13 in the stability of these two other SAC regulators.

The role of CEP57 in mitosis has not been previously well described. CEP57 has been implicated in a number of different pathways that could have an effect on mitosis including the SAC, centriole disengagement and interacting with microtubules. Crucially all other genes identified to cause

MVA have been SAC regulators. Therefore, I targeted CEP57 with AID in order to gain further insights into its function. My preliminary data confirms that CEP57 depletion leads to changes to the number of chromosomes inherited from the previous cell cycle. However, I find that mitotic timing did not change upon acute or chronic depletion of CEP57. I also confirm that in human cells CEP57 localises to the centrosome and not the kinetochore. These data indicate that CEP57 is unlikely to function in the SAC. Instead, I find that acute depletion of CEP57 leads to premature disengagement of centrioles in metaphase rather than telophase. I show that inhibition of the centriole disengagement regulator Plk1 partially rescues this timing defect, and that depletion of CEP57 in interphase does not lead to centriole disengagement until the next mitosis. The centrosome is surrounded by a complex mass of proteins known as the pericentriolar matrix (PCM). In G2 and mitosis, the PCM expands to enable increased microtubule nucleation. I show that loss of CEP57 leads to lower levels of pericentriolar matrix (PCM) components, most clearly in Cdk5rap2, at the centrosome during mitosis. My preliminary data indicates a direct link between CEP57 depletion and aneuploidy, and points toward a role for CEP57 in the expansion of the PCM during mitosis.

Acknowledgments

First and foremost, I would like to thank my supervisor, Jonathon Pines, for giving me the opportunity to pursue a PhD in his lab. I am indebted to him for his guidance, mentorship and endless passion for science. In particular I want to thank him for being a voice of reason and for always encouraging me.

I am grateful to all members of the Pines group (past and present) for useful scientific discussions, practical advice and the occasional letting off of steam. Thanks to: Chiara Marcozzi, Özgun Özer, Oxana Nashchekina, Anja Hagting, Andrew Harrison, Barbara Di Fiore, Bernhard Strauss, Camilla Rufilli, Catherine Coates, Annalisa Roberti, Keiko Yata, Luca Cirillo, Matthew Greetham, Mark Jackman, Martina Barbiero, Mirco Masi, Neha Gupta, Theresa Zeisner, and Victoria Johnson. In particular I would like to thank Chiara, Oxana and Özgün for being there as constant support throughout my project and Luca for all things image analysis related.

I thank Cancer Research UK for funding this studentship and the labs of Michel Bornens, Don Cleveland, Helfrid Hochegger, Stephen Jackson, Masato Kanemaki, and Spiros Linardopolous for key reagents.

I would like to thank Chris Bakal and Louise Evans for giving me my first experience of academic research, also at the ICR, and for encouraging me to pursue a PhD.

I am forever indebted to Alexis Barr whose research inspired me to pursue a PhD in the field of cell cycle research. I will always be grateful for her mentorship and friendship.

I would like to thank my friends, Chloe May Simpson and Jonathon Fung, for giving me a place to live when one was sorely needed at the end of my first year.

I thank all of my friends for their support and encouragement: Alan, Beccy, Becky, Chloe, David, Jack, Jonathon, Luke, Lexi, Merlin, Matt, Matthew, Madina, Sam, Trang and anyone I may have somehow forgotten!

To Elvin and Pabu, I wouldn't have been able to finish this without your support in the last couple of years.
Last and most certainly not least I would like to thank my family. My mum, Helen, for her endless support, love, patience and, for always listening to me; every single day of my PhD. I would like to thank my brother and his partner, Jon and Fiona, for their support and for taking on so much responsibility in the last 4 years at home. I would like to thank my grandparents, Anne and Eric, for their support of my education from start to finish, for inspiring me as a child and always making me believe I could do whatever I set my mind to.

This PhD is dedicated to my mum and grandparents.

Table of contents

List of figures

List of tables

Abbreviations

Table 1-1 Abbreviations

‘ (5’ or 3’)	5 prime/ 3 prime
ab	antibody
AID	Auxin Inducible Degron
AdPROM	Affinity directed protein missile system
AP	Alkaline phosphatase
APC/C	Anaphase promoting complex/ cyclosome
ATP	Adenonise triphosphate
ATM	ataxia-telangiectasia mutated
ATR	ataxia telangiectasia and Rad3-related *protein*
Bp	base pair
BSA	Bovine serum albumin
BUB	Budding uninhibited by benxamidazoles
Ca^{2+}	Calcium ion
CAK	Cyclin activating kinase
Cdc	Cell division cycle (protein)
Cdk	Cyclin dependent kinase
cDNA	Complimentary DNA
Cep	Centrosomal protein
CEP57	Centrosomal protein 57
CHK1/2	Checkpoint kinase protein
CHX	Cycloheximide

Cka	Cyclin activators
CKI	Cdk inhibitors
C-nap1	centrosomal Nek2 associated protein 1
CRISPR	Clustered regularly interspaced short palindromic repeats
DAPI	4′,6-diamidino-2-phenylindole
D-box	Destruction box
DIC	Differential interference contrast
DMA	Dimethylastron
DMEM	Dulbecco's Modified Eagle Medium
DNA	Deoxyribose Nucleic Acid
dNTPs	Deoxyribose nucleic triphosphates
D.melanogaster	*Drosophila melanogaster*
Dox	Doxycycline
ds	double stranded
dTAG	Degradation tag
DTT	Dithiothreitol
E.coli	*Escherichia.coli*
EDTA	Ethylenediaminetetraacetic acid
EMCCD	Electron multiplying charge coupled device
FACS	Fluorescent activated cell sorting
FBS	Foetal Bovine Serum
FGF2	Fibroblast growth factor 2
FIJI	FIJI is just image J
Flp	Flippase
FRAP	Fluorescence recovery after photobleaching
FRT	Flippase recognition target

G(0/1/2)	Gap phase
GC	Gibson cloning
gDNA	Genomic DNA
GFP	Green fluorescent protein
gRNA	Guide RNA
Hifi	High fidelity
HR	Homologous recombination
H.sapiens	*Homo Sapiens*
hTERT	Human Telomerase reverse transcriptase
IAA	Indoleacetic acid
ICR	Institute of Cancer Research
IF	Immunofluorescence
kbp	kilo base pair
KCl	Potassium Chloride
kDa	kilo Dalton
K-less	Lysine lacking
KO	Knock out
L15	Leibovitz's
LB	Luria-Bertani
LECA	Last eurkayotic common ancestor
LDS	Lithium Dodecyl Sulfate
MAD	Mitotic Arrest Deficient
mAID	Mini Auxin Inducible Degron
Mbp	mega base pair
MCC	Mitotic Checkpoint Complex
MeOH	Methanol
MES	2-(*N*-morpholino)ethanesulfonic acid

MOPS	3-(*N*-morpholino)propanesulfonic acid
M phase	Mitotic phase
mRNA	messenger RNA
Mt	microtubules
MVA	Mosaic Variegated Aneuploidy
NEB	New England Biotechnology
NEBD	Nuclear envelope break down
NITC	Nonense induced transcriptional compensation
nm	nanometre
ORF	Open reading frame
Os	*Oryza Sativa*
p (eg p21)	protein
p (eg pDRIVE)	plasmid
PACT	Pericentrin and AKAP450 centrosome targeting
PAGE	Polyacrylamide gel electrophoresis
PAM	Protospacer adjacent motif
PBS	Phospho-buffered-saline
PBS-T	PBS tween
PCM	Pericentriolar Matrix
PCR	Polymerase chain reaction
PFA	Paraformaldehyde
PI	Propidium Iodide
PINC	Present in N terminus of CEP57
Plk	Polo like kinase
PMSF	phenylmethylsulfonyl fluoride
PTC	Premature termination codon
PTM	Post translational modification
PVDF	Polyvinylidene difluoride

Rb	Retinablastoma protein
RFP	Red fluorescent protein
RING	Really interesting new gene
RIPA	Radioimmunoprecipitation assay buffer
RNA	Ribonucleic acid
RNAi	RNA interference
RPE1	Retinitial pigment epithelial 1
Rpm	Rotations per minute
SAC	Spindle Assembly Checkpoint
S.cerevisae	*Saccharomyces cerevisiae*
SCF	Skp1/CUL-1/F-box
S.D	Standard deviation
SDS	Sodium dodecyl sulfate
sgRNA	Single guide RNA
siRNA	Short interfering RNA
SMASh	Small molecule assisted shut off
S phase	Synthesis phase
ss	single stranded
TAE	Tris-acetate-EDTA
TE	Tris-EDTA
Tet	tetracycline
TIR1	Transport inhibitor response 1
TO	Tet operator
TPR	Tetratricopeptide repeat
TRIP13	Thyroid Hormone Receptor Interactor Protein 13
UPS	Ubiquitin proteasome system
UTR	Untranslated region
UV	Ultraviolet

V	Volts
WB	western blot
YFP	Yellow fluorescent protein
µ	micro
γ-tubulin	Gamma-tublin

1. Introduction

1.1. Historical overview

Every cell on earth relies upon the same mechanism to ensure accurate transfer of genetic material: cell division. The ability to pass on DNA as information is conserved from single cell prokaryotes to multi-cellular organisms. This feature defines what a living organism is.

Eukaryotic cell division is a highly coordinated, both spatially and temporally, regulated set of events that requires hundreds of proteins in order to be executed correctly. During cell division, the entire cytoskeleton is re-organised so that the mitotic spindle can form, constituting a huge change in architecture that effects the entire cell.

In a pathological context, aberrant cell division is a hallmark of cancer. More recently, it has become clear that mistakes in cell division subsequently lead to genomic instability, and this aneuploidy may even be a driver of cancer itself.

In the last 100 years we have made great advances in our understanding of cell division. Seminal studies in frogs, flies, sea urchin eggs and yeast have accelerated our molecular mechanistic understanding of the cell cycle.

More recently the ability to deplete specific proteins in cells has advanced our understanding of key signaling pathways in the cell cycle. In this thesis, I have used rapid and acute protein degradation in order to study how two proteins, TRIP13 and CEP57, regulate cell division. The loss of function of either of these proteins leads to a rare autosomal recessive disease in humans: Mosaic Variegated Aneuploidy syndrome (MVA) (Pinson et al. 2014; la Torre-García et al. 2019; Aziz et al. 2018; Yost et al. 2017; Sieben et al. 2020).

1.2. The Eukaryotic cell cycle

Proliferation in all organisms relies upon accurate cell cycle progression where thousands of proteins are highly coordinated in space and time to produce two identical daughter cells. Whilst the dynamics of the cell cycle can vary between species the coupling of DNA replication to the equal separation of this genetic material is conserved and crucial (Morgan 2007).

1.2.1. Phases of the cell cycle

The cell cycle has typically been defined by 4 phases: G1 (gap 1), S (synthesis), G2 (gap 2) and M (mitosis). G1, S and G2 are collectively known as interphase: the time between mitoses. Cells can also exit the cell cycle temporarily, which is known as quiescence (G0), or exit irreversibly. Cells exit the cell cycle permanently upon terminal differentiation or become senescent in certain pathologies.

The cell cycle has evolved to include checkpoints in each of these phases, which means that if mistakes have been made the cell will pause to try to correct the mistake. These checkpoints also control the transition between one phase and the next, and ensure unidirectionality of the cell cycle. If the cell is unable to repair the mistake, it will exit the cell cycle and become senescent or undergo apoptosis thereby preventing it from producing mutant daughter cells. Cells in multicellular organisms can also exit the cell cycle to differentiate.

It is important to note here that the traditional stages of mitosis described below are not universal. In some cell types chromosome condensation occurs at different points (Mazia 1961). In many types of fungi, the nuclear envelope remains intact (Kubai 1975). For human cells the following descriptions apply and therefore I will use them throughout this thesis.

1.2.1.1. G1 phase

Cells enter the G1 phase from G0 or the previous mitosis when they receive extracellular mitogenic signals that bind membrane receptors that initiate a signal cascade that results in translocation of transcription factors into the nucleus to initiate gene expression. Cells in G1 and G2 are especially responsive to both extracellular and intracellular stimulation.
Crucially, before cells enter S phase the cell must pass the restriction point and to do this it must not have DNA damage that could be propagated in future divisions. Any DNA damage detected will set off a further signalling cascade that blocks cell cycle progression (Hartwell & Weinert 1989). Once the cell passes the restriction point cells are no longer sensitive to growth factors.

1.2.1.2. S phase

The ultimate aim of S or synthesis phase is to precisely replicate the whole genome once only. In this phase each centrosome will also duplicate by growing a new daughter centriole (see 1.4.3). In order to be duplicated double stranded DNA (dsDNA) is first unwound by helicase enzymes. Helicase enzyme complexes are loaded onto DNA in G1 but remain inactive until S phase. DNA polymerase enzymes then bind small double stranded template regions created by DNA primase at origins of replications. Eukaryotic genomes are massive: *S.cerevisae* (budding yeast) have a 12 Mbp genome and *H.sapiens* have a 3 Gbp genome. In order to replicate all the DNA in a timely manner DNA replication is initiated at hundreds (yeast) or thousands (humans) of replication origins.
The replication machinery creates a replication fork whereby DNA is replicated upon both strands in a semi-conservative manner using Watson-Crick base pair rules. Each newly synthesised dsDNA molecule is made up of a nascent synthesised DNA strand and the older template strand. DNA polymerases can only replicate DNA in a 5' to 3' dependent manner which is mediated by DNA primase that creates a small template. On one

strand, the leading strand, DNA replication occurs continuously however on the other strand, the lagging strand, the DNA polymerase cannot work continuously because of the orientation of the template. In order to get around this DNA primase and DNA polymerase enzymes work together from the replication fork generating Okazaki fragments. The primase and polymerase move in opposite directions and the polymerase keeps “falling off”. DNA ligase connects these replicated fragments into a continuous strand once replication has been completed. Therefore, DNA replication occurs in a semi-discontinuous manner due to the fact that the strands are replicated by different mechanisms.

If the replication machinery encounters a DNA lesion, the fork will stall until the DNA can be repaired by one of the many DNA damage pathways. This is known as the “replication checkpoint”.

1.2.1.3. G2 phase

G2 phase marks the phase between replication and division. However, in recent years it has become clear that parts of the genome that are difficult to replicate continue to be replicated up until mitosis. Some cells even skip gap phases, such as early drosophila embryos which constantly switch between replication and division in tandem. Budding yeast have no discernible G2 phase (Demeter et al. 2000).

Despite this, cells in most organisms do not progress into mitosis unchecked and if DNA damage is discovered in this phase the cells will delay until they repair the damage. This is the “G2/M checkpoint”.

There is also the “antephase checkpoint” that is activated immediately prior to chromosome condensation in response to stress due to factors such as hypothermia and microtubule poisons (reviewed in (Chin & Yeong 2010)).

1.2.1.4. M phase

Mitosis is divided into 5 phases based on chromosome and cell morphology: prophase, pro-metaphase, metaphase, anaphase, and telophase. Prophase is defined by chromosome condensation and separation of the centrosomes to polar opposite ends of the cell. The centrosomes expand their pericentriolar matrix (PCM) by recruiting more proteins that allow them to nuclear a higher number of microtubules. Nuclear envelope break-down (NEBD) marks the transition between prophase and pro-metaphase in open mitosis. The microtubules capture chromosomes by attaching to multiprotein complexes called kinetochores at the centromere of each sister chromatid. As these attachments occur, the chromosomes align in the centre of the cell. Metaphase is defined as when all the chromosomes have congressed to the centre of the cell. When every sister chromatid is correctly attached to the most proximal centrosome (and each pair has one chromatid attached to one centrosome) anaphase is allowed to begin. This metaphase to anaphase transition is the most crucial step in mitosis: it is when a complex signalling network known as the Spindle Assembly Checkpoint (SAC) is switched off (Musacchio & Salmon 2007). The SAC ensures the accurate separation of DNA to the two daughter cells by preventing the activation of the Anaphase Promoting Complex or Cyclosome (APC/C) until all sister chromatids are correctly bi-orientated and attached to the spindle. Anaphase marks the separation of sister chromatid pairs towards opposite ends of the cell. This is mediated by shortening of microtubules that “pull” the DNA toward the centrosome. The DNA begins to decondense in telophase and the microtubules are freed from the mitotic spindle. Centriole disengagement also occurs in telophase. The nuclear envelope reassembles separately around both pools of DNA. This is followed by cytokinesis where the released microtubules form the actomyosin contractile ring, which initiates the formation of the cleavage furrow. The midbody is formed as the cleavage furrow forms between the two cells; it is eventually cleaved by abscission forming two nascent genetically identical daughter cells.

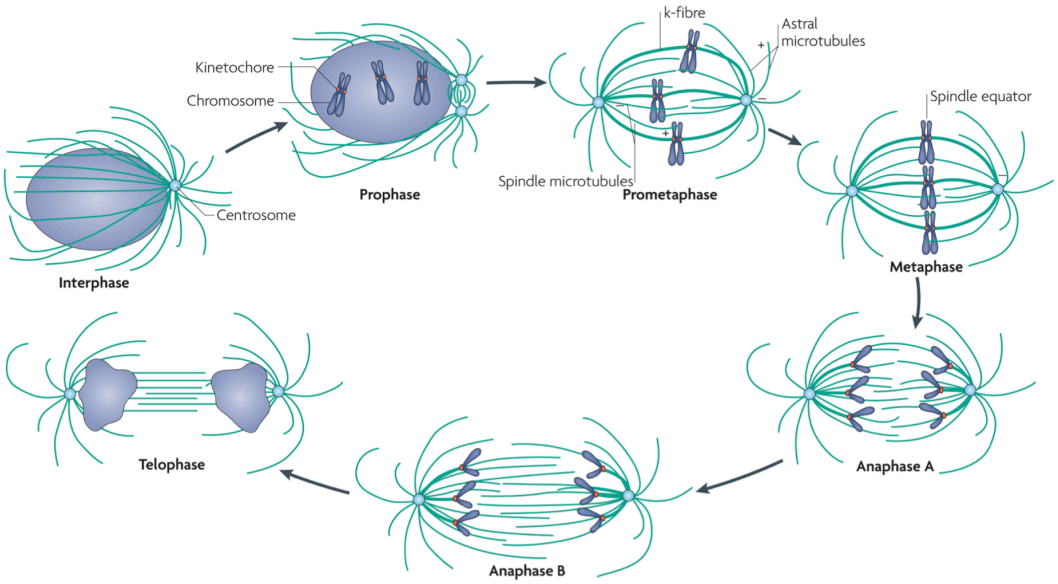

Figure 1-1. Stages of mitosis

This diagram is adapted from Walczak et.al., 2010. This schematic shows the progression of cells through the different phases of mitosis that are canonically defined by chromosome position and the status of their attachment to the mitotic spindle.

1.2.2. Cyclin dependent kinases control progression of the cell cycle

The transition between cell cycle phases is regulated by different members of the same family of serine/threonine kinases named “Cyclin-dependent kinases” or Cdks. As indicated by their name, these enzymes are active only when bound to a Cyclin. Cdk5 is active independently of Cyclin binding and therefore an exception. Their catalytic activity is also modulated by Cyclin activators (Ckas) and Cdk inhibitors (CKIs) (Hartwell 1970; Hartwell et al. 1973; Pines & Hunt 1987; Pines & Hunter 1990; Duronio & Xiong 2013).

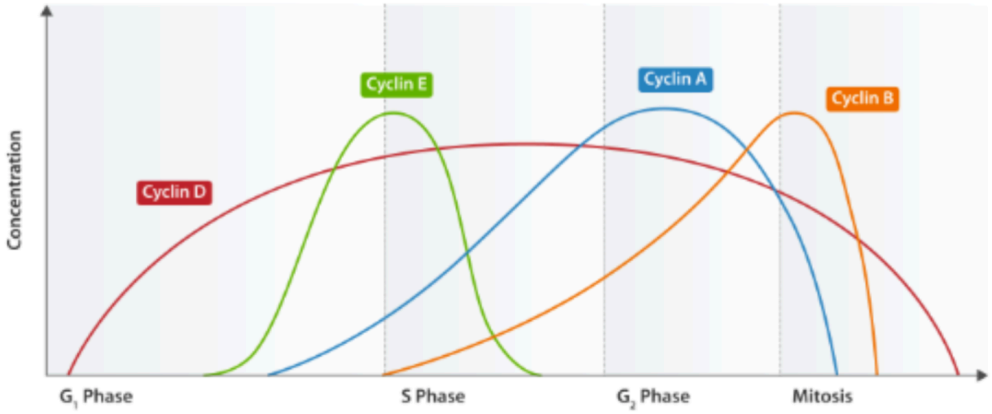

Figure 1-2 Cyclin levels throughout the cell cycle

This diagram is adapted from Pines and Hunter 1991. It shows how the levels of the 4 major types of cell cycle cyclins vary. It also represents the activation and inactivation of their partner Cdk proteins.

Whilst the levels of Cdks remains constant throughout the cell cycle, the levels of various Cyclins oscillate due to controlled destruction and consequently so does the activity of the specific Cdks that they bind (Glotzer et al. 1991; Hershko et al. 1991; Hochegger et al. 2008). Cyclin levels were originally discovered to vary in sea urchins and named “Cyclin” due to the cyclical behaviour in both their synthesis and destruction (Minshull et al. 1989; Draetta & Beach 1989; Pines & Hunt 1987; Swenson et al. 1986; Evans et al. 1983). Cyclin binding to Cdks can also influence Cdk substrate specificity (Pagliuca et al. 2011).

Cyclin/Cdk complexes target a huge range of protein substrates for phosphorylation and drive cell cycle progression through this kinase activity. They confer transfer of the gamma phosphate group from an ATP molecule to specific amino-acid sequences. The consensus motif for most Cdk substrates is [S/T]P[X][K/R] where the serine (S) or threonine (T) at the beginning is the target residue for acquisition of the phosphate (Holmes & Solomon 1996; Nigg 1991).

Cdk proteins were identified first in both fission and budding yeast using genetic screening; the Cdks were named Cdc2 and Cdc28 respectively (Nurse et al. 1976; Reed 1982). Different types of Cyclin binding in each cell cycle phase conveys substrate specificity of the single Cdk type in both

yeast species. Recently it has been shown that in fission yeast a minimal Cdk network is required and that only Cyclin B-Cdk1 is required (Coudreuse & Nurse 2010).

The complexity of higher eukaryotes is reflected in the number of Cdk and Cyclin types that they have. In human cells, 11 Cdk molecules have been identified. 4 Cdk types have been described in the active control of cell cycle progression: Cdk1, 2, 4, and 6. There are also several Cyclin families, classified by sequence conservation, that have a diverse range of functions aside from cell cycle control, including transcription. The A, B, D and E Cyclins are responsible for different parts of cell cycle control in humans.

1.2.3. Proteolysis

The controlled proteolysis of specific substrates, in both space and time, plays a key role in the progression of the cell cycle. Proteins that have served their purpose are sequentially degraded by the UPS. This selective degradation ensures unidirectionality and irreversibility and prevents re-replication or other errors that could lead to aneuploidy (Silkworth & Cimini 2012; Min & Lindon 2012; Lindon et al. 2015; Sivakumar & Gorbsky 2015). This is not limited to the degradations of Cyclins; there is a whole range of substrates degraded in mitosis including Plk1, Aurora A, and Aurora B as well Securin.

1.2.3.1. The ubiquitin proteasome system (UPS)

The UPS is a conserved method of targeting proteins for degradation (reviewed in (Maupin-Furlow 2011)) (Figure 1-3). The system uses the covalent attachment of ubiquitin to the side chain of exposed lysine residues of target proteins to mark the protein (Thrower et al. 2000). The addition of ubiquitin is not limited to targeting a protein for degradation(Schnell & Hicke 2003). Ubiquitylation has been linked to a variety of signalling processes including growth, intra-cellular transport, movement, and apoptosis. Covalent bonds between ubiquitin molecules

generates polyubiquitin chains. There are several different exposed lysines on ubiquitin which consequently increase the variability of how the chains can be made up and this influences their biological role. However, ubiquitin is best characterised for playing a key role for targeting proteins for degradation by the 26S proteasome.

The role of specific protein degradation was neglected for some time as a signalling method. It was clear that protein levels changed and underwent a periodic turnover but it was not clear that this was due to a highly regulated and specific biological process (Schimke & Doyle 1970). Originally lysosomes were considered to be the source of protein degradation (Haider & Segal 1972). This changed when proteins in the ubiquitin pathway were discovered. The field is now highly studied and it is clear the precise regulation of the destruction of specific proteins is intricately part of the biology that allows cells to function properly (reviewed in (Hershko & Ciechanover 1992)).

The conjugation of ubiquitin requires 3 types of enzymes as shown in figure 1.3. Initiation of the process is brought about by a ubiquitin activating enzyme (E1). This family of enzymes activates monomeric ubiquitin using ATP. ATP is used to generate a thiol ester intermediate, E1-S-ubuiqitin. Next an (E2) ubiquitin conjugating enzyme takes the ubiquitin from the E1 enzymes and transfers it to an E3 enzyme or the target substrate. Finally, the E3 (ubiquitin ligase) enzyme catalyses the transfer of the ubiquitin molecule from itself or the E2 to the side chain of a lysine amino acid in the target protein. The E3 forms the covalent iso-peptide bond (Pickart 2001;

Passmore & Barford 2004; Ardley et al. 2005; David et al. 2010; Plechanovová et al. 2012; Scaglione et al. 2013).

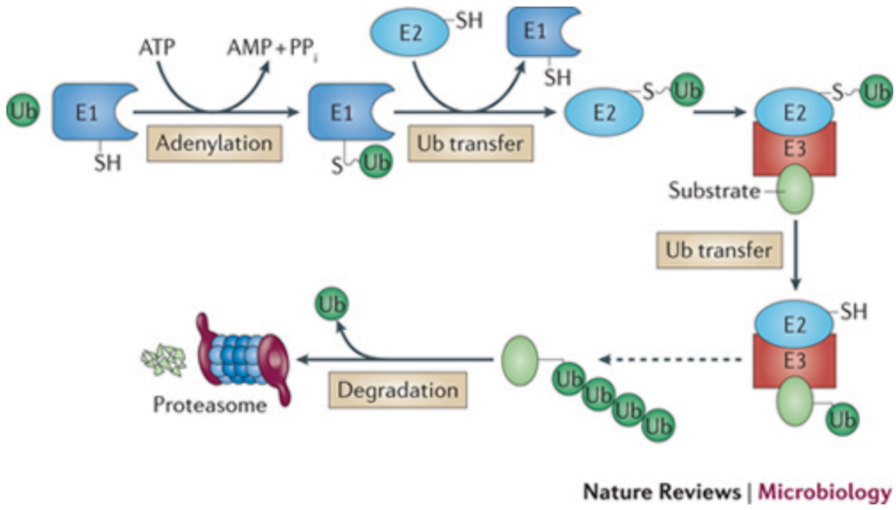

Figure 1-3 The Ubiquitin Proteasome System.

The covalent bond between ubiquitin and a target protein requires multiple steps. The E1 activating subunit forms a thioester bond using an internal cysteine residue and the C terminus of ubiquitin. This ubiquitin is now activated and can be transferred to another cysteine residue on an E2 conjugating enzyme. The E3 ubiquitin ligase catalyses transfer of the ubiquitin to the final NH_2 group of a lysine side chain. Substrates can be monoubiquitylated or polyubiquitylated by attachment of more ubiquitins to lysine side chains of ubiquitin molecules. The specific types of poly ubiquitin residues confer specificity to different cellular processes. Many chains are degraded by the 26S proteasome. (Taken from *(Maupin-Furlow 2011)*)

Activated ubiquitin molecules can be added to this ubiquitin, as stated earlier, to form polyubiquitin chains that are recognised by the 26S proteasome complex (Peters 1998; Morgan 1999; Zachariae & Nasmyth 1999). The proteasome is barrel shaped protease that breaks the targeted proteins into smaller peptides. The proteasome is formed of 2 subcomplexes: a 20S core particle that has peptidase functions, and a 19S regulatory complex with ATPase activity. This part of the complex has roles in unfolding and recognition of substrates permitting them to enter the catalytic core. A ubiquitinated protein is recognised initially by the 19S

complex in an ATP-dependent binding step(Hershko et al. 1980; Ciechanover, Heller, et al. 1980; Ciechanover, Elias, et al. 1980). The substrate is subsequently unfolded so that it can enter the central channel of the barrelled 20S particle. Proteolysis occurs here and the substrate will be reduced to polypeptides of around 8 residues in length.
The E3 ubiquitin ligase play an important role in substrate recognition as well. The cell cycle depends mostly on 2 families of Really Interesting New Gene (RING) finger protein ligases: the Anaphase Promoting Complex/Cyclosome (APC/C) and the Skp1/CUL-1/F-box protein complex (SCF) (Vodermaier 2004).

1.3. APC/C

1.3.1. APC/C structure and architecture

The APC/C was discovered in several different organisms in the mid 1990s: clam (Sudakin et al. 2001), frog (King et al. 1995), and budding yeast (Irniger et al. 1995). The APC/C functions as an E3 ubiquitin ligase that targets a range of proteins for destruction at carefully controlled points in the cell cycle, especially in mitosis. Chief among these is the coordinated destruction of the substrates Securin and Cyclin B1 at the metaphase/anaphase transition once the SAC has been satisfied. The APC/C has a triangular structure and is composed of 19 different subunits some of which exist as homodimers (Chang et al. 2015; McLean et al. 2011; da Fonseca et al. 2011; Herzog et al. 2009; Ohi et al. 2007; Dube et al. 2005; Passmore et al. 2005; Gieffers et al. 2001). It is also a member of the cullin-RING finger family of ubiquitin ligases.
Recently, studies utilising baculovirus expression of APC/C subunits have helped elucidate the complex structure, function and regulation of this key mitotic complex (Alfieri et al. 2020; Alfieri et al. 2018; Alfieri et al. 2017; Alfieri et al. 2016; Yamaguchi et al. 2016; L. Chang et al. 2015; L.-F. Chang et al. 2014; Z. Zhang, Chang, et al. 2013; Z. Zhang, Yang, et al. 2013; Uzunova et al. 2012; McLean et al. 2011; da Fonseca et al. 2011; Schreiber

et al. 2011). The APC/C is 1.2MDa in humans and is organised as 3 main sub-complexes: the catalytic core, which is also involved in substrate recognition; the scaffolding platform, and the TPR arm.

The scaffolding complex is primarily made up of APC4, APC1, APC5 and APC15. However, 85% of the subunits have been shown to have scaffolding functions.

APC8, APC6, APC3 and APC7 are the subunits that make up the TPR arm. These 4 subunits come together to form binding sites for the scaffolding subunit and one of APC/C's co-activators: Cdc20 or Cdh1. APC12, APC13 and APC16 also stabilise the arm. APC3 is involved in the recruitment of the coactivators through its TPR motifs and binding to the IR tail sequences of APC10 and to either coactivator. APC3 has a flexible loop that is phosphorylated in mitosis (S. Zhang et al. 2016). This loop is where the Cyclin Cdk complexes bind.

The catalytic core is made up of APC2, APC11 and APC10. APC10 is part of the substrate binding pocket and has a role in recognising Destruction (D) boxes. APC11 is a RING protein and recruits the E2 enzymes (UbcH10, UbcH5 and Ube2S) (Passmore et al. 2003; Carroll & Morgan 2005; Carroll:2005br da Fonseca et al. 2011). It has been shown in-vitro that UbcH10 and UbcH5 prime the substrate with ubiquitin using APC11 and that Ube2S binds a different part of APC11 to help with elongation (Wu et al. 2010; N. G. Brown et al. 2014; Kelly et al. 2014) It has been shown recently that APC1 is important for co-activator binding mediated conformational change and that depletion of APC1 WD40 domain reduces UbcH10 binding and catalytic activity but not Ube2S dependent chain elongation(Li et al. 2016). Loss of Ube2S leads to a longer time in mitosis after washout from a mitotic arrest induced with spindle poisons (Garnett et al. 2009); however, cells can adapt to the loss of both Ube2S and UbcH10 (Garvanska et al. 2016).

1.3.2. Co-activators of APC/C

The APC/C requires co-activators in order to degrade its substrates. So far three co-activators have been found: Cdc20, Cdh1, and Ama1, which is involved in meiosis. All activators identified have a C-box in their N terminus and an IR tail at the C terminus, plus a conserved WD-40 domain (Wendt et al. 2001; Vodermaier et al. 2003; Matyskiela & Morgan 2009; Thornton et al. 2006; Kraft et al. 2005; Schwab et al. 2001). Cdc20 is active from early mitosis and is replaced by Cdh1 during mitotic exit and G1 phase. The co-activators also provide substrate specificity and recognition through ternary structure interactions.

The first degradation motif identified for APC/C substrates was the D-box in Cyclin B1 (Glotzer et al. 1991; King et al. 1996 Yamano et al. 1996). This motif is present across most APC/C targets and deletion or mutation stabilises the substrate. It can also be used to target new proteins for degradation. Another common motif is the KEN box. In general, Cdc20 preferentially recognises the D-box but Cdh1 can recognise both D- and KEN-boxes.

1.3.3. APC/C regulation by phosphorylation

The APC/C is regulated by multiple kinases at various sites. Upon entry to mitosis Cdk1 and Plk1 phosphorylate the APC/C at over 30 sites to enhance binding to Cdc20; both these kinases are required for proper activation of the APC/C. More detailed studies have shown that Plk1 cannot activate the APC/C alone and that Cdk1 phosphorylation is enough for Cdc20 binding without full activation (Peters et al. 1996; King et al. 1995; Kraft et al. 2003; S. Zhang et al. 2016; Yamada et al. 1997). When APC/C is not phosphorylated, APC1 blocks the C box binding sites for Cdc20 binding with an inhibitory loop. Conversely Cdh1 is also phosphorylated upon mitotic entry but this prevents binding to the APC/C until mitotic exit when there is a shift towards phosphatase activity due to the degradation of Cyclin B1 and subsequent signal cascades (Zachariae

et al. 1998; Kramer et al. 1998; Jaspersen et al. 1999). Differential APC/C phosphorylation mediates substrate specificity as well, and this is used to coordinate the destruction of mitotic substrates in a highly organised manner as mitosis progresses.

Emi1 (Early mitotic inhibitor 1) was originally considered to inhibit Cdc20 bound APC/C and that Plk1 phosphorylation enhanced the degradation of Emi1 and released the APC/C (Moshe et al. 2004; Hansen et al. 2004; Reimann & Jackson 2002; Reimann et al. 2001). Further studies showed that Emi1 was actually an antagonist of APC/Cdh1 during G2(Di Fiore & Pines 2007).

1.4. The Spindle Assembly Checkpoint (SAC)

In all eukaryotes the SAC is responsible for ensuring the equal separation of DNA during mitosis by preventing premature sister chromatid segregation (Figure 1-4). The SAC is active from NEBD to metaphase holding the cells in mitosis until all the chromosomes have been properly attached to the bipolar spindle. This checkpoint ensures correct kinetochore microtubule attachment between each sister chromatid and the spindle (Khodjakov & Pines 2010). It ensures biorientation of the chromosomes and that the spindle will pull equal amounts of DNA into each daughter cell. In doing this, the SAC is key to preventing genome instability and aneuploid cells that could ultimately lead to cancer (Musacchio & Salmon 2007). Interestingly in the early stages of development the SAC has been shown to not become active for several divisions in frog extracts and as of yet it is unclear why (reviewed in Duro and Nilsson 2020).

The SAC ensures that two key substrates are not degraded until the cell is ready: Cyclin B1 and Securin. To do this the SAC prevents their degradation by selectively inhibiting the APC/C from destroying these substrates. The presence of Securin physically prevents cell division. Securin binds Separase, a cysteine protease that is required for sister chromatid separation. Separase targets cohesin subunits when active. Cohesin ensures physical association of sister chromatids. Cyclin B1 degradation leads to a signal cascade that organises mitotic exit. Cyclin B1

degradation in turn rapidly switches off Cdk1 activity and this rapidly changes the balance of kinases and phosphatases during mitosis.

Most SAC genes are essential in metazoans and highly evolutionarily conserved(Kops et al. 2005). These genes are not essential in yeast but become essential in the presence of spindle poisons. Genetic screens in yeast were responsible for uncovering many of the SAC components and they were so named as either MAD (Mitotic Arrest Deficient) or BUB (Budding Uninhibited by Benzamidazoles).

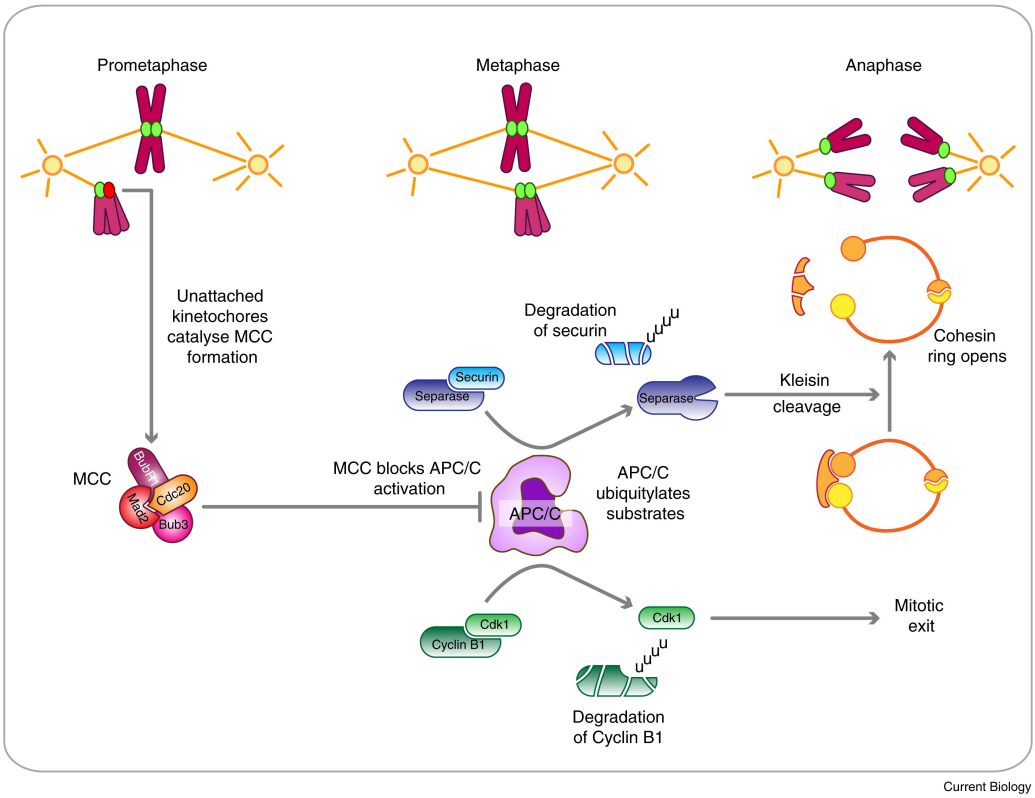

Figure 1-4 The Spindle Assembly Checkpoint.

The SAC prevents premature separation of sister chromatids by inhibition of the APC/C to ensure genome stability. The APC/C is prevented from degrading Securin and cyclinB1 by the MCC. Securin and CyclinB1 degradation promote mitotic exit as their depletion leads to activation Separase and inactivation of Cdk1. Separase cleavage of cohesin allows separation of sister chromatids whilst inactivation of Cdk1 promotes a signalling cascade that leads to mitotic exit. In order to prevent this checkpoint signalling is catalysed in pro-metaphase at unattached kinetochores whereby SAC proteins are hierarchically recruited to the outer kinetochore and the MCC is complex generated. The MCC made up of Mad2, Cdc20, Bub3 and BubR1 prevents ubiquitination activity of the APC/C by

physically binding to the APC/C and preventing recruitment of substrates or the related E2 conjugating enzyme. Once all kinetochores have properly attached to the mitotic spindle, the kinetochores no longer generate this inhibitory signal allowing activation of APC/C and progression from metaphase to anaphase. (Taken from (Lara-Gonzalez et al. 2012))

1.4.1. Wait anaphase signal

The first insight into this checkpoint came from studies on metaphase in newt lung cells. Irradiation that led to mono-orientated chromosomes arrested cells for much longer than cells that weren't treated. This was the first evidence of a "wait anaphase signal" (Zirkle 1970).
The kinetochore was marked as the site for the generation of this signal in kangaroo rat kidney (Ptk1) cells where it was shown that even one unattached kinetochore was capable of preventing cells passing into anaphase (Rieder et al. 1995). It was then discovered that key SAC components localised to the kinetochore (McIntosh 1991; Gorbsky 1995) l. The nature of the signal was not fully characterised however, it was clearly diffusible. The nature of the signal was not fully characterised: it was clearly diffusible but restricted to the spindle where it is generated because when 2 cells were artificially fused, increasing cytoplasm size and the number of spindles, chromosomes in one spindle still divided when they attached all of their microtubules despite the presence of unattached microtubules in the other spindle (Rieder & Khodjakov 1997).

1.4.2. Kinetochores

The kinetochore is a macromolecular complex that is fundamental to the normal progression of mitosis. It provides a platform for the generation of the MCC, the effector molecule of the SAC, when kinetochores are not connected to microtubules (Sacristan & Kops 2015). However, the kinetochore is also a key part of several other mitotic pathways. It

physically establishes a link between centromeric chromatin and the mitotic spindle (reviewed in (Musacchio & Desai 2017)). The kinetochore also controls microtubule dynamics and the physical separation of sister chromatids (Monda & Cheeseman 2018). It also contains many of the proteins responsible to ensure correct bioriented attachment of sister chromatids (Funabiki 2019). The kinetochore is made up of many different sub complexes, some of which are themselves dynamic depending on the state the kinetochore with respect to mitotic stage and microtubule attachment state.

1.4.2.1. Centromeres

Kinetochores assemble upon specific chromatin called the centromere. Centromeres are usually specified at the level of the epigenetic modification of histones rather than at the sequence level of the corresponding DNA. The DNA sequence for centromeres varies between species and so far, a relationship between the specific DNA sequence and kinetochore assembly has not been observed for most systems. However, there are some very specific exceptions to this such as the point centromere in *S.cerevisiae* and other fungi. The DNA sequence in budding yeast contains short “cis” elements that have a conserved sequence which enable kinetochore assembly. (Hieter et al. 1985; Lechner & Carbon 1991; Fitzgerald-Hayes et al. 1982; Clarke & Carbon 1980; Clarke & Carbon 1983) In other species, including humans and most model systems, centromeres are instead made up of highly repetitive DNA and these include retro transposons and tandem repeats, sometimes both. For humans it is a 171-bp repeat called an alpha satellite repeat. These repeats exist for up to 4.0Mbps. It has even been shown that the repetitive DNA is not critically necessary because perturbation creating artificial acentric (without a centromere) chromosome fragments has been shown to lead to neo-centromere activity at relatively unrepetitive parts of the genome (Murphy & Karpen 1995). Some species do not have repetitive elements at all of their centromeres demonstrating a potential redundancy (Shang et al. 2010). However, there is considerable evidence that repetitive elements

benefit centromere design and activity because evolutionary new centromeres have been shown to acquire repetitive elements readily when placed in non-repetitive chromatin (Montefalcone et al. 1999; Rocchi et al. 2012).

Centromere location can vary between chromosomes or across species with sub-categories including: metacentric, acrocentric and telocentric (Musacchio & Desai 2017)).

The epigenetic specification of centromeres is most often through the histone H3 variant CENP-A (Earnshaw & Rothfield 1985; Palmer et al. 1987; Sullivan et al. 1994). CENP-A is present at centromeres throughout the evolutionary tree from *S.cerevisae* (Cse4) and *H.sapiens* (however there are a few exceptions (Drinnenberg et al. 2014). CENP-A is essential for the recruitment of all other proteins in the kinetochore, so much so that artificial ectopic expression of CENP-A also promotes centromeric assembly wherever CENP-A locates in the genome (Oegema et al. 2001; Moore & Roth 2001; Howman et al. 2000; Fachinetti et al. 2013; Logsdon et al. 2015; Heun et al. 2006; Barnhart et al. 2011).

1.4.2.2. Kinetochore organisation and architecture

CENP-A is the foundation of kinetochore assembly even though the architecture has been found to be extremely different across evolution. The kinetochore is composed of over 100 proteins but most of these proteins are recruited at the onset of mitosis and rapidly disassembled at mitotic exit. Throughout interphase, 16 CENP proteins have been shown to be constitutively at the centromere and this network is aptly named the constitutive centromere associated network (CCAN) (Hinshaw & Harrison 2019; Pesenti et al. 2018; Hara & Fukagawa 2018). During mitosis, proteins are recruited to the outer kinetochore including KNL1 complexes, Mis12 and Ndc80, which comprise the KMN network (Petrovic et al. 2010). The activity of Aurora A and B kinases promote interaction between CENP-C and Mis12 (Screpanti et al. 2010; Przewloka et al. 2011). Cdk1 and Plk1 phosphorylation activity are also crucial for mitotic kinetochore assembly (Saurin 2018; Watanabe et al. 2019). These proteins form the basis of the

machinery that interacts with the incoming microtubules and in the absence of microtubules recruit SAC proteins.

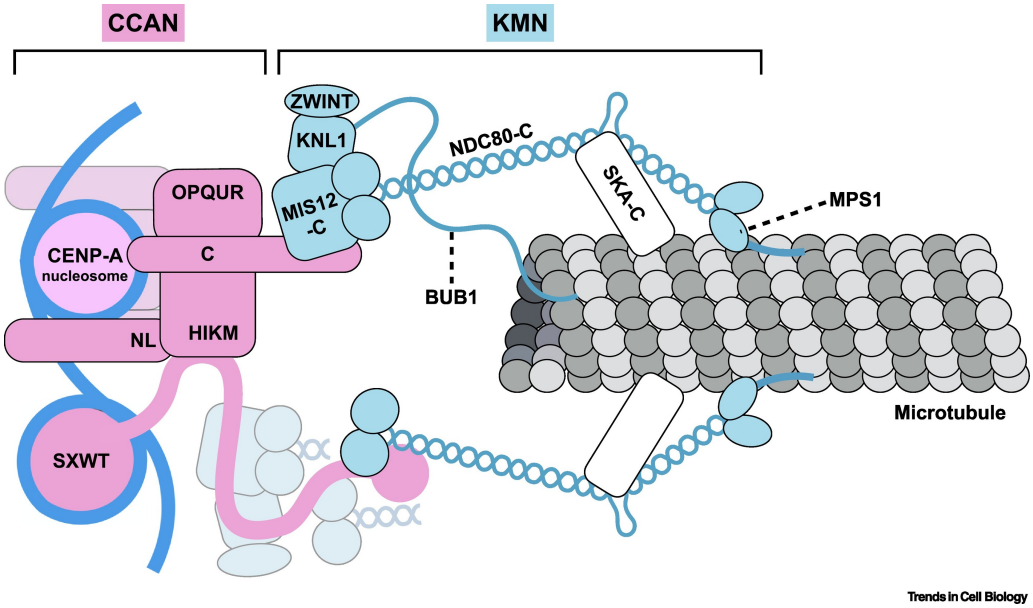

Figure 1-5 Kinetochore subunits.

The CCAN network forms a platform for the assembly with the KMN network through interactions between CENP-A and CENP-C or CENP SXWT. The KMN network is shown forming lateral attachments with a microtubule. (discussed below) SAC proteins Bub1 and MPS1 are also shown. *(Taken from (Kops & Gassmann 2020))*

A schematic summarising mitotic kinetochore machinery is shown in figure 1-5 taken directly from (Kops & Gassmann 2020). It has been shown that CENP-C and CENP-T directly recruit the KMN network. Ectopic expression of these two proteins localised to non-centromeric DNA leads to recruitment and assembly of kinetochore like structures capable of chromosome segregation (Gascoigne et al. 2011; Hori et al. 2013).

1.4.2.3. The Fibrous Corona

In pro-metaphase unattached kinetochores increase in size to assemble the fibrous corona (reviewed in (Kops & Gassmann 2020). This structure is enhanced by conditions that constitutively activate the SAC, such as a nocodazole block where microtubules cannot attach to the kinetochore. The corona begins to assemble at NEBD and was originally observed in

1967 using electron microscopy (Magidson et al. 2015)(Jokelainen 1967). This work was further validated by immuno-electron microscopy and the discovery of 4 proteins that localised there: CENP E, CENP F, tubulin and Dynenin (Cooke et al. 1997; Wordeman et al. 1991; X. Zhu et al. 1995; Rattner et al. 1993). It is now known that the corona is made up of dozens of proteins, including SAC effectors and outer kinetochore proteins. The RZZ complex of Rod, Zwilch and ZW10 has been shown to be essential for corona assembly, whereas it is unclear whether most other corona localised proteins are required for corona assembly or localise there after corona establishment (Sacristan et al. 2018) (Pereira et al. 2018) (Rodriguez-Rodriguez et al. 2018). Spindly interacts with RZZ through a C-terminal farnelysation PTM that allows it to interact with Rod (Barisic et al. 2010). This has been shown to be required for proper expansion of the corona network as a lack of Spindly prevents RZZ oligomerization (Gassmann et al. 2010) (Mosalaganti et al. 2017) (Holland et al. 2015) (Moudgil et al. 2015). In order for Spindly to mediate its interaction with the RZZ to facilitate corona expansion it must be released from its autoinhibited state. MPS1 kinase activity is required to activate Spindly; however, it is presently unclear exactly how MPS1 kinase does this. The most likely sites for MPS1-mediated phosphorylation are T13/S15 in ROD, which are also required for corona expansion (Rodriguez-Rodriguez et al. 2018). A Spindly mutant lacking part of the N terminus has been generated that cannot be auto inhibited, this mutant does not require MPS1 kinase function suggesting that MPS1's primary role in corona expansion is activating Spindly (Sacristan et al. 2018).

Many outstanding questions remain around how the corona connects to the outer kinetochore. There appear to be many redundancies between the different KMN network proteins, the RZZ complex, and SAC proteins such as Mad1 (Kops et al. 2005; Raaijmakers et al. 2018; G. Zhang et al. 2015; Caldas et al. 2015). Two of the most likely candidates are BUB1 and CENP-F. Cdk1 inhibition can be used to dislodge the corona from the kinetochore and when this happens these two proteins are the first to be lost (Pereira et al. 2018). However, there have been many issues with the depletion of BUB1, and since it is a kinase, residual BUB1 may have

sufficient activity to exert some of its function even at low levels (Currie et al. 2018; Raaijmakers & Medema 2019; Zhang et al. 2019).

The corona has been shown to play roles in several aspects of kinetochore biology. The RZZ complex interacts with several SAC proteins and the presence of the corona has been shown to increase SAC signalling (Gassmann et al. 2010; Mosalaganti et al. 2017; Holland et al. 2015; Currie et al. 2018; Raaijmakers & Medema 2019; Zhang et al. 2019). Beyond this, the corona shape aids in initial and correct microtubule attachment, to be discussed below, including encouraging lateral to end-on attachment and avoiding merotelic attachments (Sacristan et al. 2018). Many of the fibrous corona proteins interact with microtubules, and the corona has even be suggested to be a source of microtubule nucleation due to the recruitment of the gamma tubulin ring complex (Mishra et al. 2010).

1.4.2.4. Kinetochore microtubule attachment

As stated above, kinetochores bind microtubules through the KMN network and fibrous corona. In budding yeast this is a single microtubule whereas in other metazoans it is a microtubule bundle or kinetochore fibre (K fibre). Human kinetochores bind 25 microtubules on average (Musacchio & Desai 2017). KMN proteins when lost, or artificially removed, lead to mitotic errors (Kline et al. 2006; Cheeseman et al. 2006; Cheeseman & Desai 2008; Foley & Kapoor 2013).

The process by which microtubules attach to kinetochores is still not entirely well defined. The “search and capture” method was originally observed in newt cells and yeast (Hoyt et al. 1991; Rieder & Alexander 1990; Tanaka et al. 2005; Franco et al. 2007). This hypothesis was led primarily by the observation that microtubules that are relatively stable during interphase, become more dynamic during mitosis; growing and shrinking rapidly (Mitchison & Kirschner 1984). This led to the proposal that microtubules were searching stochastically for kinetochores. However, more recent models have challenged this and suggested that the model would require a strong bias, otherwise human pro-metaphase would take

several more hours to complete if 92 kinetochore microtubule interactions had to take place (Wollman et al. 2005).

The efficiency of kinetochore microtubule interactions has shown to be improved by the changing shape of the kinetochore itself: specifically the expansion of the fibrous corona, as well regulation of microtubule dynamics and a RAN GTPase gradient extending from the corona promoting attachment (Caudron et al. 2005; Kaláb et al. 2006).

Due to the dynamic and stochastic nature of the spindle, the first interaction between a microtubule and the kinetochore can occur anywhere along the length of the microtubule. The most common type of initial interaction is a lateral attachment (Rieder & Alexander 1990; Tanaka et al. 2005). CENP-E and Dynein motor proteins drive these interactions and promote chromosome alignment and subsequent conversion to end-on attachments. It is the expansion of the fibrous corona that allows these two proteins, which localise there, to drive this interaction (Magidson et al. 2015). Dynein is a minus end directed motor and sends chromosomes towards the centrosome where there is a higher density of microtubules (Y. Li et al. 2007). The plus end motor action of CENP-E subsequently promotes chromosome congression (McEwen et al. 2001). The directionality of CENP-E is guided by tubulin de-tyrosination as this PTM has been shown to be enriched in the centre of the cell and depleted elsewhere (Gundersen & Bulinski 1986).

The lateral attachment is replaced by a more stable attachment to the microtubule plus end; the end that facilitates growth of the microtubule. This is essential for accurate separation of sister chromatids. A balance between the activities of Aurora B and PP2A promote the end on attachment conversion through the recruitment of the Astrin-SKAP complex (Shrestha & Draviam 2013) (Shrestha et al. 2017).

1.4.2.5. Error correction of kinetochore microtubules

Even with several methods promoting stable end-on attachments, correct kinetochore-microtubule attachment must be amphitelic; that is one

kinetochore interacting with one centrosome through microtubules in order to ensure biorientation and the correct division of DNA. Figure 1-6, taken directly from (Cimini 2007), shows examples of incorrect attachment where chromosomes interact aberrantly with the incorrect number of spindle poles. Incorrect attachments include: monotelic (single attachment to one spindle pole); syntelic (both kinetochores are attached to the same spindle pole); and merotelic (where one kinetochore is attached to both spindle poles). These types of incorrect attachment occur during pro-metaphase and must be corrected in order to avoid genome instability (Gregan et al. 2011).

The Chromosome Passenger Complex (CPC) made up of Borealin, Survivin, INCENP and Aurora B monitors incorrect attachments and promotes correct amphitelic attachment events. The CPC is considered to sense tension between the spindle and the kinetochore and ultimately destabilises incorrect attachments and stabilises correct attachments. Aurora B has been shown to phosphorylate the kinetochore microtubule binding proteins, including Ndc80, at kinetochores that are under low tension, which subsequently causes the microtubule to detach from the kinetochore. (Cheeseman et al. 2002) (Hauf et al. 2003) (Tanaka et al. 2002). The CPC localises to the centromere and in this way is considered to regulate error correction spatially. This serves as a positive feedback because when sister chromatids begin to separate Aurora B is out of range of the target proteins.

The CPC localises to the mitotic centromere because of two histone modifcations upon histone 3. Phospho-histone H3 is a marker for mitotic cells, Haspin kinase phosphorylates threonine 3 making pH3T3 and this also enhances the binding of Survivin (Wang et al. 2011). Aurora B promotes this by activating Haspin through phosphorylation. The other histone modification takes place on histone 2A which is phosphorylated by Bub1 kinase (Kaur et al. 2007; Wang et al. 2011). Shugoshin binds phosphorylated H2A and brings with it Cdk1 phosphorylated Borealin.

The CPC is confined to the centromere rather than the kinetochore by the phosphorylation gradients setup at the kinetochore during pro-metaphase by Cdk1 and its counteracting phosphatases PP1 and PP2A (Ditchfield et

al. 2003) (Foley et al. 2011) (Suijkerbuijk et al. 2012) (Kruse et al. 2013). Cdk1 and Plk1 phosphorylate BubR1 when there is no tension and this recruits the two phosphatases (Xu et al. 2013). These phosphatases counteract any Aurora B kinase phosphorylation in this vicinity when microtubules are not bound.

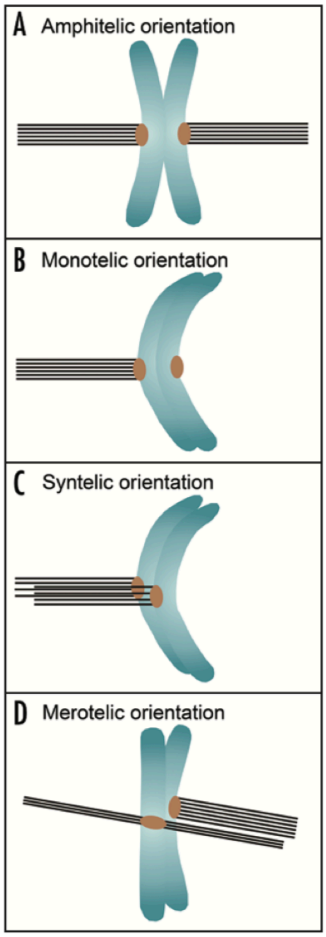

Figure 1-6 Types of kinetochore-microtubule attachment orientations

A) Amphitelic attachment. Kinetochore microtubule attachment must be amphitelic, one kinetochore corrected to one spindle pole through k-fibres to avoid mitotic errors. **B) Montotelic attachment** is where one kinetochore is attached to a spindle pole. **C) Syntelic attachment,** where both kinetochores are attached to the same spindle pole. **D) Merotelic attachment,** where one kinetochore is attached to both spindle poles. If unresolved **B)-D)** can lead to errors in mitosis. Merotelic attachment is a common mitotic error in cancer. Taken from (Cimini 2007)

1.4.3. Recruitment of SAC proteins to the kinetochore

The outer kinetochore serves as a platform that can recruit SAC proteins. Figure 1-7 taken directly from (Dou et al. 2019) shows the hierarchical recruitment of SAC proteins. SAC proteins, with some organism specific exceptions, are recruited to the kinetochore at mitotic entry (Jablonski et al. 1998) (Howell et al. 2004) (Magidson et al. 2015). Mad1 was recently shown to bring Mad2 to the kinetochore prior to NEBD and delaying this till after NEBD led to chromosome instability showing that the SAC must be ready to signal as mitosis begins (Jackman et al. 2020). Mad2, Mad1, MPS1 localisation can be used as markers for unattached kinetochores as the levels decline as attachment increases (Johnson 2004; Ito et al. 2012). However, in the case of most other SAC proteins the recruitment does not completely correlate with attachment.

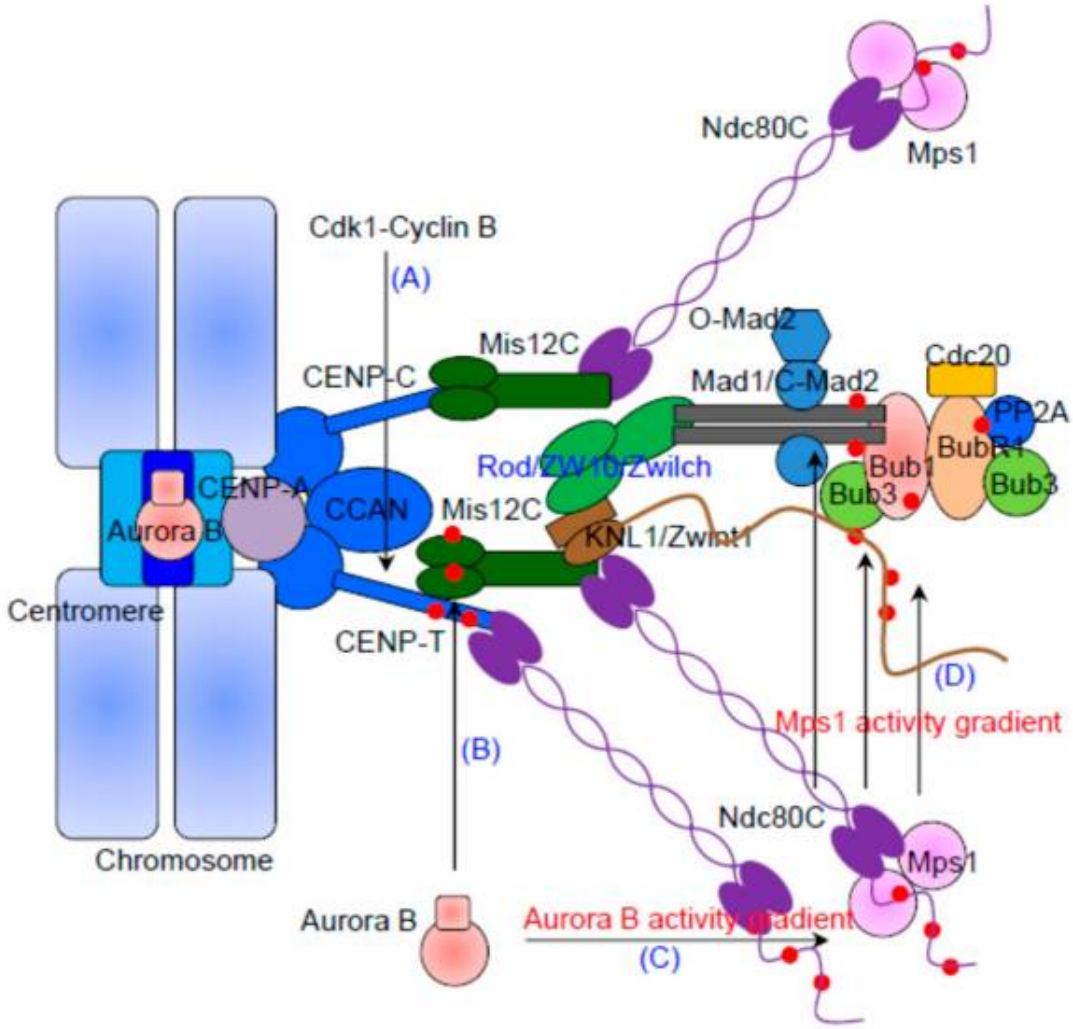

Figure 1-7 Schematic of SAC protein recruitment to the KMN network.

The diagram shows how the kinetochore is assembled from the centromere on each chromosome with recruitment of the CCAN network preceding that of the outer kinetochore components such as the KMN network of KNL1, Mis12 complex proteins, and NDC80 or the RZZ complex (Rod, ZW10 and Zwilch). These proteins in turn allow the recruitment of the MCC proteins through recruitment of Mad1 and Bub1. This is key in recruitment of the MCC complex subunits Mad2, Cdc20 and BubR1/Bub3. (A) (B) (C) (D) highlight kinase gradients that facilitate recruitment of kinetochore proteins and generation of SAC signalling. Ablation of these kinases leads to inefficient SAC signalling. Phosphorylation events are shown as red dots highlighting the complexity of the protein complex.

SAC protein recruitment to the kinetochore is highly dependent on the coordination of kinase and phosphatase activity (reviewed in (Saurin

2018)). Small molecule inhibition of Aurora B and MPS1 kinases revealed their role in the recruitment of proteins to the kinetochore. MPS1 inhibition completely ablates checkpoint signalling and this kinase activity is highly conserved (Hardwick et al. 1996; Weiss & Winey 1996) (Stucke et al. 2004) (Saurin et al. 2011) (Heinrich et al. 2012).

The N terminus of MPS1 includes an N-terminal extension and a TPR domain and these are important for its kinetochore localisation. The NTE and TPR domains both interact with different parts of the Ndc80 complex (Marquardt et al. 2016). MPS1 localisation to the kinetochore is dependent on Aurora B phosphorylation however this can be nullified by removing the TPR domain which has been shown to bind the calponin homology (CH) domain of Hec1 (Nijenhuis et al. 2013).

It has been reported that microtubule attachment displaces MPS1 localisation presenting an elegant explanation why MPS1 recruitment to the kinetochore, and in turn checkpoint signalling, negatively correlates with attachment of kinetochores to the spindle (Hiruma et al. 2015; Marquardt et al. 2016). However, more recently it has been shown that microtubule binding does not interfere with MPS1 bound to the kinetochore. (Koch et al. 2019). These data indicate that MPS1 regulation at the kinetochore is instead regulated by auto phosphorylation and that microtubule binding may instead switch off checkpoint signalling by preventing MPS1 from targeting SAC substrates and encourage it to phosphorylate itself thereby removing it (Wang et al. 2014) (Koch et al. 2019).

Once bound to the kinetochore, MPS1 phosphorylates Met-Glu-Leu-Thr (MELT) motifs of KNL1 (Yamagishi et al. 2012) (London et al. 2012) (Krenn et al. 2014). MELT motifs must be phosphorylated to recruit Bub1-Bub3 or BubR1-Bub3 complexes (Primorac et al. 2013). Plk1 has also been shown to potentiate MPS1 on shared phosphorylation sites on MELT motifs (Schubert et al. 2015). Bub3 constitutively interacts with Bub1 and BubR1 and this interaction is essential for Bub1 and BubR1's localisation to the kinetochores (Taylor et al. 1998) (Lara-Gonzalez et al. 2011) (Krenn et al. 2012) (Zhang et al. 2014). Structural studies have shown that Bub3 is able to "read" MELT repeats (Primorac et al. 2013). Bub1-Bub3 binds much

more strongly to MELT repeats than BubR1-Bub3 due to a domain in the N terminus of Bub1 (Overlack et al. 2015). The same domain region in BubR1 is required for MCC mediated inhibition of the APC/C. (Overlack et al. 2015). It is considered that BubR1 is primarily recruited through Bub1 heterodimerization rather than phosphorylation of Knl1 (Zhang et al. 2015). BubR1 has multiple roles once at the kinetochore. Ablation of Bub1-BubR1 binding to KNL1 prevents efficient generation of the MCC; however, conversely inhibiting BubR1 binding to Bub1 strengthens the SAC (Overlack et al. 2015) (Zhang et al. 2015) (Zhang et al. 2016). BubR1 also plays roles in correcting microtubule attachment by recruiting PP2A-B56 to counteract the activity of Aurora B (Foley et al. 2011; Suijkerbuijk et al. 2012) (Kruse et al. 2013). Therefore, prevention of BubR1 localisation to the kinetochore could artificially prolong this process.

Mad1-Mad2 was shown to be recruited to the kinetochore through interactions between Bub1 and Mad1. Mad1 constitutively interacts with Mad2 as a heterotetramer. This interaction requires sequential Cdk1 and MPS1 phosphorylation of Bub1. (London & Biggins 2014) (Ji et al. 2017). The sequential recruitment of Knl1, the Bubs and finally Mad1 has been referred to as the KBB pathway.

Mad1-Mad2 has also been shown to be recruited in parallel through interactions with the RZZ complex. Cells depleted of Knl1 can maintain sufficient Mad1-Mad2 levels to generate a checkpoint response. (Silió et al. 2015) It has been shown that RZZ complex functions in both Mad2 recruitment and removal after checkpoint satisfaction (Buffin et al. 2005). If Mad1 is artificially localised to the kinetochore this bypasses the need for the RZZ; however, the same redundancy is not seen upon Bub1 depletion indicating Bub1 has multiple roles in the checkpoint (Qian et al. 2017; Rodriguez-Rodriguez et al. 2018). The RZZ's primary role is now seen as Mad1 recruitment. In Drosophila, RZZ and Mad1 have been suggested to interact directly in mitosis; however, an intermediate has also been considered for some years. Recently CyclinB1 was suggested to facilitate an interaction between Mad1 and the RZZ in the corona in an MPS1 dependent manner (Alfonso-Pérez et al. 2019). Mad1 has been shown to bind CyclinB1 and a double charge substitution in Mad1's N terminus

(E53/56K) leads to B1 no longer binding (Jackman et al. 2020) (Allan et al. 2020). This interaction has been shown to be important for normal activation of the SAC for a number of reasons. Ablation of the B1-Mad1 interaction prevented localisation of Mad1 at the corona making B1 a likely candidate for the missing interactor (Allan et al. 2020). Mad1-Mad2 complexes rapidly relocate to the kinetochore from the nuclear envelope (NE) just prior to mitosis. Ablation of B1-Mad1 binding leads to a slower accumulation of Mad2 at the kinetochore and slows Mad1 leaving the NE until after NEBD (Jackman et al. 2020).

1.4.4. Generation of the MCC at the kinetochore

The “wait-anaphase” signal that has been identified as the mitotic checkpoint complex (MCC) responsible for inhibition of the APC/C during pro-metaphase. As stated above, the MCC prevents the E3 ubiquitin ligase activity of the APC/C from targeting Cyclin B1 and Securin for degradation. This complex is generated at unattached kinetochores; therefore, when all kinetochores have attached to microtubules, the SAC is satisfied and the MCC is no longer generated. The Mitotic Checkpoint Complex (MCC) is made up of Mad2, BubR1, Bub3 and Cdc20(Sudakin et al. 2001).

Mad2 is a HORMA domain protein that inhibits the APC/C when it forms a complex with Cdc20, Bub3 and BubR1 (Tang et al. 2001) (Sudakin et al. 2001; Fang 2002; Kulukian et al. 2009; Morrow et al. 2005). Mad1-Mad2 hetero-tetramers exist at the NE during interphase, and, as entry into mitosis begins, Mad1 and Mad2 rapidly re-localises to the kinetochore through Mad1’s interactions with the outer kinetochore (discussed above) (Waters et al. 1998; Skoufias et al. 2001; Logarinho et al. 2004). Due to the hierarchical nature of protein recruitment at the kinetochore, Bub1 or Mad1 depletion prevents Mad2 localising to the kinetochore. Loss of Mad2 leads to premature entry into anaphase (Gorbsky et al. 1998) (Meraldi et al. 2004). Mad1-Mad2 specifically localise to the unattached kinetochore; therefore, microtubule attachment is thought to displace them (Burke & Stukenberg 2008). Mad2 levels at the kinetochore correlate with the

number of unattached kinetochores and this can be used to demonstrate differential levels of SAC activation (Collin et al. 2013; Dick & Gerlich 2013). This is illustrated by the classical experiment whereby ablation of a single kinetochore microtubule attachment re-activates the SAC; longer delays were seen when more microtubules were ablated {Rieder:1995ex}. Furthermore addition of different spindle poisons generates differing levels of checkpoint activation that lead to variation in both the duration of the arrest and Mad2 recruitment to the kinetochore (Collin et al. 2013). Artificial targeting of SAC proteins to the outer kinetochore KMN subunits, for example Mad1 and MPS1, leads to an arrest in metaphase (Jelluma et al. 2010; Maldonado & Kapoor 2011; Ito et al. 2012; Kuijt et al. 2014; Ballister et al. 2014; Heinrich et al. 2014; Kruse et al. 2014).

Cdc20 and Mad1 have been shown to compete for the same Mad2 binding site (Luo et al. 2000) (Sironi et al. 2001) (Zhang & Lees 2001; Izawa & Pines 2012). Structural studies showed that Mad2 is capable of existing in 2 structural conformations: open (O) and closed (C) (Mapelli et al. 2006) (M. Yang et al. 2007). Structural studies have revealed that a seatbelt motif differs in the conformation and that expression of a Mad2 mutant that cannot undergo conformational change leads to a deficient checkpoint (De Antoni et al. 2005). Mad2 can only bind molecules of Cdc20 or Mad1 when in the C conformation. O-Mad2 exists freely in the cytosol. The Mad1-Mad2 hetero-dimer has been showed to be required for a second molecule of Mad2 to interact with Cdc20 (Luo et al. 2000) (Chung & R.-H. Chen 2002). This is considered to be the first step in MCC assembly. The ‘Mad2 template’ model explains how Mad2 paradoxically preferentially interacts with Cdc20 but requires Mad1 to do so. Mad2 can exist in dimers of opposite conformations (De Antoni et al. 2005). C-Mad2 bound to Mad1 as a heterodimer recruits O-Mad2 and converts it to C-Mad2, thereby enabling it to bind Cdc20. MPS1 kinase activity is required for the recruitment of Mad2 to the kinetochore. It has been shown that both O-Mad2 and C-Mad2-Mad1 require MPS1 phosphorylation of Knl1 and Bub1. (Tighe et al. 2008) (Hewitt et al. 2010) (Westhorpe et al. 2011) (Tipton et al. 2013) (Ji et al. 2017) (Faesen et al. 2017).

Mad2-Cdc20 interacts with BubR1-Bub3, recruited through MELT motifs of Knl1 (see above), to form the MCC heterotetrametric complex (Sudakin et al. 2001) (Herzog et al. 2009) (Chao et al. 2012).

.

.

1.4.5. Inhibition of the APC/C by the SAC

In order to inhibit the activity of the APC/C, the MCC sterically binds the APC/C to prevent substrate binding and recruitment, partly because Mad2 binds to the same motif on Cdc20 as does the APC/C. MCC binding induces mitotic arrest until all kinetochores are attached end-on to the mitotic spindle. The APC/C contains a co-activator molecule of Cdc20 as well as the one in the MCC. Our understanding of the interaction between the MCC and APC/C has been greatly advanced by cryo-EM structural analyses of the APC/C^{MCC} (Herzog et al. 2009) (Alfieri et al. 2016) (Yamaguchi et al. 2016). These studies confirmed previous biochemical studies that concluded that the MCC primarily blocks APC/C activity by preventing KEN box and D box interaction with substrates, as well restricting the access of the E2 enzyme UbcH10 from interacting with the APC/C(Izawa & Pines 2011; Izawa & Pines 2012). They also confirmed the conclusion that the APC/C contains a co-activator molecule of Cdc20 as well as the one in the MCC (Izawa & Pines 2015). In the structures, Mad2 exists in its C conformation in order to interact with $Cdc20^{MCC}$ and the other MCC subunits. The MCC is in the central cavity of the APC/C, and APC2 has been repositioned when compared to a structure of APC bound to its Cdh1 co-activator. The bound MCC specifically obstructs 6 degron recognition sites on the APC/C with a combination of its own KEN boxes, D boxes and ABBA motifs. (ABBA motifs bind to Cdc20 and were originally discovered in Cyclin A, BubR1, Bub1 and Acm1. BubR1 has three ABBA motifs, two of which are essential for checkpoint signalling; the third is required for initial Cdc20 recruitment to the kinetochore(Di Fiore et al. 2015).

1.4.6. Silencing of the SAC

Anaphase follows rapidly after the last kinetochore microtubule attachment is made. Cyclin B1 and Securin destruction are initiated as soon as the SAC is inactivated. This implies that MCC in the cell is rapidly inactivated. In-vitro experiments have shown that the spontaneous dissociation between Mad2 and Cdc20 is longer than the time taken for the transition from metaphase to anaphase (Simonetta et al. 2009) (Varetti et al. 2011). This means that the silencing of the SAC is likely to be an active process. Initially it was suggested that dynein stripped Mad1 and Mad2 from the kinetochore because interactions between dynactin and Mad1/Mad2 heterodimers had been shown to weaken the generation of checkpoint signalling (Howell et al. 2000). However, this “stripping” is not strong enough to silence the SAC alone.

1.4.6.1. TRIP13 and p31^{comet} mediated disassembly of the MCC

p31^{comet} was initially identified in HeLa cells as a Mad2 binding partner(Habu et al. 2002). Overexpression of p31^{comet} allows cells to progress through mitosis without proper satisfaction of the SAC(Habu et al. 2002). Depletion of p31^{comet} delays normal mitosis and prolongs arrest when cells are released from treatment with microtubule depolymerisation drugs(Xia et al. 2004; Westhorpe et al. 2011). p31^{comet} and Mad2 are structurally related (M. Yang et al. 2007) (see figure 1-8), but p31^{comet} does not have the ability to change conformation like Mad2.

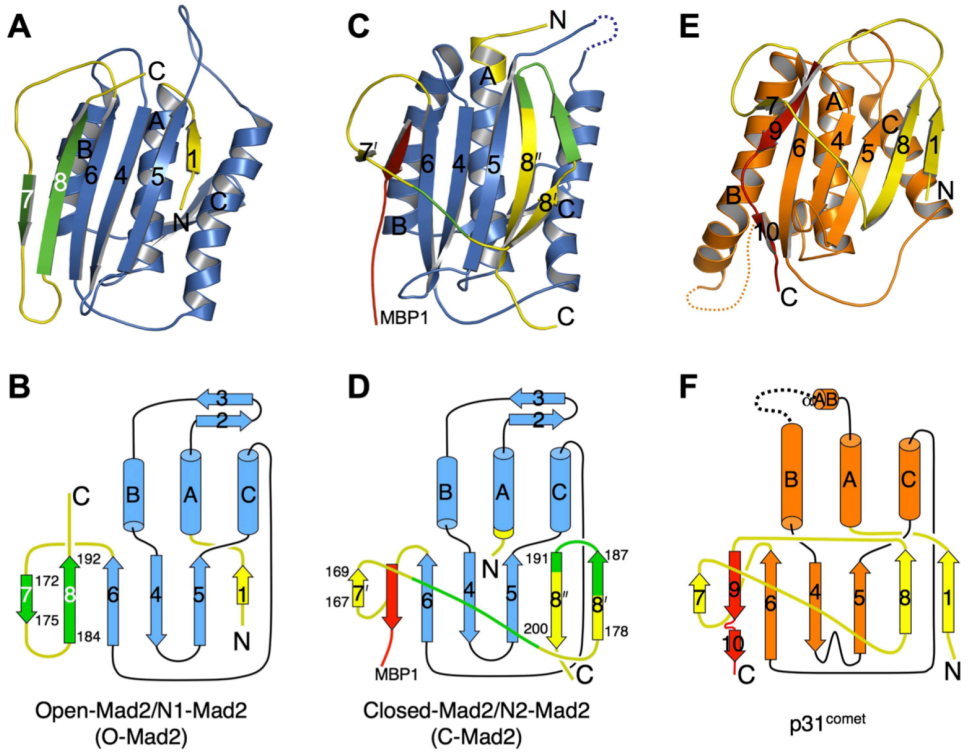

Figure 1-8 Crystal structures of Open/ Closed Mad2 and p31^{comet}.

The conformational change of Mad2 is essential for SAC signalling. This diagram illustrates the differences in the structures between Open and Closed Mad2 that confer checkpoint signalling and also how p31comet interacts with Mad2 as a heterodimer. The seatbelt domain of Mad2 (shown in yellow) is unstructured in Open Mad2 but in Closed Mad2 becomes structured allowing it to facilitate an interaction with Cdc20 (not shown). In **A) C) E)** the crystal structures, and schematics in **B) D) F)** of Open Mad2, Closed Mad2 and p31^{comet} are shown respectively. Core domains are coloured in blue for Mad2 and orange for p31^{comet}. The N and C terminus domain now known as the seatbelt domain that confer conformational change between open and closed Mad2 is coloured in yellow. The analogous domain of p31^{comet} is also yellow. MBP1 and the pseudo-C terminal tail of p31^{comet} is shown in red. Missing domains are highlighted by dashed lines. (M. Yang et al. 2007)

When Mad2 binds to p31^{comet} this prevents closed (C-Mad2) Mad2 from binding Cdc20. FRAP experiments reveal p31^{comet} is mainly cytoplasmic and constantly shuttles at the NE, but during mitosis it relocates to the

kinetochore potentially constantly interacting with Mad2 (Hagan et al. 2011).

p31^{comet} was initially considered to “cap” Mad2 but this doesn’t agree with all the data as pre-existing MCC complexes diffusing away from the kinetochore would not be effect by p31^{comet}. Mad2 levels are in a huge excess compared to p31^{comet} levels in the cell. It is now clear that p31^{comet} has an active role in MCC disassembly, interacting with all MCC subunits and the APC/C itself (Westhorpe et al. 2011). Addition of p31^{comet} in vitro to MCC will remove Mad2 from the complex (Westhorpe et al. 2011). Recombinant p31^{comet} with a mutation that doesn’t allow interaction with Mad2 is unable to disassemble the MCC (Teichner et al. 2011). The presence of ^{p31comet} also stimulates Cdk-catalysed phosphorylation of Cdc20 in the MCC and this promotes dissociation between Cdc20 and BubR1 (Miniowitz-Shemtov et al. 2010) (Miniowitz-Shemtov et al. 2012). Given that p31^{comet} does not have a yeast homologue, and that p31^{comet}-dependent release of Mad2 in vitro is an ATP driven process, it became clear p31^{comet} was not acting alone in this pathway.

Tipton et al found that Thyroid Receptor Interacting Protein 13 (TRIP13) interacts with p31^{comet} (Tipton et al. 2012). TRIP13 is a AAA-ATPase that in vitro can catalyse the conformational change from closed Mad2 to open(Ye et al. 2015). RNA interference of TRIP13 leads to a mitotic delay in cell culture and lower TRIP13 levels slows MCC disassembly in vitro (Eytan et al. 2014).

Conversely CRISPR mediated knock out of TRIP13 generates cells that do not properly activate the SAC. This led to speculation that TRIP13 may be involved in SAC activation and inactivation (Ma & Poon 2016; Ma & Poon 2018). On top of this, it has been reported that p31^{comet} knock-out does not impede the ability of cells to arrest in mitosis (Ma & Poon 2018). This is at odds with in vitro data suggesting both TRIP13 and p31^{comet} are required for extraction of Mad2 from the MCC (Ye et al. 2017). It raises the question of whether TRIP13 can interact with Mad2 independently of p31^{comet}. Recent structural insight into TRIP13 in complex with Cdc20, Mad2, and p31^{comet} suggests this is unlikely as p31^{comet} promotes TRIP13 activity and directly positions Mad2 so that TRIP13 can unwind it (Alfieri et al. 2018) It

remains unclear why the mitotic arrest phenotype of CRISPR-Cas9 mediated p31^{comet} knockout cells is different to that of TRIP13. One explanation for the difference could be that the observation that upon knock-out of either of these proteins the level of the other protein and of Mad2 changes.

1.4.6.2. APC/C mediated disassembly of the MCC

Cdc20 ubiquitylation has been implicated in causing release of Mad2(Reddy et al. 2007) (Stegmeier et al. 2007). However, this observation does not agree with the fact that a lysine-less Cdc20 (K-less), where all Cdc20 lysines have been changed to arginines, dissociates from BubR1 and Mad2 after the SAC is inactivated (Nilsson et al. 2008). Indeed, K-less Cdc20 prevented a prolonged SAC arrest in response to spindle drug treatments, indicating that ubiquitylation of Cdc20 has a more complex role in the SAC (Nilsson et al. 2008). In agreement with this, Cdc20 has been shown to be constantly synthesised and degraded during the checkpoint (Nilsson et al. 2008) (Ge et al. 2009) (Mansfeld et al. 2011; Varetti et al. 2011). Overexpression of Cdc20 ablates the checkpoint, showing that Cdc20 levels must be properly regulated during an arrest (Pan & R.-H. Chen 2004). Interestingly, although Cdc20 is primarily ubiquitylated at the C terminus on residues K485 and K490, mutating these residues did not change the dynamics of MCC disassembly suggesting that there is a lot of redundancy in the regulation of this protein (Mansfeld et al. 2011).

The SAC can be inactivated by an APC/C intrinsic mechanism. The APC15 subunit has been shown to be integral in this process (Mansfeld et al. 2011) (Uzunova et al. 2012; Foster & Morgan 2012). Loss of the yeast homolog (Mnd2) for APC15 was originally shown to lead to retention of MCC bound to the APC/C and slower activation of the ubiquitin ligase complex. MCC binding to the APC/C prevents Ube2C binding according to structural studies(Alfieri et al. 2016; Yamaguchi et al. 2016). APC/C lacking APC15

is catalytically active; however, it cannot mediate Cdc20 ubiquitylation, which links it to checkpoint silencing.

Crucially, co-depleting APC15 and p31^{comet} has an additive effect, which indicates that there are two independent pathways for checkpoint silencing (Mansfeld et al. 2011) (Uzunova et al. 2012) (Foster & Morgan 2012). Co-depletion of TRIP13 and APC15 has also been shown to lead to permanent mitotic arrest, indicating that these 2 pathways are the key ways in which the SAC is silenced(D. H. Kim et al. 2018).But this observation is at odds with the view that TRIP13 KO cells cannot generate a checkpoint response (Ma & Poon 2016); thus, there are still unanswered questions about the dynamics of these pathways. Both appear to be active throughout the checkpoint rather than activated upon SAC satisfaction, and it is likely that MCC production exceeds MCC disassembly rates until the final kinetochore is attached tipping the scales in favour of disassembly. It is attractive to consider that these pathways are constantly recycling Mad2 back to its open form through TRIP13 and this allows regeneration of the MCC complex until proper kinetochore attachment is completed. One hypothesis is that the TRIP13-p31^{comet} pathway mediates MCC disassembly in the cytosol and APC15 is responsible for MCC bound to the APC/C.

1.5. Centrosomes

The centrosome was discovered in 1883 by Edouard Van Beneden; however, it wasn't until 1888 that Theodor Boveri first used the term centrosome. Over the last few decades, centrosome biology has become a key area of study for many research areas (reviewed in (Kellogg et al. 1994) (Bornens 2012) (Arquint et al. 2014) (Conduit et al. 2015)). The centrosome is the main microtubule organising centre (MTOC) of the cell (reviewed in (Lüders & Stearns 2007) and (Sanchez & Feldman 2017)). However, it is clear that centrosomes play fundamental roles in many other cellular processes through its microtubule and protein recruitment (reviewed in (Rieder et al. 2001; Doxsey et al. 2005)). Centrosomes can

be traced back to the last eukaryotic common ancestor (LECA) through the centrin genes that make up the body of the centrosome (Gräf 2018), although centrosomes do diversify widely through metazoans (Conduit et al. 2015).

Whilst it has become clear that some organisms, such as Drosophila, do not require centrosomes to go through cell division, centrosome loss leads to p53 dependent arrest in G1 in mammalian cells (Basto et al. 2006) (Wong et al. 2015). In animal cells, centrosomes are also important for cilia formation in non-dividing quiescent cells, and aberrant cilia function has been linked to many human diseases (Fry et al. 2014; Kurkowiak et al. 2015). As early as the 1920s, centrosomes have been known to play a role in cancer (discussed in 1.5.3).

1.5.1. Structure

The centrosome is made up of two different centrioles surrounded by a pericentriolar matrix (PCM). These centrioles differ in age because centrosomes duplicate semi-conservatively once per cell cycle. This occurs during S phase at the same time as DNA replication. The “old” mother has distal and sub distal appendages that were elucidated through electron microscopy (Paintrand et al. 1992). Contrastingly, the “young” daughter centriole lacks these extra structures and will only gain them in the next cell cycle when it becomes a mother centriole. Whilst both centrioles are capable of nucleating microtubules, only the mother centriole can anchor microtubules using these appendages (Piel et al. 2000). These appendages are not always conserved in invertebrate centrioles but it is clear that these appendages on the mother centriole are required for the growth of the primary cilium in non-dividing cells (Ishikawa et al. 2005). Vertebrate centrioles have been shown to have a nine-fold symmetry of microtubules assembled around the inner cartwheel structure (Bobinnec et al. 1998). This is simplified in some organisms, including worms and flies, both in size and complexity: the modified microtubule triplets forming the

wall are reduced to doublets for instance (Conduit et al. 2015). In humans, the size of a centriole is around 200 nm in diameter and 500 nm long.

The structural basis of the centriole shape has been found to be dependent on the oligomerization of Sas6(Bld12p) (Kitagawa et al. 2011; van Breugel et al. 2011).

Electron microscopy showed that the PCM surrounds the centrioles regardless of cell cycle phase. The centrosome is a membrane-less organelle that the PCM encompasses, creating a spatially restricted region capable of its own biochemical signalling. The PCM is where the majority of microtubule nucleation occurs; however, it is important to note that centrioles have the ability to nucleate microtubules on their own (Gould & Borisy 1977). Initially, researchers used the auto-immune sera of scleraderma patients to identify proteins at the dynamic PCM structure(Tuffanelli et al. 1983) (Gosti-Testu et al. 1986). This led to the initial identification and characterisation of pericentrin (PCNT) in spindle behaviour (Doxsey et al. 1994). Through proteomic studies from purified centrosomes and large scale RNAi and localisation screens in *C.elegans* or *D.melanogaster* it is now clear that hundreds of proteins are recruited to the centrosome and that most of these proteins probably reside in the PCM (Andersen et al. 2003) (Sönnichsen et al. 2005) (Goshima et al. 2007) (Dobbelaere et al. 2008) (Hutchins et al. 2010) (Neumann et al. 2010) (Alves-Cruzeiro et al. 2014).

After the discovery that a lot of the main PCM components, like PCNT (PLP), Cdk5rap2 (Cnn), Cep152 (Asterless) contained large coiled-coil domains the idea of the “centromatrix” was considered. Coiled-coil domains consist of interlaced alpha-helices that mediate interactions between proteins due to hydrophobic surfaces that energetically favour forming hydrophobic cores.

The organisation of the interphase PCM has become clearer after advancements made in light microscopy. 3D stochastic optical reconstruction microscopy (STORM) and 3D structured illumination microscopy (SIM) are both sub-diffraction-limit light microscopy techniques that have been used to show a specific concentric toroid shape exists in the interphase PCM (Mennella et al. 2012) (Sonnen et al. 2012) (Fu &

Glover 2012). Interestingly, the PCM changes shape dynamically between interphase and mitotic cells. The same proteins remain recruited to the PCM but there appears to be no clear ordered or discrete structure (Lawo et al. 2012).

For the cell to enter mitosis, the PCM expands and recruits many more proteins to facilitate the increased demand for microtubule nucleation to form the mitotic spindle. The activity of Plk1 has been shown to be essential in expansion of the mitotic PCM, with numerous proteins failing to be recruited upon Plk1 depletion (Santamaria et al. 2011). This is known as centrosome maturation (1.5.2.4).

1.5.2. The centrosome cycle

The centrosome cycle runs concurrently to the cell cycle. It ensures that centrosomes duplicate and separate equally once per cell cycle much like DNA does in a semiconservative manner (Nigg & Stearns 2011). The centrosome cycle is shown below in figure 1-9 adapted from (Barr & Gergely 2007).

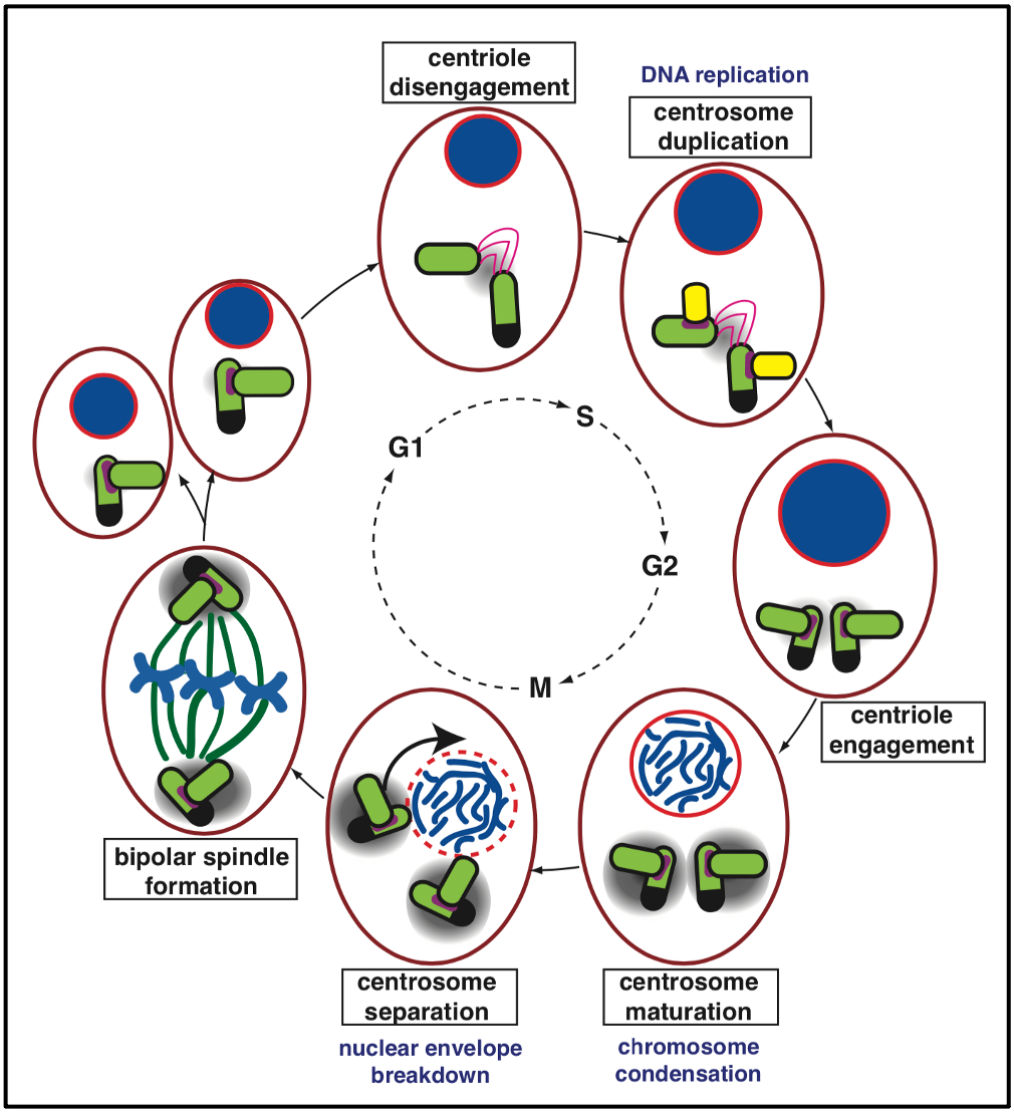

Figure 1-9 The centrosome cycle

Diagram shows the coordination of the centrosome cycle with the cell cycle. Red boxes indicate key centrosome events. Disengagement of centrioles at the end of mitosis licenses centrosome duplication in S-phase. Both centrioles nucleate the growth of a procentriole (yellow cylinders). In S/G2, the daughter centriole from the previous cell cycle (green centriole) fully matures to become a mother centriole (black mark). Duplicated centrosomes undergo centrosome maturation in the subsequent G2 by recruiting extra protein to the PCM (grey circle). Mature centrosomes separate at the G2/M transition, to form the bipolar spindle in mitosis. In a normal cell cycle these events ensure the inheritance of one centrosome, centriole pair of differing age to each daughter cell (mother and daughter).Adapted from (Barr & Gergely 2007)

1.5.2.1. Centriole disengagement

In G1 phase, cells have one centrosome consisting of two centrioles that in the previous cell cycle were a single centrosome mother and daughter pair but in G1 phase they are “disengaged”. This means that they do not exhibit the regular orthogonal geometry to one another. In the next S phase, they will both be mother centrioles that disengaged in the previous mitosis in late anaphase or telophase (Piel et al. 2000). Centriole disengagement must occur before the next S phase otherwise cells will arrest and duplication cannot occur. (Tsou & Stearns 2006; Nigg 2007; C. S. Fong et al. 2018). When G1 and G2 cells were fused, G1 centrosomes duplicated but G2 centrosomes did not. Centriole disengagement therefore acts as a checkpoint for preventing reduplication. Centrosome amplification has been implicated in many cancers. A p53-dependent arrest has been shown to arrest cells in both cells with losses and gains of centrosomes.

Separase, the protease that drives sister chromatid separation through the cleavage of cohesion, was identified as playing a fundamental role in centriole disengagement in *Xenopus laevis* extracts (Tsou & Stearns, 2006). Two main substrates for Separase have now been identified: PCNT and centrosome localised $Scc1^{Rad21}$(Nakamura et al. 2009; Schöckel et al. 2011; Matsuo et al. 2012; K. Lee & Rhee 2012). When PCNT and Scc1 mutants were expressed with the Separase cleavage sites mutated from ExxR to RxxE, centriole disengagement was delayed into G1 phase (Schöckel et al. 2011; Matsuo et al. 2012; K. Lee & Rhee 2012). In some organisms including worms and flies, the requirement for cohesin cleavage is thought to be non-essential (Oliveira & Nasmyth 2013; Cabral et al. 2013). Interestingly, fluorescence reporters for both of these proteins have shown that centrosome localised Separase becomes active at the metaphase to anaphase transition even though centriole disengagement occurs much later at telophase suggesting that Separase activity is not the final step in centriole disengagement. (Chestukhin et al. 2003), (Agircan & Schiebel 2014).

The other key regulator of centriole disengagement is Plk1. Co-inhibition of both Separase and Plk1 prevents centriole disengagement indefinitely and leads to cell cycle arrest. (Tsou et al. 2009). Plk1 was subsequently shown to be an upstream effector of Separase mediated cleavage of both PCNT and $Scc1^{Rad21}$. Phosphorylation by Plk1 is required for recognition of PCNT by Separase most likely through PP2A binding (Kim et al. 2015). Kim et al showed that phospho-resistant mutants of PCNT cannot be cleaved and delayed centriole disengagement, whereas phospho-mimetic PCNT mutants were able to rescue this in the presence of Plk1 inhibitors (J. Kim et al. 2015). PP2A binding also links Plk1 to the cohesin cleavage pathway because PP2A interacts with small Shugoshin 1 (sSgo1) (Tsang & Dynlacht 2008; Wang et al. 2008). Despite this it is clear that Plk1 must phosphorylate other substrates in order to control centriole disengagement as inhibition of both Separase and Plk1 are required to completely inhibit centriole disengagement, whereas inhibiting either one alone allowed cells to progress into S phase and duplicate their centrioles (Tsou et al. 2009)

Plk1 has a multitude of roles during G2 phase and mitosis: in centrosome maturation it is essential for the maturation of the PCM (Santamaria et al. 2011) (Lee & Rhee 2011). It is likely that the any other target of Plk1 is one of the many proteins within the PCM (Santamaria et al. 2011).

It is important to note that it has been shown, through electron microscopy and high resolution light microscopy, that centriole duplication is no longer blocked once the centrioles reach a distance of around 80nm from one another (Shukla et al. 2015). Shulka et al then went on to show that the distance is actually reached at prophase rather than upon the metaphase anaphase transition when centriole disengagement is canonically thought to occur. Despite this in recent times, the context of “precocious centriole disengagement” has been referred to and this is more often than not referring to premature occurrence of centriole disorientation where the centrioles are completely free of one another like in the subsequent G1 (Watanabe et al. 2019). Unlike centriole disengagement, centriole disorientation is more easily detected by conventional confocal light microscopy.

1.5.2.2. Centrosome cohesion

After disengagement the two centrioles inherited from the previous cell cycle establish a linker. Purified centrosomes analysed by electron microscopy showed that centrosomes are held together in G1, S and G2 phase by a proteinaceous linker between the proximal ends of the older centriole in each pair (Paintrand et al. 1992). The proteinaceous linker is composed of C-Nap1/Cep250 and the filamentous protein rootletin (Mayor et al. 2000; Bahe et al. 2005; J. Yang et al. 2006). Prior to entry to mitosis the linker is destroyed in order to facilitate bi-polar spindle assembly.
It was shown that c-Nap1 was at the proximal ends of both centrioles and that rootletin fibres extended between them by immunogold electron microscopy. Rootletin localisation depends on c-Nap1. RNA interference (RNAi) and antibody injection assays have revealed that both of these proteins are required for centrosome cohesion. Nocodazole treatment of interphase cells also leads to centrosome splitting showing that microtubules also play a key role in cohesion.

1.5.2.3. Centrosome duplication

As stated earlier, centrosome duplication is coupled with DNA replication in S phase. Centrosome duplication was shown to be semi-conservative by the injection of biotin labelled tubulin. This showed that only new daughter centrioles incorporated tubulin. These experiments elucidated that the new daughter grew from the proximal end of each mother centriole during S phase. The procentrioles are immediately engaged as showed by their orthogonal conformation relative to the mother. This engagement lasts until late anaphase /telophase of the following mitosis, see 1.5.2.1. These procentrioles then begin to grow and mature during G2 phase up until mitosis.
Nucleation of the new centriole begins at the base of each centriole. Cep192 and Cep152 are key proteins for initiation of centrosome duplication. Cep192 is responsible for recruitment of Cep152 which is considered to be responsible for the recruitment of Plk4 (Sonnen et al.

2013) (T.-S. Kim et al. 2013). Plk4 recruitment is essential for centriole duplication (Habedanck et al. 2005) (Bettencourt-Dias et al. 2005) (Kleylein-Sohn et al. 2007). Both Ceps localise outside the centriole structure as a ring (Lüders 2012). An interaction between Cep63 and Cep152 at the proximal end of mother centrioles has also been shown to be required in order to properly recruit Plk4 (Sir et al. 2011) (N. J. Brown et al. 2013) (Lukinavičius et al. 2013). Plk4 once recruited is transferred by competitive binding from Cep192 to Cep152 and then to the sites of procentriole assembly where it recruits STIL, which it phosphorylates to recruit SAS-6(Ohta et al. 2014; Kratz et al. 2015). These proteins in turn recruit CPAP and this protein trigger assembly of the procentriolar microtubules (Kleylein-Sohn et al. 2007; C.-J. C. Tang et al. 2011).

Sas6 is responsible for assembling the 9-fold cartwheel structure elucidated by EM (Kitagawa et al. 2011) (van Breugel et al. 2011). Structural studies revealed that SAS6 homodimerizes using it's coil-coil domain and N terminus domain and assembles into the 9 fold symmetrical structure (Brito et al. 2012; C. S. Fong et al. 2014). This assembly process transiently occurs within the empty lumen of the mother centriole, and through interactions with STIL and Plk4 is transferred to the luminal wall in order to facilitate elongation and maturation. The cartwheel is removed from new centrioles in the next mitosis and stabilisation of cartwheel-less centrioles is mediated by Cep295 (Izquierdo et al. 2014; Arquint & Nigg 2014). Procentriole formation is completed by the assembly of microtubule triplets (in most animal cells).

Centriole elongation begins in S phase. For it to occur, STIL, CPAP and Sas6 must interact and centrioles grow to a specific size depending upon the organism. CPAP is important for stabilisation of the cartwheel and recruitment of microtubules. Overexpression of CPAP disrupts this process and leads to larger centrioles(Kohlmaier et al. 2009; Schmidt et al. 2009). Cep135, Cep120 and centrobin are all recruited to the daughter centriole specifically to promote assembly and elongation. CP110 caps elongating centrioles by localising to the distal end. CP110 interacts with Cep97 and the kinesin-13 homolog Kif24. Depletion of CP110 or Cep97 leads to over-elongated centrioles as well (Schmidt et al. 2009) (Spektor et al. 2007).

Kif24 depletion results in loss of CP110 from centrioles but not over elongation (Kobayashi et al. 2011).

Plk4 is not the only kinase activity required for centriole duplication. The activity of Cdks has been shown to be important in the regulation of centriole duplication (J. Chang et al. 2010). Inhibition of DNA replication using aphidicolin to prevent the activity of DNA polymerases does not prevent centriole duplication but instead repeated centrosome assembly in both *Xenopus laevis and Drosophila melanogaster* embyros (Raff & Glover 1988; Hinchcliffe et al. 1999). In the frog extracts, centrosome duplication could be inhibited by adding Cdk inhibitors and rescued by overexpressing Cdk2-cyclinE (Lacey et al. 1999). Centrosome duplication requires active Cyclin Cdk complexes in the cell at the start of S phase: several substrates have been identified: CP110 (Z. Chen et al. 2002), MPS1 (Kasbek et al. 2007), nucelophosmin (Okuda et al. 2000) and MCM5 (Ferguson & Maller 2008) however, many questions remain about Cdk activity during centriole duplication.

1.5.2.4. Centrosome maturation

In G2, more proteins begin to be recruited to the PCM and how this process occurs is the focus of many studies. It results in an increase in the microtubule nucleation capacity of the centrosomes during mitosis due to the increased amount of γ-tubulin ring complexes (γTRCs) in the PCM. In early mitosis, during prophase and pro-metaphase, even more γ-tubulin is recruited independent of microtubules which demonstrates that there is a centrosome-intrinsic mechanism for the accumulation.

As the cell progresses towards mitosis there is also a shift in the relative kinase and phosphatase balance in the cell. As more and more proteins become phosphorylated this allows recruitment to the centrosome. Cdk11, Pak1, Aurora A, and Plk1 have all been implicated in phosphorylation that increases centrosome maturation recruitment. Cdk11 and Pak1 recruit Aurora A and Plk1 to the centrosomes. Pak1 can fully activate Aurora A by phosphorylation of T288 in the activation loop (Littlepage et al. 2002).

In flies, polo, the homolog of Plk1, is essential for centrosome maturation and the progression of mitosis (Dobbelaere et al. 2008).

Plk1 phosphorylates many of the PCM components including: PCNT, Cep192, Cep215 and NEDD1(Santamaria et al. 2011). Phosphorylation of PCNT by Plk1 is critical for the recruitment of gamma-tubulin, AuroraA, NEDD1 and itself. γ-tubulin and NEDD1 heavily rely upon PCNT and Cep192, who require each other for centrosomal localisation (Haren et al. 2006; F. Zhu et al. 2008). Cep215 and PCNT also promote each other's localisation at the PCM. Cep215 has been shown to interact with γTRCs to stimulate microtubule nucleation (K.-W. Fong et al. 2008) (Conduit, Feng, et al. 2014).

Whilst all of these proteins are clearly required for centrosome maturation, the exact mechanisms of how and why they are required remain unclear. In flies and worms, centrosome maturation relies on fewer proteins. Recently, a positive feedback loop has been identified in flies where the homologs of Cep215, Plk1 and Cep192 (Cnn, polo, and spd2, respectively) cooperate to rapidly increase the size of the PCM at mitotic onset (Alvarez-Rodrigo et al. 2019). The authors mutate S-S/T motifs in Spd2 to perturb the binding of polo through its PBD and show that this ablates centrosome maturation. These three proteins are essential for centrosome maturation, much like their vertebrate homologs (listed above). (Conduit, Richens, et al. 2014) (Conduit, Feng, et al. 2014) (Woodruff et al. 2015; Wueseke et al. 2016) (Woodruff et al. 2017) (Feng et al. 2017). Interestingly, Plp, the homolog of PCNT, seems to play a more minor role in fly centrosome maturation (Martinez-Campos et al. 2004) (Richens et al. 2015).

Centrosome maturation has been extensively studied across model organisms but many questions still remain, such as how do split centrosomes recruit the same amount of PCM and subsequently nucleate the same number of microtubules in order to not upset the balance of the mitotic spindle?

1.5.2.5. Centrosome separation

At the end of G2, prior to mitosis, the 2 duplicated centrosomes move to the opposite ends of the cell in order to facilitate the assembly of the bipolar spindle for mitosis; this is known as centrosome separation. Centrosome cohesion must be dissolved; the proteinaceous linker must be disrupted and the centrosomes must physically separate through the action of the motor protein Eg5 (Mardin & Schiebel 2012).

As explained above, the linker is composed of C-nap1/Cep250 and Rootelin. C-nap1 is responsible for the localisation of Rootelin, which binds in between the two ends of the centriole. Cep68 and Cep135 are important for the localisation of c-nap1 at the proximal end of each mother centriole (Fry, Mayor, et al. 1998) (K. Kim et al. 2008) (Graser et al. 2007).

The dissolution of the linker has shown to be dependent on the kinase activity of Nek2 and can be induced by overexpression of Nek2 (Fry, Meraldi, et al. 1998). Nek2 phosphorylates C-nap1, Cep68 and Rootelin (Bahe et al. 2005) (Guoliang Fang et al. 2014) (Hardy et al. 2014). Nek2-dependent phosphorylation of C-nap1 disrupts the interactions with Cep135 (Hardy et al. 2014). When Cep68 is phosphorylated this promotes dissociation and subsequent degradation during mitosis (Graser et al. 2007) (Man et al. 2015).

Nek2 activity is coordinated so that centrosome separation occurs at the optimal time just prior to mitosis. The activity of Nek2 unsurprisingly peaks at the end of G2 phase. Nek2 is counteracted by the phosphatase, PP1a, but PP1a is inhibited by Cdk1 at mitotic onset (Puntoni & Villa-Moruzzi 1997) (Smith et al. 2011). Cdk1 activity also ramps up during G2 and is at its maximum during the first half of mitosis (Gavet & Pines 2010). Pericentrin has also been shown to prevent Nek2 activity (Matsuo et al. 2010).

After the removal of the linker, centrosomes are physically separated by the motor protein, Eg5. Eg5 is targeted to the centrosomes by Plk1, Nek6 and microtubules (Mardin et al. 2011) (Smith et al. 2011) (Bertran et al. 2011). This typically occurs before NEBD but in some animals it occurs after. Eg5 is a plus end-directed kinesin motor protein that slides antiparallel microtubules past each other to drive the centrosomes away from one another (Blangy et al. 1995) (Kapitein et al. 2005). Dynein, a

minus end-directed motor protein, is also required for separation to provide counteracting forces that drive centrosomes apart (Raaijmakers et al. 2012). In addition to this, myosin II provides extra support for dynein after NEBD at the cell cortex where it mediates interactions with astral microtubules, attaching them to the cortex to help centrosomes reach polar ends of the dividing cell (Rosenblatt et al. 2004) (Tame et al. 2014). It has recently been shown that actin plays a crucial role in the correct formation of the bipolar spindle due to its role in the control of centrosome separation (Stiff et al. 2020).

The inhibition of Eg5 is often used to cause mitotic arrest because without centrosome separation a bipolar spindle cannot form; therefore the error correction pathway continuously detaches kinetochores to generate a SAC response (Blangy et al. 1995).

1.5.3. Centrosomes in disease

Abnormal centrosome behaviour has been linked to several diseases including cancer, microcephaly and dwarfism (Nigg & Raff 2009) (Bettencourt-Dias et al. 2011). Despite this, centrosomes are redundant, for cell division at least, in animal cells although these cells show decreased efficiency at assembling the mitotic spindle. As stated above, flies can develop without centrosomes but loss of centrosomes in humans and many animal cells triggers the activation of p53 in G1 phase (Bazzi & Anderson 2014); loss of p53 allows acentrosomal cells to cycle indefinitely (Lambrus et al. 2015). However, aneuploidy is not the trigger of p53 activation because it is activated in all acentrosomal cells through a yet undefined signalling mechanism (Conduit et al. 2015). p53 is also activated in centrosome amplified cells but this is through another pathway as the Hippo pathway is activated in tetraploid cells but not in acentrosomal cells (Ganem et al. 2014) (Wong et al. 2015). Centrosome amplification is a hallmark of several cancers and has been directly linked to causing tumour formation (Pihan et al. 1998) (D'Assoro et al. 2002) (Basto et al. 2008). However, whilst there is a correlation between the increase in the number

of centrosomes and an increase in genome instability, centrosome genes are not often mutated nor do they act as oncogenes/tumour suppressors (Lingle et al. 1998) (Pihan et al. 1998) (Lingle et al. 2002). Due to centrosome clustering, most multipolar spindles events result in normal bipolar divisions (Quintyne et al. 2005) (Basto et al. 2008). However, multipolar spindles could result in an increase in genome instability through merotelic kinetochore attachments (Ganem et al. 2009) (Silkworth et al. 2009). Conversely, unlike cancer, there is a clear genetic link between centrosome genes and microcephaly. Autosomal Recessive Primary Microcephaly is a congenital neurodevelopmental disorder where the brain is much smaller than the average for age or gender. Interestingly gene mutations identified to cause microcephaly nearly always reside at the centrosome, but why this is the case remains unclear.

1.6. Aims of this thesis

1.6.1. TRIP13

The complex signalling of the SAC makes it hard to study and despite many recent advancements there are still many things we do not understand. A key missing piece of information is how the disassembly of the MCC is regulated during SAC silencing at metaphase. The ATPase activity of TRIP13 has been shown biochemically to convert Mad2 from closed to open; however, it is still unclear how this activity is important for the checkpoint. There was a difference between the partial siRNA knock down phenotype and complete CRISPR knock out of TRIP13 phenotype. In many CRISPR knock out studies it has been shown that cells have time to adapt to the long-term loss of a protein by changing the expression of related genes in the same signalling pathway. Indeed, there was a large upregulation of $p31^{comet}$ in TRIP13 KO cells, which could interfere with the observed phenotype of checkpoint override. On top of this there was also a large reduction in the levels of Mad2 in TRIP13 KO cells. Mad2 levels have been shown to directly correlate with the strength of the SAC and it has been shown that overexpression of $p31^{comet}$ leads to cells progressing prematurely through the checkpoint by our lab (unpublished) and several others.

One of the mains aims of this thesis was therefore to understand how the SAC behaved in response to acute loss of TRIP13. To do this, I spent a large proportion of my time generating and optimising cell lines capable of depleting TRIP13 using the auxin inducible degron (AID) system.

1.6.2. CEP57

During my research, I became aware that TRIP13 loss was non-essential in humans but led to an extremely rare autosomal recessive disease known as mosaic-variegated-aneuploidy (MVA) syndrome. At the start of this project, only genes with crucial roles in the SAC had been identified to lead

to this disease; with BubR1 being the other main gene. The third gene identified however, was CEP57.

The function of CEP57 is poorly characterised in the literature with lots of contradictions. The most interesting contradiction, with regards to my project, is whether CEP57 really has a role in the SAC. There are papers that show a difference in mitotic timing and others that show no change.

CEP57 had also been shown potentially to affect the normal timing of centriole disengagement. Normally centriole disengagement occurs at mitotic exit in telophase. If the centrioles disengage prior to metaphase there is a potential for aneuploid events due to improper formation of the bipolar spindle. Premature centriole disengagement has been shown to lead to genome instability but this process had never been linked to MVA before specifically.

Due to the acute nature of the AID system, I judged CEP57 an ideal novel candidate to study using inducible degradation. I aimed to deplete CEP57 at different periods during the cell cycle and centrosome cycle to understand whether CEP57 was really a SAC protein, centrosome protein, or both. The main aim for this part of my project was to understand more about the molecular function of CEP57 and potentially use that information to understand more about how this protein leads to MVA syndrome.

2. Materials and Methods

2.1. Materials

2.1.1. Cell lines

hTERT RPE-1 cells (RPE1) were originally derived from *Homo sapiens* retinal pigment epithelial cells. They were immortalised using stable ectopic expression of human telomerase reverse transcriptase (hTERT) combined with a hygromycin resistance cassette to enable selection. Throughout this thesis these cells will be referred to as RPE1.

RPE1-osTIR1 cells were a kind gift from Don Cleveland that ectopically express the F-box protein Transport Inhibitor Response 1 (TIR1) from the rice plant *Oryza Sativa*.

The RPE1 FRT/TR cell line was generated by Mark Jackman and Felicia Pagliuca in order to create stable cell lines more readily and reproducibly. This cell line is stably expressing the Tet repressor. To make the stable cell line, the hygromycin cassette in the plasmid pcDNA5 FRT/TO was replaced with a neomycin cassette.

The RPE1/TR/ROSA26-OsTIR1myc cell line was a kind gift from Helfrid Hochegger. In his lab CRISPR was used to target osTIR1myc into the safe harbour locus, ROSA26 under the control of the Tet-ON 3G system (Takara).

All 3 of these cell lines were used for gene targeting and subsequently to test and optimise the Auxin Inducible Degron (AID) system in.

Centrin-GFP stable cell lines were made and maintained in using 0.4µg/µL neomycin.

E.coli DH5α cells were used for all molecular biology as hosts for cloning. They were created by Catherine Coates and Oxana Naschekina. They had the following genotype: F–Φ80*lac*ZΔM15 Δ(*lac*ZYA-*arg*F) U169 *rec*A1 *end*A1 *hsd*R17 (rK–, mK+) *pho*A *sup*E44 λ– *thi*-1 *gyr*A96 *rel*A1

Table 2-1 List of cell lines and clones used in this study

Cell line	Origin	Clones described in this study
RPE1	Clontech	-
RPE1 osTIR1	Don Cleveland	-
RPE1 osTIR1 FLAG-Venus-TRIP13	Jordan Holt / Theresa Zeisner / Chiara Marcozzi	
RPE1 FRT/TO	Mark Jackman / Felicia Pagliuca	-
RPE1 FRT FLAG-osTIR1	Chiara Marcozzi / Jordan Holt	-
RPE1 FRT FLAG-osTIR1 +/+ FLAG-Venus-TRIP13	Jordan Holt / Theresa Zeisner / Chiara Marcozzi	-
RPE1 FRT FLAG-osTIR1 +/+ FLAG-Venus-mAID-TRIP13	Jordan Holt / Theresa Zeisner / Chiara Marcozzi	D2, E1, D11, A9, E5, H1, H8, H11, E2
RPE1 /TR ROSA26 osTIR1myc	Helfrid Hochegger	-
RPE1 /TR ROSA26 osTIR1myc +/+ FLAG-Venus-mAID-TRIP13	Jordan Holt	2F11, 2G2, 4B4
RPE1 /TR ROSA26 osTIR1myc +/+ FLAG-Ruby-mAID-CEP57	Jordan Holt	1B1, 1F8, 1H2
RPE1 /TR ROSA26 osTIR1myc +/+ FLAG-Ruby-mAID-CEP57, Centrin-GFP	Jordan Holt	1B1-CentrinGFP, 1F8-CentrinGFP, 1H2-CentrinGFP
E.coli DH5a	Catherine Coates / Oxana Nashchekina	-

2.1.2. Plasmids

Table 2-2 List of plasmids

Plasmid	Origin
pD1401-AD:CMV-Cas9-2A-GFP-TRIP13	ATUM / Chiara Marcozzi
pD1401-AD: CMV-Cas9-2A-mCherry -TRIP13	Jordan Holt
pJ247 FLAG-Venus-TRIP13	ATUM/ Chiara Marcozzi
pJ247 FLAG-Venus-mAID-TRIP13	Jordan Holt/ Theresa Zeisner
pcDNA5 FRT/TO Neomycin FLAG-osTIR1	Chiara Marcozzi
All-in-one-Cas9D10-T2A-GFP	Stephen Jackson
All-in-one-Cas9D10-T2A-GFP-CEP57	Jordan Holt
pDrive	Qiagen
pDrive FLAG-Ruby-mAID-CEP57	Jordan Holt
pEGFP-C1-Centrin	Abraham Yann/Michel Bornens

2.1.3. sgRNAs for gene targeting

Table 2-3 List of sgRNAs

Sequence of target	Target name
GCGCCTGCTTCAGGTCGCCCA	TRIP13 gRNA1
CTGTGTGGCCGAGTCGCCAA	TRIP13 gRNA2
TAACATTCCCAAGGGCCGGC	CEP57 gRNA1
GGGTTGGTTGCTACGCCAAA	CEP57 gRNA2

2.1.4. Oligonucleotides for clone validation

Table 2-4 List of oligonucleotides used for screening clones

Sequence	Forward / Reverse	Use
GTTGGGTCCCCACTGCTC	Fw	Screening/ sequencing TRIP13 N terminus
AGCACGCAATAATGTTGGC	Rv	Screening/ sequencing TRIP13 N terminus
CTACGGAGAACCCGAGAGC	Fw	Screening CEP57 N terminus
CGACAAGTGAGAACCAGAAGC	Rv	Screening CEP57 N terminus
TCCCGAGTCTTGGAGAAGAG	Fw	Sequencing CEP57 N terminus
TCCCTCACCATCCTTCTTTTT	Rv	Sequencing CEP57 N terminus

2.1.5. Small molecules

Table 2-5 List of small molecules

Small molecules	Origin	Stock Concentration	Final Concentration
Colcemid	Calbiochem	10µg/ml	100ng/mL
Dimethylastron (DMA)	Calbiochem	10mM	10µM
Indoleacetic acid (IAA) salt	Sigma	5mM	500µM
Nocodazole	Sigma	5mg/mL	0.33µM or 55nM
Reversine	Cambridge Biosciences	10mM	0.5µM

Taxol	Sigma	5mg/mL	0.33μM
MG132	Calbiochem	10mM	10μM

2.1.6. Antibodies

Table 2-6 List of antibodies

Antigen	Species	Origin	Product code /epitope	Technique	Dilution
Beta Tubulin	mouse	Sigma	(T4026)	WB	1:5000
Beta Tubulin	rabbit	Abcam	Ab6046	WB IF	1:2000 1:200
Cdc20	mouse	Santa Cruz	Sc-13162	WB	1:1000
Cdk5rap2	rabbit	Bethyl	IHC-00063-T	IF	1:1000
Centrin	mouse	Merck	20H5	IF	1:1000
Cep63	rabbit	Millipore	#06-1292	IF	1:100
Cep152	rabbit	Bethyl	A302-480A-T	IF	1:1000
CP110	rabbit	Proteintech	12780-1-AP	IF	1:500
CREST	human	Cortex Biochem		IF	1:1000
FLAG (M2)	mouse	Sigma	M2	WB IF	1:4000 1:1000
Gamma Tubulin	mouse	Abcam	(GTU-88)	IF	1:1500
Mad2	rabbit	Bethyl	(A300-301A)	WB	1:1000
Myc	mouse	Cell Signalling	9B11	WB	1:1000

p31^{comet}	Rabbit	Moravian	Full length	WB	1:1000
Pericentrin	rabbit	Abcam	Ab4448	IF	1:1000
Pericentrin	mouse	Abcam	Ab28144	IF	1:2000
TRIP13	rabbit	Bethyl	A303-605A)	WB	1:1000
TRIP13	rabbit	Abcam	Ab128171	WB	1:1000

WB = Western blot. IF = Immunofluoresence

2.1.7. Molecular biology reagents

Table 2-7 List of molecular biology reagents

Reagent	Origin	Specification
Agarose	Sigma	1% w/v in TAE buffer
Ampicillin	Sigma	Dissolved to 50mg/mL in dH_2O, filter sterilised
Calf intestinal alkaline phosphatase	Roche	1U per 50µL reaction
DNA loading dye	Fermentas	5x stock
dNTPs	Roche	100mM stock
Ethidium Bromide	Sigma	10mg/mL stock
Expand high fidelity DNA polymerase	Roche	-
Gel extraction kit	NEB	-
GeneJET Plasmid Miniprep kit	Fermentas	-
Gibson Assembly kit HiFI	NEB	
Kanamycin	Sigma	Dissolved to 50mg/mL in dH_2O, filter sterilised

LB plates	ICR	Supplemented with either ampicillin or kanamycin
Luria-Bertani (LB) medium	ICR	10g bacto tryptone, 5g bacto yeast extract, 10g NaCl – to final volume of 1L with H_2O; pH to 7.0 with NaOH
Quick ligase	NEB	-
Restriction enzymes	NEB	-
Spi Maxiprep kit	Qiagen	-

2.1.8. Tissue culture reagents

Table 2-8 List of tissue culture reagents

Reagent	**Origin**	**Specification**
24-well plate	Nunc	-
6-well plate	Nunc	-
96-well plate	Nunc	-
AmphotericinB. Fungizone	Thermo-scientific	250mg/mL stock
Black BD Falxon Optilux 96-well clear bottom plates	Nunc	-
CellTrics mesh	Partec	30μM
DMEM Nutrient Mixture F12 HAM	Sigma	-
Foetal Bovine Serum (FBS)	Thermo-scientific	Heat inactivated
Glutamax	Thermo-scientific	200mM stock
Leibovitz's L-15	Thermo-scientific	

Minisart filter sterilisation unit	Sartorius Stedium Biotech	0.22µm
Penicillin/Streptomycin	Thermo-scientific	10000U/mL / 10000mg/mL respectively
Phospho-buffered-saline (PBS)	ICR	-
Qualified FBS	Thermo-scientific	Heat inactivated and tetracycline free
Sodium Bicarbonate	Thermo-scientific	-
Trypsin-EDTA	Sigma	10 x
µ-well slide chamber	Ibidi	-

2.1.9. Protein Analysis reagents: SDS-PAGE, western blotting

Table 2-9 List of cell lysis reagents

Reagent	Origin	Specification
NuPAGE LDS Sample buffer	Invitrogen	4x
Dithiothreitol (DTT)	Sigma	1M in dH_2O
PBS	ICR	10mM Na_2HPO_4, 1.8Mm KH_2PO_4, 137mM NaCl, 2.7mM KCL; pH 7.4
EDTA-free protease inhibitor cocktail tablets	Roche	1 per 10mL lysis buffer

Table 2-10 List of Western blotting reagents

Reagent	Origin	Specification
Bradford reagent	Thermo-scientific	Coomassie Plus Protein Assay Reagent
Immobilon-FL PVDF transfer membrane	Millipore	-
LICOR protein marker	LICOR	-
Mark12 protein molecular weight marker	Invitrogen	-
MES SDS PAGE running buffer	Invitrogen	20x diluted to 1x in dH_2O
Milk, dried with non milk fat	Pritchitt Foods	Dissolved to 5% w/v in PBS-T
MOPS SDS PAGE running buffer	Invitrogen	20x diluted to 1x in dH_2O
NuPage 4-12% Bis Tris precast protein gels	Invitrogen	10, 12 and 15 wells
PBS-T	ICR	0.1% Tween
PFilter paper	Whatmann	
Ponceau S	Sigma	0.7% Ponceau S Red, 1% acetic acid
Transfer buffer	-	1x MOPS buffer + 20% ethanol in dH_2O

2.1.10. Other reagents

Table 2-11 List of other reagents used in this study

Reagent	Origin	Specification
Acetic acid	Sigma	-
Ethanol	Sigma	-
Isopropanol	Sigma	-
Methanol	Sigma	-
PMSF	Sigma	100mM in Isopropanol
Propidium Iodide	Sigma	50mg/mL dissolved in dH_2O
RNAse A	Qiagen	-
Spectrophosphometer cuvettes	Fisher	-

2.1.11. Equipment

Table 2-12 List of equipment used in this study

Equipment name	Origin
4RT rocking table	Luckham
96-well plate spinner	Eppendorf
Centrifuge 5714R	Eppendorf
Centrifuge Mistral 2000	MSE
Centrifuge RC3B plus	Sorvall
CO_2 Incubators	Sanyo
Deltavision	Imsol
EPS 601 Power supply	Amersham Biosciences
Fluorescence-activated cell sorting Aria	
Horizon 58 Gel Electrophoresis Apparatus and power cords	Thistle Scientific
Leica SP8	Leica
Li-COR Odyssey gel scanning system	Li-COR Bioscience

Mastercycler nexus Gradient PCR system Thermomixer	Eppendorf
Micro Centrifuge EL5000 Ultra Compact	Alpha Laboratories
Milli-Q Ultrapure water purifier	Millipore
NanoDrop Photospectrometer	Thermo scientific
Neon Transfection System for microporation	Invitrogen
Nikon Eclipse TiE	Nikon
Optima TLX Ultracentrifuge	Beckman Coulter
PS 250-2 Power Supply	Sigma
PTC-200 Peltier thermal cycler PCR machine	MJ Research
Shaker	Biorad
Spinning disc confocal microscope	3i
StepOne Plus	Applied Biosciences
UltraSpec 3300 Pro Spectrophotometer	Amersham Biosciences
Vibracell Sonicator	Sonics
VibraMax	Heidolph
Vortex mixer	VWR
Wheel	Biorad
XCell Surelock Novex Mini-Cell Electrophoresis system	Invitrogen

2.2. Methods

2.2.1. Molecular Biology

2.2.1.1. Cloning Via Restriction Digest

Constructs used in this study were made by restriction digest or Gibson (GC) techniques (see 2.2.1.2. for GC) depending on the DNA sequence or complexity of the cloning attempted.

For restriction digest-based cloning, NEB enzymes were used to digest the sequence of interest from the donor vector for 1-2 hours at 37°C. Digests were typically conducted in a 50µL reaction, sometimes in duplicate. The backbone vector was digested in the same way in parallel and subsequently treated with alkaline phosphatase (AP) for 30 minutes at 37°C. These digest reactions were mixed with 5x DNA loading dye in order to be run on 1% agarose gels made with TAE buffer. The DNA was visualised by adding 100ng/mL of Ethidium Bromide into the agarose mix after boiling and prior to casting. Gel electrophoresis was performed in TAE buffer at 175V for 30 minutes in order to separate pieces of DNA. Ultra-violet (UV) light was used to visualise DNA and the correct bands were excised using a molecular weight marker ran in parallel. These bands were purified using NEB's gel extraction kit according to the manufacturer's protocol. For constructs where there were no suitable restriction enzyme sites, polymerase chain reaction (PCR) primers were designed to anneal to the target sequence with restriction sites added to the 5' end. This DNA was amplified using PCR (reaction in table 2-13) with the thermal cycler program described in table 2-14.

Table 2-13 Molecular biology reaction mixes

Reaction type	Ingredients
Restriction digest (NEB) reaction	1-2µg DNA, 10U restriction enzyme, in 1x Cutsmart buffer. Reaction made up to 50µL in dH_2O
TAE buffer	40mM Tris acetate, pH 8.4, 1mM EDTA, in dH_2O
PCR reaction	10-100ng template, 1µM of each primer, 20µM of each dNTP, 1U DNA polymerase in 1x DNA polymerase buffer. Reaction made up to 50µL in dH_2O
Colony PCR reaction	Potential colony, 5µL myTaq buffer. 4.6µL water 0.2µL of each primer at 2.5µM
Ligation reaction	1µL vector, 3µL insert. 2.5U Quick Ligase (T4), 10µL 2x Quick Ligase buffer made up to 20µL total volume in dH_2O.

A small volume of these PCR products was run on an agarose gel to check it had worked. In the meantime, this PCR product was purified using the PCR clean up kit from NEB according to manufacturer's instruction. Then it was digested and purified from an agarose gel as described previously in the same way as plasmids.

Table 2-14 PCR thermal reaction

Step	Temperature (°C)	Time
Initial Denaturation	98	30 s
Amplification	98	30 s
4 cycles	45-55	1 min
	72	1 min/kb
35 cycles	98	30 s
	Tm -5	1 min
	72	1 min/kb
Final extension	72	10 min
End	4	Until switched off

Tm = melting temperature of primers

The Quick Ligase kit from NEB was used to ligate DNA inserts into the target vector. A reaction where only the digested backbone vector was included as a negative control. The reaction is described in table 2-13.

The products from ligation reactions were then used to transform 30µL DH5a competent cells. The bacteria were thawed on ice for 20 minutes before being mixed very gently with 7µL of the ligation reaction and left on ice for a further 20 minutes. Heat shock was used to transform the bacteria for 1 minute at 42°C. After this the bacteria were placed back on ice immediately to recover for at least 2 minutes. If the vector was ampicillin resistant the bacteria were plated immediately, using glass beads in sterile conditions, on Agar plates supplemented with 50µg/mL ampicillin. For kanamycin resistant vectors the bacteria were left in 1mL of LB media at 37°C for 1 hour in order to allow time for expression of antibiotic resistance prior to plating on Agar plates supplemented with 50µg/mL of kanamycin. Plates were placed upside down overnight for 37°C.

In order to check for positive ligation reactions, plates were compared to the negative control plate for an increase in colonies or screened using colony PCR.

Table 2-15 Colony PCR cycle

Step	Temperature (°C)	Time
Initial Denaturation	95	30 s
Amplification 30 cycles	95 45-68 72	30 s 1 min 1 min/kb
Final extension	72	10 min
End	4	Until switched off

For colony PCR screening (reaction in table 2-13) single colonies were picked and added to 10µL PCR reaction (table 2-15). These colonies were also re-plated individually and labelled. These colonies were lysed in the initial screening step.

Positive colony reactions were amplified in 3mL LB supplemented with the appropriate antibiotic and grown overnight at 37°C. The DNA was purified using a miniprep kit according to the manufacturer's protocol. These plasmids were sent for sequencing using appropriate primers. Using the "re-plate", a successful cloning reaction transformant was then grown using a starter colony approach (1-2mL of LB containing the appropriate antibiotic) for at least an hour to amplify the bacteria initially. This was then amplified further by growing it in 200mL LB culture overnight at 37°C. The DNA from this culture was purified using a Maxiprep kit according to the manufacturer's instructions. The DNA was stored in TE buffer for transfections into human cells.

2.2.1.2. Cloning via Gibson Assembly

Gibson Assembly, or Gibson cloning, was sometimes used in combination with restriction digest-based cloning. This was often when adding multiple fragments into the same target vector at once.

The reaction relies on several enzymes all available in a single reaction kit (NEB):

- The exonuclease creates single-stranded 3´ overhangs that facilitate the annealing of fragments that share complementarity at one end (the overlap region)
- The polymerase mends gaps within each annealed fragment
- The DNA ligase seals nicks in the assembled DNA

The end result is a double-stranded fully sealed DNA molecule that can be transformed and amplified using bacterial preps.

Snapgene software was used to design overlapping PCR primers. The overlap was always between 25-40 base pairs. The overlap was sometimes used to introduce smaller extra sequences such as start or stop codons and novel restriction sites. These primers were subsequently ordered from Integrated DNA technologies (IDT) are described in table 1-5. PCR reactions were carried out using the instructions in Tables 2-13 and 2-14. These reactions were then purified by Gel extraction and the Gibson Assembly was performed according to the manufacturer's protocol for 60 minutes (NEB).

In this time the backbone was cut by restriction digest as described in section 2.2.1.1 and table 1-14. However, AP was not used to dephosphorylate the backbone in this case.

Transformation is performed with 2-5µL of final assembly reaction and all subsequent validation and purification steps were completed as described in 2.2.1.1.

2.2.2. Cell culture

2.2.2.1. Cell culture

RPE1 and RPE1 based cell lines were cultured in F12:DMEM medium supplemented with 10% FBS, 0.348% sodium bicarbonate, 100U/mL penicillin, 0.1mg/mL streptomycin, 0.3mg/mL L-GlutaMAX and 0.5µg/mL Fungizone.

All RPE1 FRT FLAG-osTIR1, RPE1 /TR ROSA26 osTIR1myc and cell lines derived from either of these 2 parent cell lines were cultured in tet-free conditions by replacing the normal heat-inactivated FBS with Qualified FBS free of tetracycline/doxycycline impurities. This ensured osTIR1 was only expressed upon the addition of these antibiotics in a controlled manner.

2.2.2.2. Synchronisation by Serum starvation

RPE1 cells have an intact restriction point and therefore can be synchronised in G1 by removing growth factors which prevents downstream signalling and phosphorylation of Retinoblastoma protein. This will hold cells in a G0/G1 like state until they are subsequently stimulated by the reintroduction of growth factors.

To do this, complete media was replaced with serum starve media (complete media lacking FBS) after washing 3x with warm PBS first. The cells were put back in the incubator during these washes for several minutes.

After 24 hours cells should have nearly all divided once and be held in G0/G1. 20% FBS is added back. These cells will then progress in the cell cycle. Typically, the mitotic peak is around 28 hours after re-addition of FBS.

2.2.2.3. Plasmid transfection

Plasmid DNA was inserted into cells using microporation. Neon Transfection System (Invitrogen) was used according to manufacturer's protocol. Buffers were kept cold until use. Cells were kept in R buffer for the minimal time possible. 1µg of DNA per 1 million cells was transfected. For RPE cells condition 16 was the most optimal: 1400V, 20ms, 2 pulses. Cells were typically assayed 2 or 3 days later.

2.2.2.4. Gene targeting by CRISPR

Flow cytometry strategies were used to select for positive CRISPR clones. To establish homozygous knock-in TRIP13 or CEP57 fluorescent/AID cell lines two types of constructs were made: Cas9 targeting plasmid and a repair template.

For the Cas9 targeting plasmid, an All-in-One plasmid was used. For TRIP13, the All-in-One plasmid (ATUM) came with sequences corresponding to sgRNAs already synthesised. This construct had already been generated for a previous study to make TRIP13 knock out cells (Chiara Marcozzi).

In the case of CEP57 guides were cloned into a different All-in-One vector (a gift from Stephen Jackson's lab). The All-in-One plasmid design contain one (ATUM) or two (Stephen Jackson's lab) U6 promoter driven sgRNA cassettes alongside a sequence encoding for Cas9D10A nickase coupled via a ribosomal skipping motif 2A peptide linker to an mCherry or GFP fluorescent protein marker.

To clone sgRNA sequences into this vector, pairs of complementary DNA oligos (4-mer overhang+20-mer sgRNA sequences) were purchased as standard (de-salted) from IDT. The DNA oligonucleotides were annealed by pooling in a thermocycler for 10 minutes at 95°C; 5 minutes at 65°C; 15 minutes at 25°C and held at 4°C till used. Each DNA oligo duplex had 5' overhangs (forward: ACCG, reverse: AAAC in reference to the PAM sequence) designed to be directly cloned into the BbsI or BsaI-digested

All-in-One vector. The Oligo pairs were then phosphorylated using T4 PNK in T4 ligase buffer. Phosphorylation was achieved by heating oligo pairs in a thermocycler for 30 minutes at 37°C and then the enzyme was inactivated at 70°C for 10 minutes. The sgRNA DNA duplexes were ligated (see table 1-14) sequentially in individual transformation reactions and confirmed by Sanger sequencing at Genewiz at the end.

The repair template was synthesised for TRIP13 (ATUM/ Chiara Marcozzi) and the miniAID sequence was added using restriction digest (with the help of summer student Theresa Zeisner/ see 2.2.1.1.). For CEP57 the repair template was made by 6 fragment Gibson assembly (see 2.2.1.2).

Both repair templates contained the sequence for the FLAG epitope, a fluorescent marker, and the miniAID degron sequence. These sequences were flanked by homology arm regions corresponding to the N terminus of the target protein. The left homology arm was identical to the 5'UTR region and the right homology arm corresponded to exon 1 and the following sequence. Homology arm length varied between 600-1000bp. The (protospacer adjacent motif) PAM and sgRNA sequences were in the right homology arm. These sequences were "Wobbled" or silently mutated in order to lower the likelihood of re-cutting by the Cas9 enzyme in the event of homologous recombination with the repair template.

The homology arms were PCR amplified from genomic DNA purified from RPE1 cells and cloned into destination vectors such as TOPO or pDRIVE in order to be sanger sequencing. Amplification from genomic DNA (gDNA) required a touchdown PCR approach (Table 2-16).

Table 2-16 Touchdown PCR

Step	Temperature (°C)	Time
Initial Denaturation	98	30 s
Amplification	98	30 s
4 cycles	63	1 min
	72	1 min/kb
4 cycles	98	30 s
	60	1 min
	72	1 min/kb
30 cycles	98	30s
	57	1 min
	72	1 min/kb
Final extension	72	10 min
End	4	Until switched off

The Cas9 targeting plasmid and a repair template were maxiprepped (Qiagen) and then co-transfected into RPE1 cell lines using microporation (2.2.2.3); 1µg of each plasmid was used per 1 million cells.

After 3 days cells were bulk sorted using flow cytometry (2.2.2.5) for Cas9 expression using the fluorescent marker from that vector. These cells were expanded and then single cell sorted into 96 well plates. 600 cells were initially sorted for screening and more were bulk sorted here in case of further need. After 10 days 96 wells were "spotted" using a light microscope in tissue culture for individual colonies to ensure homogeneity in the population. They were then screened by PCR (see 2.2.2.6).

2.2.2.5. Flow cytometry

After transfection, live cells were sorted in the ICR flow cytometry facility on a BD FACS Aria II (BD Biosciences). Cells were first trypsinised and washed in PBS before being filtered for clumps or aggregates using a 30µM filter (PARTEC) into polypropylene FACS tubes.

These cells were then gated for living cells using forward and side scatter before doublets were eliminated. These cells were then sorted for positive fluorescence either GFP, Venus or RFP using the filters shown in table 1-18. In order to distinguish between autofluorescence and positive cells the cells were shown using filters for RFP vs GFP/Venus. This offset the auto-fluorescent cells at a 45-degree angle. The cells were sorted into complete media.

Table 2-17 FACS filter sets

Fluorescent marker	Filter (nm)
Venus /eGFP	530/30
mRuby	580/40

2.2.2.6. Clone validation by PCR

Clones typically reached confluency 2 weeks after single cell sorting (2.2.2.5.). At this point genomic DNA was extracted using DirectPCR lysis buffer supplemented with Proteinase K to a final concentration of 0.4mg/mL This buffer was aliquoted into a separate 96 well plate. In parallel cells were washed with PBS and trypsinised in 30µL 2x trypsin. After several minutes 10µL of the trypsin cell mix was added to 25µL lysis buffer. This lysis plate was then sealed and lysis was carried out in a thermal cycler using the conditions shown in (Table 2-18.)

Table 2-18 Genomic DNA extraction program

Time	Temperature (°C)	Note
1 hour	55	Lysis
1 hour	95	Inactivation of proteinase K
Hold	4	-

These cell lysates were then used as PCR templates to screen for knock-in of the protein tag sequences. These primers can be found in table 2-4.

The design of this PCR addressed two things:

- Integration of knock-in sequence
- Integration into the correct-locus

One primer was designed to anneal to a sequence outside the homology arm sequence, ensuring that the integration was in the correct part of the genome and not an off-target effect. The other primer annealed to whichever homology arm furthest away from the original primer. As a result the PCR amplifies the sequence regardless of integration event and you can differentiate a negative clone (smaller band size) with positive clones (bigger band size). This also allows the separation of homozygote and heterozygote events because a heterozygote clones have 2 bands, one of each size. These PCRs were also from genomic DNA so the touchdown program described in table 2-16 was used. Finally, positive bands were Sanger sequenced at Genewiz either after insertion into the TOPO destination vector or directly after gel extraction.

2.2.3. Biochemical analysis

2.2.3.1. Whole cell lysate extraction

Cells were collected as normal by trypsinisation after washing with PBS. These cells were pelleted at 1000rpm for 5 minutes before being washed with PBS and centrifuged once more. The PBS was then aspirated and the cells were either flash-frozen here and stored at -80 or cells were taken directly for lysis.
Cells were lysed in either of the following lysis buffers:

Table 2-19 Lysis buffers

Lysis buffer	Ingredients
NP-40	50mM Tris pH=7.5 150mM NaCl
RIPA	20 mM Tris-HCl (pH 7.5) 150 mM NaCl, 1 mM Na2EDTA 1 mM EGTA 1% NP-40 1% sodium deoxycholate 2.5 mM sodium pyrophosphate 1 mM β-glycerophosphate 1 mM Na3VO4 1 µg/ml leupeptin.

For NP-40 lysis buffer, 0.5% NP-40 and protease inhibitors were added on the day. For RIPA buffer protease inhibitors were added on the day.
Cells were kept on ice at all times before and after lysing; lysates were incubated on ice for 20 minutes and then clarified by spinning for 15 minutes at 14000rpm at 4°C. The supernatant was taken and protein concentration was measured using the Bradford assay and Coomassie Plus Protein Assay Reagent (Thermo scientific). Absorbance was measured at 595nm on a spectrophotometer (Amersham).

2.2.3.2. Protein analysis: SDS-PAGE and Western blotting

1x LDS was used to prepare samples for SDS PAGE. LDS was supplemented with 10mM fresh DTT and boiled for 5 minutes. Samples were then loaded onto a 4-12% Bis-Tris acrylamide gel (NuPAGE, Invitrogen). The samples were run at 100V for 20 minutes through the stacking gel and then at 175V for around 45 minutes after. LICOR fluorescent marker was used, only 1µL per gel. For small proteins, under 30kDa, 1xMES was used. For other proteins 1x MOPS was used as a running buffer.
The gel was then transferred onto PVDF membrane in transfer buffer (1xMOPS supplemented with 20% Ethanol) at 400mA for 1 hour. Ponceau

stain was used to check for efficient transfer and then cells were blocked in 5% low fat milk diluted in 0.1% w/v PBS tween for 1 hour.
Membranes were incubated in 2.5% milk blocking buffer with primary antibodies overnight at 4°C (table 1-7). The next day, cells were washed for at least 10 minutes in PBS tween followed by incubation with secondary antibodies in the dark for 1hour in 2.5% milk blocking buffer. Alexa Fluor680 and 800 (LiCOR) were used at 1/10000. Secondary antibodies were then washed off with 3 more PBS Tween washes. Membranes were imaged on an infrared imaging system Odyssey Clx (LiCOR) and quantification was performed using the software for this machine.

2.2.4. Live cell imaging

2.2.4.1. Mitotic timing

Cells were imaged using a Nikon widefield microscope using a DIC 20x air objective. The microscope was controlled using micromanager software. Cells were seeded onto µ-well dishes (Ibidi) 1 or 2 days before imaging. Cells were filmed in L15 media supplemented with P/S and the appropriate FBS
For assays where nuclear envelope breakdown (NEBD) – anaphase timing cells were filmed every 3 minutes for at least 24 hours. For assays where the SAC was challenged using spindle poisons (eg Nocodazole, Taxol or DMA) cells were filmed every 10 minutes for at least 24 hours. Quantifications were performed using FIJI software.

2.2.4.2. Single cell analysis of AID

Cells were filmed using a 40x Oil objective on a Deltavision microscope. The Deltavision is equipped with an EMCCD camera. Cells were seeded onto µ-well dishes (Ibidi) 1 or 2 days before imaging. Cells were filmed in L15 media supplemented with P/S and the appropriate FBS.

In order to measure single cell degradation kinetics, cells were filmed every 5 minutes using the appropriate fluorescent channel; YFP for TRIP13 and RFP for CEP57. Cells were filmed and then doxycycline, IAA and/or MG132 were added. IAA was added on top at 6x concentration in 50µL of media on top of 250µL of dox/tet containing media.
For CEP57 6 3µM Z stacks were taken because of the small focal localisation of the protein to the centrosome.
Quantification was performed using FIJI software.

2.2.4.3. DMA washout

Cells were filmed using a 40x Oil objective on a Deltavision microscope. The Deltavision is equipped with an EMCCD camera. Cells were seeded onto µ-well dishes (Ibidi) 1 or 2 days before imaging. Final concentration of 10µM DMA was used. Media containing DMA was gently taken out of the µ-well dish and replaced with L15 as quickly as possible without losing focus. Images were taken every 5 minutes. In order to see cells rounded up in mitosis Z stacks were used like in 2.2.4.2. Quantification was performed using FIJI software.

2.2.4.4. Mitotic errors with sirDNA or sirTubulin

Cells were either filmed using a 40x Oil objective on a Nikon Widefield or Deltavision. The Deltavision is equipped with an EMCCD camera. Cells were seeded onto µ-well dishes (Ibidi) 1 or 2 days before imaging. 3 hours prior to imaging normal media containing final concentration 50nM sirDNA or sirTubulin was added to cells. This media was changed to L15 prior to imaging. Cells were filmed with 3µM Zstacks x8. Images were taken every 2 or 5 minutes.
Quantification was performed using FIJI software.

2.2.4.5. Live cell imaging of centriole disengagement

Time-lapse confocal imaging was performed on a Marianas confocal spinning-disk microscope system (Intelligent Imaging Innovations, Inc.) comprising a laser stack for 445 nm/488 nm/514 nm/561 nm lasers; an Observer Z1 inverted microscope (Carl Zeiss) equipped with Plan-Apochromat 63× 1.4 NA lens; an OKO stage top incubator set to 37°C (OKO); a CSU X1 spinning disk head (Yokogawa); a Gemini W view optical splitter attached to a Flash4 CMOS camera (Hamamatsu), and a QuantEM 512SC camera (Photometrics). The microscope was equipped with Brightline filters (Semrock) for GFP/RFP, for CFP/YFP/RFP, and for RFP670.

Cells were seeded onto µ-well dishes (Ibidi) 1 or 2 days before imaging. 3 hours prior to imaging 50nM Sirtubulin was added (2.2.4.4). Cells were filmed every 5 minutes.

In order to visualise centrosomes throughout all cell cycle phases using either CEP57 or Centrin markers; 25 0.5µM stacks were used. Quantification was performed using FIJI software by eye.

2.2.5. Immunofluorescence

2.2.5.1. Fixation

Cells were grown on 0.22µM coverslips from a low confluency and fixed at around 80-90% confluency. Cells were either fixed using 4% Paraformaldehyde (PFA) and permeabilised using 0.1% TritonX100 or they were fixed using ice-cold Methanol (MeOH) for 10 minutes. Fixation was washed off 3x in PBS 0.2% Tween. For experiments involving centrosome staining MeOH was used. For kinetochore localised proteins PFA/2XPHEM was used.

2.2.5.2. Staining and Mounting

Coverslips were blocked in 2% bovine serum albumin (BSA) for 30 minutes at room temperature. On a piece of parafilm, 50µL of blocking buffer containing antibodies (see table 1-7) was placed as a droplet. The coverslip was inverted onto the droplet so that the blocking buffer completely covered that side of the coverslip. Primary antibodies were incubated overnight at 4°C.

Cells were then washed 3x in PBS 0.2% Tween for 10 minutes each time. Secondary antibodies Alexa 488 Rabbit or Alexa 594 Mouse were placed in the same manner as primary antibodies on fresh parafilm at 1/400. This time inverted coverslips were stored in the dark and incubated for 1 hour at room temperature.

After 3 more washes with PBS 0.2% Tween, cells were mounted using prolong antifade reagent containing DAPI onto glass slides. These slides were sealed using clear nail varnish and stored at 4°C in the dark.

2.2.5.3. Imaging

Slides were imaged on the same microscope as above. Images of antibodies staining for centrosomally localised proteins were taken as follows: 2 x zoom,18 0.3µM stacks.

Images were processed and analysed using FIJI.

2.2.6. Metaphase spreads

2.2.6.1. Preparation of samples

Cells were plated in T175 flasks at a low density. When cells reached 50-60% confluency, colcemid was added to induce arrest at prometaphase for 2-3 hours. Cells were trypsinised and collected before being washed with PBS. 37.5nM KCl solution was added for 15-30 minutes. This hypotonic environment causes cells to swell. From this point onwards all spins were done at 200g in order to prevent cells from bursting. Cells were spun down and KCl was gently removed from the enlarged pellets.

2.2.6.2. Fixation

Carnoy's fixative (3:1 MeOH:Acetic acid) was prepared on the day of fixation in a fume hood. 5mL of this fixative solution was carefully added dropwise in the fumehood to each pellet whilst shaking the tube with the other hand. Cells could be stored here at -20.

2.2.6.3. Spreading

The night before spreading glass slides were washed in ethanol and stored in water overnight in order for them to be cold. Cells were re-pelleted and resuspended in 200-1000µL of fresh Carnoy's fixative before spreading. A humidity chamber was constructed using a plastic square dish with wet towel inside.

Spreading was performed in the fumehood. With a P200 cells were taken up. Slides were only removed from cold water at the last possible moment and placed in the humidity chamber. 2 drops were dropped on each slide placed in the humidity chamber from a height. A lid was placed on the humidity chamber immediately to cover any slides with cells on to keep the humidity and allow spreading. Samples were left to dry in the fumehood for a few hours, taking away the wet towel a couple of hours after spreading.

2.2.6.4. Staining

Slides were aged overnight at room temperature before being stained with 1:50 reusable Giema stain diluted in dH_2O for 10 minutes at 4°C. Slides were left to dry before a coverslip was mounted for imaging. This was also done in the fume hood. Slides were left to dry for a few hours.

2.2.6.5. Imaging

Slides were imaged on a spinning disc confocal microscope using a 63x objective to take images using brightfield. Chromosome spreads were quantified in FIJI software by eye.

2.2.7. Propidium Iodide staining and cell cycle analysis by FACS

Propidium Iodide staining was used to see the distribution of cell cycle phase and roughly as a guide for whether cells were maintaining normal genome stability.

Cells were harvested using trypsinisation, pelleted and washed in PBS and re-pelleted. Ice cold 70% Ethanol was used to fix cells dropwise on a vortex. Samples were stored at -20°C for 24 hours at least.

Cells were stained with 5µg/mL Propidium iodide and 0.25U/mL RNAse at 37°C for 15 minutes before being imaged on the BD Facs AriaII. Cells were sorted using forward and side scatter and doublets were eliminated before gating cells for G1/S/G2-M using PE Texas Red A vs count. Images were quantified using FloJo software.

2.2.8. Image analysis

2.2.8.1. Measuring centriole distance

Dr Luca Cirillo designed a FIJI macro which allowed sequential segmentation of centrioles using CP110 staining in IF. Cells were classified, followed by centrosomes. Centrioles were then selected manually and distance in µM was calculated using known magnification and pixel sizes. This experiment was performed unbiased by double blinding the images.

3. Generation of an Auxin Inducible Degron system in RPE1 cells to target TRIP13

3.1. Introduction

3.1.1. Background

In the last 30 years our understanding of complex signalling pathways, such as the Spindle Assembly Checkpoint (SAC), has been greatly accelerated by perturbing signalling pathways through removing a specific protein to understand its role. There are many ways to deplete proteins in human cell culture such as: genetic knock out (KO), RNA interference (RNAi) and small molecule inhibitors.

The introduction of CRISPR/Cas9 has made gene editing a viable tool to perturb protein function in mammalian cells lines (Ran et al. 2013) (Mali et al. 2013). For cell line-based studies this is a much more efficient way of doing both “knock in” and “knock out” experiments. Gene knock outs are a powerful way of perturbing protein function; however, the recombination frequency when transfecting Cas9 constructs is still so low that it is pertinent to generate clonal cell lines since the analysis of initially transfected cells can be widely heterogeneous. Although clonal CRISPR “knock out” assays take much longer to generate than small molecule or RNAi experiments, crucially CRISPR/Cas9 can in theory be designed to target any gene without off target effects. The caveat to this is that KO cell lines are typically generated by targeting Cas9 to a specific gene sequence where the enzyme will cut and introduce random frameshifts, insertions and deletions, all of which are highly likely to lead to premature termination

codons (PTCs). In 2019, it was reported that PTCs can lead to nonsense induced transcriptional compensation (NITC) (El-Brolosy et al. 2019) (Z. Ma et al. 2019). NITC is a mechanism by which mutant gene alleles upregulate homologous genes in order to compensate for their loss of function.

RNAi has been a staple technique for quickly reducing the levels of a target protein for several years. RNAi causes a reduction or “knock down” of protein expression in the cell by targeting the corresponding messenger RNA (mRNA) for degradation. RNAi knock down is much quicker than CRISPR knock outs; typically assayed 48 hours after addition of siRNA. In an asynchronous population of RPE1 cells, with a normal doubling time of around 20 hours, most cells will have divided at least twice during this incubation time. On top of this, RNAi often leads to incomplete RNA degradation in human cells and this makes interpretation of phenotypes challenging. RNAi is also prone to off target effects through the targeting of other mRNAs with similar sequences. Complicating things further, many cell cycle enzymes have been shown to be able to function at very low expression levels and this had led to misinterpretation of phenotypes in RNAi (and CRISPR) experiments (Currie et al. 2018; Raaijmakers & Medema 2019).

Both CRISPR and RNAi cause protein depletion indirectly by targeting the corresponding DNA or RNA. Small molecules are used to target proteins directly. Small molecules usually give a homogenous phenotype that is rapid and sometimes reversible by washout. However, small molecules are generally only suitable for targeting enzymes that contain an active site that can be blocked. Scaffold proteins are much harder to target; therefore, it is unlikely that there will be a small molecule made for every protein. Unfortunately, small molecules are also prone to off-target effects because of the evolutionarily highly-related nature of many protein kinases. They often have similar active sites, making specific kinase inhibitors challenging to design. Phenotypes specific to one kinase can be masked by the inhibition of multiple related kinases at once using a single molecule.

The study of cell cycle regulators is challenging because regulation of protein expression is a method the cell cycle exploits to ensure accurate

progression. Thus, some proteins have different roles depending on the cell cycle phase. Studying the SAC poses an additional challenge because it is a highly complex and dynamic system that in a normal mitosis is only active for a very short period of time; in RPE1 cells the checkpoint is active for less than 30 minutes. In those 30 minutes, hundreds of proteins are re-organised after nuclear envelope break down. I wanted to introduce a technique that should overcome a key issue that encumbers both RNAi and KO cell lines: the time between the perturbation and the downstream assay is too long.

3.1.2. Inducible Degradation

Several techniques have emerged over the last two decades that can be harnessed to target a specific protein for destruction. (Table 3-1). Moreover, these techniques are inducible, and for some proteins the time taken to deplete their levels significantly has been measured at under an hour. Since the perturbation is occurring rapidly and at the protein level it is unlikely that this will be immediately communicated back to the nucleus and lead to immediate changes of expression on the genetic or epigenetic level of related genes. I wanted to harness inducible degradation to target proteins for destruction during specific cell cycle phases, and eliminate the possibility of adaptation in previous mitotic divisions.

On the whole conditional protein inactivation techniques have several commonalities. Firstly, they generally require the protein of interest to be tagged in order to target it for degradation. The endogenous protein can now be studied by targeting the tag to the gene's locus using CRISPR. Secondly, these techniques require the addition of a small molecule to selectively target the protein for degradation. These small molecules interact with both the tag and with an E3 ubiquitin ligase. The proximity of the target protein with an E3 ubiquitin ligase causes them to be ubiquitylated and targeted to the proteasome for degradation.

Table 3-1 Conditional protein inactivation techniques

Technique	Tag	Small molecule	Reference
Auxin-inducible-degron (AID)	AID or miniAID (mAID)	Auxin /IAA/ NAA	(Nishimura et al. 2009)
Small molecule assisted shutoff (SMASh)	SMASh	Asunaprevir	(Chung et al. 2015)
Affinity directed protein missile (AdPROM)	GFP	Anti GFP-nanobody	(Fulcher et al. 2016)
Degradation Tag (dTAG)	FKBP12	dTAG	(Nabet et al. 2018ij)

The requirement for CRISPR/Cas9 gene editing makes inactivation of proteins at the endogenous level time consuming and low-throughput. An alternative is Trim-Away which only requires a high-affinity antibody specific for the target protein rather than prior modification of the genome, plus exogenous expression of the immune E3 ubiquitin ligase TRIM21 (Clift et al. 2018).

It important to note that during the time of my PhD some of these systems have been further developed, including hybrid systems such as an AID-SMASH and AID-nanobody based approach (Lemmens et al. 2018) (Daniel et al. 2018).

3.1.3. Auxin Inducible Degron

The Auxin Inducible Degron (AID) was developed in 2007. Auxin is a plant hormone that regulates growth. Auxin induces rapid destruction of transcription repressors belonging to the IAA/AUX family using a specific form of the SCF E3 ubiquitin ligase complex. Humans and other eukaryotes lack the auxin response but utilise the Skp1-Cullin-F-box protein (SCF) system. This allowed the Kanemaki lab to create the Auxin Inducible

Degron by introducing the system into mammalian cells (Nishimura et al. 2009).

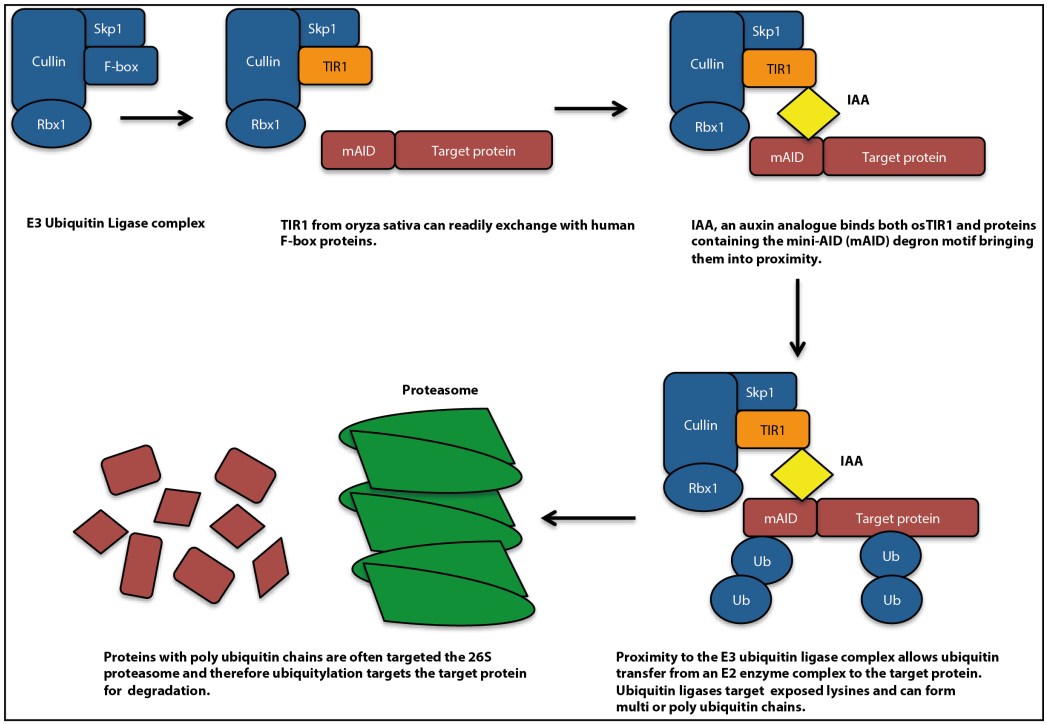

Figure 3-1 Schematic describing the Auxin Inducible Degron (AID) system

The system needs several components in order to work. Firstly, the target protein must be tagged with the AID motif. Secondly, the TIR1 F-box protein, must be exogenously expressed. TIR1 is normally only expressed in plant cells (Kepinski & Leyser 2005). The system is inducible because TIR1 only binds with a high affinity to the AID motif sequences in the presence of auxin or derivatives such as Indole Acetic Acid (IAA). Over the last few years improvements have been made to the system including reducing the size of the tag from 27 to 9 kDa (AID and miniAID respectively) (Natsume et al. 2016).

3.1.4. TRIP13

TRIP13 forms a 6 subunit ATPase that has been implicated in promoting a conformational change in the MAD2 protein from ‘closed’ to ‘open’. (Ye et al. 2015) I chose TRIP13 as my proof of principle protein because its role in mitosis had already been partially characterised; in particular the phenotype of cells in which TRIP13 had been depleted had been characterised by Dr Chiara Marcozzi and Oxana Naschekina. When Chiara used siRNA to lower TRIP13 protein levels in RPE1 and HeLa cells and quantified the time from Nuclear Envelope Break Down (NEBD) to anaphase she observed a delay in mitosis. Chiara also generated knock out clones of TRIP13. In these clones, the timing of unperturbed mitosis was also slower. However, she also observed that some clones did not maintain an arrest in the presence of nocodazole whilst other clones arrested normally despite being made in the same way in parallel (Appendix A). She also observed that the clones that did not arrest had lower levels of Mad2 and high levels of $p31^{comet}$. High $p31^{comet}$ levels has been shown to override the SAC and low levels of Mad2 have been shown to be unable to maintain a SAC arrest (Habu et al. 2002).

Both the conflicting phenotypes, and the changes in fundamental SAC protein levels, made TRIP13 a perfect candidate for pilot studies on inducible degradation. In this chapter, I describe the strategies employed to test and optimise the AID on TRIP13.

3.2. Results

To test the AID system, I had to establish cell lines capable of auxin mediated degradation. I chose RPE1 cells, which are immortal but untransformed, have wildtype p53 and a near diploid karyotype that is chromosomally stable. RPE1 cells still have an intact restriction point in G1 and arrest in response to DNA damage. As a result, RPE1 cells are considered to be a good system in which to study normal signalling pathways.

3.2.1. Targeting TRIP13 in RPE1 cells with constitutive osTIR1 expression

I started by using RPE1 cells that constitutively expressed Transport Inhibitor Response 1 (TIR1) protein from the rice plant *Oryza Sativa*. These cells were a kind gift from Don Cleveland's lab. This cell line will be referred to as RPE1 OsTIR1 from here on.

Figure 3-2 shows how both alleles of TRIP13 were targeted using CRISPR/Cas9-mediated gene targeting. To generate knock in clones, cells were co-transfected with a targeting construct and a repair template construct. For the targeting construct I used an All-in-One plasmid that contained Cas9 D10A nickase plus sgRNAs targeting exon1 of TRIP13 driven by a U6 promoter (ATUM). This cassette was coupled to a GFP cDNA sequence via a peptide 2A (P2A) linker ribosomal skipping sequence.

Two different constructs were used for the repair template; 3xFLAG-Venus was used as a positive control because it already had been used to generate TRIP13 knock-in HeLa clones in the lab. This construct was modified using restriction digest by an undergraduate summer student, Theresa Zeisner, to include the miniAID (mAID) degron sequence after the Venus open reading frame (ORF). These repair templates contained homologous sequences to the 5' Untranslated Region (5'UTR) in the left homology arm (LHA) and exon 1 of TRIP13 onwards in the right homology

arm (RHA) respectively. The epitope tag, fluorescent marker and/or the degron sequence were inserted between these 2 homology arms (Fig. 3-2).

The original 3xFLAG-Venus repair template designed by Chiara Marcozzi had been synthesised by ATUM. The protospacer adjacent motif (PAM) and corresponding sgRNA sequences in the repair template that would be recognised by the Cas9 were modified using synonymous silent mutations to reduce the likelihood of re-cutting after homologous recombination (HR) with the repair template.

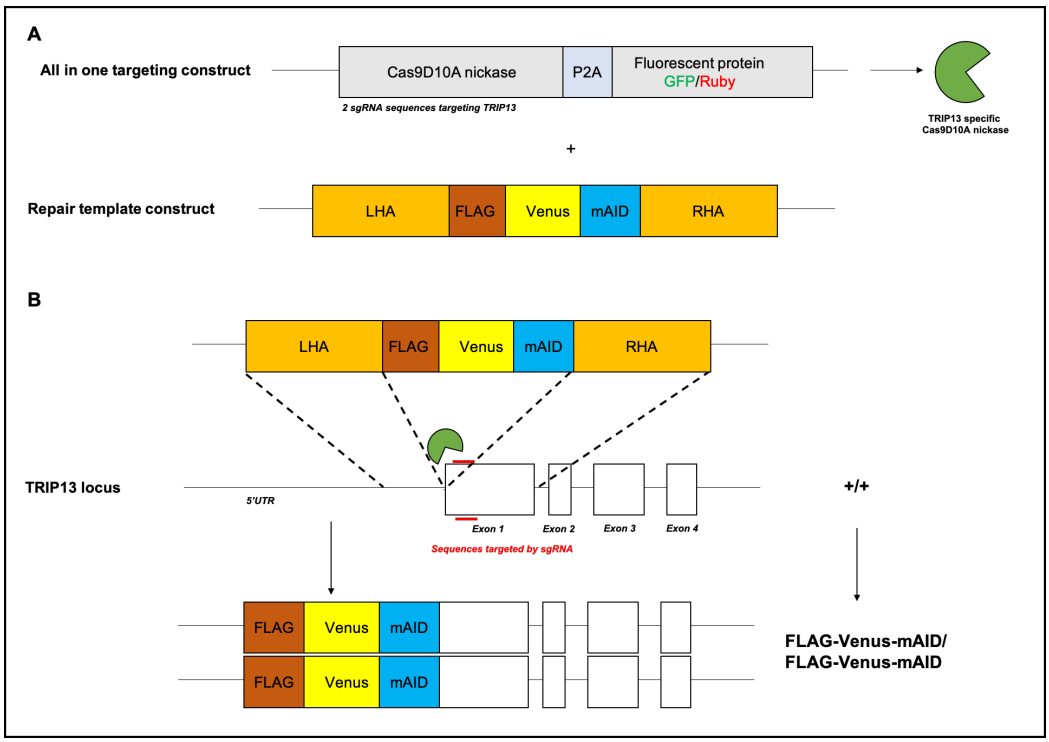

Figure 3-2 CRISPR/Cas9 Knock in strategy for FLAG-Venus-mAID-TRIP13

A) Knock in cell lines were generated by co-transfection of 2 plasmids. 1) All in One plasmid expressing a Cas9 D10A nickase with 2 sgRNAs targeting TRIP13 and a fluorescent marker; either GFP or Ruby. 2) A repair template containing homology arms for TRIP13 flanking tags: FLAG Venus and/or mAID. Corresponding sgRNA target sequences were "wobbled" to avoid re-cutting after successful integration of repair template. **B)** Schematic shows homology directed repair targeting the new terminus of TRIP13.

Electroporation was used to transfect the plasmids into RPE1 osTIR1 cells. Transfected cells were left to recover and expand for 3 days. Both the Cas9 plasmid and the repair templates contained fluorescent markers so that I could enrich for positive cells using Fluorescent Activated Cell Sorting (FACS). The cells were sequentially sorted, initially for GFP expression as

a marker for Cas9 expression (Figure 3-3A). At least 50,000 GFP positive cells per condition were sorted into a 6-well plate and expanded for at least 7 days. At this point cells were single-cell sorted for Venus-TRIP13 expression. Index-sorted Venus positive cells are shown in figure 3-3 B. Subsequently, 300-500 cells were sorted as single cells into 96 well plates. After 9-10 days cells were analysed by eye to ensure a single colony was growing in each well. The cells were expanded for another week and were processed at 70% confluency. The cells were first shuffled into new 96-well plates to reduce the waste of downstream reagents because not all cells survive or continue to grow after FACS. These shuffled plates were then lysed for genomic DNA (gDNA) using the Direct Lysis reagent in combination with Proteinase K to prevent degradation of the gDNA by DNAses in the lysate.

The clones were then screened using PCR designed to show whether there had been successful HR events with the repair template into the TRIP13 locus. Primers were designed to amplify across the region where FLAG, Venus and mAID should be inserted. One primer was always designed to amplify to a region outside either of the homology arms. This ensured that the PCR was specific to the TRIP13 locus and that HR had not taken place in another random part of the genome. Therefore, the PCR was designed to amplify from both negative and positive clones. A representative example of the PCR is shown in figure 3-3C. It shows two bands, a smaller negative wild-type band (1.5kb) and a larger positive band (2.3kb for FLAG-Venus and 2.5kb FLAG-Venus-mAID ((not shown))) showing that the 3xFLAG-Venus sequence has been inserted into the DNA.

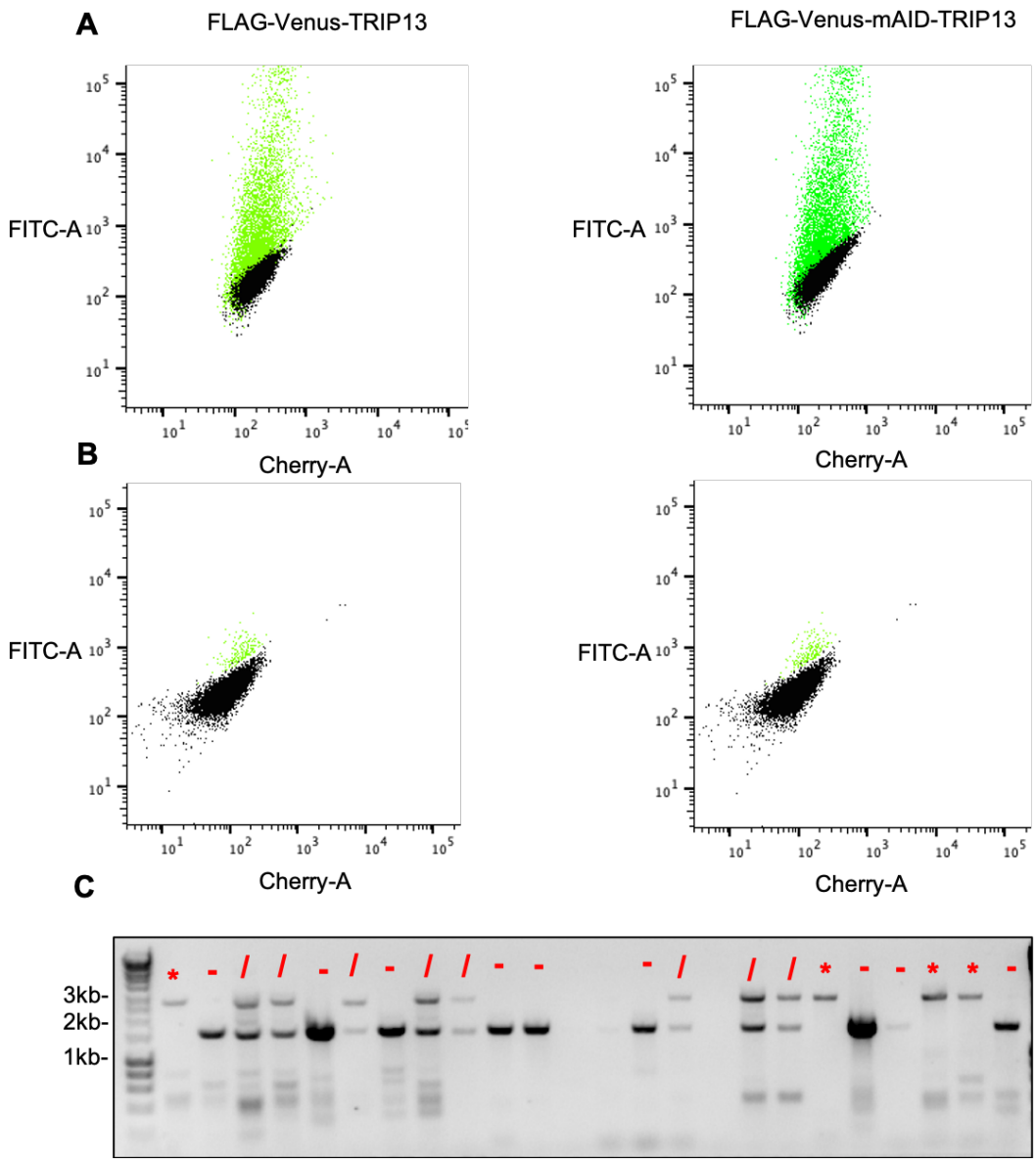

Figure 3-3 Initial FACS sort in RPE osTIR1 and PCR screen

A) Bulk sort for Cas 9 positive cells using GFP as a marker. Cells in green were sorted into a 6 well plate for further expansion **B)** Single cell sort for Venus positive cells. Cells in green were index sorted singularly into 96 well plates **C)** Example PCR screen used to screen for FLAG-Venus-TRIP13 events. * marks homozygote knock-in clones; / marks heterozygote clones, and – marks negative wild type cells. The negative band is around 1.5kb and the positive band is around 2.3Kb because it includes the sequence for FLAG and Venus – 800bp.

Using this approach, it was relatively easy to generate FLAG-Venus-TRIP13 homozygous “knock-in” clones. However, when using the repair construct that also included the mAID sequence no homozygous or heterozygous clones were observed by PCR.

I repeated the transfection, FACS, and screening for the FLAG-Venus-mAID construct multiple times and never observed any positive clones

despite seeing a positive signal by FACS similar to that of the FLAG-Venus construct.

I knew that the filter sets in the FACS Aria I was using were unable to distinguish between GFP and Venus positive cells; however, since the GFP signal was transient and overexpressed I had assumed that waiting between the bulk and single cell sorts would eliminate the majority of this signal. I decided to check whether this was really the case by changing the colour in the Cas9 targeting construct from GFP to Ruby via restriction digest cloning. I then repeated the FACS sorts with my new ruby targeting construct as shown in figure 3-4. Using this construct, I detected no Venus positive cells for the FLAG-Venus-mAID construct indicating that I had been screening false-positive cells the whole time.

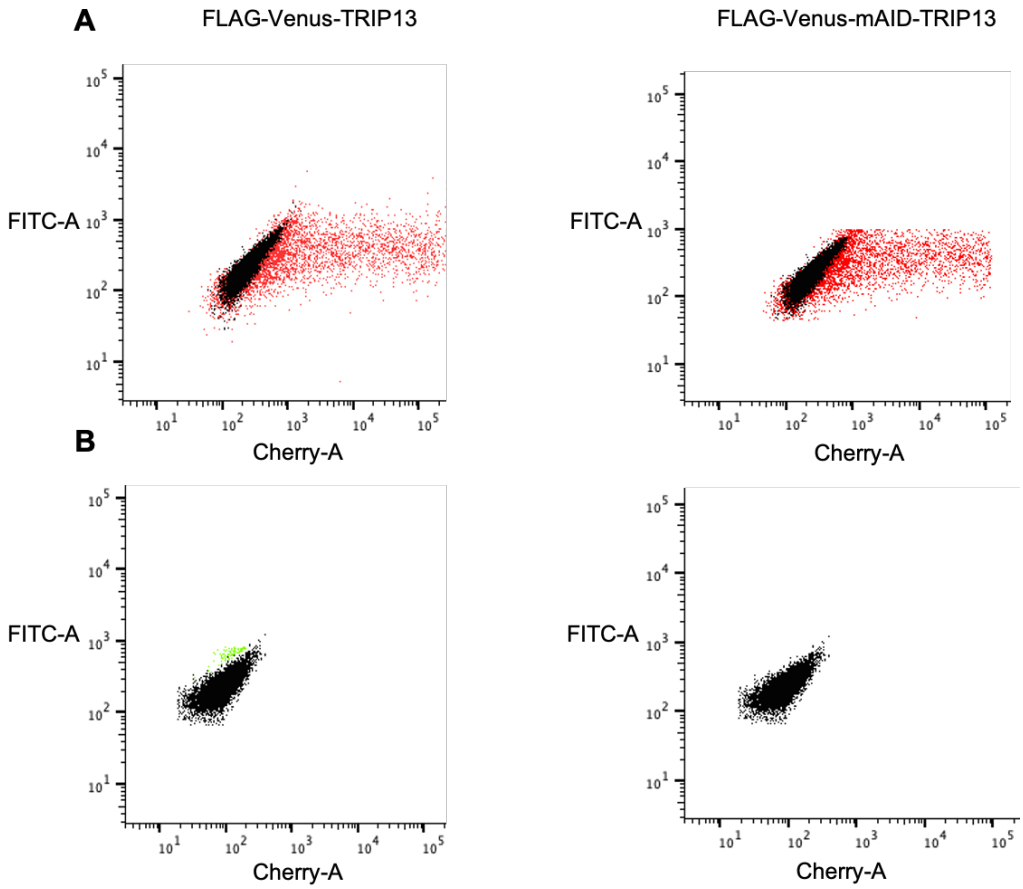

Figure 3-4 FACS sort using Cas9 ruby in RPE osTIR1

A) Bulk sort for Cas 9 positive cells using Ruby as a marker. Cells in red were sorted into a 6 well plate for further expansion **B)** Single cell sort for Venus positive cells. Cells in green were index sorted singularly into 96 well plates There were no positive clones for FLAG-Venus-mAID and fewer for FLAG-Venus indicating that in Figure 1.3B only false positives were sorted. PCR screen was as in figure 1.3C.

3.2.2. Targeting TRIP13 in RPE1 FRT/TR osTIR1 cells

Through personal communication with multiple labs, it became clear that the AID system was potentially capable of non-specific degradation of the target protein when TIR1 was expressed freely. Whether this was due to high levels of TIR1 or contamination of FBS with auxin derivatives was not clear. I decided to set up the AID system in a cell line where TIR1 expression was controlled with a doxycycline specific promoter to eliminate both of these problems.

I used RPE1 FRT/TR cells that were originally generated by Mark Jackman and Felicia Walton.

I used a neomycin resistant FRT construct containing FLAG-osTIR1. This construct was then microporated at a 1:9 ratio with another construct, pOG44, expressing the flippase enzyme that switches the empty FRT cassette with the osTIR1 containing cassette. 5 days post transfection these cells were plated sparsely and selected using neomycin. From this point onwards the cell line and all derivative cell lines were grown in media supplemented with qualified FBS meaning that it was free from tetracycline impurities.

This new cell line, RPE1 FRT/TR osTIR1 only expressed FLAG-osTIR1 after addition of tetracycline. (Figure 3-5). I then repeated CRISPR/Cas9 targeting of TRIP13 with the All-in-One (ruby) and repair plasmids. This time the FACS signal between Venus and Venus mAID populations was more comparable. (Figure 3-6B). From around 500 clones screened, I obtained 2 homozygous knock-in cell lines for FLAG-Venus-mAID-TRIP13 that were confirmed by western blotting and sequencing.

Representative immunoblots are shown in figure 3-7. These blots also show that the TRIP13 antibodies that recognised the wildtype species did not recognise the fusion species. I confirmed the homozygote knock ins using an anti-FLAG antibody in parallel.

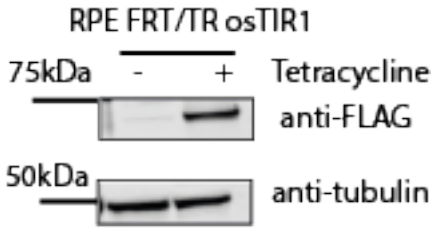

Figure 3-5 FLAG-osTIR1 expression requires tetracycline induction

Immunoblot of RPE FRT/TR osTIR1 pool. Cells were blotted for using anti FLAG and anti-beta tubulin as a loading control. 0.1µg/mL Tetracycline was added for 2 hours in order to induce expression of FLAG-osTIR1. osTIR1 is 64kDa.

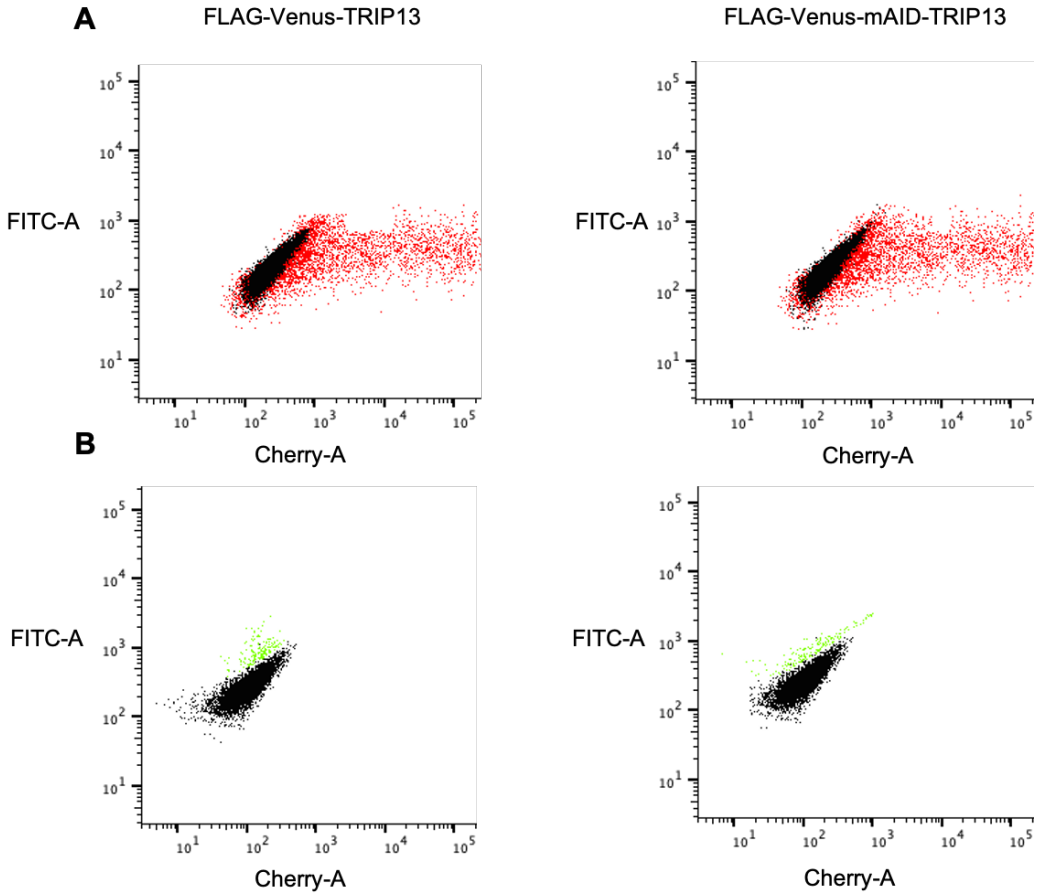

Figure 3-6 FACS sort for RPE FRT FLAG-osTIR1

A) Bulk sort for Cas 9 positive cells using Ruby as a marker. Cells in red were sorted into a 6 well plate for further expansion **B)** Single cell sort for Venus positive cells. Cells in green were index sorted singularly into 96 well plates. This time positive colonies were isolated from both FLAG-Venus and FLAG-Venus-mAID populations. PCR screens were performed as in Figure 3-3C

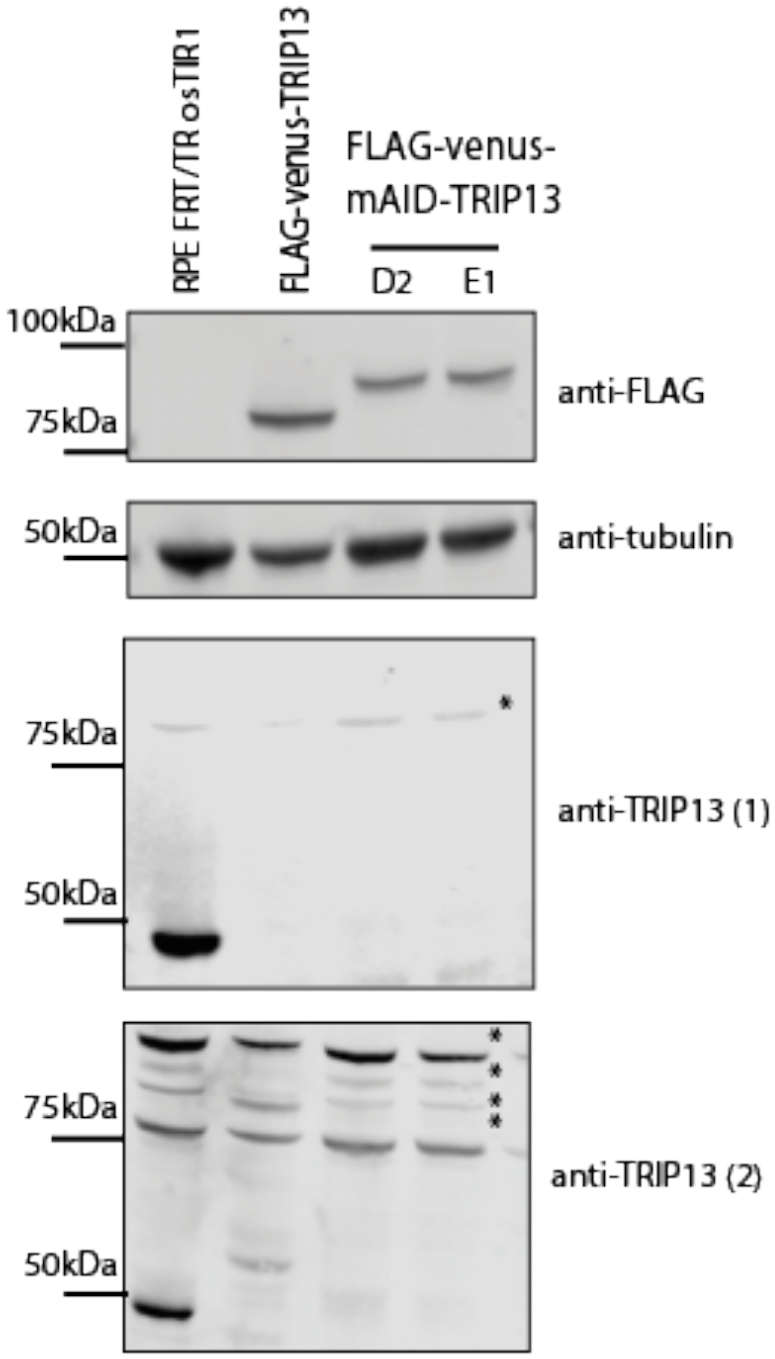

Figure 3-7 Validation of 2 homozygote knock in clones for FLAG-Venus-mAID-TRIP13

2 positive clones identified using PCR and validated by sequencing were subjected to immunoblotting to confirm the zygosity of the TRIP13 locus. The parental cell line and a previously validated clone were used as negative and positive controls respectively. TRIP13 is 49kDa. Venus is 25kDa. Anti-FLAG antibodies detected a singular band at the expected size which shifted in size in the clones with miniAID (9kDa). Anti TRIP13 antibodies only detected normal TRIP13 in the wild-type sample and not in any of the clones. They did not detect the fusion protein.

3.2.3. Initial characterisation of TRIP13 AID in RPE1 FRT/TR osTIR1 cells by immunoblotting

Initially I induced osTIR1 expression for 4 hours using 0.1µg/ml tetracycline followed by the auxin derivative Indole-3-acetic-acid (IAA) at 500µM in clone D2. I then assayed the levels of TRIP13 using an anti-FLAG antibody, 1 and 3 hours after adding IAA (Figure 3-8).

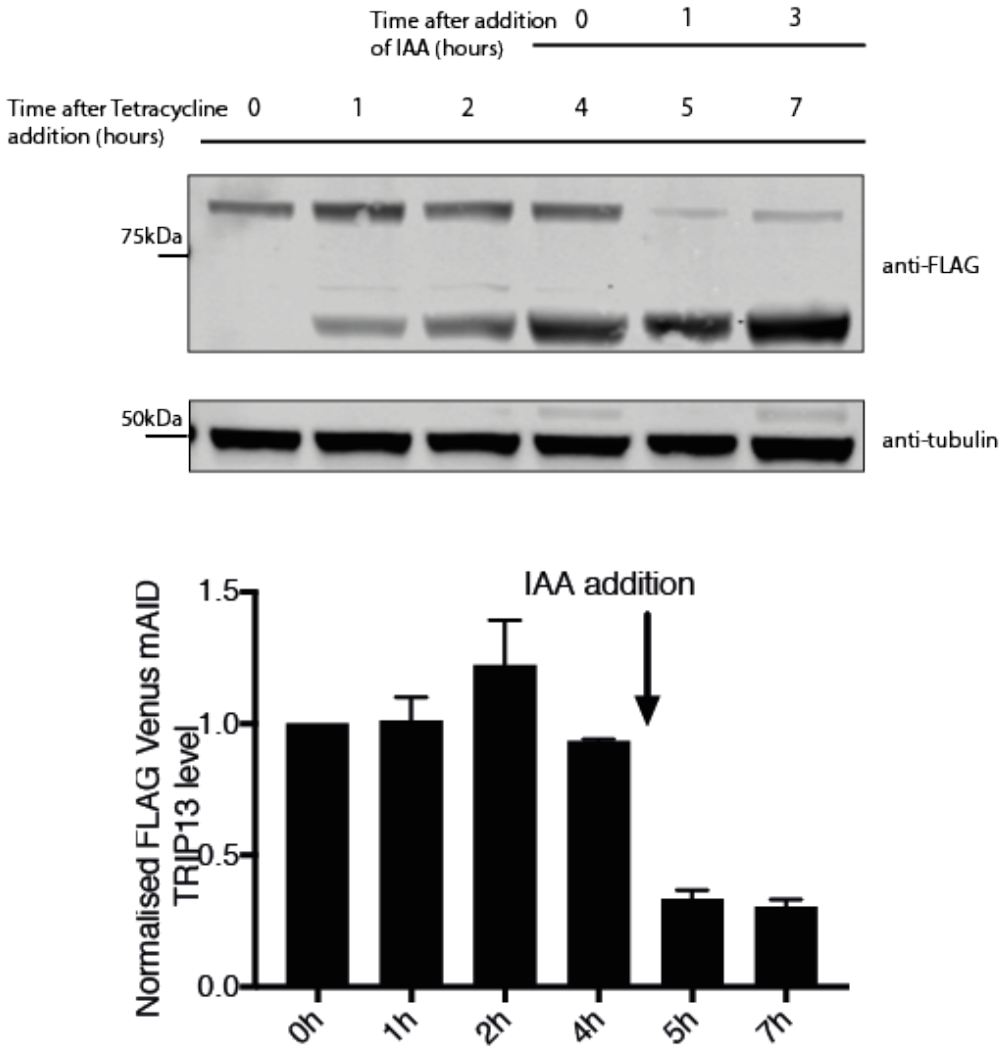

Figure 3-8 Immunoblot analysis of clone D2 confirms AID reduces level of FLAG-Venus-mAID-TRIP13

A short time course of tetracycline /IAA for clone D2 indicates that TRIP13 levels reduce in the first hour of IAA treatment. Tetracycline was added at 0.1µg/mL and IAA was added at 500µM. Anti-FLAG in this case shows both FLAG-Venus-mAID-TRIP13 (higher band) and FLAG-osTIR1 (lower band). IAA was added to the last 2 timepoints for 1 and 3 hours respectively leading to a 70-80% drop in TRIP13 levels at both time points. Experiment was repeated twice more. Graph shows quantification of the FLAG-Venus-mAID-TRIP13 band normalised against the tubulin loading control and to the first time point. Analysis was performed using Image studio lite and graphpad prism.

In cells treated with IAA and tetracycline there was a reduction in TRIP13 levels immediately after the IAA was added. However, the levels did not drop below 20%.

I repeated the assay and measured the levels of TRIP13 at longer time points, this time in both clones. The levels of TRIP13 dropped rapidly upon induction with IAA but not at later time points (Figure 3-9). I assayed whether higher initial levels of osTIR1 led to a greater reduction of TRIP13 levels but this did not reduce the levels of TRIP13 anymore than previously observed (figure 3-10).

Next I checked whether this residual TRIP13 population was due to new synthesis of the protein. After inducing with tetracycline for 2 hours, I added IAA at short frequent time points, with and without cycloheximide (CHX) to inhibit new translation of TRIP13. There was still a residual amount of TRIP13 that was never degraded (figure 3-11).

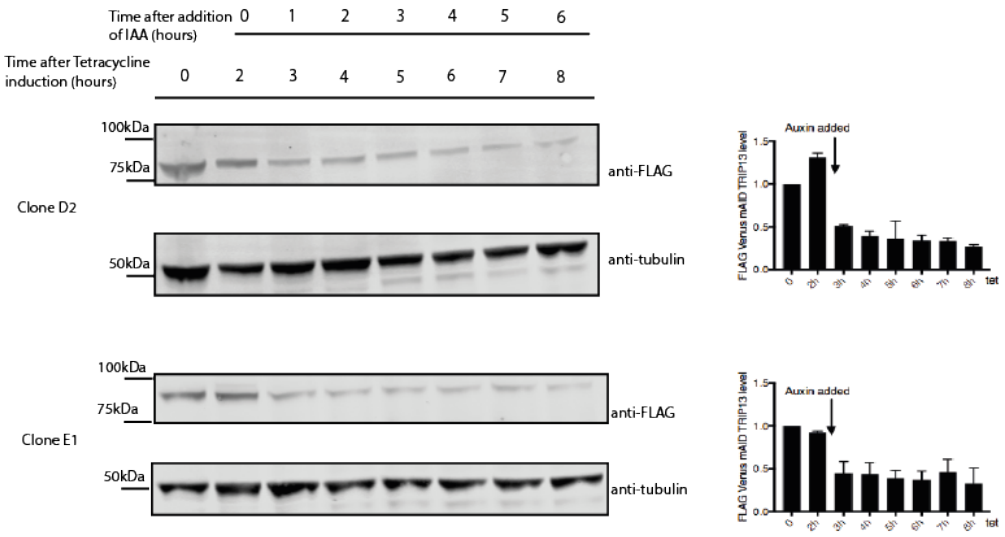

Figure 3-9 IAA reduces TRIP13 levels within the first hour but not anymore at longer time points

A longer time course of tetracycline /IAA for clones D2 and E1 indicates that TRIP13 levels do not reduce more than after the first hour of IAA treatment. Tetracycline was added at 0.1µg/mL and IAA was added at 500µM. Anti-FLAG in this case shows only the FLAG-Venus-mAID-TRIP13. IAA was added after 2 hours tetracycline treatment this time. Experiment was repeated once more. Graph shows quantification of the FLAG-Venus-mAID-TRIP13 band normalised against the tubulin loading control and to the first time point. Analysis was performed using Image studio lite and graphpad prism.

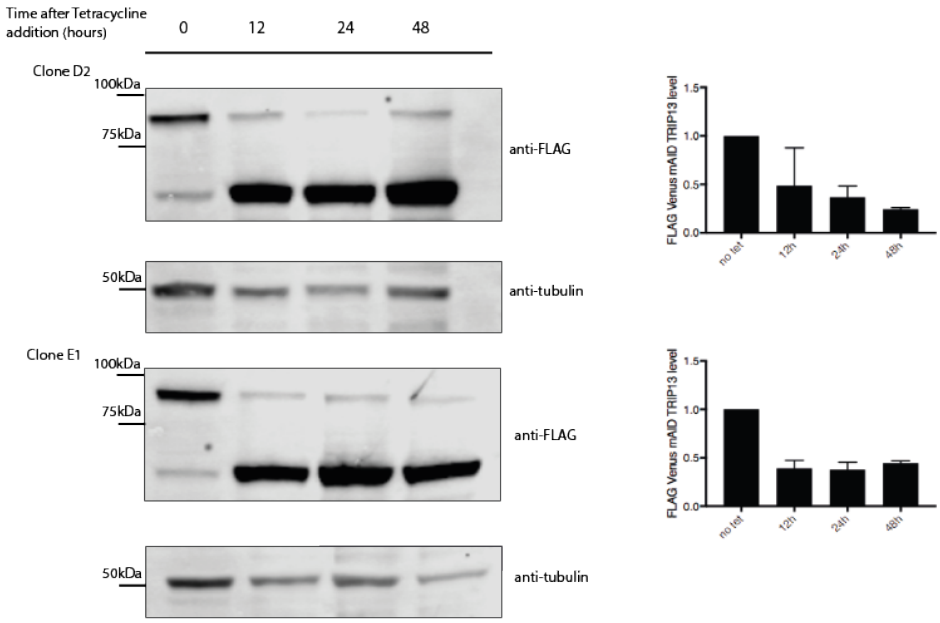

Figure 3-10 Long term induction of osTIR1 using tetracycline does not reduce levels of TRIP13

FLAG-osTIR1levels were varied in this time course by addition of tetracycline for longer periods. In all 3 treatments IAA was only added for 1 hour prior to cell lysis. TRIP13 levels do not reduce below 70% in both clones. All other variables were as described in figure 3-9

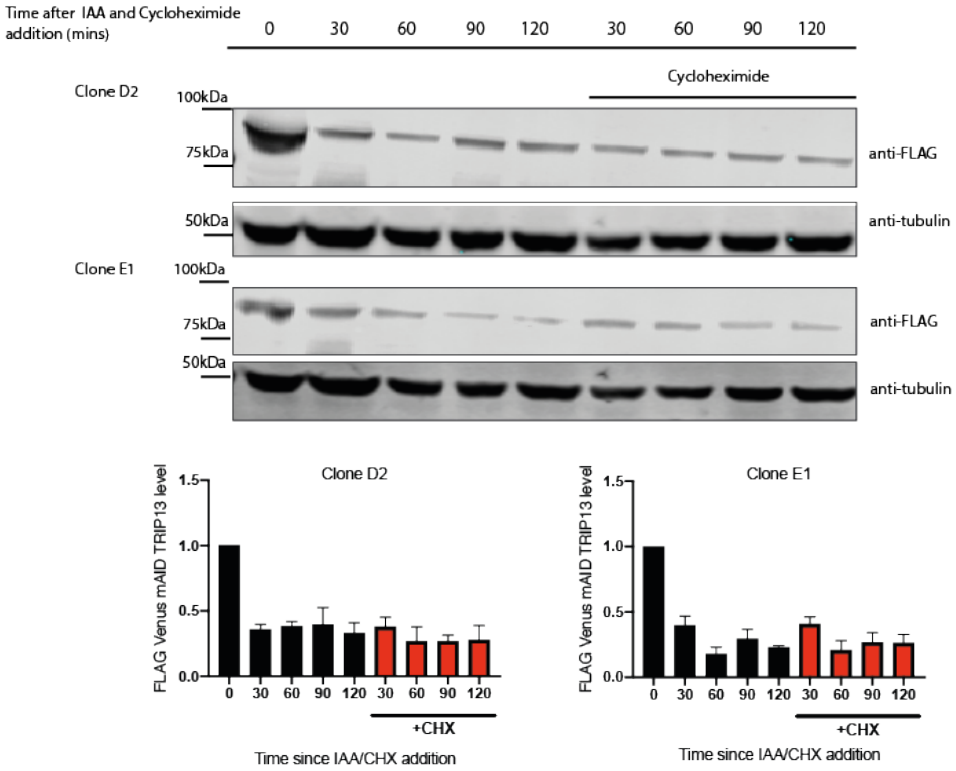

Figure 3-11 New synthesis of TRIP13 is not affecting TRIP13 levels during AID

Cells were treated with tetracycline for 2 hours and then subjected to short treatments of IAA and or Cycloheximide (CHX). Inhibition of protein synthesis did not have a significant effect on levels of TRIP13.

3.2.4. Single cell characterisation of TRIP13 AID in RPE1 FRT/TR osTIR1 cells

Tagging TRIP13 with Venus as well as mAID this allowed me to measure the degradation on a single cell level (Figure 3-12). I had not seen much variation between clones D2 and E1 by western blotting and decided to move forward with clone D2. I had also not seen different levels of induction of osTIR1 having an effect on TRIP13 levels using immunoblotting. To assay cells by time-lapse fluorescence microscopy, I added tetracycline and IAA in parallel and started to image cells every 5 minutes. Every 5th frame is shown in figure 3-12A. After a lag phase, where tetracycline addition switched on expression of osTIR1, I observed rapid degradation of TRIP13 to undetectable levels.

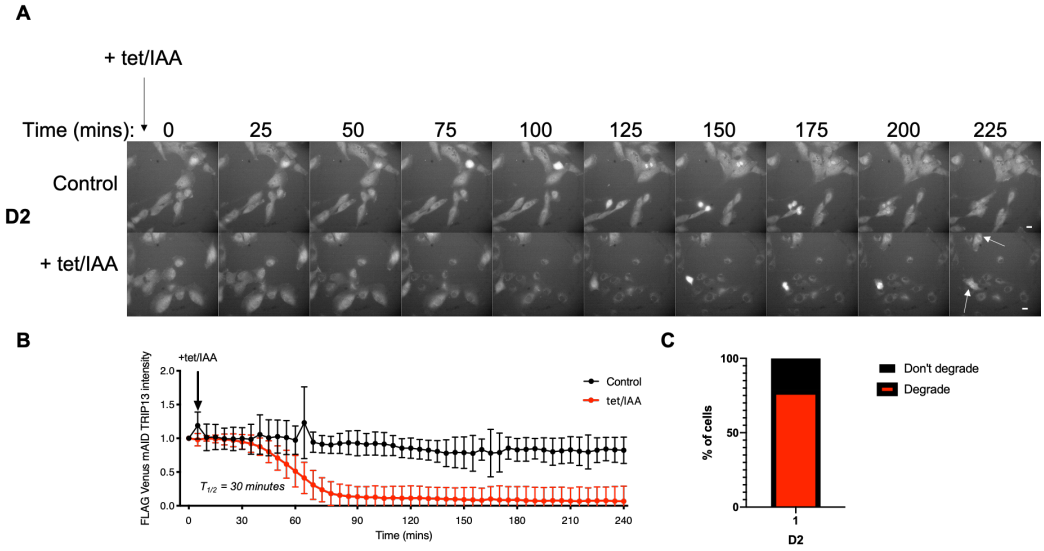

Figure 3-12 Single cell degradation of FLAG-Venus-mAID TRIP13

Widefield microscopy was used to film clone D2. Tet/IAA were added in frame 2. Cells were filmed every 5 minutes and every 5th frame is shown. EMCCD camera with 4x4 binning was used. Scale bar = 20μM Venus intensity was calculated for 10 cells by drawing manually around each cell in each frame. Intensity was normalised to background and cell area and the first frame. Cells rapidly degraded after a lag in 60 minutes. The half-life was 30 minutes. Some cells did not degrade at all and they are highlighted in the final frame (bottom right) with white arrows. These cells were not included in either quantification. However, they were quantified by eye in the bar chart. FIJI software was used for analysis and graphpad prism was used for quantification. (See Appendix C for larger images.)

TRIP13 levels were quantified, in figure 3-12B, by measuring the total cell intensity of Venus manually using FIJI software. Background intensity levels were also measured for each frame. For each cell, the total cell

intensity was normalised to background levels by multiplying both against the cell area and then subtracting the background from the cell intensity value. The level of TRIP13 intensity was treated as 1 in the first frame and all subsequent values were normalised against it. The half-life of TRIP13 was on average 30 minutes. Complete degradation occurred over 50-60 minutes from when levels first began to drop and this corresponded to the time taken to observe a drop in levels by immunoblot. Crucially, I observed that degradation only occurred in some cells and that other cells - highlighted by white arrows in figure 3-12A - never degraded TRIP13. The percentage of cells that degraded TRIP13 is shown in figure 3-12C.

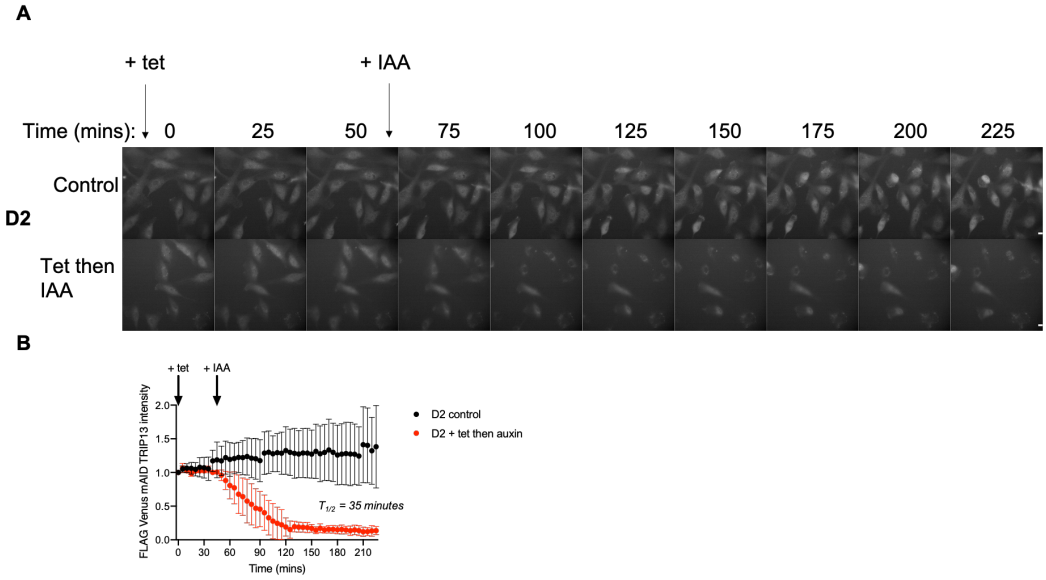

Figure 3-13 Addition of tetracycline and IAA sequentially does not make improve the rate of degradation of TRIP13

Clone D2 cells were subjected to sequential tet and IAA treatment. This time cells degraded immediately upon IAA addition however, the time taken for cells to reach background levels remained the same. Acquisition and analysis were performed the same as in figure 3-12. (See Appendix C for larger images.)

I next wanted to see whether higher initial osTIR1 levels could reduce the half-life of TRIP13 even further. Figure 3-13 shows cells in which I added tetracycline and IAA sequentially, filming throughout. The half-life in this experiment was slightly longer at 35 minutes. I considered adding tetracycline for a long time but I was also aware of reports that this could have non-specific effects so I decided to test this first by filming cells in the presence of tetracycline alone. Figure 3-14 shows that prolonged

expression of osTIR1 does lead to a decrease in Venus intensity and therefore I decided to not test adding IAA at any later time points.

Single cell microscopy had shown that the system was working but not in all the cells. This was also true for clone E1. I repeated the CRISPR/Cas9-mediated gene targeting once again and generated several more homozygote knock-ins to ensure that this was not a clonal problem (figure 3-15). I quantified the percentage of cells that degraded TRIP13 in each clone. This is shown in figure 3-15B. The first clone I had generated, clone D2 had the highest number of cells degrading in each experiment. I sub-cloned D2 using FACS to see whether I could isolate a pure population of cells that degraded TRIP13, but when I subjected the subclones to the same analysis I did not see an improvement in the percentage of cells degrading TRIP13.

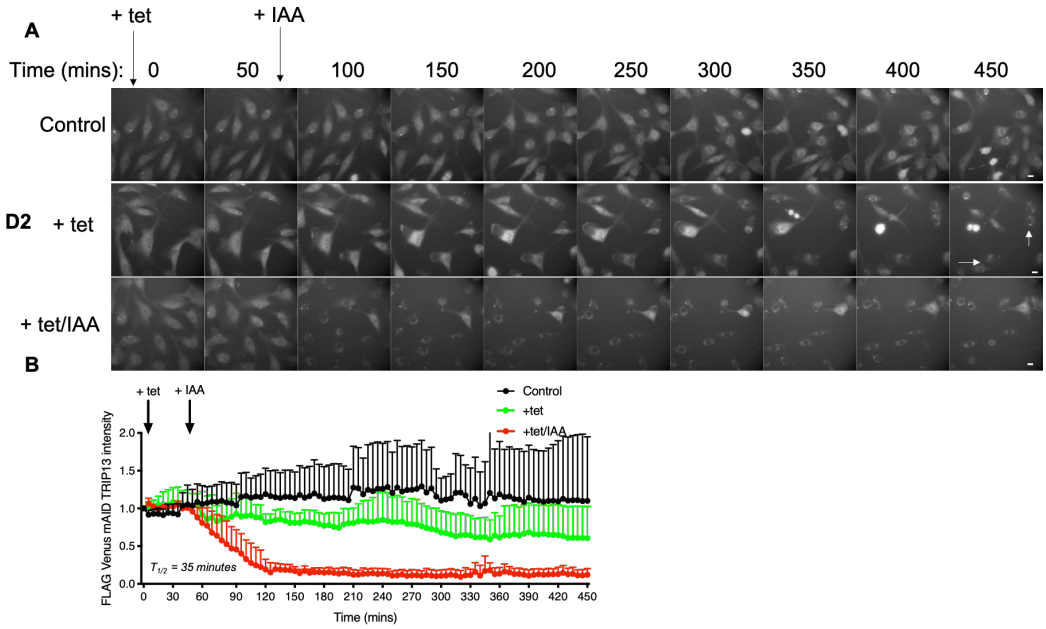

Figure 3-14 Prolonged expression of osTIR1 reduces levels of TRIP13 without IAA

Clone D2 cells were subjected to sequential tet and IAA treatment. A third condition where only tet was added this time. The tetracycline treated cells gradually lowered in Venus intensity indicating osTIR1 expression alone has an effect. Acquisition and analysis were performed the same as in figure 3-12. (See Appendix C for larger images.)

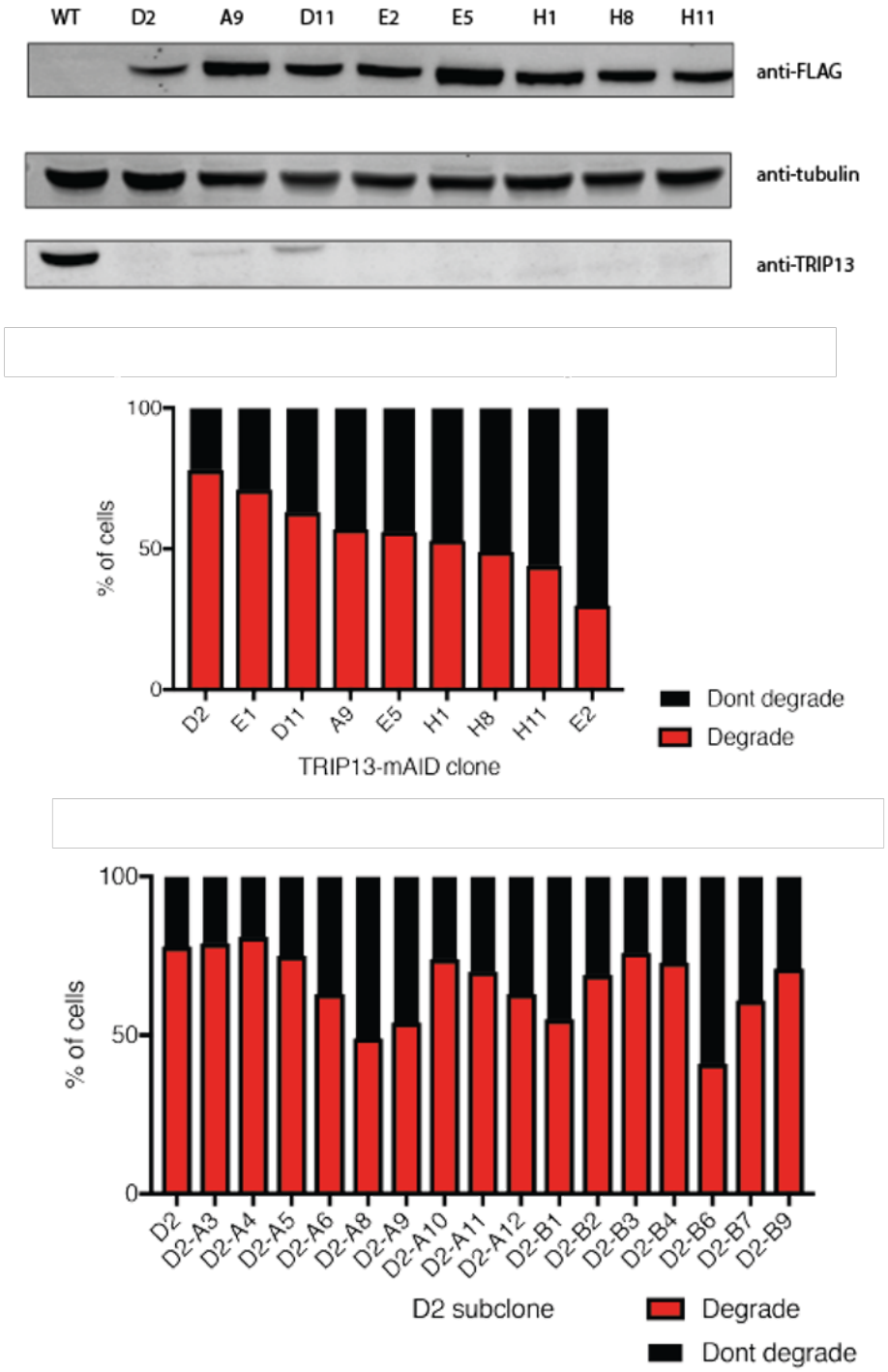

Figure 3-15 All RPE FRT osTIR1 FLAG-Venus-mAID-TRIP13 clones are heterogenous for degradation of TRIP13

Immunoblot shows validation of new FLAG-Venus-mAID TRIP13 clones using anti TRIP13 and anti FLAG antibodies with beta tubulin used as a loading control. These clones were then filmed as in figure 3-13 and number of cells that do and do not degrade were quantified by eye. 100 cells were quantified per sample. None of the clones exhibited a greater percentage of degradation than D2. D2 was then subcloned using FACS and these clones were then subjected to the same assay. None of the sub-clones achieved a 100% of cells degrading TRIP13 either.

3.2.5. The SAC does not function effectively in response to acute loss of TRIP13

Once I had established that some cells depleted TRIP13 to a very low level, I proceeded to check how the SAC behaviour changed with and without TRIP13. I measured both NEBD-anaphase timing and time in mitosis after SAC activation in response to 0.33μM nocodazole (Figure 3-16).

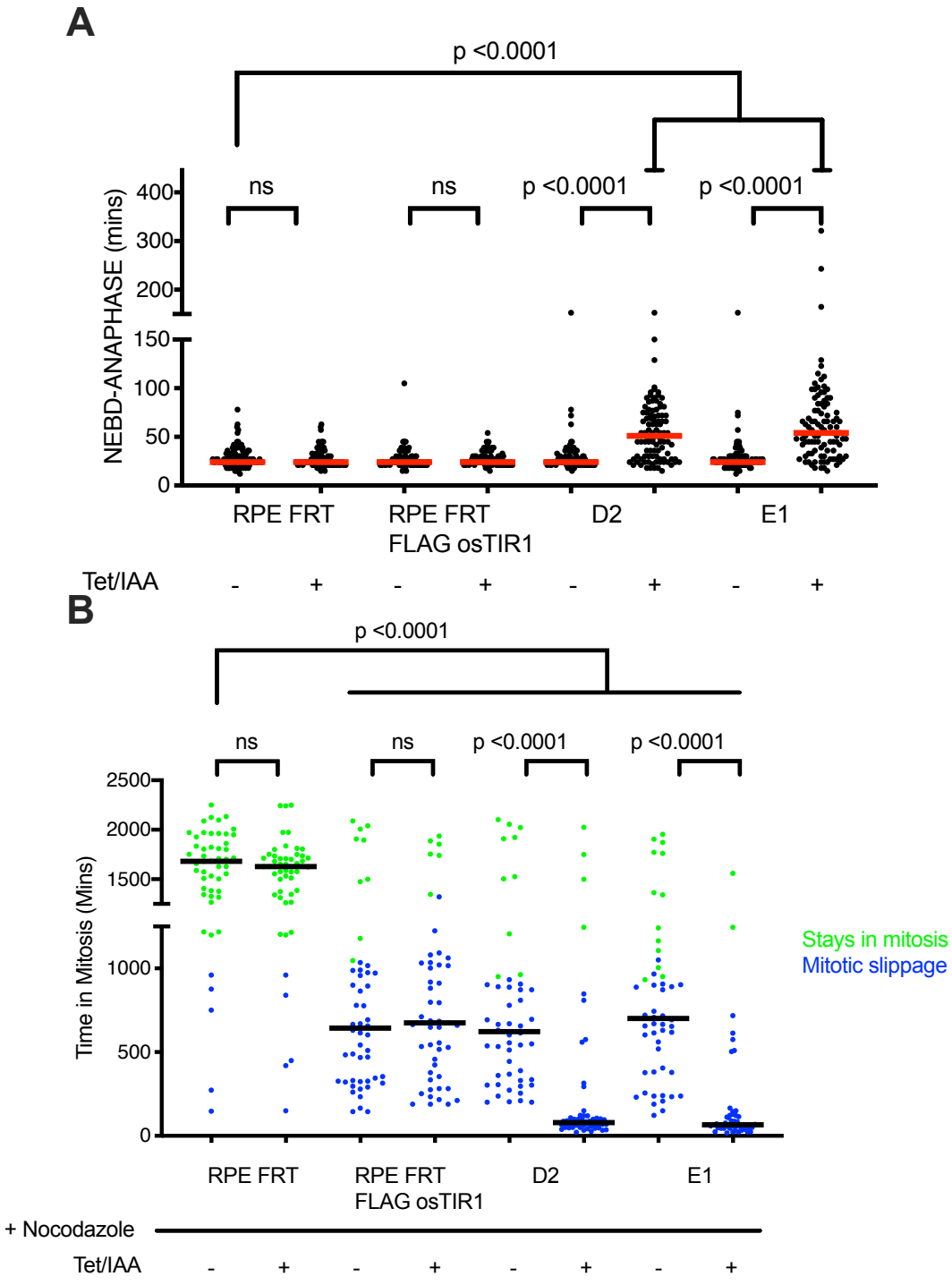

Figure 3-16 Acute TRIP13 depletion leads to both mitotic delay and checkpoint override.

A) Time-lapse analysis of NEBD-Anaphase timing for both the parent cell lines and clones D2 and E1. Measurements were made with and without TRIP13 acute depletion by adding tetracycline and IAA 2 hours prior to filming. **B)** Time lapse analysis of the same cells with 0.33μM nocodazole added to all conditions to activate the SAC. Green cells represent cells that remained in mitosis at the end of the movie whereas blue represents cells that slipped out of mitosis back into interphase. Cells were filmed using a 20x DIC air lens every 3 minutes for 24 hours and 30 hours respectively. Horizontal bars represents median in both graphs. n = 100 in A and 50 in B. Timing was quantified by eye using FIJI software and quantified using graphpad prism. One way ANOVA was used for statistical analyses

In both clones NEBD-anaphase is delayed when tetracycline/IAA are added to deplete FLAG-Venus-mAID-TRIP13 but not in the control parent cell lines (figure 3-16A). Timing increased from 27± 9mins in all control samples and in untreated D2 and E1, to 54 mins± 28mins in D2 tet/IAA and 63± 42mins in E1 tet/IAA. This is in line with siRNA data (Chiara Marcozzi, unpublished data).

When the SAC was activated using nocodazole, 95% of cells arrested in the parent RPE FRT cell line for the duration of the movie, and addition of tetracycline/IAA had no effect. Unexpectedly, RPE FLAG osTIR1 and the clones derived from this line did not have the same mitotic behaviour as RPE FRT cells when filmed only in nocodazole. The majority of cells in these lines (over 80%) arrested in mitosis for a prolonged but much shorter period than RPE FRT cells: the average time in mitosis was reduced from 1590±437mins in RPE FRT to 750±523mins; 764±527 and 774±478mins in RPE FRT osTIR1, D2 and E1, respectively. The majority of these cells also slipped out of mitosis.

In the clones, this arrest was ablated by addition of tetracycline and IAA to remove TRIP13 from the system, showing that acute depletion of TRIP13 leads to loss of the checkpoint. When tet/IAA was added, timing was reduced from 764± 527mins and 774± 478mins to 249±454mins and 178±307mins in D2 and E1, respectively.

Although these experiments showed that acute depletion of TRIP13 recapitulated both phenotypes seen using siRNA and CRISPR KO, the AID capable cell line did not exhibit a wildtype checkpoint arrest therefore I decided to not proceed with using these cell lines.

3.3. Discussion

In this chapter I have described the strategies exploited to generate knock-in cell lines that are able to degrade TRIP13. To do this I used CRISPR/Cas9 to drive homologous recombination with an exogenous repair construct containing the miniAID degron sequence in a cell line where osTIR1 was controlled by the tet-repressor.

In recent years, the AID system has been widely adopted in cell line-based systems and as a result a number of improvements have been made (Nishimura et al. 2009a). I decided to adopt many of these changes. Firstly, the use of a mAID degron motif sequence rather than the original full size AID tag (Natsume et al. 2016). The mAID is only 9kDa whereas the full-size tag is over 25kDa. TRIP13 is 49kDa and adding both Venus and the full-size AID tag would have doubled the mass of TRIP13. Control of TIR1 expression is another way that clearly improves the AID system (Natsume et al. 2016). In RPE1 cells it is was impossible to select for AID tagged TRIP13 clones using fluorescence without repressing TIR1 expression. This is likely due to the fact that TIR1 can cause degradation of target proteins without auxin derivatives; therefore, the Venus signal was suppressed on the FACS read out. I also observed IAA independent degradation in live-cell imaging in the presence of only TIR1 expression. However, I never eliminated potential auxin derivatives in the media as a potential variable.

In this case, Venus tagging of TRIP13 was important because it also allowed me to measure the single cell kinetics of TRIP13 degradation. Single cell assays explained the residual TRIP13 visualised using the western blot population-based assay. I saw that Venus tagged TRIP13 was depleted to undetectable levels in some cells but that some cells never degraded TRIP13 at all.

These clones had a number of drawbacks that in combination precluded their further study. The first problem was the heterogeneity in the population that I observed when TRIP13 was degraded. This phenotype, whilst overcome by single cell imaging, would have made biochemistry challenging.

In the early stage of this project, I introduced FLAG-tagged TRIP13 into a cell line which already contained FLAG-tagged osTIR1. Therefore, I couldn't determine whether the cells in which TRIP13 did not degrade were also not expressing TIR1 by immunofluorescence. I suspected that there may be methylation of the promoter of the exogenous TIR1 gene leading to its silencing, and that prevented some cells from degrading TRIP13 (Hsu et al. 2010; Moritz et al. 2015). However, I was unable to test this due to the conflicting FLAG tags and lack of a good TIR1 antibody.

The final limitation of the cell line was the difference in mitotic timing between RPE FRT osTIR1 cells and the parental RPE FRT cells, for which I have no explanation.

During the time I was making and characterising the cell lines described in this chapter, Dr Helfrid Hochegger published work describing the use of the AID system combined with the SMASh system in RPE1 cells where he saw homogenous depletion of target proteins (Lemmens et al. 2018) (Hegarat et al. 2020). Dr Jörg Mansfeld also published papers where he combined the AID system with a nanobody that recognised GFP derivatives (Daniel et al. 2018) . Both these systems seemed like stronger choices to study the biology of TRIP13 than my own so I decided to proceed with the cell line from the Hochegger lab.

4. TRIP13 – a proof of principle for the AID

4.1. Introduction

In the previous chapter, I described the strategies employed to generate TRIP13-AID cell lines in the RPE FRT/FLAG-osTIR1 background. The clones generated had a number of drawbacks, including heterogeneous TRIP13 degradation and abnormal mitotic timing. In this chapter I describe how I generated new TRIP13-AID cell lines using a different RPE parental cell line developed in Dr Helfrid Hochegger's lab: RPE ROSA26/osTIR1-myc (Lemmens et al. 2018) (Hegarat et al. 2020). In this cell line, CRISPR was used to knock osTIR1-myc into the ROSA26 safe harbour locus under the control of a doxycycline sensitive promoter. After characterising new clones made in this cell line, I use TRIP13 as a proof of principle to validate the AID by comparing my results to the TRIP13 KO data generated by Chiara Marcozzi (Appendix A). As stated above, the original reason to use AID to target TRIP13 for rapid degradation was due to conflicting phenotypes observed in TRIP13-KO cell lines and subsequent changes to the levels of Mad2 and $p31^{comet}$. In parallel with this study, Dr Chiara Marcozzi subsequently identified, using mass spectrometry, that there were residual TRIP13 levels in the clones that could generate a SAC response and we now assume this is the reason for the observed discrepancy in behaviour between clones (Appendix A). Therefore, KO of TRIP13 leads to cells unable to maintain a SAC mediated arrest when challenged with spindle poisons. This is in line with published work (Ma & Poon 2016). TRIP13-AID therefore represents a way to test whether AID is capable of reducing protein levels to extremely low levels as the discrepancy between clones indicated that TRIP13 was capable of exerting it's AAA-ATPase function and changing the conformational state of Mad2

at extremely low levels. Another question that still remained was whether it was TRIP13 KO or the subsequent changes in Mad2 and p31^{comet} levels that lead to the observed phenotype in mitotic cells.

The dynamic connections between microtubules and kinetochores are perturbed when the cells are treated with spindle poisons. Since the SAC is generated at unattached kinetochores, spindle poisons maintain SAC activation because there are always unattached kinetochores in these cells. Studies from our lab (Collin et al. 2013) and others have showed that the SAC works like a "rheostat" rather than a digital on/off signal, and therefore can be activated to different levels. The level can be changed according to the concentration of spindle poison added and cell type (Rieder et al. 1995; Z. Yang et al. 2009). SAC "strength" correlates with the levels of Mad2 recruited to kinetochores, which are indicative of the MCC produced (Collin et al. 2013). Nocodazole and Taxol treatments both lead to prolonged mitotic arrest by interfering with microtubule dynamics. Taxol-arrested cells remain in mitosis for a shorter amount of time than nocodazole-arrested cells, and typically display a higher rate of mitotic slippage. This is reflected in the levels of Mad2 at the kinetochore in these 2 arrests: Taxol arrested cells recruit lower amounts of Mad2. The strength of the SAC can also be measured using the degradation kinetics of Cyclin A and Cyclin B (Collin et al. 2013). Taxol arrest is weaker than both nocodazole and monastrol arrests because it stabilises microtubules and this eventually leads to syntelic attachments (Z. Yang et al. 2009). Syntelic attachments are in turn detected and corrected by Aurora B and converted to amphitelic attachments that satisfy the SAC (Santaguida et al. 2011).

MPS1 kinase activity is required for proper activation of the checkpoint. Without it, recruitment of checkpoint components to the kinetochore is severely impaired and as a result MPS1 inhibition drives cells to progress through mitosis rapidly.

I use time-lapse microscopy assays to investigate how mitotic progression is affected by acute loss of TRIP13, both in an unperturbed mitosis and under conditions where the SAC is kept active by the addition of spindle poisons, or inactivated by the MPS1 inhibitor, Reversine (Hewitt et al. 2010).

I also show that cell cycle phase is important for when TRIP13 is depleted. Depletion of TRIP13 before mitosis does not lead to the same mitotic timing as depletion during mitosis.

4.2. Results

4.2.1. Generation of FLAG-Venus-mAID-TRIP13 clones in RPE1 ROSA26/osTIR1-myc

To begin with, I repeated the steps from section 3.2.2 to generate new clones in RPE1 ROSA26/osTIR1-myc using CRISPR/Cas9 gene targeting. This cell line will be herein referred to as “parental” or WT. I only generated FLAG-Venus-mAID TRIP13 clones this time. Figure 4-1 shows FACS plots for both bulk and single cell index experiments with RPE1 FRT/osTIR1 FLAG-Venus-mAID-TRIP13 clone E1 from chapter 3 as a positive control (figure 4-1B) to gate and select for new positive cells that are represented by index sorts in figure 4-1C.

From these FACS experiments, I obtained several homozygous knock-in clones using the same PCR validation set up as before. In this chapter I have characterised 3 of these clones in detail: 2F11, 2G2 and 4B4. I further confirmed the zygosity of these clones by sequencing and western blotting (figure 4-2)

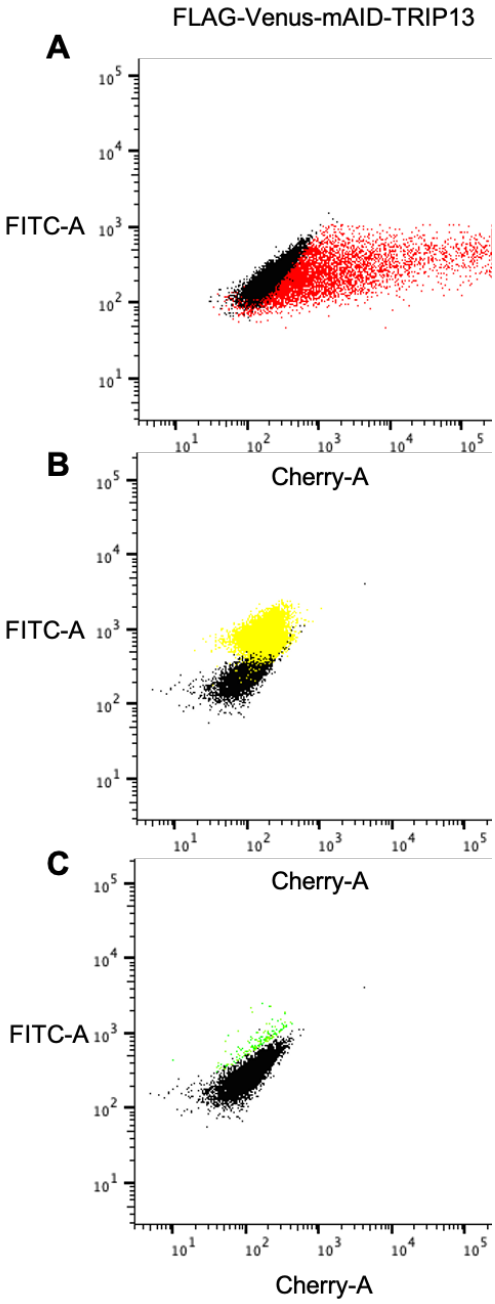

Figure 4-1 FACS sorting for FLAG-Venus-mAID-TRIP13 in RPE1 ROSA26 osTIR1-myc background

A) Bulk sort for Cas 9 positive cells using Ruby as a marker. Cells in red were sorted into a 6 well plate for further expansion **B)** FLAG-Venus-mAID TRIP13 E1 clone shown in yellow and used as a positive control to single cell sort the indexed cells in green in **C)**. Untransfected control cells are shown in black throughout.

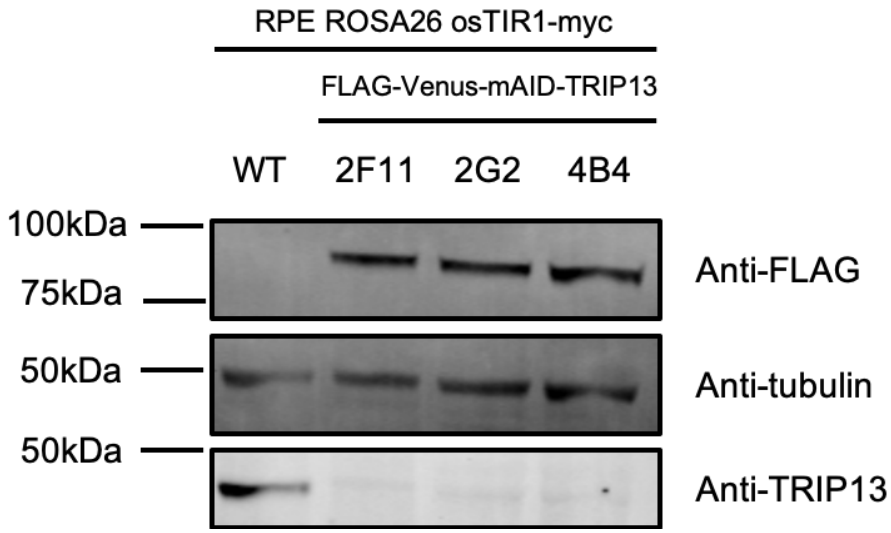

Figure 4-2 Three new homozygote FLAG-Venus-mAID TRIP13 clones

3 positive clones identified by PCR and sequencing were subjected to immunoblotting with anti-FLAG and anti TRIP13 to confirm zygosity as before in figure 3-7. Tubulin was used as a loading control

4.2.2. TRIP13-AID is more homogenous and faster in clones generated from RPE1 ROSA26/osTIR1-myc parental cells

To ascertain whether the AID system was improved in this cell line system, I repeated western blotting and single cell time-lapse microscopy to measure the degradation at both the population and single cell level.

In this system, the expression of TIR1 was under the control of the Tet-ON3G ® promoter (Takara). This promoter is only sensitive to doxycycline and there is no tet repressor integrated into this cell line. Therefore, I thought it was likely that the expression of TIR1 could be different from my previous cell line. Figure 4-3 shows parental cells treated with doxycycline and collected every 2 hours. After 4 hours TIR1 was detectable. According to recent literature, and from my own cell experiments described in chapter 3, it is clear that high TIR1 levels can cause non-specific degradation of AID targets, and that higher levels of TIR1 do not induce faster degradation. Therefore, I decided to induce for 4 hours prior to adding IAA. This method was used in all subsequent experiments.

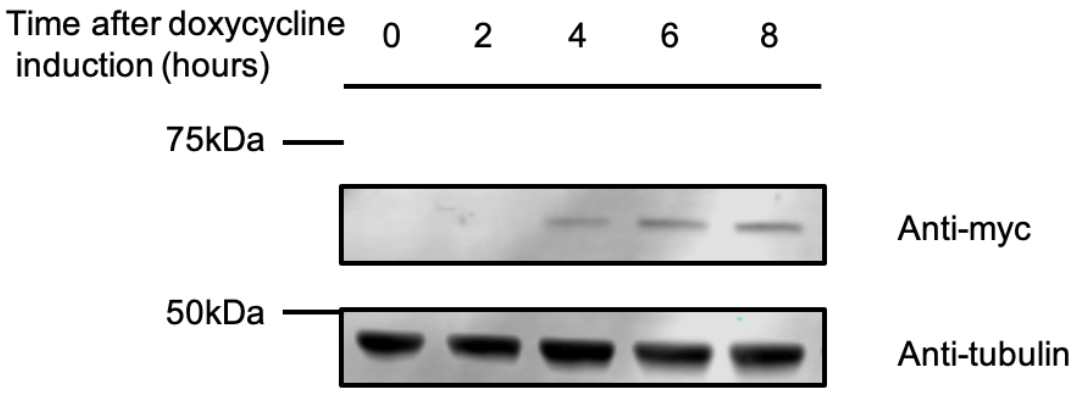

Figure 4-3 Expression of osTIR1-myc is detected 4 hours after doxycycline induction

Parental cells were treated with 1µg/mL Doxycycline and collected every 2 hours. Anti-myc was used to detect osTIR1 and anti-tubulin was used as a loading control.

I measured the levels of TRIP13 after Dox and IAA addition in all clones (Figure 4-4). TRIP13 levels remained the same in the parental line, as expected. In the three TRIP13-AID clones, TRIP13 levels were reduced to around 30% within one hour of IAA addition continued to decrease to an almost undetectable level in the subsequent 5 hours. This is in contrast to clones generated in the previous cell line where levels of TRIP13 initially decreased rapidly but never decreased below 20%.

Figure 4.4 Time course analysis of TRIP13 degradation in all 3 clones

Cells were treated with doxycycline as before for 4 hours before addition of 0.5µM IAA was added. Cells were collected every hour for 6 hours and blotted for with Anti-FLAG and Anti Tubulin (loading control). Parental cells were blotted with anti-TRIP13 because of the lack of FLAG tag. TRIP13 levels were reduced by at least 70% in all 3 clones within the first hour and this level continued to reduce for the following 5 hours until a negligible signal was observed. Graphs show average of 3 biological repeats. Error bars represent S.D.

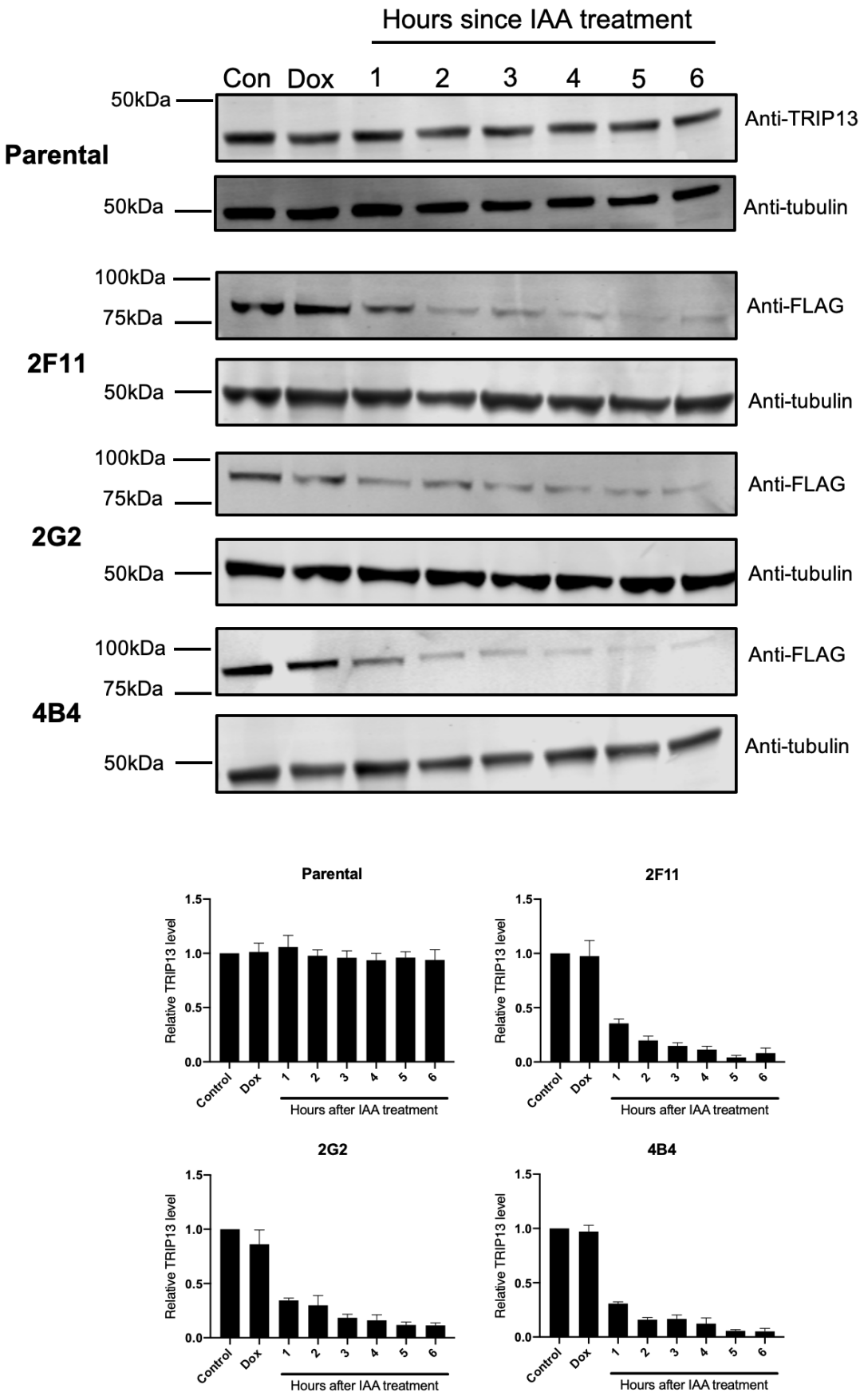

Figure 4-4 Time course analysis of TRIP13 degradation in all 3 clones (see previous page)

I then performed time-lapse microscopy in order to measure the time taken for TRIP13 to be depleted on a single cell level and ascertain whether this cell line behaved homogenously. Figure 4-5A shows single cell degradation of TRIP13-AID in all 3 clones. The assay was quantified as described in figure 3-12 (figure 4-5B). In the new clones the half-life of TRIP13-AID is slightly shorter upon addition of IAA (2F11 and 2G2: 20 minutes, 4B4: 25 minutes) and Venus-tagged TRIP13 is undetectable between 40 and 60 minutes after IAA addition for the majority of cells. Importantly, the degradation of TRIP13 in these cells was much more homogenous; in 2 out of the 3 clones >95% of cells degrade the protein immediately upon the addition of IAA (figure 4-5C). There was a small sub-population of cells, most noticeably in clone 2G2, which did not degrade TRIP13 immediately but instead delayed and then degraded TRIP13 with similar kinetics to the rest of the population (data not shown). This delayed population could be an explanation for why the levels of TRIP13 are still detectable by western blotting for a few hours after addition of IAA. However, these assays are not directly comparable and this could just be a sensitivity issue.

I confirmed that the disappearance of FLAG-Venus-TRIP13-mAID was due to proteasome degradation by adding the proteasome inhibitor MG132. In figure 4-6 I repeated the single cell degradation assay and added 10μM MG132 in parallel with IAA. This prevented the degradation of TRIP13 as expected.

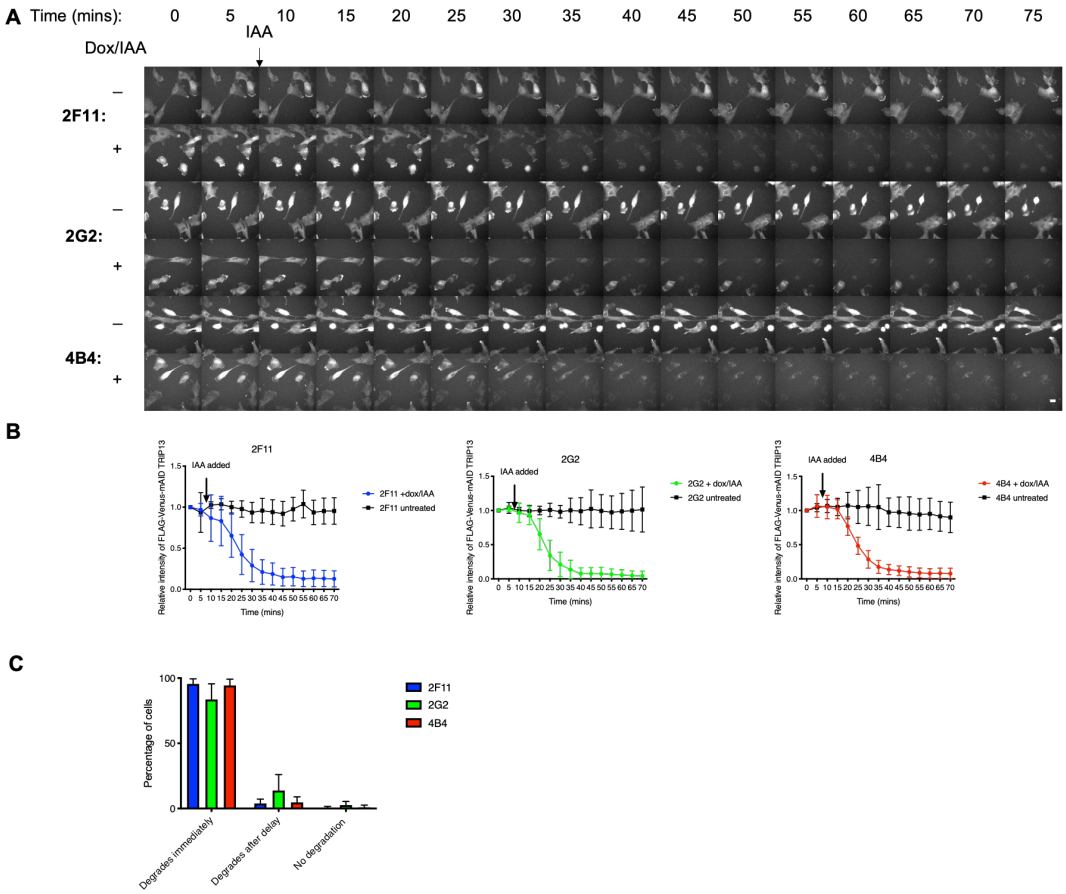

Figure 4-5 Single cell degradation of FLAG-Venus-mAID TRIP13 is faster and more homogenous in these clones

A) Widefield microscopy was used to film all clones as described in figure 3-12. This time cells were treated with doxycycline for 4 hours prior to filming and IAA was added after the second time point. **B)** Graphs show normalised Venus intensity averaged for at least 10 cells. Half-life is between 20 and 25 minutes for all 3 clones. **C)** The number of cells degrading TRIP13 was calculated manually in 3 separate biological repeats. At least 80% of the cells degraded cells immediately. The remaining cells degraded with the same kinetics at random later times. Very few cells did not degrade at all. Error bars represent S.D. (See Appendix C for larger images.)

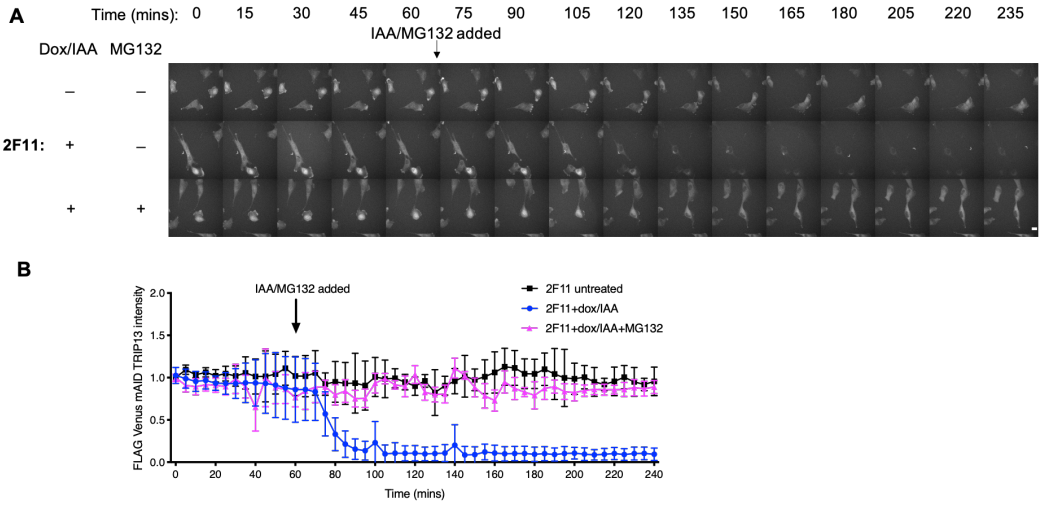

Figure 4-6 MG132 prevents AID mediated degradation of TRIP13

A) The experiment from figure 4-5 was repeated but 10μM MG132 was added which reduction in Venus signal. **B)** Quantification of **A)** was performed exactly the same as in figure 4-5.

4.2.3. Acute degradation of TRIP13 alters the levels of Mad2 and p31^{comet}

As stated previously, TRIP13 is required for the conversion of closed Mad2 to open Mad2. This originally led to speculation that TRIP13 is required for the disassembly of the MCC upon SAC satisfaction as siRNA depletion of TRIP13 has been shown to prolong Mad2 interacting with Cdc20 (Miniowitz-Shemtov et al. 2015). More recently, however, it has been shown that TRIP13 -/- cells cannot generate a proper SAC response in the presence of spindle poisons, which led to the hypothesis that TRIP13 is required for the activation or maintenance of the MCC rather than just the disassembly (Ma & Poon 2016). Our own lab confirmed these changes in mitotic timing in both Hela and RPE TRIP13 -/- cells. (Chiara Marcozzi, unpublished). Interestingly in both published studies and our own study, SAC deficient TRIP13 -/- cells have higher levels of p31^{comet} and lower levels of Mad2.

It was unclear whether these changes were directly due to the loss of TRIP13, or the result of long-term adaptation in these CRISPR/Cas9-generated cell lines. Therefore, I assayed whether acute TRIP13 loss leads to changes in the levels of Mad2 or p31^{comet}. To my surprise the levels of these two proteins rapidly change when TRIP13 is acutely removed, indicating that these proteins depend upon one another for stability: p31^{comet} levels were upregulated at least 2-fold in all clones, and Mad2 levels were reduced by nearly half only 2 days after TRIP13 removal (Figure 4-7).

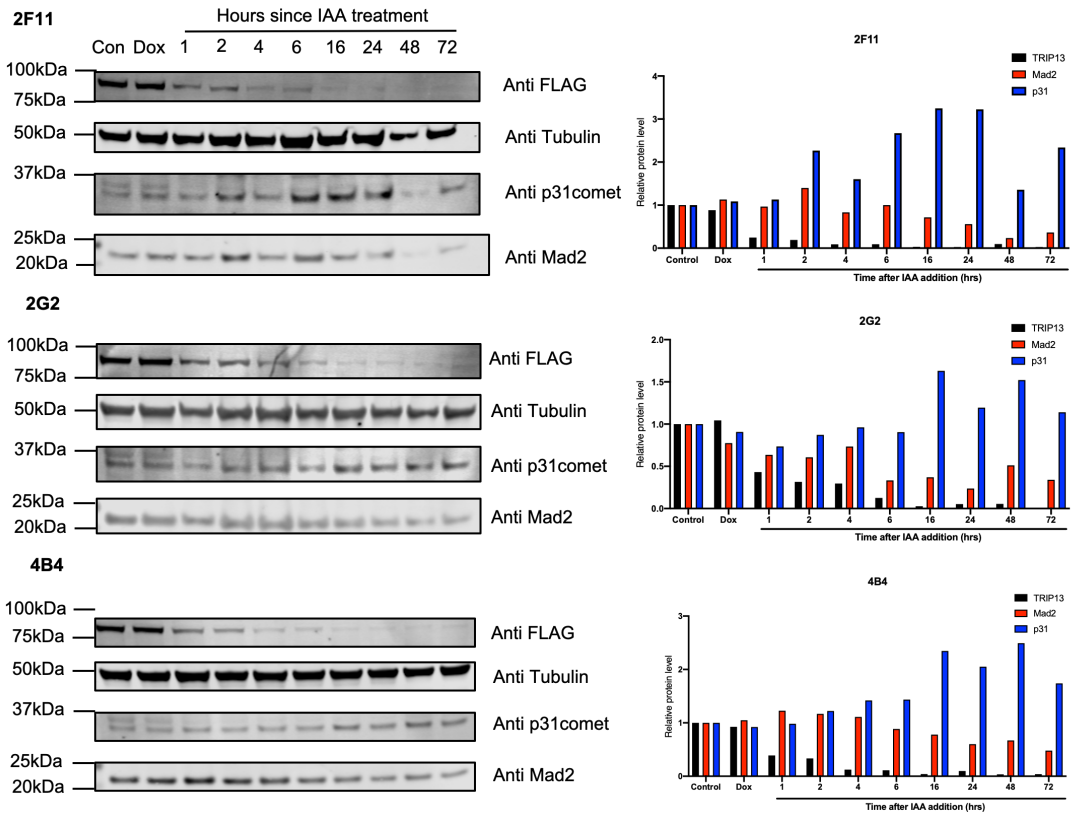

Figure 4-7 Acute TRIP13 degradation causes p31^{comet} levels to increase and Mad2 levels to decrease

Asynchronous cells were lysed at different time points after dox/IAA treatment as described previously. In all 3 clones, p31^{comet} levels were increased at least 2-fold and Mad2 levels were reduced at least by half after 16-24 hours of IAA treatment.

p31^{comet} and TRIP13 only interact with closed Mad2. Most of the Mad2 in the cell is in the open conformation, and whilst the conversion of open to closed Mad2 can occur spontaneously, it is very slow (Ye et al. 2015). In mitosis, kinetochores accelerate this conversion when Mad1 and Mad2 heterodimers interact with free open Mad2, converting it to closed to generate the MCC. The western blot in figure 4-7 was performed on asynchronous cells, therefore I decided to ask whether the open to closed conformational change was important for the changes in p31^{comet} and Mad2 levels by repeating the assay on cells synchronised in interphase by release from serum starvation. I released cells after 24 hours of serum starvation by adding back 20% FBS and depleted TRIP13 with doxycycline and IAA addition (Figure 4-8).

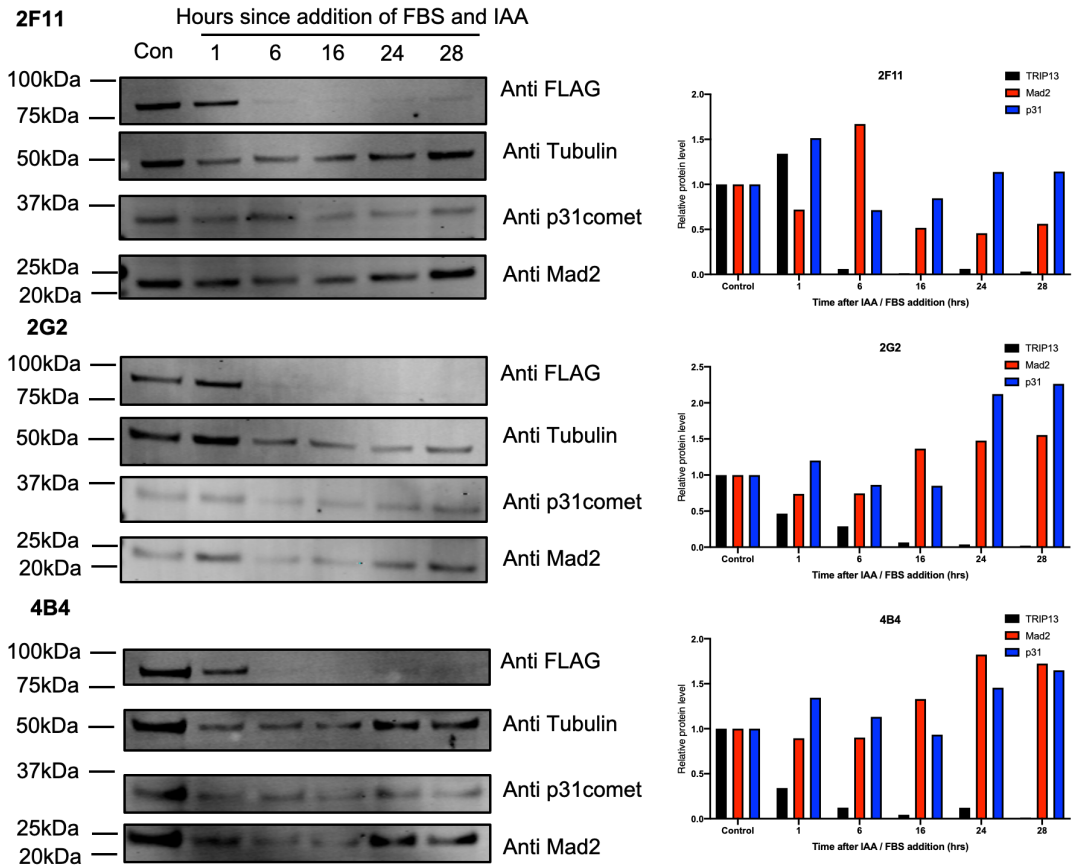

Figure 4-8 Cells released from serum starvation do not clearly upregulate p31^{comet} or downregulate Mad2 levels

Cells were serum starved for 24 hours. Upon re-addition of 20% FBS, IAA was added too. (Dox was added at 20 hours).

In this assay, I did not observe the same trend of increasing p31^{comet} levels and decreasing Mad2 levels, implying that cells have to undergo mitosis where Mad2 p31^{comet} and TRIP13 interact together before any changes to protein levels occur. These data indicate that the conformational switch that Mad2 undergoes during mitosis is likely required for the change in the cellular levels of these proteins.

These data would greatly benefit from a technique that directly separates Mad2 conformations but up to now we have not had any success with published methods, including chromatography separation and conformational specific antibodies.

4.2.4. Acute degradation of TRIP13 changes mitotic timing with or without spindle poisons

The AID system presented a way of assaying the response of the SAC to only TRIP13 loss rather than chronic depletion where the levels of Mad2 and p31^{comet} have also been altered. TRIP13-AID can therefore be used to check whether TRIP13 loss leads to dysfunction of the SAC directly. To do this, I performed time lapse microscopy to assay the strength of the SAC in response to acute loss of TRIP13.

When the 3 clones were treated with IAA for an hour prior to filming all clones had prolonged NEBD-anaphase timing compared to untreated cells, as well as the parental control (IAA untreated: parental = 25min; 2F11 = 29min; 2G2 = 29min; 4B4 = 28min vs IAA treated parental = 25 min; 2F11 = 77min; 2G2 = 81min; 4B4 = 71min respectively. All +- 3 minutes) (Figure 4-9). This implies that TRIP13 is required for normal timing of mitosis in unperturbed conditions. These data could mean TRIP13 has a role in normal SAC inactivation.

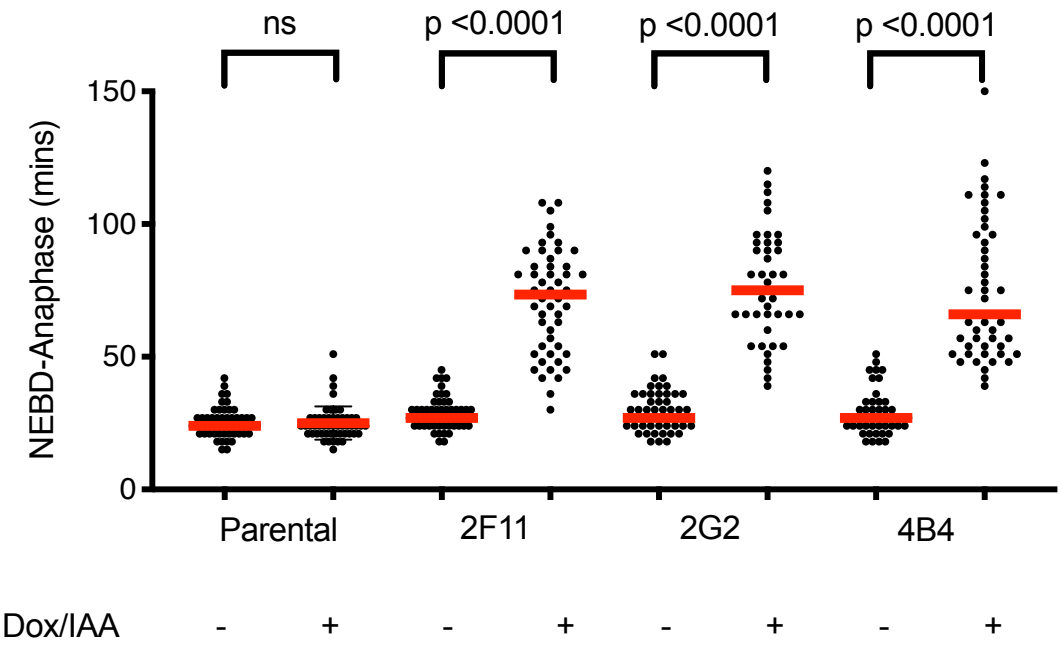

Figure 4-9 NEBD-Anaphase timing is delayed by acute TRIP13 degradation

Cells were treated with doxycycline for 4 hours and IAA for 1 hour before being filmed using 20x air DIC objective on Nikon Widefield microscope. Cells were filmed every 3 minutes. Median value is shown in red. 50 cells were quantified per condition. Experiment was repeated twice. One way ANOVA was used for statistical analysis.

To determine whether TRIP13 had a role in prolonged activation of the SAC, I then repeated the experiment but I added either 0.33μM

Nocodazole, 0.1μM Taxol or 10μM DMA at the same time as I added IAA. Each of these drugs causes prolonged activation of the SAC by interfering with the formation of the bipolar spindle. Nocodazole and Taxol interfere with the polymerisation and depolymerisation of microtubule fibres, respectively, whilst DMA inhibits the motor protein Eg5 that drives the two centrosomes to opposite poles of the cell at the beginning of mitosis. Under all these conditions there are always a number of kinetochores that generate MCC complexes because they do not have properly attached microtubules. Since the SAC is not binary, but rather behaves like a rheostat, this means that it can be activated to different degrees depending on how it is activated. These three conditions all activate the SAC to different extents, with nocodazole being the strongest and taxol the weakest.

However, under all 3 conditions, cells acutely depleted of TRIP13 could not maintain an arrest and the checkpoint was severely compromised. This is shown in figure 4-10. The treated cells underwent mitotic slippage instead of properly dividing in all cases.

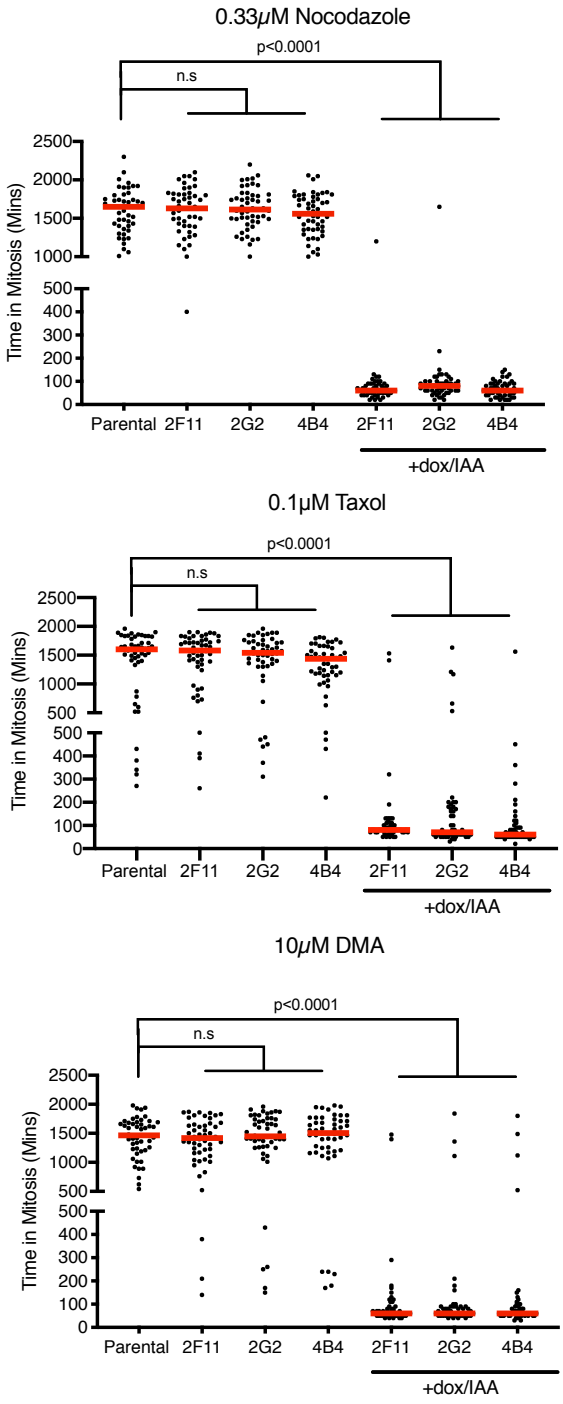

Figure 4-10 Acute TRIP13 degradation in interphase cells causes a defective checkpoint and mitotic slippage in spindle poisons

Cells were filmed and treated as in figure 4-10 but upon addition of IAA, spindle poisons were added at the concentrations shown above each graph. Experiment was performed at least twice. 50 cells were quantified per position and statistical analysis was done as described in figure 4-10. All cells in dox/IAA conditions exhibited mitotic slippage.

I noticed that the delay the clones experienced when treated with IAA in unperturbed conditions was very similar to that observed when the cells

were treated with nocodazole and IAA. I have replotted this data in figure 4-11. This implied that RPE cells still had the ability to activate the checkpoint when depleted of TRIP13, and that TRIP13 is required for the normal timing of mitosis. To confirm this, I treated the WT parental cells and a single clone, 2F11, with Reversine in parallel to IAA treatment. 0.5μM Reversine treatment rescued the TRIP13-AID mediated delay indicating that this delay requires the checkpoint.

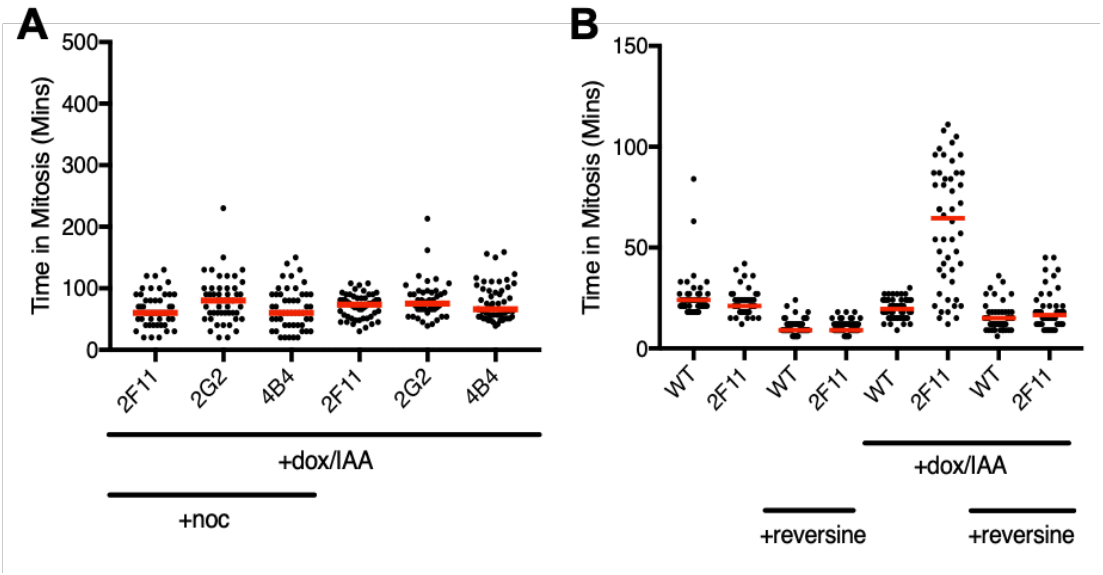

Figure 4-11 There is a minor activation of the SAC after acute TRIP13 degradation that can be inhibited by addition of MPS1 inhibitor

A) The time of all clones after IAA treatment in both NEBD-anaphase timing from figure 4-10 and nocodazole treatment in figure 4-11 is very similar. **B)** Addition of 0.5μM Reversine rescues this delay indicating that this delay is mediated by the SAC.

4.2.5. Acute TRIP13 depletion during mitosis is different to acute depletion during interphase

Since TRIP13 has been implicated in both activation and inactivation of the SAC, I decided to exploit the AID system and deplete TRIP13 during a mitotic arrest and compare this to the previous assays where depletion was done on asynchronous cells, the majority of which were in interphase. In this way, I could bypass SAC activation and deplete TRIP13 in a cell in which the checkpoint was already active.

In order to do this on a high number of cells, I pre-synchronised clone 2F11 cells using serum starvation. One thing that was important to consider was that transcription and translation are heavily repressed during mitosis;

therefore, I added doxycycline at the same time as DMA 4-5 hours prior to mitosis. This ensured that the majority of the cells responded to IAA because they had built up TIR1 levels before entering mitosis.

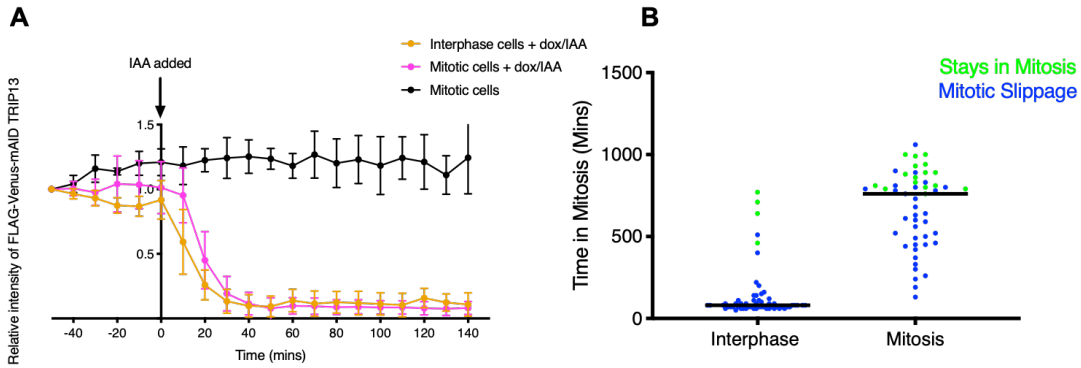

Figure 4-12 Acute TRIP13 degradation does not cause immediate SAC override in cells arrested prior to degradation

A) The time taken for TRIP13 to degrade in arrested mitotic cells is very similar to the time taken in interphase cells. Experiment was performed and quantified as described in figure 4-5. **B)** The time taken for cells to exit mitosis was measured. Black line represents the median. Experiment was performed at least 3 times.

I first measured whether TRIP13 degradation in arrested cells was comparable to interphase cells (Figure 4.12A). Both interphase cells and mitotic cells degraded TRIP13 with similar kinetics. I then measured the time in mitosis of cells depleted of TRIP13 when they were arrested in DMA and observed a very different phenotype when TRIP13 was depleted in mitosis rather than interphase. Cells depleted during DMA arrest did not slip out of mitosis but rather remained for a variable amount of time. On average the time remaining in mitosis was at least 10-fold longer.

It is important to consider effects on Mad2 and p31^{comet} levels during these experiments. I specifically analysed cells that divided at the beginning of the movies as they would not have time to adapt to TRIP13 by altering their p31^{comet} levels or Mad2 levels. In the case of the cells depleted in interphase just before mitosis the loss of TRIP13 had an immediate effect and the cells experienced mitotic slippage. In cells where TRIP13 was depleted during mitosis the I cannot rule out that changes in p31^{comet} or Mad2 levels might contribute to the cells eventually slipping out of mitosis.

4.2.6. TRIP13 does not localise to the kinetochore during mitosis

TRIP13 has been reported to localise to the kinetochore (Tipton et al. 2012) but my tagged FLAG-Venus-mAID-TRIP13 construct did not; rather, it localised everywhere in the cell except on chromatin (Figure 4-4 and 4-5). To check that my tag did not interfere with the correct localisation of TRIP13, I assayed TRIP13 localisation using immunofluorescence (Figure 4-13). I used two different TRIP13 antibodies on parental cells arrested in DMA for 6 hours then fixed with methanol or paraformaldehyde, with or without pre-extraction, and co-stained with CREST. Consistent with my live cell imaging experiments I could not see TRIP13 at the kinetochore with any of these conditions.

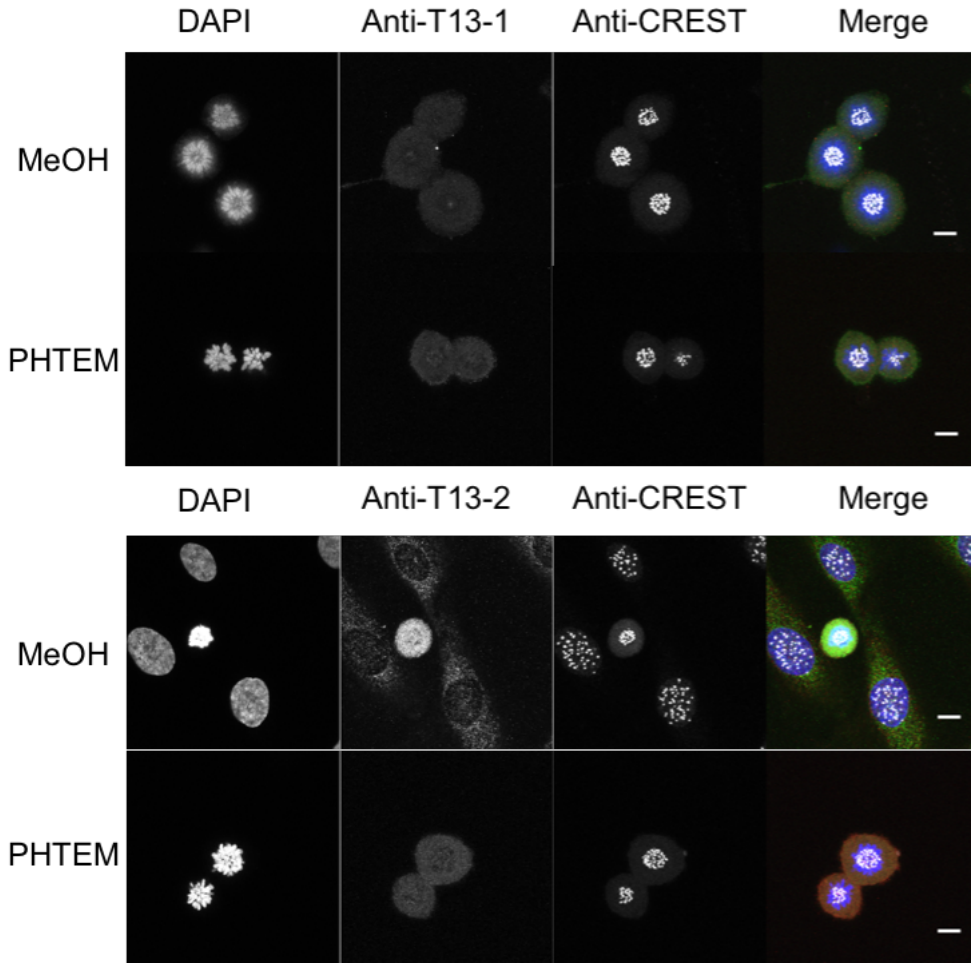

Figure 4-13 Immunofluorescence analysis of parental cells suggests endogenous TRIP13 localisation is not normally at the kinetochore

All cells were arrested in DMA for 5 hours prior to fixation. Cells were fixed in either PHTEM or MeOH then stained in the same way with 2 separate TRIP13 antibodies in parallel to CREST to detect centromere/kinetochores in the cell.

4.3. Discussion

In this chapter I analysed the effect of acutely removing TRIP13 from RPE1 cells using an improved AID system expressing TIR1 from the ROSA26 safe harbour locus. In 3 separate homozygote knock-in clones I found that the majority of TRIP13 was depleted in the vast majority of cells in under an hour after adding IAA.

When TRIP13 was depleted for longer time periods - 16 hours or more - the levels Mad2 and p31^{comet} also changed. Mad2 levels were reduced by up to 50% and p31^{comet} levels increased by over 100%. This behaviour has been observed previously in TRIP13 -/- knock out cells (Ma & Poon 2016). Here I have shown that this is not a result of adaptation as it occurs rapidly; therefore, TRIP13 levels are important for the levels of Mad2 and p31^{comet}. Mad2 has two conformations and only the closed conformation readily interacts with TRIP13 and p31^{comet}. Closed Mad2 is generated at the kinetochore and TRIP13 and p31^{comet} act together to convert it back to open Mad2. Thus, when TRIP13 is depleted, closed Mad2 should accumulate and bind p31^{comet}. Since there is more Mad2 in the cell than p31^{comet}, I suggest a model whereby p31^{comet} is stabilised by binding closed Mad2, but the remaining unbound closed Mad2 is less stable, which would lead to an overall reduction in its level. This hypothesis is supported by data showing that more p31^{comet} is bound to Mad2 in TRIP13 KO cells (Ma & Poon 2016) but to support my hypothesis I would need to measure directly the amount of open and closed Mad2 in cells. It has also been shown that Mad2 recruitment to the kinetochore is impaired in MVA patient derived cells with a TRIP13 mutation p.Arg354X (Yost et al. 2017). This mutation prevents translation of TRIP13 protein due to mRNA decay. I did not specifically examine the levels of Mad2 at unattached kinetochores during my studies however, this observation could also be due to a general reduction in the total Mad2 population.

I have examined how the SAC responds to acute removal of TRIP13 using live-cell microscopy. Both reduction of Mad2 and increase in p31^{comet} levels have been shown to lead to changes in SAC behaviour; therefore, I sought to eliminate this variable by measuring cells as soon as they were depleted of TRIP13. I showed that TRIP13 removal delays cells in unperturbed mitosis, but prevents cells from arresting for long periods when challenged with spindle poisons. In both assays, cells depleted of TRIP13 remain in mitosis between 50-90 minutes on average, and this delay depends on the SAC because it is eliminated by adding an MPS1 inhibitor.

By contrast, depleting TRIP13 in mitosis rather than in interphase leads to different SAC behaviour. Cells already in a checkpoint arrest do not require TRIP13 to maintain it and remain in mitosis nearly 10x longer than cells which lost TRIP13 prior to going into mitosis.

During my studies with the TRIP13-AID system, two other labs also produced papers focusing on the response of the checkpoint to acute TRIP13 depletion (Ma & Poon 2018; D. H. Kim et al. 2018). These studies largely agreed with my own in that acute depletion of TRIP13 was required for a proper mitotic arrest. Both of these studies went on further to conclude that TRIP13 loss led to an imbalance in the levels of open and closed Mad2, and that TRIP13 depletion could be rescued by ectopic expression of Mad2 because Mad2 is synthesised in the open conformation.

Kim et al suggested that acute TRIP13 depletion of one hour leads to a mild arrest due to the formation of the MCC in interphase; however, this contradicts the work of Ma and Poon who suggested that formation of the MCC is not impaired when TRIP13 is lost. My own results show TRIP13 is not required for activation of the checkpoint because the subsequent delay can be reversed by inhibition of MPS1 kinase. Indeed, the difference in mitotic timing observed by Kim et al could also be due to the fact that Mad2 and p31^{comet} levels will be different after 1 and 16 hours of TRIP13 depletion.

Another factor could be that these studies were completed in different cell lines. Whilst I depleted TRIP13 in a non-transformed, chromosomally stable RPE1 background, the published studies were completed in DLD1 and HeLa cells, both of which are aneuploid. Another minor difference is

that both these studies use the full-size AID tag. Ma and Poon also generated their cells using a different strategy to that followed by me and by Kim et al in that HeLa cells were subjected to CRISPR to knock out the endogenous TRIP13 before being infected with TRIP13-AID. Taken together these small variations could explain some of the minor phenotypic differences observed.

Overall my results combined with published data point towards a model whereby TRIP13 recycles Mad2 to be used in a prolonged a SAC arrest. In normal cells the population of Mad2 will be open and when the SAC is activated it will be converted to closed to generate the MCC and TRIP13 will be free to convert closed Mad2 back to open. In cells rapidly depleted of TRIP13, this no longer occurs and leads to all the Mad2 becoming closed. Closed Mad2 alone cannot be used to generate more MCC which is required in a prolonged arrest. My TRIP13-AID system supports this model as there is an initial checkpoint response but cells cannot hold this arrest. This could be due to the fact that all the Mad2 in the cell is converted to closed in this time and as MCC is no longer generated the cells slip back out of mitosis. This model is supported by Kim et al rescuing TRIP13 defects with Mad2 overexpression.

One unresolved issue that I would like to have pursued but did not have time to explore is that it is generally considered that there are 2 distinct pathways for the MCC to be disassembled: the $p31^{comet}$-TRIP13 pathway and auto-ubiquitination of Cdc20 by the APC/C. It would have been interesting to determine whether the cells could disassemble the MCC when both TRIP13 and Cdc20 ubiquitination were inhibited. Kim et al addressed this indirectly by inhibiting APC15 using siRNA and showed that cells depleted of TRIP13 never exited mitosis.

Given these competing studies, and how well TRIP13 has now been studied in-vitro and at a structural level, I decided to focus my time on a new protein for the remainder of my PhD.

5. Using AID to characterise the role of CEP57 in mitosis

5.1. Introduction

In the previous chapter I characterised the acute degradation of TRIP13 using the AID system in the RPE1 ROSA26/osTIR1 cell line system. I showed that degradation in this system is rapid and homogenous for TRIP13 and that acute degradation leads to a phenotype very similar to the one observed in TRIP13 KO RPE1 cells. Mutations in TRIP13 have been associated with. Mosaic Variegated Aneuploidy syndrome (MVA), and now that I had validated the AID using TRIP13 as a proof of principle, I decided to use the system to analyse CEP57, another gene implicated in MVA. MVA typically presents phenotypically with a variety of abnormalities including, but not limited to, growth retardation, microcephaly, and developmental delay (Dery et al. 2020). A subset of cells taken from patients are aneuploid and around 1/3 of MVA patients develop cancer. MVA is an extremely rare autosomal recessive disease with around only 50 individuals characterised worldwide. Mutations in TRIP13 or BUB1B or CEP57 are the most commonly mutated genes identified accounting for nearly 50% of the total cases so far. Most recently mutations in CENATAC, a minor spliceosome component, have been shown to lead to MVA through its regulation of the retention of A-type introns in a specific subset of genes, including some that regulate chromosome segregation (de Wolf et al. 2020.).

Thus far, nearly all the MVA genes identified have a well-defined function in the SAC and therefore likely maintain genome stability in this way. The contributions of the TRIP13 and BubR1 proteins to the SAC, as well as to correct kinetochore-microtubule attachment in the case of BubR1, are well described in the literature (Kim et al. 2018; Ye et al. 2015; G. Zhang et al. 2016; Di Fiore et al. 2016); however, there are limited data on what the protein, CEP57, does on a molecular level.

Initially CEP57, also named Translokin, was reported to regulate the growth factor FGF2 as an intracellular trafficking protein (Bossard et al. 2003). Since then CEP57 has been implicated in many cellular processes that could affect the accuracy of mitosis including: microtubule dynamics, the spindle assembly checkpoint, centriole biogenesis, centriole disengagement, and cytokinesis (Wu et al. 2012; Zhou et al. 2016; Watanabe et al. 2019)

CEP57 has been linked specifically to the SAC through a reported interaction with Mis12 at the kinetochore and with Mad1(Zhou et al. 2016). SiRNA depletion of CEP57 led to a decrease in Mad1 and Mad2 at the kinetochore, which in turn led to changes in the strength of the SAC as measured by the length of mitosis in response to spindle poisons. The authors suggest this weaker SAC response could be the reason for CEP57 loss leading to aneuploidy (Zhou et al. 2016). Xenopus CEP57 has also been shown to localise to the kinetochore (Emanuele & Stukenberg 2007). Most recently, depletion of CEP57 by siRNA has been implicated in the timing of centriole disengagement (Watanabe et al. 2019). In direct contrast to the previous literature, this report saw no change in SAC timing when CEP57 was depleted and also claimed that CEP57 localised to the centrosome rather than the kinetochore.

Abnormal centriole behaviour has also been reported in mouse studies where a CEP57 MVA mutant was expressed. Homozygous CEP57 knockout embryos did not survive to term; however, a homozygous truncation mutant mimicking one MVA patient survived to term but died soon after (Aziz et al. 2018). The study concluded that these mice did not produce a CEP57 product. So far 11 individuals have been identified with CEP57 mutations(Lane et al. 2002; García-Castillo et al. 2008; la Torre-García et al. 2019; Aziz et al. 2018; Brightman et al. 2018). All of these mutations are spread throughout the gene and lead to premature termination codons (PTCs). However, cancer has not been reported in any of the CEP57 individuals despite 75% incidence in individuals with BUB1B mutations.

Due to these conflicting reports, I chose CEP57 as an ideal candidate to analyse using AID and study the behaviour of cells after both short term

and long-term depletion. I hypothesised that acute depletion of CEP57 using AID would be a good proxy for studying how CEP57 loss leads to aneuploidy. I also hoped to understand more about the true localisation of CEP57 by studying fluorescently tagged CEP57 expressed from the endogenous locus.

In this chapter I show that, in agreement with recent literature, (Watanabe et al. 2019), AID mediated depletion of CEP57 affects the normal timing of centriole disengagement but does not have a clear role in the SAC in human cells1.

5.2. Results

5.2.1. Generation of FLAG-Ruby-CEP57 and FLAG-Ruby-mAID-CEP57 clones

To begin with, I targeted the 5' end of the first exon of CEP57 using CRISPR/Cas9 using the strategy described previously in figure 3-2. To do this, I designed and assembled repair templates containing homology arms amplified from RPE1 genomic DNA and the FLAG, mRuby, and miniAID cassettes using Gibson cloning. As there were no suitable guides in the first exon, I inserted two sgRNAs that targeted the first intron of CEP57 into the All-in-One Cas9 D10 nickase plasmid. The PAM sequences in the repair template were modified to reduce the likelihood of re-cutting after successful HR events.

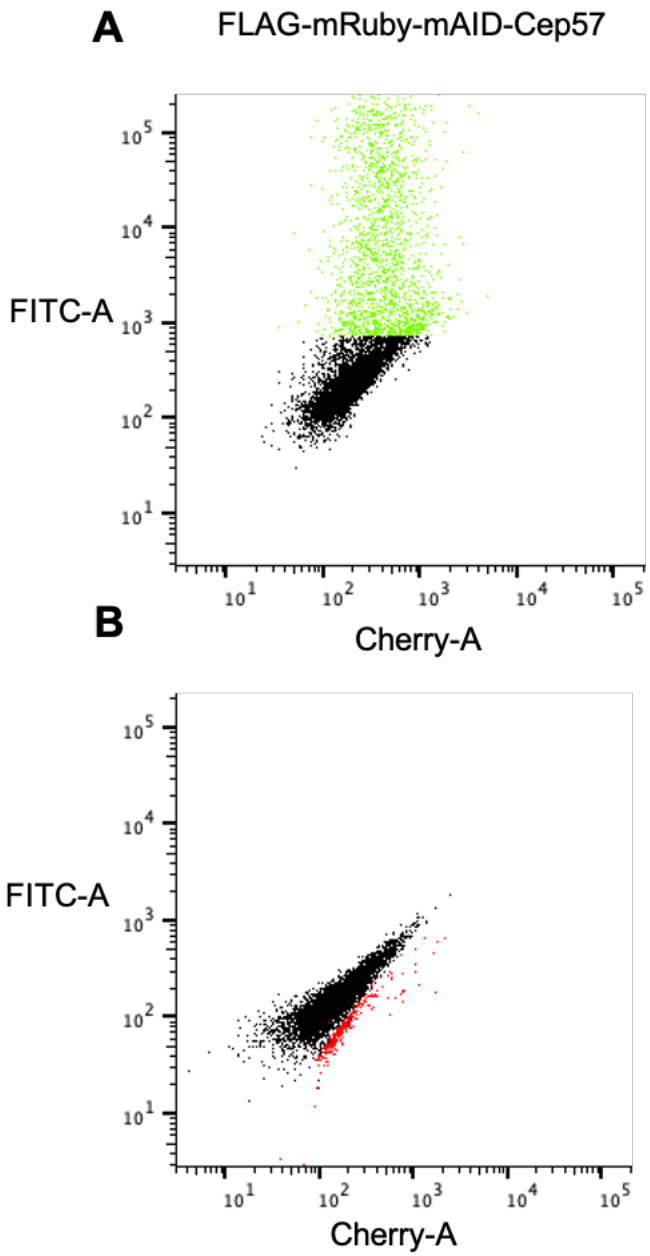

Figure 5-1 FACS profiles for the generation of FLAG-mRuby-mAID-CEP57 clones

A) Bulk sort for Cas 9 positive cells using GFP as a marker. Cells in green were bulk sorted into a 6 well plate for further expansion **B)** Potential FLAG-mRuby-mAID-CEP57 clones are visualised in red using indexed sorts. Unsorted control cells are shown in black in both **A)** and **B)**.

As before, these plasmids were co-transfected and sequentially sorted using FACS (figure 5-1). Homozygote clones were assessed by PCR and validated by sequencing. In this chapter I have characterised the following 3 FLAG-mRuby-mAID-CEP57 clones: 1B1, 1F8 and 1H2.

First, I confirmed fusion protein expression using western-blotting (figure 5-2). The fusion protein's predicted molecular mass is 94kDA (3xFLAG: 3kDa, mRuby: 25kDa, mAID: 9kDa and CEP57: 57 kDa).

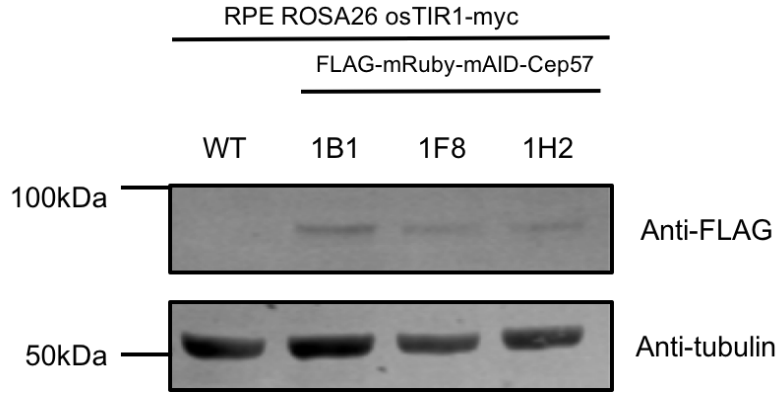

Figure 5-2 Fusion band expression of FLAG-mRuby-mAID-CEP57 in 3 homozygote clones

3 clones identified by PCR and sequencing were immunoblotted for anti-FLAG. Tubulin is used as a loading control.

In the previous chapters, I used both anti-TRIP13 antibodies and anti-FLAG antibodies and whilst the anti-TRIP13 antibodies didn't recognise my fusion protein they allowed me to conclude that there was no detectable expression of wild-type TRIP13 in these cell lines.

I attempted to detect CEP57 directly using several commercial antibodies and antibodies from the previous literature. However, I did not detect proteins of the expected molecular mass with any of these (data not shown). Therefore, I attempted to raise my own antibody using synthesised peptides. In total, 4 peptides were synthesised: 2 from sequences close to each terminus of CEP57. The peptides were paired as shown below and injected into 2 rabbits each in order to increase the likelihood of an immune response; however, after extensive testing of both the sera and affinity purified fractions, I did not find a suitable antibody to use.

5.2.2. Localisation of CEP57

I used confocal time-lapse fluorescence imaging to determine where the CEP57-AID localised. By immunofluorescence, CEP57 had been reported to localise to the centrosome as well as kinetochores during mitosis (Zhou

et al. 2016; Wu et al. 2012). Fluorescently labelled CEP57 fragments have been expressed exogenously and showed that the N terminus of CEP57 localises to the centrosome and the C terminus localises to microtubules (Momotani et al. 2008). Since I had tagged CEP57 using CRISPR/Cas9 in the endogenous locus, I hoped to go one step further in understanding its localisation throughout the cell cycle.

Figure 5-3 shows stills of CEP57-AID clones in different cell cycle phases. All clones had single or double foci in all cell cycle phases. During the cell cycle these foci behaved as expected for centrosomes, separating prior to mitosis and migrating to the spindle poles after nuclear envelope break down. I later confirmed this directly by co-expressing Centrin-GFP as a centriole marker (see figures 6-5, 6-6 and 6-7 below).

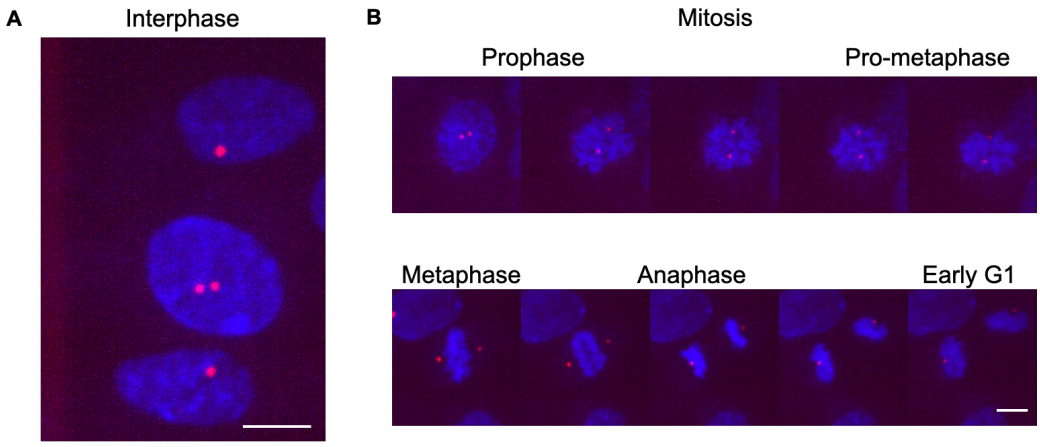

Figure 5-3 Endogenously tagged CEP57 localises to the centrosome in all cell cycle phases

1B1 clone cells were filmed using a 63x oil objective on a confocal spinning disc microscope (3i). Prior to filming 50nm sirDNA was added to visualise DNA. Maximum projection images are shown of 25 0.5µM stacks. sirDNA = blue. FLAG-mRuby-mAID-CEP57 = red. **A)** In interphase cells one or two foci were observed in all cells. More than two foci were never observed. **B)** In mitosis these foci exhibited typical centrosome behaviour moving to the spindle poles after separating prior to NEBD. Scale bar in **A)** 10µm **B)** 5µm. All cells in all clones exhibited the same localisation (data not shown for 1F8 and 1H2).

5.2.3. Characterisation of CEP57-AID

Next, I characterised the AID mediated degradation of CEP57 in all 3 clones by adding doxycycline for 4 hours to induce TIR1, followed by IAA and imaging as described previously in chapters 3 and 4. The half-life of CEP57-AID was 170mins, 135mins, and 100mins in clones 1B1, 1F8, and

1H2 respectively. The difference in these values may be due to the heterogeneous behaviour in the individual cells' degradation tracks. On average the levels of FLAG-mRuby-mAID-CEP57 were comparable to background levels after 4 hours in all 3 clones (figure 5-4B).

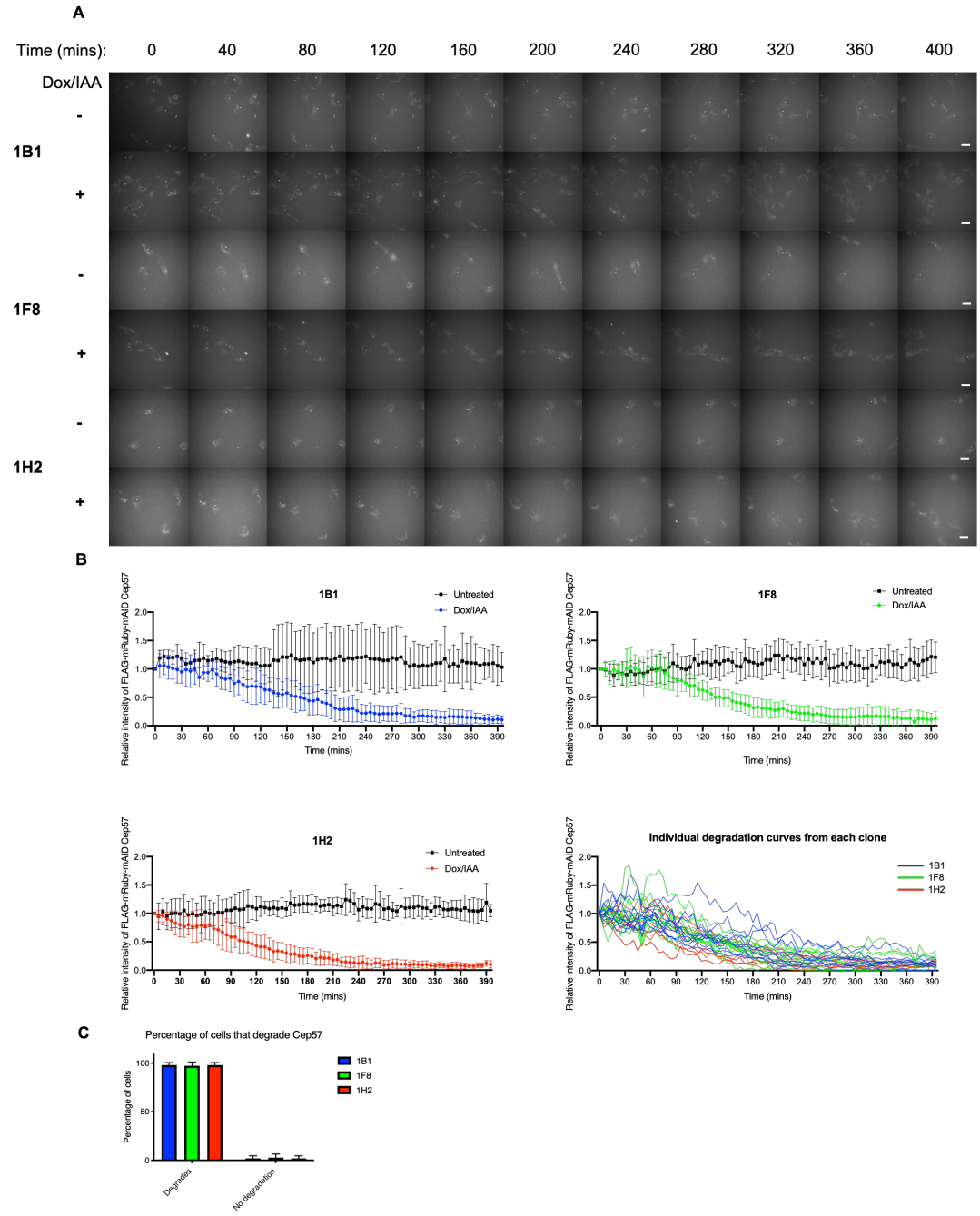

Figure 5-4 Single cell degradation of FLAG-mRuby-mAID-CEP57

A) Each clone was left untreated or treated with doxycycline for 4 hours prior to filming. IAA was added at the 11th frame. Cells were filmed using a 40x air objective and EMCCD camera on a Deltavision Widefield microscope. Images were taken every 5 minutes, every 8th frame is shown here. **B)** Quantification of **A).** After IAA addition, intensity of centrosomally localised CEP57 reaches undetectable levels after 3-5 hours in all clones as shown by average intensity for each clone or single cell degradation tracks. 10 cells were analysed for each condition. Images were quantified manually using FIJI software. Max intensity was normalised to background max intensity, area and the first time point. **C)** The percentage of cells which degraded CEP57 is shown. 100 cells per

condition were analysed by eye. The graph shows an average of 3 repeats. (See Appendix C for larger images.)

Only 10 cells were counted for each condition in figure 5-4B. In figure 5-4C I counted the number of cells qualitatively after 4 hours with visible CEP57 foci and concluded that after 4 hours nearly all cells had degraded CEP57. I then performed western blot analysis staining for FLAG-mRuby-mAID-CEP57 using anti-FLAG and could also no longer detect tagged CEP57 5 hours after adding IAA. Therefore, I decided to proceed with these conditions in my future experiments.

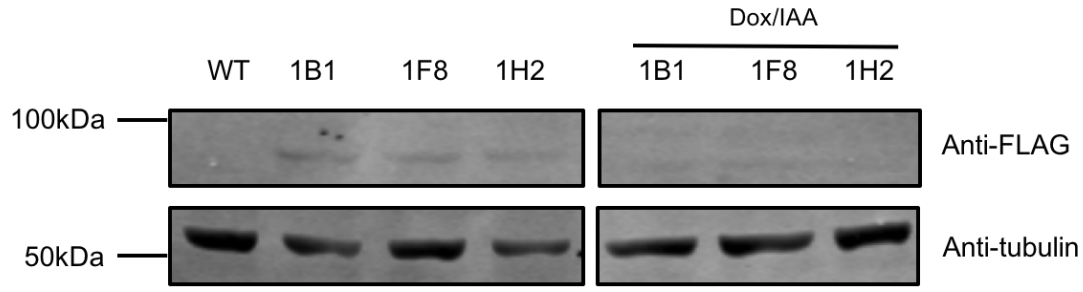

Figure 5-5 CEP57 is undetectable by immunoblotting after 5 hours of IAA treatment

Cells were treated for 4 hours with doxycycline followed by 5 hours of IAA. FLAG tagged CEP57 was no longer detectable after IAA treatment. Tubulin was used as a loading control.

5.2.4. Acute depletion of CEP57 does not affect mitotic timing

Now that I had optimised conditions for CEP57 degradation I started to investigate how removing CEP57 affected mitosis. Despite seeing no localisation to the kinetochore during mitosis, I assessed whether CEP57 plays a role in the SAC by measuring mitotic timing with and without AID mediated destruction of CEP57. As described in the previous chapter for TRIP13, perturbations to the levels of SAC proteins usually changes the ability of a cell to progress through mitosis or to maintain an arrest when microtubule dynamics are altered.

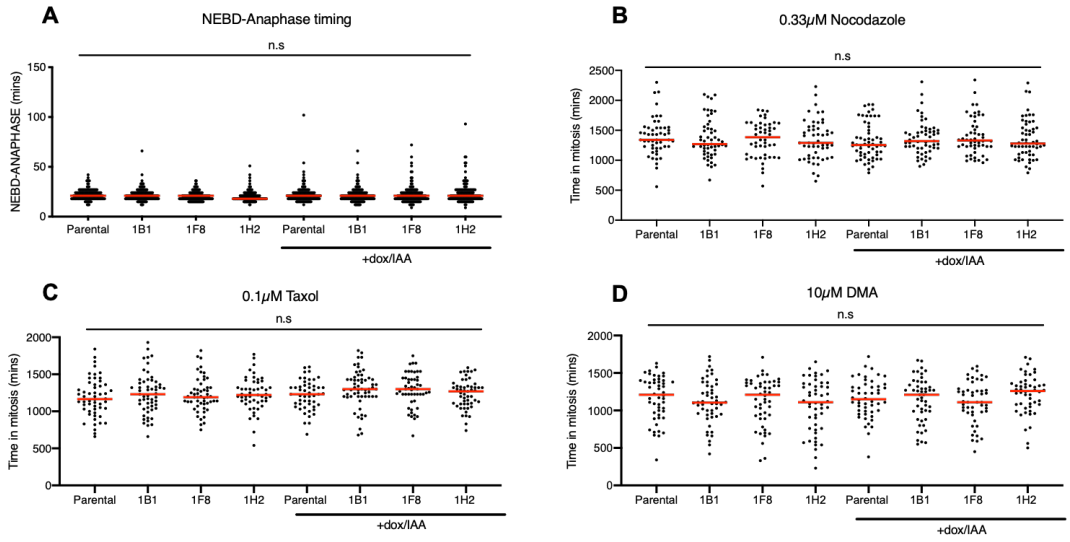

Figure 5-6 Acute depletion of CEP57 does not affect the progression of mitosis in unperturbed or SAC-activated conditions

In all assays, cells were either left untreated or treated with doxycycline for 4 hours followed by IAA for 5 hours. For assays including spindle poisons, this was added after IAA treatment just prior to filming. For **B)** 0.33μM Nocodazole; **C)** 0.1μM Taxol or **D)** 10μM DMA. Cells were filmed on a Nikon Widefield Microscope using a 20x air DIC objective. For **A)** cells were imaged every 3 minutes and for **B-D** every 10 minutes. Red bars represent median. Experiments were repeated once. At least 50 cells were quantified per condition.

I filmed CEP57-AID clones using DIC microscopy, as described above. I depleted CEP57 by adding doxycycline for 4 hours and then IAA for 5 hours and used each untreated clone as a control (figure 5-6). In both unperturbed (5-6A) and SAC activated conditions (5-6B-D), I observed no significant change to the length of mitosis when CEP57 was acutely depleted.

In figure 5-6 I was looking at asynchronous cells with only 5 hours of depletion. I filmed for 20 hours but prioritised looking at cells that went into mitosis at the beginning of the movies. Previous reports showing changes or no changes to mitotic timing had used siRNA against CEP57(Zhou et al. 2016; Watanabe et al. 2019). SiRNA typically takes at least 48 hours to deplete the relevant mRNA and in turn reduce the levels of the corresponding protein. Therefore, these assays look at cells that have progressed through up to 2 cell cycles in this time. To replicate these conditions with my system, I repeated the experiment but this time I depleted CEP57 for 24 hours or 48 hours respectively (figure 5-7). I confirmed CEP57 levels were still depleted by eye at the beginning of filming. However, I observed no significant changes in mitotic timing for

unperturbed cells or DMA arrested cells after either 24- or 48-hour IAA treatment. Since I do not observe CEP57 localisation at the kinetochore nor changes in mitotic timing, I conclude that CEP57 is unlikely to have a role in the SAC.

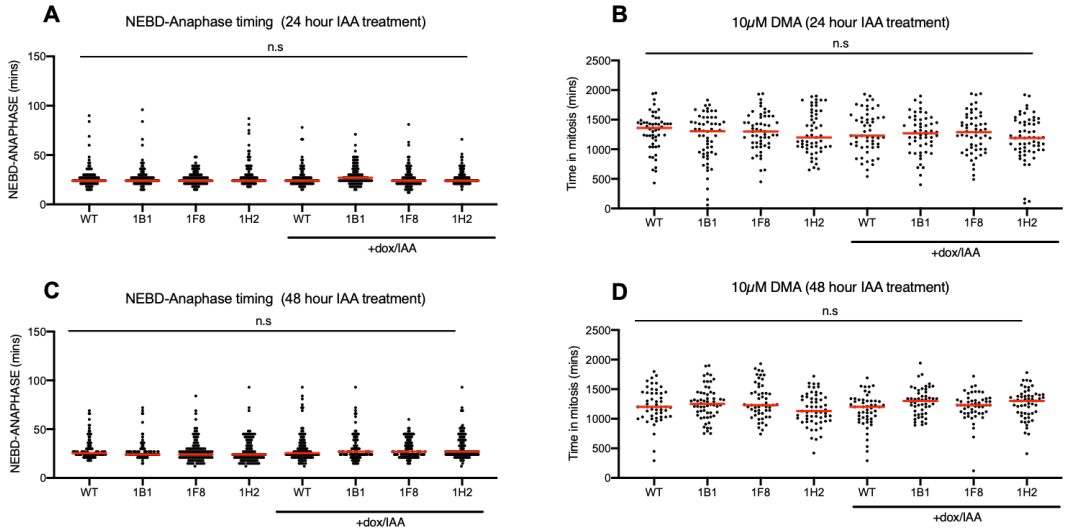

Figure 5-7 Depletion of CEP57 for 24 or 48 hours does not affect the progression of mitosis

In all assays, cells were either left untreated or treated with doxycycline for 4 hours followed by IAA for 24 or 48 hours. For assays including DMA this was added after IAA treatment just prior to filming (**B)** and **D)**) Cells were filmed on a Nikon Widefield Microscope using a 20x air DIC objective. For **A)** and **C)** cells were imaged every 3 minutes and for **B) and D)** every 10 minutes. Red bars represent median. Experiments were repeated once. 100 cells per condition were analysed in NEBD to Anaphase timing and 50 per condition for DMA experiments.

5.2.5. Acute depletion of CEP57 causes mild genome instability

When I filmed cells depleted of CEP57 with DIC I did not observe any major mitotic defects. Therefore, I filmed the cells again and added 50nm sirDNA for 3 hours prior to filming to see whether I could detect lagging chromatin (Watanabe et al. 2019). I also quantified the percentage of tripolar spindles observed as well “asymmetric divisions”. An example of an asymmetric division is shown in the panels of figure 5-8A. These cells had greater than two masses of DNA separating around metaphase but ultimately divided into 2 cells. Tripolar spindles resulted in 3 cells. In figure 5-8A, the graphs show that the percentage of tripolar spindles and asymmetric divisions

increased upon depletion of IAA for 4 hours or 24 hours; however, the percentage of lagging chromosomes did not increase in either condition, as previously reported (Watanabe et al. 2019). This was consistent in all 3 clones.

Figure 5-8B shows flow cytometry where the proportion of cells with 2n, 4n or >4n DNA using propidium iodide staining was measured. For this experiment, I depleted CEP57 for either 7 or 14 days, replenishing the doxycycline and IAA every 3 days. In all 3 clones, I observed a small population of >4n cells at both 7 and 14 days.

Finally, in figure 5-8C I quantified the number of chromosomes per cell using metaphase spreads. I performed this experiment once upon parental cells as well as clone 1B1 +/- IAA for either 1 day or 14 days. After 14 days, I observed sporadic cells with random gains and losses of chromosomes as shown by the two examples in 5-8C. It is important to note that both the PI staining and metaphase spreads have not been repeated but all 3 of these assays clearly point to aneuploidy developing after acute CEP57 depletion.

A) Quantification of mitotic errors observed by time-lapse imaging. CEP57 was depleted as previously described (5-6 or 5-7) however, 50nM SiR-DNA was added to media for 3 hours prior to filming and washed out when media was changed to filming media. Cells were filmed using a 40x oil objective on a Nikon Widefield Microscope. 8 3μM stacks were taken per image in order to visualise mitotic cells. Images were taken every 2 minutes. Representative maximum projection images of mitotic errors are shown on the panels to the right. Experiments were repeated at least twice, 300 cells were counted per condition. **B)** Flow cytometry analysis of CEP57 depleted cells. Cells were treated with doxycycline/IAA as indicated and collected for PI staining. Cells were gated in order to visualise >4n populations**.** In all clones, a small population of cells was observed with greater than 4n DNA content indicating mitotic division failure. Experiment was not repeated. **C)** Example images of metaphase spreads stained with DAPI from cells with more than 46 chromosomes: 58 and 48 respectively. Graphs show individual experiments where CEP57 was depleted in clone 1B1 for either a day or 14 days before cells were enriched using colcemid and processed for spreads. Number of cells counted, n, is shown underneath each condition on the graphs. CEP57 was depleted throughout both **B)** and **C)** by re-addition of doxycycline and IAA every 3 days when cells were passaged.

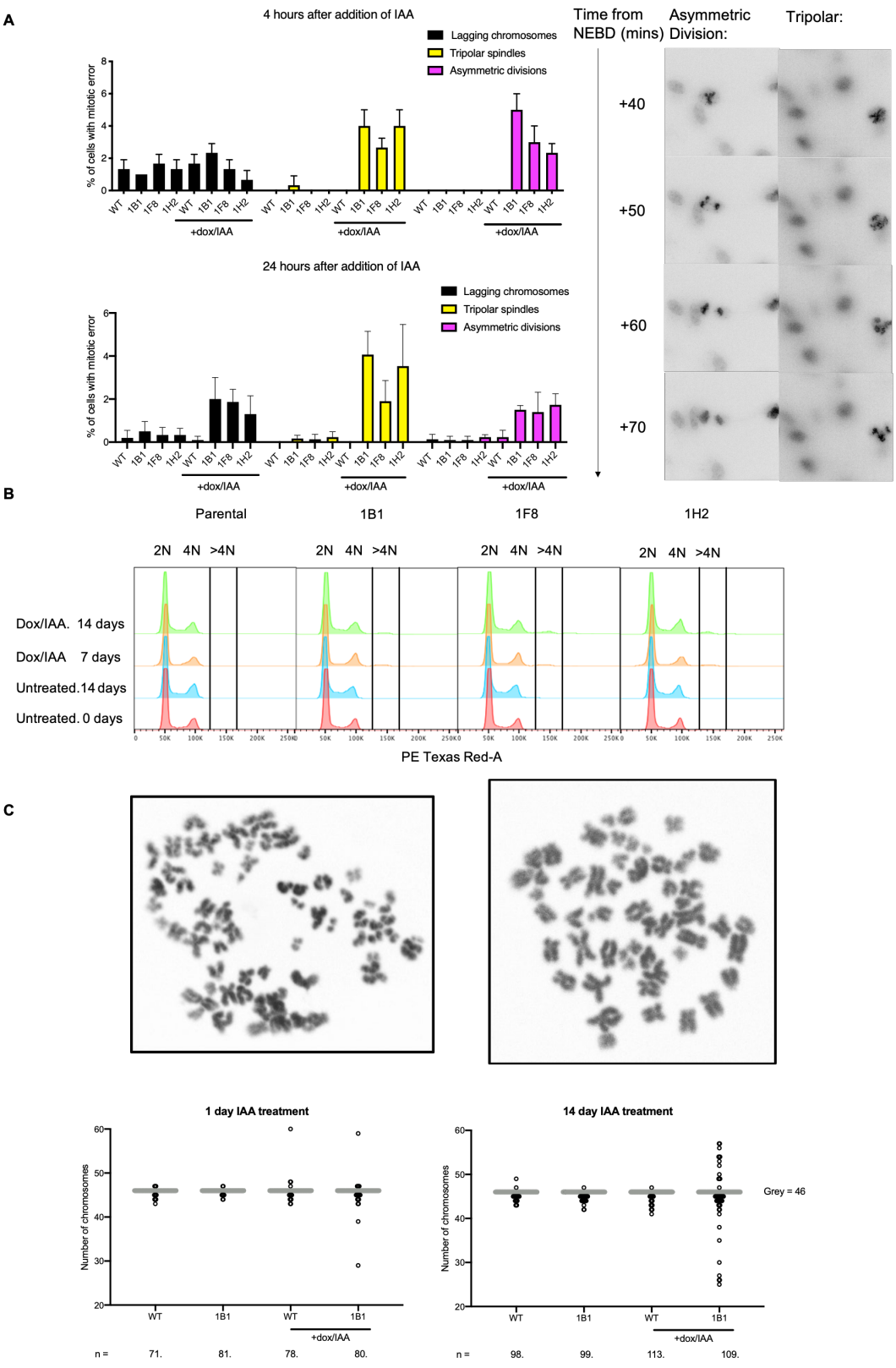

Figure 5-8 Acute depletion of CEP57 leads to mild genome instability (see previous page)

5.2.6. Acute depletion of CEP57 leads to premature centriole disengagement

Now that I had determined that endogenously tagged CEP57 localised to the centrosome and that errors in cell division were not due to aberrant behaviour of the SAC, I investigated whether CEP57 was required for the normal progression of the centrosome cycle. Specifically, I investigated centrosome localisation during mitosis.

I synchronised cells using serum starvation and depleted them of CEP57 before cells started to enter mitosis. I then fixed cells using methanol and performed immunofluorescence staining. Initially, I used anti-FLAG to determine CEP57 localisation and depletion and observed centrosome localisation throughout the cell cycle in all three clones. CEP57 had been previously reported to localise to microtubules when overexpressed (Momotani et al. 2008) and I noticed some weak localisation to the mitotic spindle that I did not see in my live cell imaging (figure 5-3); therefore, I co-stained with anti-beta-tubulin plus anti-FLAG. This confirmed that CEP57 weakly localises to the spindle as well as the centrosome (figure 5.9). In CEP57 depleted cells, some cells did not form bipolar spindles (figure 5.9; plus dox/IAA). (Panels show representative cells from all clones.) As in my live cell assays, depletion of CEP57 leads to loss of signal at the centrosome.

Having established robust CEP57 depletion, I asked whether CEP57 depletion caused whether centrioles to become disengaged earlier in mitosis. To do this, I stained for centrioles plus the PCM using anti-CP110 and anti-gamma tubulin, respectively (figure 5-10). In agreement with recent literature, I observed improper localisation of centrioles prior to anaphase indicating that centrioles had become disengaged (figure 5-10A, +dox/IAA). Centriole disengagement normally occurs later in telophase. Crucially I only found this phenotype in cells depleted of CEP57 (figure 5-10B). These mis-localised centrioles had recruited gamma tubulin and were therefore capable of nucleating microtubules (Kollman et al. 2011), in agreement with previously published microtubule re-growth

assays(Watanabe et al. 2019). This could be an explanation for the observed mitotic division failures in figure 5-8A.

I also observed a very small number of cells that had undergone centriole amplification (figure 5-11A). The percentages of cells with centriole amplification are quantified in figure 5-11B. Centriole disengagement has been reported to be the licensing step for centriole duplication; therefore this observation is a strong indicator that these cells have undergone centriole disengagement (Tsou & Stearns 2006; Tsou et al. 2009).

My results were in agreement with previous literature; however, I observed fewer cells with centriole disengagement than in cells treated with siRNA against CEP57 (figure 5-10B). Watanabe et al had characterised centriole disengagement in their live cell assays as any pair of centrioles from the same centrosome that had an average distance of double that of wild-type (Watanabe et al. 2019); therefore, I measured the distance between centrioles using a semi-automated macro (designed by Dr Luca Cirillo). This was performed in an unbiased way by double blinding the images. I observed that on average centriole pairs were further apart in CEP57-AID cells at metaphase but centrioles were rarely double the distance compared to those in control cells. The centrioles that were more than double the distance were clearly identifiable as disengaged by eye.

In conclusion, my data indicate that CEP57 is involved in centriole disengagement, but not the SAC, and that this is the likely manner by which loss of CEP57 leads to aneuploidy.

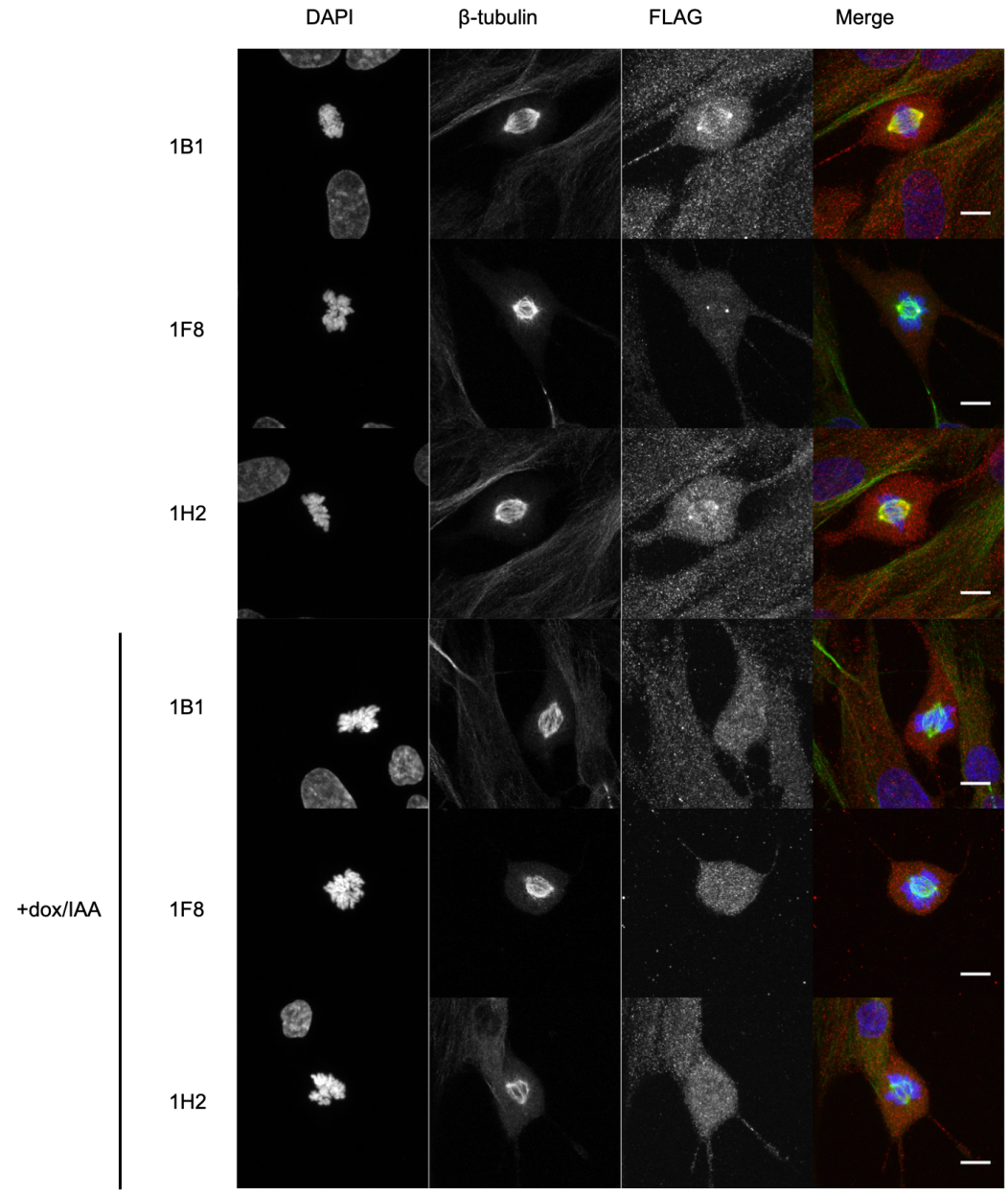

Figure 5-9 CEP57 detection and depletion using immunofluorescence

Panels show representative maximum projected images of CEP57-AID clones stained with anti-FLAG and anti-alpha tubulin. Merge images show DAPI in blue, Tubulin in green and CEP57 in red. CEP57 localises as expected to the centrosome. Some cells have weak localisation on the spindle itself. Alpha Tubulin used as a co-stain for the mitotic spindle. In CEP57 depleted panels, example images show non-bipolar spindles at pro-metaphase/metaphase cells. Cells were filmed using a 63x oil objective on a Leica SP8 confocal microscope. 30 0.3µM stacks were used per image.

Figure 5-10 Depletion of CEP57 leads to mis-localised centrioles prior to the metaphase-anaphase transition

Cells were treated and imaged as described in 5-9. **A)** Anti-CP110 was used as a centriole marker, shown in green, and gamma-Tubulin was used as a PCM marker, shown in red. DAPI is shown in blue. A small population of cells was observed where centrioles did not localise only to the spindle pole and far from their respective partner. These cells also displayed lower amounts of gamma-Tubulin. **B)** Graph shows quantification of 3 experiments.

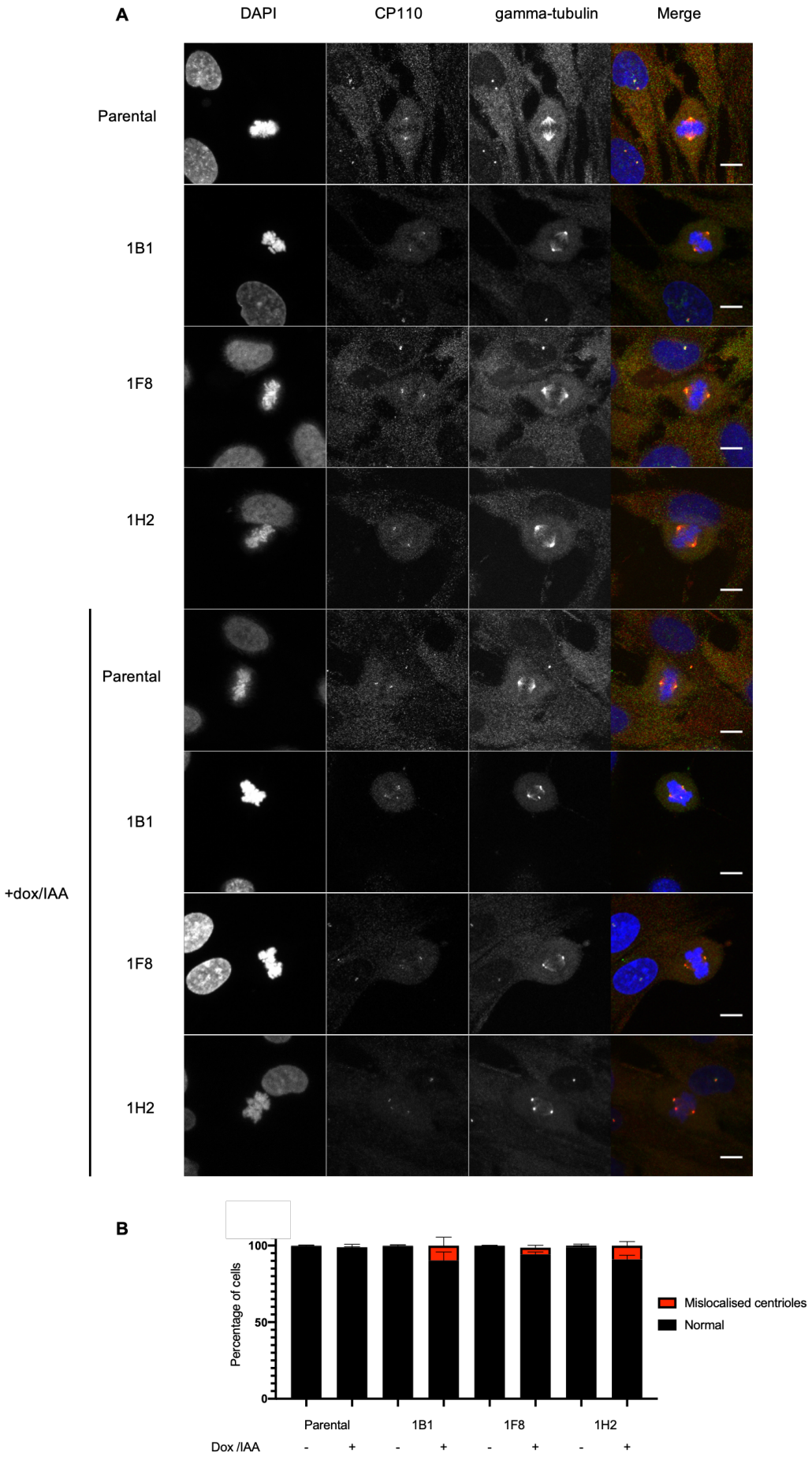
A
DAPI
CP110
gamma-tubulin
Merge
Parental
1B1
1F8
1H2
+dox/IAA
Parental
1B1
1F8
1H2
B
Percentage of cells
100
50
0
Mislocalised centrioles
Normal
Parental
1B1
1F8
1H2
Dox /IAA
- + - + - + - +

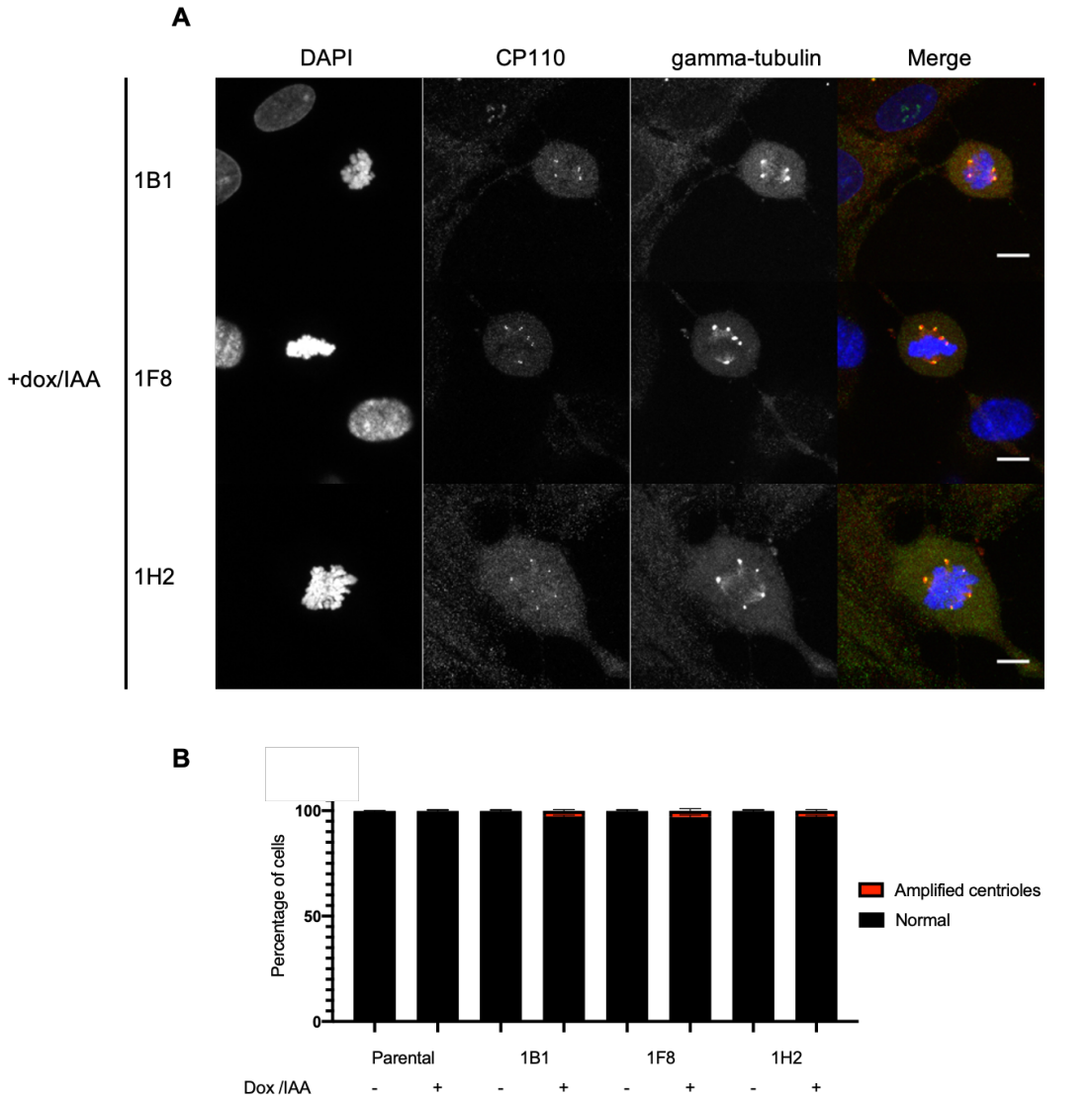

Figure 5-11 Figure 5-11 Centriole amplification is also observed in cells acutely depleted of CEP57.

These images are representative examples from the same assays as figure 5-10.

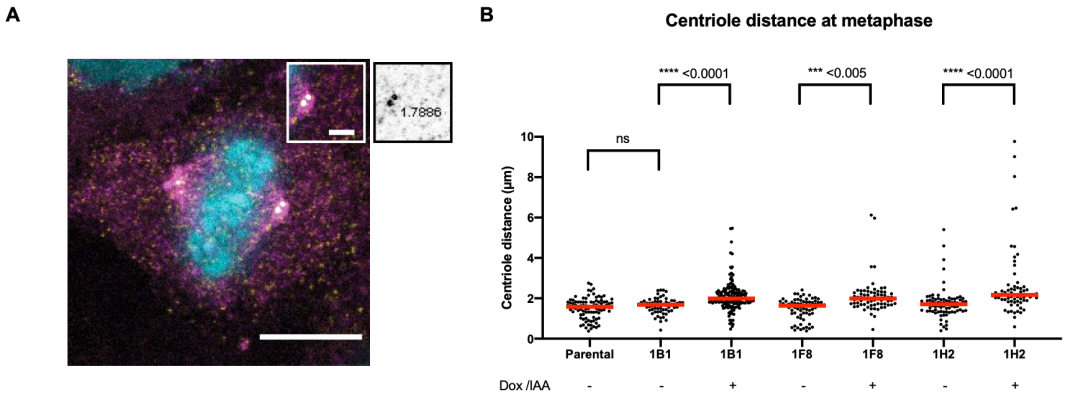

Figure 5-12 The average distance between centrioles at metaphase is higher in CEP57 depleted cells

A) Example image from semi-automated macro designed to measure centriole distance. DAPI is shown in cyan, CP110 in white and gamma-Tubulin in pink. Offset box shows distance in µms. **B)**

Quantification of centriole distance. Experiments were repeated twice. Each condition has at least. 30 cells, 60 pairs of centrioles quantified. ANOVA was used as a statistical test.

5.3. Discussion

In this chapter I have examined the effect of acute depletion of CEP57 on mitosis using 3 individual CEP57 AID clones. I targeted RPE1 ROSA26 osTIR1-myc cells using CRISPR Cas9 to tag CEP57 at the N terminus with FLAG, mRuby and miniAID.

In these clones, I observed either a singular foci or pair of foci per cell that strongly resembled the centrosomes in their behaviour throughout the cell cycle. This is in agreement with previous literature that CEP57 localises to the centrosome. Recent data show specific sub-cellular localisation to the mother centriole but I did not specifically confirm this in my assays; however, in my data I only observed one focus per centrosome during mitosis indicating that it localises to a specific type of centriole.

I did not observe any cells with many foci that co-localise with chromatin during mitosis that would indicate CEP57 localises to the kinetochores, despite previous reports. Moreover, I observed only centrosomal localisation when I stained with FLAG in immunofluorescence assays; therefore, I conclude that CEP57 is only localised to the centrosome throughout the cell cycle.

I found that upon addition of dox/IAA, all three clones degraded CEP57 much more slowly than TRIP13: 5 hours vs 1 hour, respectively, in live cell imaging assays. I also observed that unlike in TRIP13 AID clones, CEP57 seemed to be degraded at different rates in different cells (figure 5-4B). This could indicate that cells have different levels of CEP57 at the centrosome; however, I have not specifically examined this.

It is not surprising that the AID system has the ability to target different proteins to different extents. TRIP13 and CEP57 have distinctly different localisations. Venus-TRIP13 localises throughout the cytosol whereas super resolution microscopy has shown that CEP57 specifically localises to the proximal end of the mother centriole (Lukinavičius et al. 2013). CEP57 may be less accessible to ubiquitin ligases and the proteasome if it is within the PCM or in the body of the centrosome itself. There could

also be different levels of these 2 protein candidates in RPE1 cells, which I was unable to specifically examine due to a lack of antibodies targeting either tagged species.

In future it may be more pertinent to degrade CEP57 faster. One improvement that could be made is adding the SMASh tag as utilised in Lemmens et al where the authors combined 2 separate inducible degradation systems. In this instance the authors could only achieve proper destruction of the target proteins when both small molecules, IAA and Asuvprenir were used to bring the protein into the proximity of E3 ubiquitin ligases. It has also been reported that modifying TIR1 as well as the ligand IAA can improve degradation rates by improving the binding specificity (Nishimura et al. 2020; Sathyan et al. 2020). This system also reduces non-specific degradation in the sole presence of TIR1. However, this system would require the regeneration and recharacterization of all cell lines.

After characterising the degradation of CEP57 I measured mitotic timing to determine whether loss of CEP57 perturbed the SAC in some way. I measured mitotic timing in unperturbed conditions as well as 3 different spindle poisons but did not see any strong changes in timing after 4, 24 or 48 hours of CEP57 depletion.

Given that my data indicate that CEP57 does not localise to the kinetochore or change mitotic timing as previously reported, I believe CEP57 is probably not a SAC protein. However, it isn't a requirement for a SAC protein to localise to the kinetochore, TRIP13 being a prime example. Furthermore, it is possible that CEP57 is just localised to the kinetochore at a specific time point or at such low levels that my microscopy assays did not detect it. Measuring mitotic timing is a robust way of identifying SAC proteins. It has been shown in the case of some SAC enzymes such as Bub1 that they must be depleted to very low levels in order to see an effect. One limitation of my assays is that perhaps the AID system does not deplete CEP57 to a low enough level to see the resulting effect upon the SAC. One way to eliminate any residual CEP57 would be generation of a knock out. However, it has been shown that CEP57 knockouts are lethal in mice and therefore I did not pursue this avenue of work.

When I repeated live cell imaging with sirDNA as a chromatin marker, I did observe mitotic errors at a low frequency in CEP57 depleted cells. The frequency of these errors was extremely low but most frequently seemed to be

spindle errors. It has been shown previously that CEP57 depletion leads to lagging chromosomes; however, I did not observe an increase in these when CEP57 was depleted (figure 5-8A). One reason for this could be the resolution of my images. This assay could be repeated using DAPI staining and immunofluorescence but it is important to point out that throughout my IF assays in this thesis I have not noticed an increase in lagging chromatin. To ask directly whether CEP57 was leading to aneuploidy, I used metaphase spreads to count the number of chromosomes in one clone at 1- and 14-day(s) post degradation and observed cells with both massively increased and reduced numbers of chromosomes. Whilst these assays need to be repeated and performed on multiple clones, this does indicate that CEP57-AID can serve as a mimic for studying the effects of MVA syndrome.

CEP57 was recently implicated in the timing of centriole disengagement, which built on earlier work that showed lots of spindle related errors. I confirmed that premature centriole disengagement occurred upon acute depletion of CEP57. Watanabe et al. used siRNA to deplete CEP57 and observed a much higher frequency of centriole disengagement; however, their definition of centriole disengagement was unclear, defined as any centriole pair with double the average length of wild-type centriole distance. I measured centriole distance and whilst there was a clear increase in average centriole distance between untreated and IAA treated cells, I did not observe the same percentages of abnormal centriole disengagement. This could be due to the method used to deplete CEP57 or the difference in depletion time, or it could be because I used a different assay to observe centriole disengagement.

6. Characterising the role of CEP57 in the normal timing of centriole disengagement

6.1. Introduction

In the previous chapter, I showed that acute depletion of CEP57 did not lead to a clear defect in the Spindle Assembly Checkpoint (SAC) but instead led to premature centriole disengagement during early mitosis. This implicates premature centriole disengagement as a potential cause of the genome instability observed in MVA patients with CEP57 mutations, and that aberrant SAC function is not the only way this condition can manifest.

Centriole disengagement is the process by which the mother and daughter centrioles separate during telophase (Piel et al. 2000). Disengagement licenses centrioles for the next S-phase because without it, centriole duplication cannot occur (Tsou & Stearns 2006; Nigg 2007; Fong et al. 2018). Separase and Plk1 have been shown to be key regulators of this process as centriole disengagement is completely blocked when small molecule inhibition of Plk1 was used in human Separase KO cell lines. (Tsou et al. 2009). Neither perturbation alone prevented disengagement completely; each only delayed it into G1.

Separase was originally shown to be important for centriole disengagement in *Xenopus laevis* egg extracts, where human S-phase centrioles were shown to disengage when mixed with extract containing active Separase (Tsou & Stearns 2006). It was also shown to partially localise to the centrosome during mitosis (Chestukhin et al. 2003). Separase cleaves two substrates through its cysteine protease activity at the centrosome: pericentrin/kendrin (PCNT) and $Scc1^{Rad21}$, a subunit of centrosome-localised cohesin (Nakamura et al. 2009; Schöckel et al. 2011;

Matsuo et al. 2012; Lee & Rhee 2012). Expression of non-cleavable forms of PCNT or Scc1 have been shown to delay centriole disengagement into G1 (Schöckel et al. 2011; Matsuo et al. 2012; Lee & Rhee 2012). However, it is still not completely clear whether the cleavage of cohesin is strictly required for centriole disengagement. In *Drosophila melanogaster*, cohesin cleavage does not promote centriole disengagement, and in *Caenorhabditis elegans* microtubule forces were shown to take a more important role than Separase (Oliveira & Nasmyth 2013; Cabral et al. 2013).

Another complication concerning Separase regulation of centriole disengagement is rationalising when it occurs. Separase is well characterised in its role in sister chromatid separation where it cleaves chromatin bound cohesin subunit $Scc1^{Rad21}$. The chromatin pool of Separase becomes active when Securin is degraded by the APC/C after satisfaction of the SAC at the metaphase/anaphase transition. (Ciosk et al. 1998; Uhlmann et al. 1999) but centriole disengagement normally occurs in telophase. Cleavage of both substrates has been shown to begin at metaphase using fluorescent biosensors artificially targeted to the centrosome using the PACT domain of AKAP450 (Agircan & Schiebel 2014). Interestingly, despite being cleaved, PCNT remains at the centrosome throughout anaphase. It has been suggested that PCNT has to be removed before disengagement occurs (Kim et al. 2019). Furthermore, the regulation of Separase at the centrosome involves other proteins compared to the chromatin bound fraction. Both astrin and Aki1 have been shown to inhibit centrosomal Separase and their depletion leads to centriole disengagement in the formation of multipolar spindles (Yuan et al. 2009; Nakamura et al. 2009). Prolonged arrest has also been suggested to lead to precocious centriole disengagement through leaky APC/C activity and subsequent premature activation of Separase (Karki et al. 2017). Small shugoshin 1 (sSgo1), a spliceoform of shugoshin 1 (Sgo1), has been shown to localise to the centrosome. Sgo1 prevents sister chromatid separation prior to Separase activation and a similar role has been proposed for sSgo1 regarding centrosomal Separase because dominant negative sSgo1 and total Sgo1 depletion both trigger centriole

disengagement early (Tsang & Dynlacht 2008). Whilst it is clear Separase cleavage of PCNT and Scc1 play roles in centriole disengagement, it remains unclear what is the exact sequence of events required to trigger this process that ultimately occurs long after Separase activation.

Inhibition of Plk1 has also been shown to delay centriole disengagement (Tsou et al. 2009). Initially, it was considered that Plk1 was involved in the recruitment of sSgo1 and in doing so PP2A as well. In this way, Plk1 activity was initially considered to promote centriole engagement and then subsequently disengagement by initiating cohesin cleavage (Tsang & Dynlacht 2008; Wang et al. 2008). Plk1 was subsequently shown to be important for the maturation of the PCM at the onset of mitosis (Lee & Rhee 2011). Phosphorylation of PCNT by Plk1 is also required for Separase mediated cleavage of PCNT (Kim et al. 2015). Phospho-resistant mutants of PCNT were not cleaved and resulted in a delay in centriole disengagement and phospho-mimetic PCNT mutants were able to rescue this in the presence of Plk1 inhibitors (Kim et al. 2015). The fact that Plk1 kinase activity is important in the regulation of both proteins that are cleaved by Separase activity points towards redundant regulation. However, this does not explain the observation that both proteins must be prevented from performing their function to completely prevent centriole disengagement (Tsou et al. 2009).

A recent study has shown that CEP57 and PCNT interact and that ablation of the interaction leads to premature centriole disengagement (Watanabe et al. 2019). Watanabe et al. showed that CEP57 interacts with the C terminal “Pericentrin/Akap450 Centrosome Targeting” (PACT) domain of PCNT and mapped the corresponding binding domain in CEP57 subsequently named “Present In N-terminius of CEP57” (PINC). This interaction is potentially evolutionary conserved in *Schizosaccharomyces pombe* at the spindle pole body SPB, the yeast equivalent of a centrosome. Ppc89, potentially the functional homolog of CEP57, interacts with Pcp1, the functional homolog of PCNT(Rosenberg et al. 2006). This interaction may also be between the N terminus of Ppc89 and C terminus of Pcp1 (Bestul et al. 2017). Watanabe et al. showed that this interaction is important for centriole timing by rescuing premature centriole

disengagement, mediated by si-PCNT, through expressing a fusion of PCNT and CEP57. (Watanabe et al. 2019) Loss of PCNT, and its *Drosophila* homolog PLP, both have been shown to lead to premature centriole disengagement and amplification (Roque et al. 2018) (Kim et al. 2019). However, many questions remain about why this interaction is important and whether it is the only way that CEP57 contributes to ensure normal timing.

In this chapter I have started to investigate why, on a molecular level, loss of CEP57 leads to premature centriole disengagement. In agreement with Watanabe et al. (Watanabe et al. 2019) I find that CEP57 is only required for centriole engagement at the mitotic centrosome, and that Plk1 inhibition rescues CEP57 mediated premature centriole disengagement.

6.2. Results

6.2.1. Cep63 and Cep152 localisation are unaffected by acute CEP57 depletion

To better understand how CEP57 leads to improper timing of centriole disengagement, I decided to check whether acute removal of CEP57 leads to mis-localisation of other centrosomal proteins.

CEP57 has been shown to interact with both Cep63 and Cep152 by selective chemical crosslinking (Lukinavičius et al. 2013). Super resolution microscopy revealed that these 3 proteins interact at the proximal end of centrioles. Unlike CEP57, Cep63 and Cep152 have not been reported to have functions in centriole disengagement but both proteins have been shown to have important roles in centriole duplication and the recruitment of PLK4 (Sonnen et al. 2013; Brown et al. 2013). Interestingly, when mutated both CEP63 and CEP152 lead to the same diseases: Seckel syndrome and autosomal recessive primary microcephaly (MCPH) (Kalay et al. 2011; Marjanović et al. 2015). Microcephaly is a characteristic of MVA syndrome as well; however, the fact that CEP57 leads to a different pathology indicates that these proteins could function in different pathways despite their interaction. Even so, recent literature indicates that these proteins may depend upon one another for their localisation. One study claims that CEP57 and Cep63 must interact for the recruitment of Cep152 and as a consequence normal centriole duplication (Wei et al. 2020). Contrary to this, CEP57 has a homolog in humans, CEP57L1, and (Zhao et al. 2020) reports that these two proteins function redundantly and only when they are both depleted is centriole biogenesis impaired - due to the failure to recruit Cep63 and Cep152. Overall, it remains unclear why CEP57 interacts and localises with these two proteins. It has even been suggested that these proteins are all recruited together to new mother centrioles in late G1 (Lee et al. 2020).

Due to this conflicting literature, I hypothesised that CEP57 depletion may be affecting the localisation of these two other Cep proteins. Furthermore, since centriole duplication happens prior to centriole disengagement, and disengagement is required for the next cell cycle's duplication, I thought it would be best to check whether CEP57 depletion had any detrimental effects on centriole duplication. Therefore, I stained for the localisation of Cep63 and Cep152 when CEP57 was depleted (Figure 6-1 and 6-2). In the absence of CEP57, I saw normal Cep63 and Cep152 localisation in metaphase cells that had progressed through S and G2 without CEP57. I also saw normal centriole numbers throughout interphase in both live cell and fixed cell images (data not shown) indicating that CEP57 AID was not adversely affecting centriole duplication.

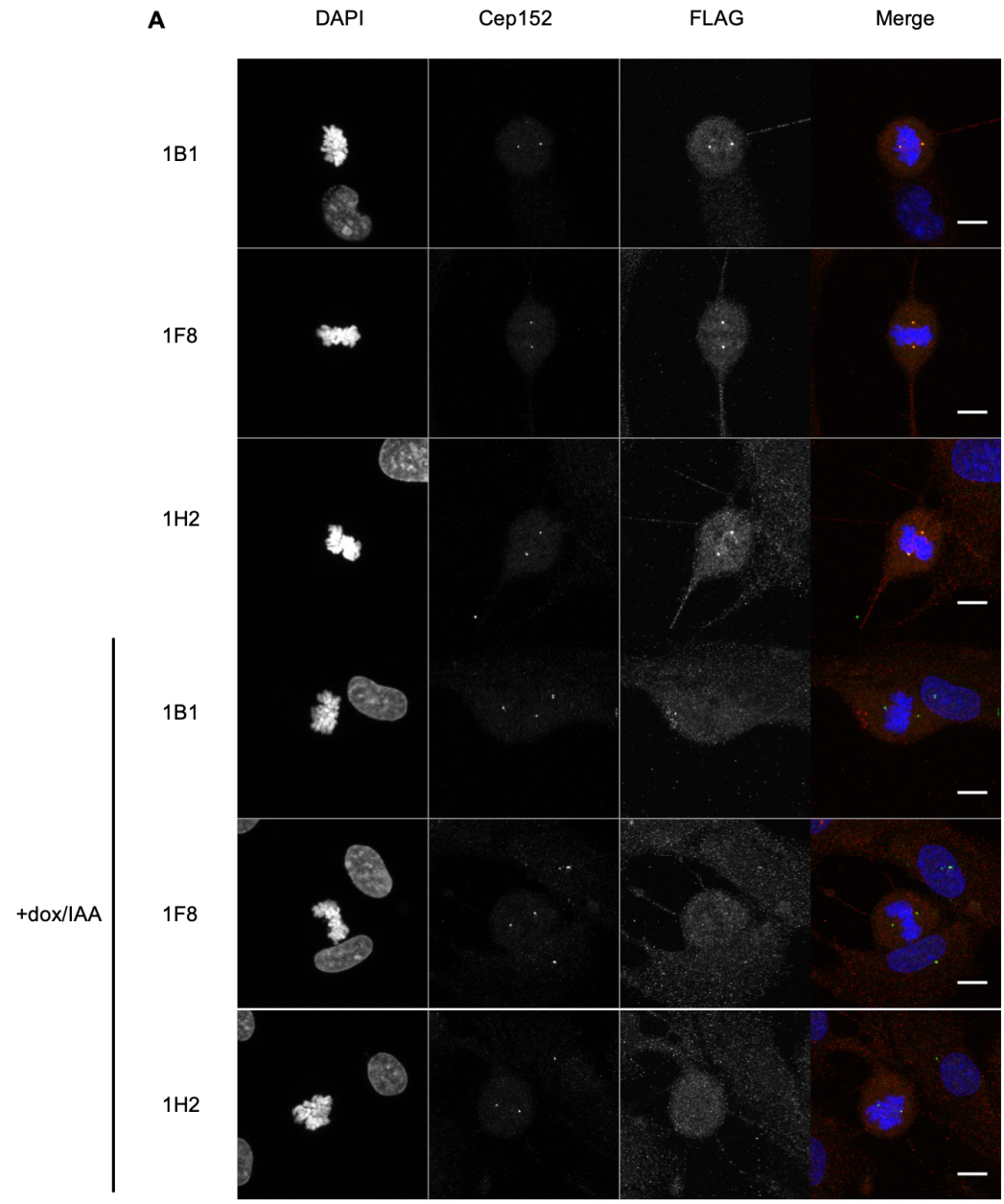

Figure 6-1 Acute depletion of CEP57 does not change the localisation of Cep152.

Cells were stained with Cep152 (green) and FLAG for CEP57 (red) to compare localisation and intensity. Representative images are shown. Images were taken on a Leica SP8 confocal microscope, with 30x 0.3μM stacks. Scale bar = 10μm. 30 cells per condition were analysed, experiment was repeated once.

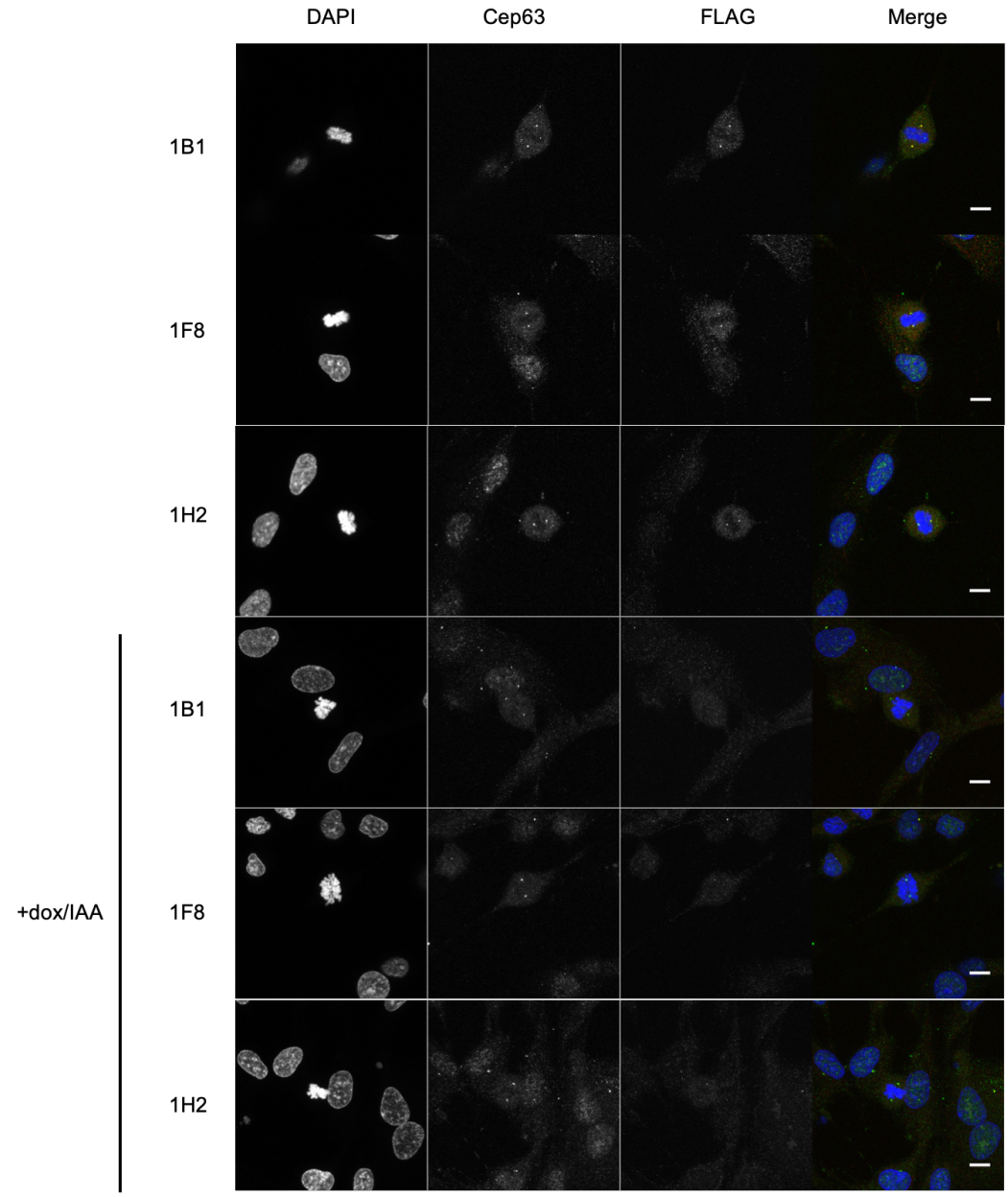

Figure 6-2 Acute depletion of CEP57 does not change the localisation of Cep63

Cells were stained with Cep63 (green) and FLAG for CEP57 (red) to compare localisation and intensity. Representative images are shown. Images were taken on a Leica SP8 confocal microscope, with 30x 0.3µM stacks used. Scale bar = 10µm. 30 cells per condition were analysed, experiment was repeated once.

6.2.2. Levels of Cdk5rap2 are reduced in mitosis after acute CEP57 depletion

Upon CEP57 depletion I observed a strong reduction in the intensity of Cdk5rap2 at the centrosome (Figure 6-3). Cdk5rap2, or centrosomin (cnn)

in *Drosophila*, is a key component of the PCM. In flies Cnn is required for the connection between the PCM and centrioles and loss leads to severe cell division failure in embyros and in somatic cells (Lucas & Raff 2007). Loss of function mutations in mice have led to loss of centriole engagement and subsequent centriole amplification resulting in multipolar spindles (Barrera et al. 2010). During mitosis, depletion of Cdk5rap2 leads to detachment of the centrosome from the spindle pole through abrogating interactions with AKAP450 and Dynenin/Dynactin (Barr et al. 2010; Lee & Rhee 2010)

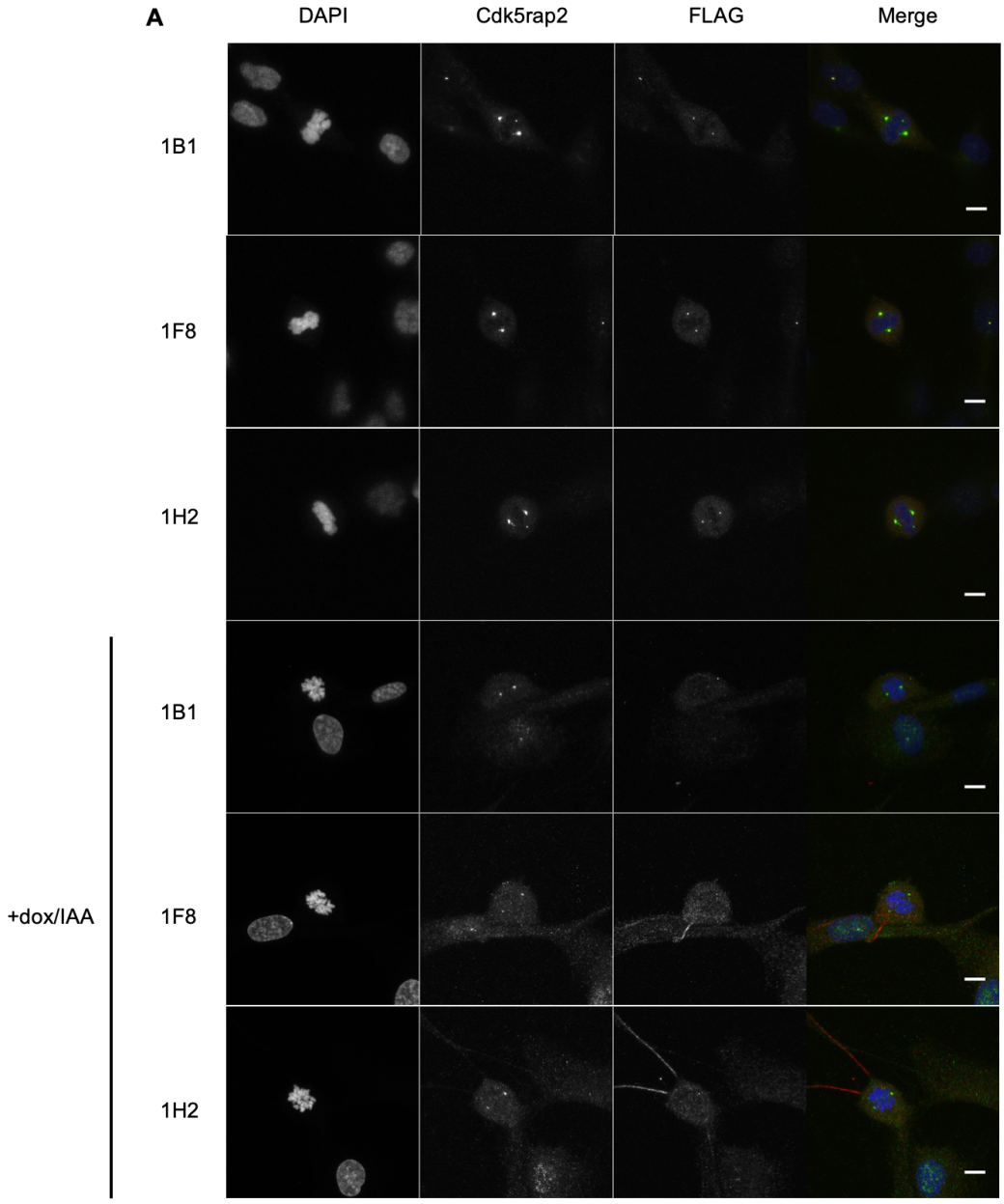

Figure 6-3 Acute CEP57 depletion reduces the intensity of Cdk5rap2 at the centrosome during mitosis

Cells were stained with Cdk5rap2 (green) and FLAG for CEP57 (red) to compare localisation and intensity. Representative images are shown. Images were taken on a Leica SP8 confocal microscope, with 30x 0.3µM stacks used. Scale bar = 10µm. 30 cells per condition were analysed, experiment was repeated once.

Depletion of Cdk5rap2 leads to premature centrosome separation in a pathway independent of C-nap1 and Rootelin (Graser et al. 2007). I have not observed either of these phenotypes upon CEP57 depletion; however, I did not directly analyse a Cdk5rap2 knockdown. Homozygous mutations in Cdk5rap2 have also been linked to MCPH (Bond et al. 2005).

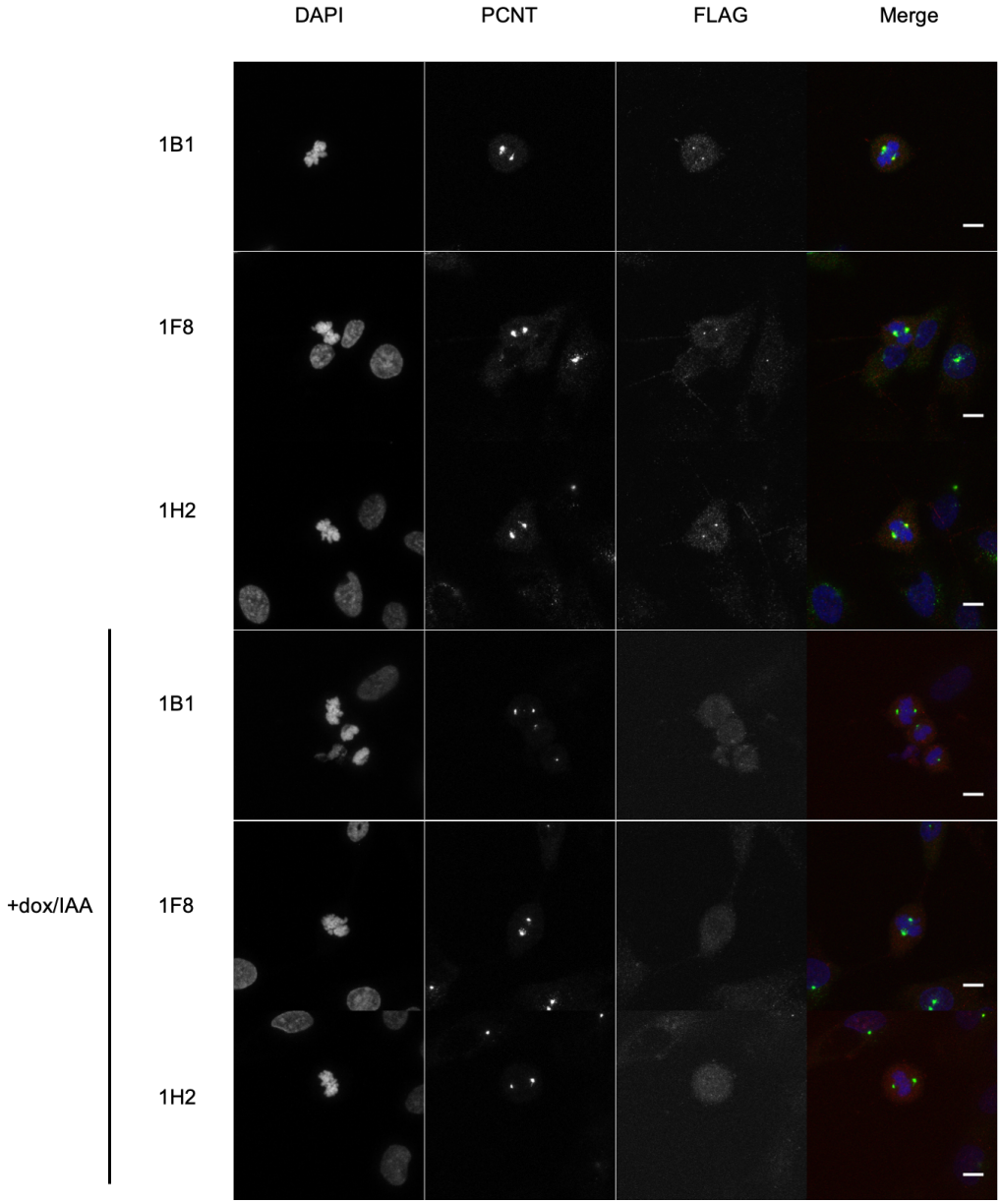

Figure 6-4 Acute CEP57 depletion does not consistently change PCNT intensity at the centrosome during mitosis

Cells were stained for immunofluorescence with PCNT (green) and FLAG for CEP57 (red) to compare localisation and intensity. Representative images are shown. Images were taken on a Leica SP8 confocal microscope, with 30x 0.3μM stacks used. Scale bar = 10μM. 30 cells per condition were analysed, experiment was not repeated.

I also stained for PCNT with and without CEP57 depletion and observed a reduction in levels in some cells, but not others (Figure 6-4). Cdk5rap2 and PCNT interact throughout the centrosome cycle in the PCM (Kim & Rhee 2014). As previously stated, PCNT is a key centriole disengagement protein interacting with both master regulators Separase and Plk1. Cdk5rap2 and PCNT have been shown to require each other for localisation in the PCM (Kim & Rhee 2014). It has also been shown that PCNT and Cdk5rap2 levels both drop concurrently upon centriole disengagement (Kim et al. 2015). It is, therefore, interesting that when I see reduced Cdk5rap2 levels upon CEP57 depletion I don't always see a decrease in PCNT levels (figure 6-4). This indicates that CEP57 may interact with Cdk5rap2 independently of PCNT.

6.2.3. Studying centriole disengagement using live cell imaging

In the previous chapter I studied centriole disengagement in fixed cells. One drawback of this method is that it is impossible to observe the same cell in different phases of the cell cycle. In order to study centriole disengagement in living cells, I generated stable cell lines expressing Centrin-GFP by transfecting my CEP57-AID clones with a Centrin-GFP construct (kind gift of Michel Bornens). I selected for Centrin-GFP positive cells using 0.4μg/μL neomycin for 2 weeks before pooling colonies and sorting cells by FACS to select low GFP-expressing cells. I then sorted single cells and selected clones with comparable expression levels by eye for each CEP57-AID clone. However, it should be noted that intra-clonal levels of Centrin-GFP remained highly variable. These cell lines were maintained in neomycin when in culture and will be referred to as 1B1, 1F8 and 1H2 Centrin-GFP.

6.2.4. Acute CEP57 depletion leads to centriole disengagement in mitosis but not in G2.

I repeated my AID setup on serum synchronised CEP57-AID Centrin-GFP cell lines using confocal microscopy. Since CEP57 was fluorescently tagged with mRuby I used it to confirm whether or not the cell had degraded CEP57. In order to visualise spindle errors, I added sirTubulin as before. In figure 6-5A, I show representative examples of cells progressing through mitosis +/- CEP57 degradation. Normal cells tend to progress until late anaphase or even G1 before centrioles are clearly separated. In the case of CEP57-depleted cells, separation of centrioles occurs much earlier in mitosis, from pro-metaphase onwards. The frame marking centriole disengagement is indicated by a white arrow and magnified inset (figure 6-5A). I quantified premature centriole disengagement by classifying disengagement by eye before or after metaphase (Figure 6-5B). In clone 1B1 Centrin-GFP I observed an increase in disengaged cells before metaphase from 19%+/-16.5% to 50+/-21.0% respectively. In clone 1H2 Centrin-GFP I observed an increase from 5%+/-8.2 to 49%+/-28.2. These experiments were repeated 3 times; however, these data are from repeats with low numbers of cells which led to a high standard deviation. (1B1 untreated: n = 11, 9, 8. 1B1 dox/IAA: n = 12, 15, 8. 1H2 untreated: n = 10, 7, 5. 1H2 dox/IAA: n = 13, 8, 8.) I have not quantified 1F8 Centrin GFP due to the low number of cells imaged but I observed similar results in this clone.

From these experiments, I quantified the percentage of cells in clones 1B1 and 1H2 that exited mitosis with an abnormal number of centrioles. As with centriole disengagement prior to metaphase, I saw a clear increase in both clones (1B1 7%+/-2.5 to 20%+/-4.5, 1H2 3%+/-1.5 to 20%+/-8.0) however, despite premature disengagement many divisions ultimately resulted in daughter cells with a normal number of centrioles. Each daughter cell, rather than each division, was scored even though most parent cells had 4 centrioles; this ensured that rare cells with more than >4 centrioles were also taken into account.

I observed that the majority of premature disengagement events occurred in early mitosis rather than G2. I reclassified the same data sets scoring each cell's centrioles as engaged or disengaged prior to G2 (figure 6-5C). The percentage of cells with disengaged centrioles in CEP57 depleted conditions was reduced from to 50%+/-21.0 and 49%+/-28.2 in mitosis to just 4.5%+-3.2 and 5.5%+/-1.1 in G2 phase in clones 1B1 and 1H2 respectively. Moreover, these numbers were similar in untreated cells (4.5%+/-2.5 for both clones) indicating that CEP57 is not having a specific effect on cells which disengage their centrioles in G2. An example cell with disengaged centrioles prior to nuclear envelope break down is shown in figure 6-5A (1H2 Dox/IAA). Due to the low number of cells and subsequent high variation these data should be repeated but so far, they are in agreement with previous observations and suggest that CEP57 is more important for centriole engagement in mitosis than interphase (Watanabe et al. 2019).

I did not observe an increase in the number of tripolar or multipolar divisions between untreated and CEP57 depleted conditions. In many experiments I did not observe a single tripolar division event and therefore decided not to quantify these mitotic errors from this assay. However, it was clear from sirTubulin localisation that disengaged centrioles in divisions that resulted into two cells are interacting with the mitotic spindle.

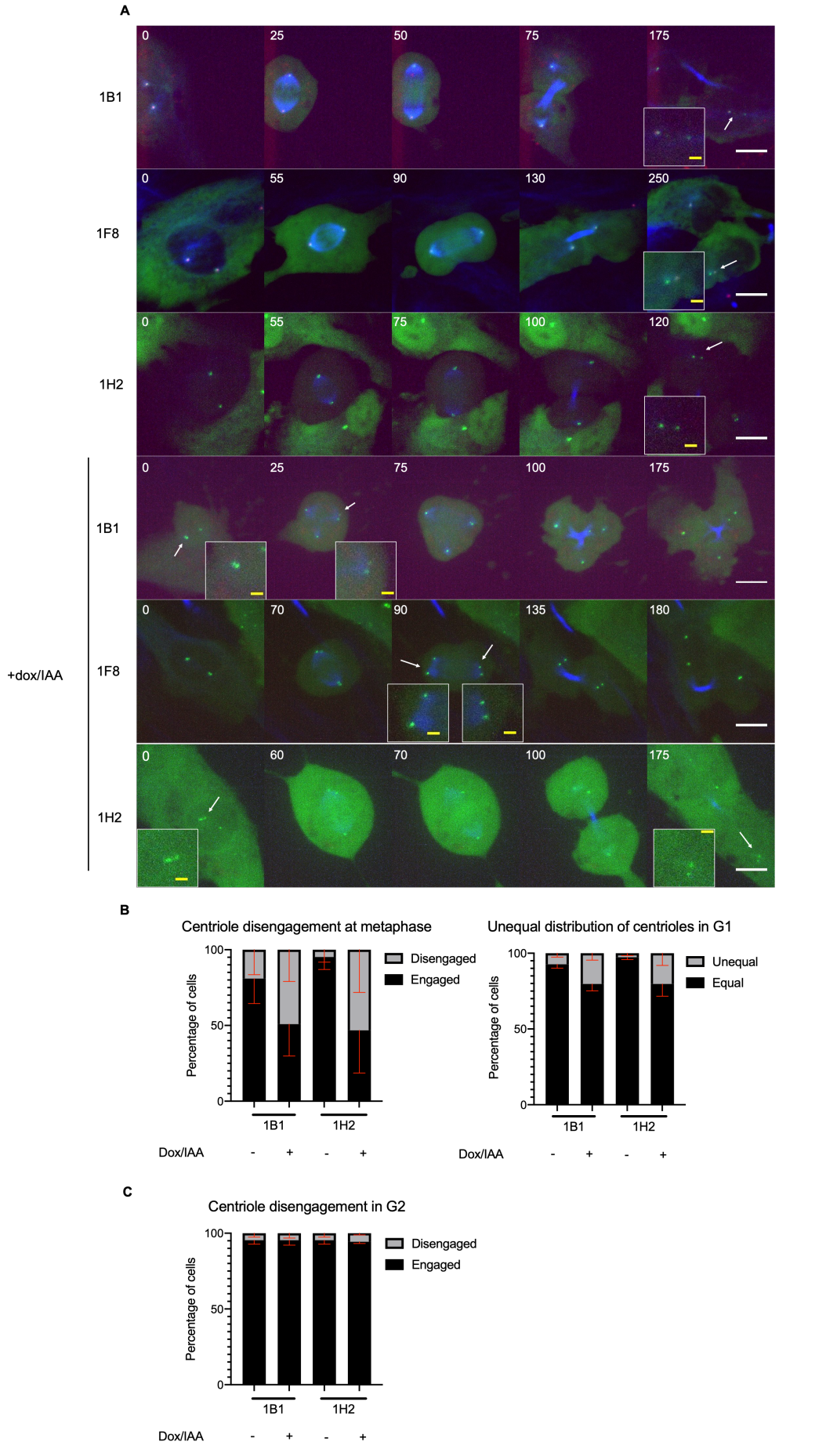
A
1B1
1F8
1H2
+dox/IAA
1B1
1F8
1H2
0
25
50
75
175
0
55
90
130
250
0
55
75
100
120
0
25
75
100
175
0
70
90
135
180
0
60
70
100
175
B
Centriole disengagement at metaphase
Disengaged
Engaged
Percentage of cells
100
50
0
1B1
1H2
Dox/IAA
- + - +
Unequal distribution of centrioles in G1
Unequal
Equal
Percentage of cells
100
50
0
1B1
1H2
Dox/IAA
- + - +
C
Centriole disengagement in G2
Disengaged
Engaged
Percentage of cells
100
50
0
1B1
1H2
Dox/IAA
- + - +

Figure 6-5 CEP57 leads to premature centriole disengagement in mitosis but not in G2

A) Panels show stills from live cell imaging. Serum synchronised CEP57-AID Centrin-GFP clones were filmed every 5 minutes for 8-12 hours. Time is shown in white (minutes). Cells were filmed 24 hours after serum re-addition in order to capture mitotic cells. SirTubulin is shown in blue, Centrin-GFP in green and FLAG-Ruby-mAID-CEP57 in red. Cells were either left untreated or treated with Dox/IAA 18 hours prior to filming. Centriole disengagement is indicated by white arrows and magnified inset boxes. If only one arrow is shown, other centriole pair did not divide in time filmed. In untreated images these events primarily occur after cytokinesis in G1 daughter cells. In IAA treated clones, these events occur during mitosis, often prior to sister chromatid separation. Sir tubulin also shows that disengaged centrioles recruit gamma tubulin. White scale bar = 10μm. Yellow scale bar in inset = 2μM. **B)** Quantification of 3 repeats for each clone. Number of cells quantified was between 5-15. Exact numbers in text. **C)** Re-quantification of same data set counting cells with centriole disengagement prior to mitosis. *For movies see Appendix B 1-6*

6.2.5. Centriole disengagement after DMA washout

To improve the number of cells I could analyse, I decided to repeat the experiment and then briefly arrest cells in mitosis for 3 hours using the Eg5 inhibitor DMA (figure 6-6A). I only arrested cells briefly because prolonged mitotic arrest has been suggested to lead to centriole disengagement through leaky APC/C activity, which enables Separase to prematurely cleave PCNT (Karki et al. 2017).

DMA washout allowed me to quantify more cells by selecting cells that had already arrested in mitosis. In figure 6-6C the average number of cells quantified was 20-25 per condition. As before, I observed a clear increase in the percentage of cells with premature centriole disengagement prior to metaphase (1B1 6%+/-5.5 to 53%+/-11.6 1F8 17%+/-12.6 to 48%+/-14.6 1H2 9%+/-7.9 to 43%+/-3.5 respectively). In many cases the disengagement was clear (figure 6-6B) because the centrioles were separated even before the cell started to reassemble the mitotic spindle after DMA washout. These observations are in line with what I observed above in cells progressing through mitosis and indicate that lack of CEP57 in pro-metaphase enables centrioles to disengage.

Unlike in normal cells, after CEP57 depletion the percentage of divisions that resulted in unequal distribution of centrioles after DMA washout remained very similar to the percentage of cells that prematurely disengaged their centrioles prior to metaphase (Unequal division Dox/IAA: 1B1 43%+/-10.1, 1F8 45%+/-15, 1H2 38%+/-5.3) (figure 6-6C).

I also used sirTubulin as a marker to quantify the types of spindle that developed in these conditions (figure 6-6D). For these experiments, I quantified 30-40 cells per condition. In 2 out of 3 clones I observed an increase in the number of asymmetric spindles. These spindles were classified by eye as cells that clearly had >2 poles that nucleated tubulin but ultimately divided into two cells. I did not observe a strong increase in tripolar and multipolar divisions after CEP57 depletion indicating that these asymmetric divisions could lead to CEP57 mediated aneuploidy. However, these events were extremely rare and therefore quantification may be skewed by one or two positive cells.

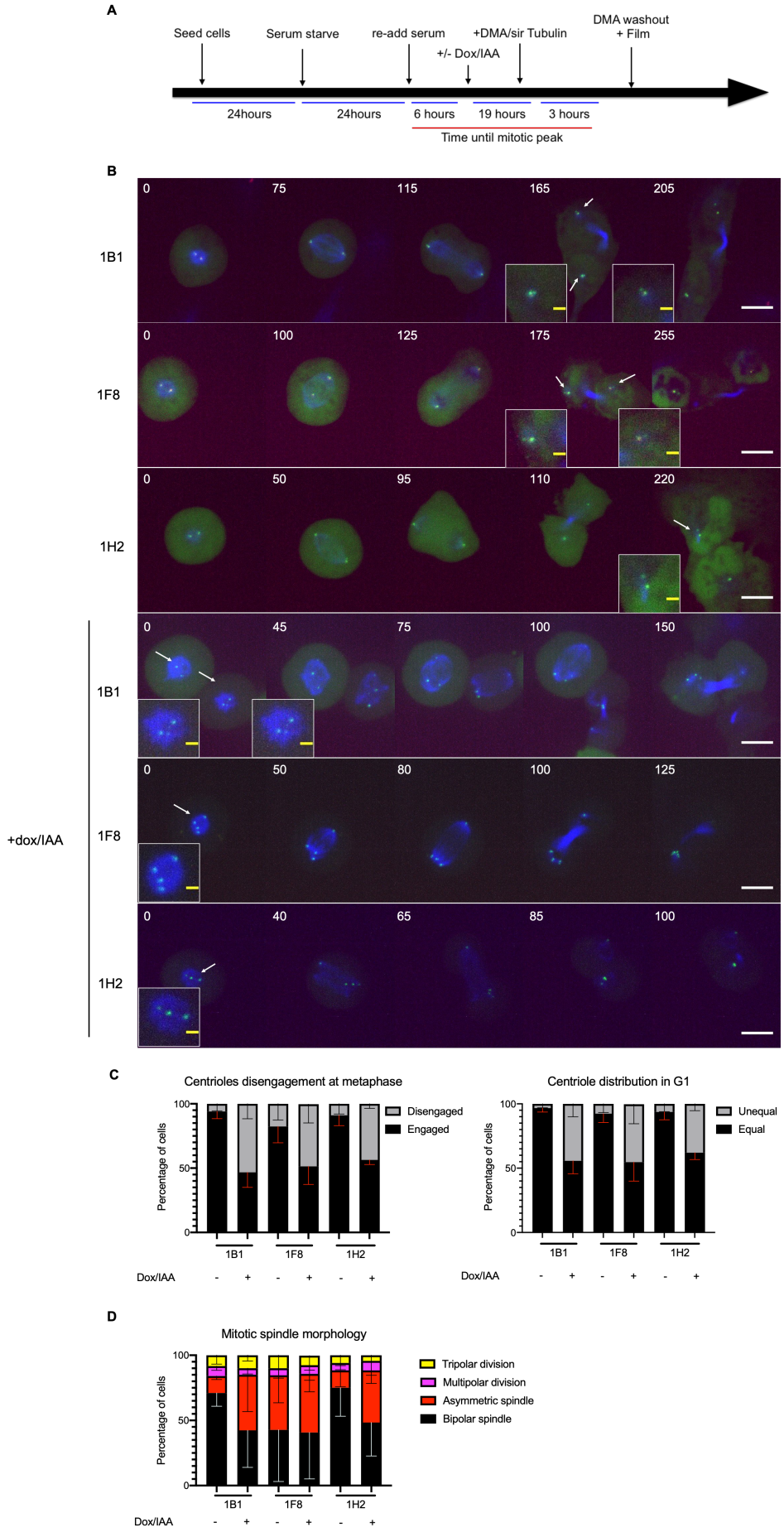
A
Seed cells
Serum starve
re-add serum
+DMA/sir Tubulin
+/- Dox/IAA
DMA washout
+ Film
24hours
24hours
6 hours
19 hours
3 hours
Time until mitotic peak
B
1B1
1F8
1H2
+dox/IAA
C
Centrioles disengagement at metaphase
Disengaged
Engaged
Percentage of cells
Dox/IAA
Centriole distribution in G1
Unequal
Equal
D
Mitotic spindle morphology
Tripolar division
Multipolar division
Asymmetric spindle
Bipolar spindle

Figure 6-6 Centriole disengagement after DMA washout

A) Schematic for experimental setup. **B)** Panels show stills from live cell imaging. CEP57-AID Centrin-GFP clones were washed out of DMA prior to filming. As before, frames were taken every 5 minutes for 8-12 hours. Time is shown in minutes. Sirtubulin is shown in blue, Centrin-GFP in green and FLAG-Ruby-mAID-CEP57 in red. Cells were either left untreated or treated with Dox/IAA for 18 hours prior to filming. Centriole disengagement is indicated by white arrows and magnified inset boxes. If arrow not shown, these centrioles did not disengage during filming. Untreated cells progressed to G1 before disengagement. In treated clones, cells often began filming with disengaged centrioles or immediately disengaged centrioles after DMA washout. White scale bar = 10μm. Yellow scale bar in inset = 2μM. **C)** Quantification of 3 repeats for each clone. Number of cells quantified per repeat per clone was 25-30. Cells were scored for centriole disengagement prior to metaphase and then number of centrioles during G1 manually. **D)** Re-quantification of same data set classifying spindle morphology after DMA washout. *For movies see Appendix B 7-12*

6.2.6. Inhibition of Plk1 partially rescues CEP57 mediated premature centriole disengagement

As stated previously, Plk1 phosphorylation greatly enhances recruitment of proteins to the PCM in G2 phase and during early mitosis. Inhibition of Plk1 has been shown to prevent centriole disengagement until later in G1, and combined with Separase knock-down prevents centriole disengagement completely (Tsou et al. 2009). Plk1 activity is specifically co-ordinated with mitotic entry and this period seems to be when CEP57 is specifically required at the centrosome to ensure normal centriole disengagement timing. To test whether Plk1 activity had any effect on CEP57 mediated premature centriole disengagement, I repeated the DMA washout experiment adding 40nM BI2536 at the same time as DMA and sirTubulin for 3 hours. I used a low dose of BI2536 due to the pleiotropic nature of Plk1. Plk1 is important in coordinating events leading to entry to mitosis as well as the SAC and during anaphase (Hansen et al. 2004) (O'Connor et al. 2015) (Schubert et al. 2015) (Thomas et al. 2016) (Parrilla et al. 2016) (Gheghiani et al. 2017). Inhibition at any point in mitosis leads to cells not progressing into the next phase or cell death. Even at this low concentration of BI2536, I noticed fewer cells entered mitosis prior to filming or exited mitosis during filming. I ignored cells that failed to exit mitosis, and quantified only the cells which entered G1. Despite these issues, I was able to quantify multiple experiments for two clones (1B1 n = 5 and 1H2 n = 4) (figure 6-7C). In 1B1 Centrin-GFP I observed a reduction

in the percentage of premature centriole disengagement from 41%+/-4.6 to 23+/-7.6 In 1H2 the reduction was less pronounced going from 35%+/-2.3 to 28%+/-4.6 (figure 6-7C.) The percentage of cells with unequal distribution of centrioles followed this trend as expected (figure 6-7C). However, I was not expecting Plk1 inhibition to specifically affect this phenotype. Examples of cells treated with dox/IAA and 40nM BI2536 that exit mitosis normally are shown in figure 6-7B.

This experiment has again been performed on a low number of cells however, it clearly indicates that premature centriole disengagement induced by CEP57 depletion can be partially reversed by Plk1 inhibition. This points towards CEP57 being involved in the expansion of the PCM at the onset of mitosis.

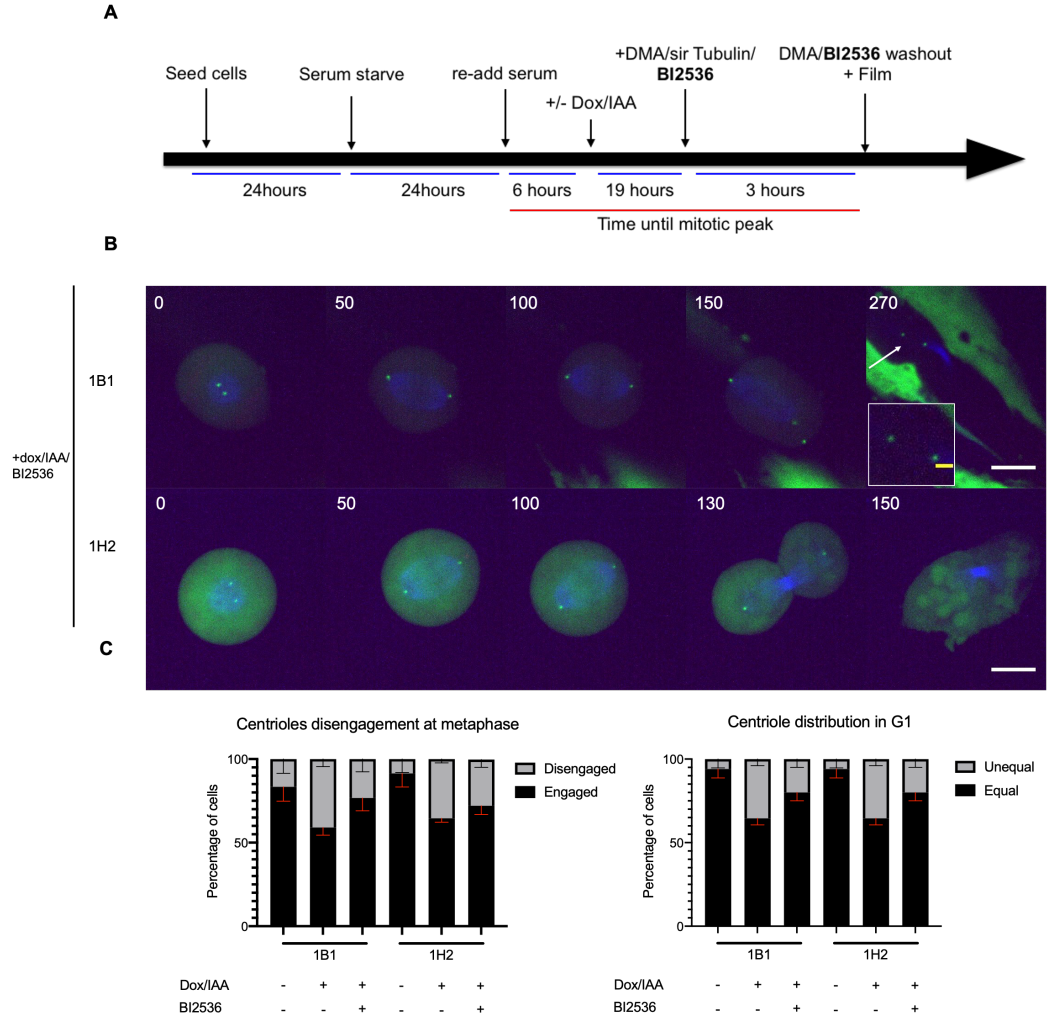

Figure 6-7 Inhibition of Plk1 partially rescues CEP57 mediated premature centriole disengagement

A) Schematic for experimental setup. Experiment was repeated as in 6-6 but BI2536 was added for 3 hours. **B)** As in 6-6. Panels show examples of BI2536 treated cells exiting mitosis with engaged centrioles. White scale bar = 10μm. Yellow scale bar in inset = 2μM. Centriole disengagement is indicated by white arrows and magnified inset boxes. If arrow not shown, these centrioles did not disengage during filming**. C)** Quantification of 5 and 4 repeats for each clone. Number of cells quantified per repeat per clone was between 6-15 Cells were scored for centriole disengagement prior to metaphase and then number of centrioles during G1 manually. *For movies see Appendix B 13 and 14*

6.3. Discussion

In this chapter, I have shown in 3 individual CEP57-AID clones that acute depletion of CEP57 leads to perturbation of the normal timing of centriole disengagement. I confirmed this in living cells after observing the same phenotype in fixed assays in chapter 5. I then went on to show that most cells only disengage their centrioles during mitosis rather than in G2, even when CEP57 is depleted long before G2. This observation implies that CEP57's role in centriole engagement is specific to the mitotic centrosome. I performed qualitative immunofluorescence assays to check whether the localisation of some other centrosomal proteins was changed by CEP57 depletion and observed that the levels of the PCM component Cdk5rap2 were reduced in these conditions. Despite this, I did not observe clear changes in many known CEP57 interactors including Cep63/Cep152 that are thought to be responsible in some way for the localisation of CEP57 to the centrosome (Lukinavičius et al. 2013; Wei et al. 2020); nor consistent changes in levels of PCNT, which is a well described Cdk5rap2 interactor and a recently described CEP57 binding partner (Watanabe et al. 2019). These data point towards a role for CEP57 in the structure or expansion of the PCM during mitosis. Since CEP57 has been reported to localise specifically to the proximal end of the mother centriole rather than in the PCM itself, it is not clear how it would provide such a function. The observation that PCNT levels do not reduce as clearly as Cdk5rap2 levels is at odds with previous literature showing they are co-dependent on one another for their localisation during mitosis (Kim et al. 2019). It would be interesting to see whether CEP57 interacts directly with Cdk5rap2, and to which parts of these proteins, given that the CEP57 PINC domain has been

shown to interact with the PACT domain of PCNT (Watanabe et al. 2019). Further analysis would also benefit from studies with increased resolution of the mitotic centrosome in normal and CEP57 treated conditions. Super resolution microscopy, or more specifically expansion microscopy, has recently proved to be an excellent technique when it comes to the study of centrioles (Sahabandu et al. 2019; Kong et al. 2020).

The PCM is capable of acting as a microtubule organising centre (MTOCs) independent of centrioles (Rieder et al. 2001; Basto et al. 2006). In flies and mammals, these cells often fail division at cytokinesis or fail to progress into the next cell cycle (Debec & Abbadie 1989). (Piel et al. 2001). Interestingly, siRNA depletion of CEP57 has very recently been shown to rescue bi-polar spindle formation in cells treated with centrinone (a Plk4 inhibitor) so that they only have one centrosome. In this paper, the authors suggest that CEP57 acts an anchor between the centriole and the PCM and that releasing the PCM from this interaction allows cells to form bipolar spindles using just PCM material (Takumi et al. 2020). This work provides indirect evidence that CEP57 is important for the interaction between the centriole and the expanded PCM network.

Finally, I showed that CEP57 mediated premature centriole disengagement can be partially rescued by inhibition of Plk1. These assays would benefit from repetition as rescue was clearer in one clone,1B1, than the other, 1H2. This has been corroborated by recent published literature (Watanabe et al. 2019). However due to the complex nature of Plk1 in centriole disengagement as well as mitosis in general, these data on their own are not sufficient to provide an explanation for what CEP57 is doing. It is likely that we do not know all the substrates that Plk1 phosphorylates in the control of centriole engagement during mitosis. Plk1 activity is important, perhaps essential, in the cleavage of both $Scc1^{Rad21}$and PCNT by Separase. However, this cannot be Plk1's only role in centriole disengagement as the activity of both Plk1 and Separase must be inhibited in order for centriole disengagement to be fully blocked. This implies that either Plk1 or Separase regulate centriole disengagement in an unknown manner on top of the pathways elucidated so far. Further study where the activity of Separase is monitored or perturbed in conjunction with CEP57

depletion would help separate out exactly why Plk1 phosphorylation can rescue the effects of CEP57 depletion. This could be achieved using the Separase biosensors (Agircan & Schiebel 2014) or by directly depleting Separase by siRNA. I have attempted both of these assays but without success so far.

In both chapter 5 and chapter 6 I have referred to the aberrant centriole behaviour that I observed as centriole disengagement occurring too early. Shulka et al showed by electron microscopy that if centrioles separate to a distance above 80nm in the presence of active Plk1 they are able to duplicate and that by prophase centrioles are already at this distance during mitosis. Since centriole disengagement is considered to be a block to centriole duplication this raises the question of what else is blocking this occurring during mitosis and why Separase and Plk1 are so important in the regulation of centriole behaviour in late mitosis. However, since my assays were performed in both fixed and live conditions with confocal microscopy I cannot study the separation to the same resolution as Shulka et al. Whilst my assays are unsuitable to corroborate whether the centrioles move apart at prophase, they do show a measurable difference when CEP57 is removed.

One aspect of CEP57 biology that I did not investigate is its apparent ability to bind to microtubules. Improper formation of the bipolar spindle could lead to indirect consequences on centrosome structure. CEP57 has also been reported to interact with NEDD1. I observed a mild decrease in the recruitment of gamma tubulin in some cells (figure 5-10A). However, much like my observations of the levels of PCNT in figure 6-4, these experiments would benefit from more repeats and improvements in either quantification or resolution.

7. General discussion

7.1. Utilising inducible degradation as a tool

The work presented in this thesis aimed to use inducible degradation as a tool to understand more about the roles of TRIP13 and CEP57 in mitosis and maintaining genome stability.

Initially, I developed my own RPE based cell line to test the Auxin Inducible Degron (AID). The expression of OsTIR1 from the FRT site was induced using tetracycline. However, this cell line had a number of drawbacks including: mosaic degradation of TRIP13; IAA-independent degradation of TRIP13; and changed mitotic timing. These limitations precluded continuing my work; therefore, I changed to an RPE1 cell line where osTIR1 was expressed from the ROSA26 safe harbour locus(Lemmens et al. 2018) (Hegarat et al. 2020). In this cell line, degradation of TRIP13 was more homogenous and the untreated cells retained normal mitotic timing. I also did not detect non-specific degradation in the conditions that I used for my assays. I continued with this system for the rest of my studies.

In recent years, there have been several improvements made to a range of inducible degradation techniques. Two key drawbacks of AID-mediated degradation have been incomplete degradation of the target protein and non-specific degradation due to TIR1 expression. Hybrid systems have been developed to reduce the level of the protein as much as possible. This includes using the AID system in parallel with the Small Molecule Assisted Shut-off (SMASh) system for the degradation of cyclin A and cyclin B (Lemmens et al. 2018) (Hegarat et al. 2020) as well as fusing the AID tag to a nanobody in order to degrade APC subunits (Daniel et al. 2018). Most recently, AID2 has been developed (Yesbolatova et al. 2020). AID2 utilises a mutated TIR1 protein (F74G) combined with a new ligand 5-Ph-IAA. Combined, these 2 innovations lead to quicker degradation and previously difficult genes to target have been successfully degraded across model systems: yeast, mice and human cells. This is due to a range of improvements that include: increased cell permeability of the ligand

allowing it to be used at much lower concentrations; higher stability of TIR1 (F74G) leading to more ternary complexes between the TIR1, ligand and target protein tagged with mAID; and that TIR1 (F74G) does not interact well with IAA, thereby preventing IAA contaminants in FBS leading to non-specific degradation (Uchida et al. 2018; Yesbolatova et al. 2020). In my system, I did not detect non-specific basal degradation and both proteins degraded to undetectable levels using western blotting and live-cell imaging. However, the degradation of CEP57 was much slower than that of TRIP13. This could be potentially due to the differing localisations and respective accessibilities of the two proteins to the SCF ubiquitin ligase machinery containing TIR1, though I did not investigate this. Further studies should consider the choice of inducible degradation system carefully.

7.2. – TRIP13

TRIP13 was used as a proof of principle to establish the viability and usefulness of the AID system. Previous studies, including unpublished data from our laboratory, had indicated that TRIP13 was required to generate a normal SAC response alongside p31^{comet}. Our lab had already shown that co-depletion of APC15 and p31^{comet} had an additive effect to delay mitotic progression and therefore suggested that there were two independent pathways involved in checkpoint silencing(Mansfeld et al. 2011). Further unpublished data sought to understand whether TRIP13 KO led to a further additive effect (Appendix A). Published In-vitro studies strongly implied that TRIP13 and p31^{comet} worked together to allow disassembly of the MCC, whereas APC15 was part of a separate pathway in agreement with our unpublished (Ye et al. 2015).

However, at the beginning of this study, we had conflicting data concerning the phenotype of TRIP13 KO clones generated by CRISPR/Cas9 in both Hela and RPE1 cells. Some clones had a normal SAC response to spindle poisons whereas other clones were unable to maintain an arrest when treated in the same way. To complicate matters further, the clones that did not arrest had altered levels of TRIP13 interactors: Mad2 and p31^{comet}.

Both low Mad2 levels and high p31^{comet} levels have been shown to alter the strength of the SAC; therefore, it was unclear whether the phenotype observed was due to TRIP13 loss or possible adaptation in response to the loss of TRIP13.

It had also been suggested that TRIP13 was required for the activation of the checkpoint as well as the silencing of the checkpoint (Ma & Poon 2018). This paper also reported changes to the levels of Mad2 and p31^{comet} as well as a shift in the balance of the conformation of Mad2. It was unclear how TRIP13 could be required for both activation and silencing of the SAC. I decided that targeting TRIP13 for acute degradation with the AID should help further our understanding of TRIP13s role in the SAC and overcome some of the limitations observed in TRIP13 KO cell lines.

First, I characterised the levels of Mad2 and p31^{comet} in TRIP13-AID at short- and long-term timings. I observed that after 16-24 hours of TRIP13 depletion Mad2 and p31^{comet} levels resemble those observed in TRIP13 KO cells. Mad2 levels were reduced by nearly half in all clones assayed and p31^{comet} levels were doubled or tripled. These data imply that the KO clone changes observed were not due to adaptation but instead a true response to the loss of TRIP13. These data suggest that the levels of Mad2 and p31^{comet} are dependent on TRIP13 expression.

To further understand whether TRIP13 played a role in the stability of Mad2 and p31^{comet}, I repeated the assay upon serum starved cells that would not undergo mitosis for at least 20-24 hours after release. In this way I could assay whether the conformational change of Mad2 was important for the changes in levels observed upon TRIP13 depletion because only closed Mad2 interacts with TRIP13 and p31^{comet} and closed Mad2 is primarily generated when cells undergo mitosis. I did not observe the same level changes at the same timings; however, this experiment provides indirect evidence because I did not actively assay the conformation of Mad2 throughout.

Mad2 is required to generate MCC and reducing the amount of Mad2 in the cell will lower the amount of MCC generated and reduce the strength of the SAC. In normal cells overexpression of p31^{comet} drive cells to exit mitosis and strongly implies that TRIP13 and p31^{comet} play an active role in

SAC silencing. It would be interesting to see whether overexpression of p31^{comet} drives cells to exit mitosis independent of TRIP13.

Next, I depleted TRIP13 in otherwise untreated asynchronous cells and saw that depletion of TRIP13 immediately caused a short delay in the time taken between nuclear envelope break down and anaphase. This was in agreement with previous siRNA depletion of TRIP13 data and suggests that TRIP13 contributes to the normal progression of mitosis and could imply that it slows inactivation of the SAC. In addition, this short delay could be removed by adding the MPS1 inhibitor, Reversine, to completely inactivate the SAC. Interestingly these data do not agree with current literature that TRIP13 is required to activate the SAC. This phenotype could be specific to RPE1 cells or non-transformed cells. It could also due to be differences in when the AID system was applied. Kim et al. report that there is only a delay in cells treated for less than 24 hours and attribute this to the generation of interphase MCC that needs to be disassembled (Kim et al. 2018). I have not shown data on the NEBD-Anaphase timing where TRIP13 has been depleted for 24 hours. However, one other difference between cells treated for 1 hour or 24 hours is the levels of Mad2 and p31^{comet} and this could account for the removal of the delay they observed. It is also important to note that by immunoprecipitation the lab can only detect MCC components interacting when mitotic cells are lysed (unpublished data).

Acute depletion of TRIP13 for one hour was also enough to prevent cells arresting in nocodazole, taxol or DMA which generate different SAC responses due to their effect on microtubule dynamics. Cells that enter mitosis without TRIP13 are unable to mount a proper checkpoint response. However, if the checkpoint is activated prior to depletion of TRIP13, some cells remain arrested for several hours. These experiments demonstrate the importance of using the AID at different times during the cell cycle. However, it remains unclear why loss of TRIP13 during an arrest does not lead to the same phenotype as loss of TRIP13 immediately prior to an arrest.

Published literature has indicated that p31^{comet} does not lead to loss of the checkpoint and that the respective balance of open and closed Mad2

remains unchanged(Ma & Poon 2018). Whilst I did not directly study p31^{comet} in this thesis, I would expect p31^{comet} depletion to have the same phenotype as TRIP13 depletion as TRIP13 requires p31^{comet} to exert its interaction and interact with Mad2 in-vitro(Ye et al. 2017; Ye et al. 2015; Alfieri et al. 2018).

Overall, I decided to not pursue this project further after a different publication (Kim et al. 2018) using a TRIP13-AID system published results broadly in agreement with my own. This paper went on to characterise that overexpression of Mad2 levels ultimately rescued the effect of TRIP13 depletion suggesting that TRIP13's crucial role in the SAC is to replenish O-Mad2 levels. Without being able to assay O vs C Mad2 it was challenging to pursue this project further.

7.3. – CEP57

Previous studies of CEP57 had not achieved a convincing consensus on the protein's role in mitosis. One of the key reasons CEP57 is interesting is that it is the only locus linked to MVA syndrome whose gene product does not have a clear role in the SAC. I found that CEP57-AID did not change mitotic timing and CEP57 did not localise to the kinetochore and concluded it was unlikely to be a SAC protein. On the other hand, endogenously tagged CEP57 localised to the centrosome in all cell cycle phases and I observed clear but infrequent mitotic errors that suggested issues with bipolar spindle formation using time-lapse fluorescent imaging of sirDNA treated cells. I confirmed these errors led to aneuploidy by counting the number of chromosomes in cells chronically depleted of CEP57. I therefore investigated what effect CEP57 had on the progression of the centrosome cycle and found that acute loss of CEP57 leads to de-regulation of when cells disengage their centrioles. The disengaged centrioles recruited, or maintained, PCM components including gamma-tubulin indicating that they were capable of microtubule nucleation. This indicates that they were likely able to cause the observed defects in bipolar

spindle formation that led to mitotic errors. These data were in direct agreement with observations made by Watanabe et al. 2019.

Whilst there is a clear correlation between centrosome dysfunction and cancer, in flies this centrosome loss did not lead to genome instability. So far there has been no direct link established between aneuploidy and centrosome dysfunction. However, my data clearly indicate that loss of CEP57 leads to aneuploidy. However, I would like to repeat metaphase spreads on more clones to be more certain of this. The link between aneuploidy and CEP57 is also emphasised by individuals with MVA (la Torre-García et al. 2019). It may be beneficial to directly show that centriole disengagement leads to chromosomal instability. One potential way that premature centriole disengagement could lead to aneuploidy is through merotelic attachments and subsequent incorrect division of chromatids that is not sensed by the SAC. However, I cannot rule out that CEP57-AID is leading to some other mechanism of genome instability that I have not yet detected.

After establishing a link between the aneuploidy and premature centriole disengagement, I proceeded to study CEP57's role in this pathway. In order to study centriole disengagement more closely, I established live cell imaging assays of centriole disengagement by stably expressing Centrin-GFP in my CEP57-AID clones. This led to the observation that CEP57 mediated premature centriole disengagement primarily occurs in mitosis and not G2.

Previous studies have showed that the activities of Separase and Plk1 are required for centriole disengagement to occur. I showed that small molecule inhibition of Plk1 reduced the effect on abnormal timing of centriole disengagement mediated by CEP57 depletion. These experiments were not consistent between clones and one clone remains to be assayed but preliminarily suggest that phosphorylation by Plk1 is important for CEP57's role in this process.

So far, I have been unable to assay whether inhibition of Separase can also rescue the effect of CEP57 depletion. Separase dependent cleavage of PCNT is considered to be dependent on prior Plk1 phosphorylation. Since CEP57 has recently been shown to interact with PCNT and that

ablation of this interaction leads to premature disengagement, it would be important to establish whether this is related to Separase cleavage of PCNT. Interestingly there are a number of potential ExxR sites in CEP57 that could be Separase cleavage sites. Compared to the known Separase cleavage sites the residues in between E and R are more hydrophobic and bulkier. Whilst I think it is unlikely these are cleavage sites; it is something that could be investigated in future studies.

Plk1 kinase typically phosphorylates substrates with the consensus: [D/E]X[pS/T][IVLM]X[E] (Nakajima et al. 2003) (Bibi et al. 2013). This phosphorylation is considered to also require a polo binding domain (PBD) which initially recruits Plk1, with a consensus S-[pS/T]-[P/X] (Lee et al. 1998; Elia et al. 2003). I manually searched the primary sequence of CEP57 in humans and did not see any strong candidates for Plk1 phosphorylation sites. However, there is an uncharacterised conserved SP phosphorylation site close to the N terminus of CEP57 (S53) (Santamaria et al. 2011) (Houjiang Zhou et al. 2013) (Mertins et al. 2016). SP sites are typically targeted by Cdk1. As my data has indicated a specific requirement for CEP57 in mitosis but not interphase, a Cdk1 site is of potential interest since Cdk1 activity is at its highest during mitosis prior to anaphase. Interestingly one of the datasets this phosphorylation was detected was a study upon Plk1 targets during mitosis despite the sequence not resembling either the PBD or Plk1 kinase consensuses (Santamaria et al. 2011). Interestingly constitutive Plk1 activation has been shown to promote daughter centriole maturation and subsequent amplification in early mitosis (Shukla et al. 2015). Shulka et al propose that centrioles actually physically disengage much earlier in mitosis (i.e lose their orthogonal conformation) and a physical separation of 80nm is enough to promote amplification. This observation also promotes the idea the structure of the PCM is important to maintain centriole distance rather than “engagement” as such. It also indicates that if CEP57 is involved in Plk1’s role in centriole disengagement earlier in mitosis, it is unlikely that Separase function would be perturbed when CEP57 is depleted.

Overall, it is still relatively unclear what CEP57 interacts with at the centrosome. I began a low-throughput method of checking the localisation

and levels of which proteins are affected by CEP57 depletion. The most striking observation I made was to the levels of Cdk5rap2. Cdk5rap2 is a crucial part of the PCM and depletion of it leads to many centrosome defects including centriole disengagement and centrosome separation in interphase. Cdk5rap2 also interacts with PCNT throughout the centrosome cycle. However, whilst I did observe some cells with lower PCNT levels it was not as striking as in Cdk5rap2 stained cells. This in itself is an interesting observation as multiple studies have reported that Cdk5rap2 and PCNT depend upon one another for localisation. This preliminary data suggests that CEP57 and Cdk5rap2 may also interact and maybe only during mitosis.

The phenotype of CEP57 depletion is very similar to that of PCNT KO(Roque et al. 2018) (Kim et al. 2019). An interaction between the two proteins has been recently characterised(Watanabe et al. 2019). In my thesis, I did not specifically investigate that interaction however, I would have liked to understand more about whether the interaction with PCNT was related to Separase dependent cleavage as mentioned above. However, I believe the more likely reason for CEP57 and PCNT interaction to be related to the expansion of the PCM. Removal of PCNT has been shown to be required for centriole disengagement however, I did not see a consistent correlation between lower PCNT levels and centriole disengagement in my IF. Another possible way of studying this would be to introduce a live cell marker for PCNT. For some reason premature centriole disengagement was more easily detectable during live cell imaging assays than in IF.

It is also still unclear why CEP57 interacts with Cep63 and Cep152 at the proximal end of the mother centriole. Despite this interaction, removal of CEP57 has not consistently been reported to lead to the same effects as depletion of Cep63 or Cep152 suggesting that the proteins are important in different signalling pathways. It is still broadly unknown what is required for CEP57 to localise to the centrosome and what CEP57 is subsequently able to recruit to the centrosome. I did not specifically check when CEP57 is recruited to new mother centrioles but this may help gain insight into its function.

To summarise, my data indicate that CEP57 is important for the structure of the PCM during mitosis. Lower levels of Cdk5rap2 and PCNT indicate that potentially the expansion of the PCM for mitosis is compromised without CEP57. Plk1 phosphorylation is known to be required for this process as well, which may explain why Plk1 inhibition can partially rescue CEP57 effects. Previous data have already suggested that CEP57 is important for the connection between the centriole and the PCM. CEP57 was shown by super resolution microscopy to localise to the wall of the mother centriole specifically at the proximal end (Watanabe et al. 2019). However, further investigation is required into understanding why this interaction is only required during mitosis when the PCM is expanded. In this respect, controlled degradation of CEP57 via AID will be a useful tool in order to examine the differences between the structure of the interphase and mitotic PCM. So far, I have only used confocal microscopy to investigate this. Higher resolution microscopy such as super-resolution and electron microscopy should now also be considered.

7.4. Future perspectives

Many unanswered questions remain about CEP57's role in centriole disengagement. It is also unclear if CEP57 is required for any other aspect of the centrosome cycle in other phases. In this thesis, I did not specifically investigate CEP57 depletion in other cell cycle phases; however, it should be noted I did not see any issues in interphase at the centrosome or in cell cycle progression generally.

In the immediate future, areas of focus should include: examining whether inhibition of Separase effects timing in CEP57 depleted cells; study of the structure of mitotic PCM and whether CEP57 and Cdk5rap2 interact biochemically.

If these studies do not advance our knowledge significantly a comprehensive study into what CEP57 interacts with on a proteomic level may reveal unknown players in centriole disengagement. Further study would benefit from identifying the proteins that recruit CEP57 to the centrosome and what proteins CEP57 is required for. There are very little

biochemical studies on CEP57 and in general CEP57 is missing from some systematic mass spectrometry-based centrosome studies. In my experience, robust antibodies against CEP57 are still lacking and improvement in this area will advance study of this protein.

Whilst CEP57L1 has not been implicated in centriole disengagement or MVA syndrome, there are now reports that the two proteins share a redundant function in S phase. Therefore, co-depletion of CEP57 and CEP57L1 may also be of benefit.

8. Bibliography

Agircan, F.G. & Schiebel, E., 2014. Sensors at centrosomes reveal determinants of local Separase activity. J. M. G. Higgins, ed. *PLoS Genetics*, 10(10), p.e1004672.

Alfieri, C. et al., 2016. Molecular basis of APC/C regulation by the spindle assembly checkpoint. *Nature*, 536(7617), pp.431–436.

Alfieri, C., Chang, L. & Barford, D., 2018. Mechanism for remodelling of the cell cycle checkpoint protein MAD2 by the ATPase TRIP13. *Nature*, 559(7713), pp.274–278.

Alfieri, C., Tischer, T. & Barford, D., 2020. A unique binding mode of Nek2A to the APC/C allows its ubiquitination during prometaphase. *EMBO reports*, p.e49831.

Alfieri, C., Zhang, S. & Barford, D., 2017. Visualizing the complex functions and mechanisms of the anaphase promoting complex/cyclosome (APC/C). *Open biology*, 7(11), p.170204.

Alfonso-Pérez, T. et al., 2019. MAD1-dependent recruitment of CDK1-CCNB1 to kinetochores promotes spindle checkpoint signaling. *The Journal of Cell Biology*, 218(4), pp.1108–1117.

Allan, L.A. et al., 2020. Cyclin B1 scaffolds MAD1 at the kinetochore corona to activate the mitotic checkpoint. *The EMBO Journal*, 39(12), p.e103180.

Alvarez-Rodrigo, I. et al., 2019. Evidence that a positive feedback loop drives centrosome maturation in fly embryos. *eLife*, 8, p.D430.

Alves-Cruzeiro, J.M.D.C., Nogales-Cadenas, R. & Pascual-Montano, A.D., 2014. CentrosomeDB: a new generation of the centrosomal proteins database for Human and Drosophila melanogaster. *Nucleic acids research*, 42(Database issue), pp.D430–6.

Andersen, J.S. et al., 2003. Proteomic characterization of the human centrosome by protein correlation profiling. *Nature*, 426(6966), pp.570–574.

Ardley, H.C., Hung, C.-C. & Robinson, P.A., 2005. The aggravating role of the ubiquitin-proteasome system in neurodegeneration. *FEBS letters*, 579(3), pp.571–576.

Arquint, C. & Nigg, E.A., 2014. STIL microcephaly mutations interfere with APC/C-mediated degradation and cause centriole amplification. *Current biology : CB*, 24(4), pp.351–360.

Arquint, C., Gabryjonczyk, A.-M. & Nigg, E.A., 2014. Centrosomes as signalling centres. *Philosophical transactions of the Royal Society of London. Series B, Biological sciences*, 369(1650), p.20130464.

Aziz, K. et al., 2018. Mosaic-variegated aneuploidy syndrome mutation or haploinsufficiency in CEP57 impairs tumor suppression. *The Journal of clinical investigation*, 128(8), pp.3517–3534.

Bahe, S. et al., 2005. Rootletin forms centriole-associated filaments and functions in centrosome cohesion. *The Journal of Cell Biology*, 171(1), pp.27–33.

Ballister, E.R., Riegman, M. & Lampson, M.A., 2014. Recruitment of Mad1 to metaphase kinetochores is sufficient to reactivate the mitotic checkpoint. *The Journal of Cell Biology*, 204(6), pp.901–908.

Barisic, M. et al., 2010. Spindly/CCDC99 is required for efficient chromosome congression and mitotic checkpoint regulation. S. Doxsey, ed. *Molecular biology of the cell*, 21(12), pp.1968–1981.

Barnhart, M.C. et al., 2011. HJURP is a CENP-A chromatin assembly factor sufficient to form a functional de novo kinetochore. *The Journal of Cell Biology*, 194(2), pp.229–243.

Barr, A.R. & Gergely, F., 2007. Aurora-A: the maker and breaker of spindle poles. *Journal of cell science*, 120(Pt 17), pp.2987–2996.

Barr, A.R., Kilmartin, J.V. & Gergely, F., 2010. CDK5RAP2 functions in centrosome to spindle pole attachment and DNA damage response. *The Journal of Cell Biology*, 189(1), pp.23–39.

Barrera, J.A. et al., 2010. CDK5RAP2 regulates centriole engagement and cohesion in mice. *Developmental Cell*, 18(6), pp.913–926.

Basto, R. et al., 2008. Centrosome amplification can initiate tumorigenesis in flies. *Cell*, 133(6), pp.1032–1042.

Basto, R. et al., 2006. Flies without centrioles. *Cell*, 125(7), pp.1375–1386.

Bazzi, H. & Anderson, K.V., 2014. Acentriolar mitosis activates a p53-dependent apoptosis pathway in the mouse embryo. *Proceedings of the National Academy of Sciences of the United States of America*, 111(15), pp.E1491–500.

Bertran, M.T. et al., 2011. Nek9 is a Plk1-activated kinase that controls early centrosome separation through Nek6/7 and Eg5. *The EMBO Journal*, 30(13), pp.2634–2647.

Bestul, A.J. et al., 2017. Molecular model of fission yeast centrosome assembly determined by superresolution imaging. *The Journal of Cell Biology*, 216(8), pp.2409–2424.

Bettencourt-Dias, M. et al., 2011. Centrosomes and cilia in human disease. *Trends in genetics : TIG*, 27(8), pp.307–315.

Bettencourt-Dias, M. et al., 2005. SAK/PLK4 is required for centriole duplication and flagella development. *Current Biology*, 15(24), pp.2199–2207.

Bibi, N., Parveen, Z. & Rashid, S., 2013. Identification of potential Plk1 targets in a cell-cycle specific proteome through structural dynamics of kinase and Polo box-mediated interactions. K. S. Lee, ed. *PloS one*, 8(8), p.e70843.

Blangy, A. et al., 1995. Phosphorylation by p34cdc2 regulates spindle association of human Eg5, a kinesin-related motor essential for bipolar spindle formation in vivo. *Cell*, 83(7), pp.1159–1169.

Bobinnec, Y. et al., 1998. Centriole disassembly in vivo and its effect on centrosome structure and function in vertebrate cells. *The Journal of Cell Biology*, 143(6), pp.1575–1589.

Bond, J. et al., 2005. A centrosomal mechanism involving CDK5RAP2 and CENPJ controls brain size. *Nature genetics*, 37(4), pp.353–355.

Bornens, M., 2012. The centrosome in cells and organisms. *Science*, 335(6067), pp.422–426.

Bossard, C. et al., 2003. Translokin is an intracellular mediator of FGF-2 trafficking. *Nature Cell Biology*, 5(5), pp.433–439.

Brightman, D.S., Ejaz, S. & Dauber, A., 2018. Mosaic variegated aneuploidy syndrome caused by a CEP57 mutation diagnosed by whole exome sequencing. *Clinical case reports*, 6(8), pp.1531–1534.

Brito, D.A., Gouveia, S.M. & Bettencourt-Dias, M., 2012. Deconstructing the centriole: structure and number control. *Current Opinion in Cell Biology*, 24(1), pp.4–13.

Brown, N.G. et al., 2014. Mechanism of polyubiquitination by human anaphase-promoting complex: RING repurposing for ubiquitin chain assembly. *Molecular Cell*, 56(2), pp.246–260.

Brown, N.J. et al., 2013. Cep63 and cep152 cooperate to ensure centriole duplication. D. Cimini, ed. *PloS one*, 8(7), p.e69986.

Buffin, E. et al., 2005. Recruitment of Mad2 to the kinetochore requires the Rod/Zw10 complex. *Current Biology*, 15(9), pp.856–861.

Burke, D.J. & Stukenberg, P.T., 2008. Linking kinetochore-microtubule binding to the spindle checkpoint. *Developmental Cell*, 14(4), pp.474–479.

Cabral, G. et al., 2013. Multiple mechanisms contribute to centriole separation in C. elegans. *Current biology : CB*, 23(14), pp.1380–1387.

Caldas, G.V. et al., 2015. The RZZ complex requires the N-terminus of KNL1 to mediate optimal Mad1 kinetochore localization in human cells. *Open biology*, 5(11), p.150160.

Carroll, C.W. & Morgan, D.O., 2005. Enzymology of the anaphase-promoting complex. *Methods in enzymology*, 398, pp.219–230.

Caudron, M. et al., 2005. Spatial coordination of spindle assembly by chromosome-mediated signaling gradients. *Science*, 309(5739), pp.1373–1376.

Chang, J. et al., 2010. PLK2 phosphorylation is critical for CPAP function in procentriole formation during the centrosome cycle. *The EMBO Journal*, 29(14), pp.2395–2406.

Chang, L. et al., 2015. Atomic structure of the APC/C and its mechanism of protein ubiquitination. *Nature*, 522(7557), pp.450–454.

Chang, L.-F. et al., 2014. Molecular architecture and mechanism of the anaphase-promoting complex. *Nature*, 513(7518), pp.388–393.

Chao, W.C.H. et al., 2012. Structure of the mitotic checkpoint complex. *Nature*, 484(7393), pp.208–213.

Cheeseman, I.M. & Desai, A., 2008. Molecular architecture of the kinetochore-microtubule interface. *Nature reviews. Molecular cell biology*, 9(1), pp.33–46.

Cheeseman, I.M. et al., 2002. Phospho-regulation of kinetochore-microtubule attachments by the Aurora kinase Ipl1p. *Cell*, 111(2), pp.163–172.

Cheeseman, I.M. et al., 2006. The conserved KMN network constitutes the core microtubule-binding site of the kinetochore. *Cell*, 127(5), pp.983–997.

Chen, Z. et al., 2002. CP110, a cell cycle-dependent CDK substrate, regulates centrosome duplication in human cells. *Developmental Cell*, 3(3), pp.339–350.

Chestukhin, A. et al., 2003. Processing, localization, and requirement of human Separase for normal anaphase progression. *Proceedings of the National Academy of Sciences*, 100(8), pp.4574–4579.

Chin, C.F. & Yeong, F.M., 2010. Safeguarding entry into mitosis: the antephase checkpoint. *Molecular and Cellular Biology*, 30(1), pp.22–32.

Chung, E. & Chen, R.-H., 2002. Spindle checkpoint requires Mad1-bound and Mad1-free Mad2. D. Koshland, ed. *Molecular biology of the cell*, 13(5), pp.1501–1511.

Ciechanover, A., Elias, S., et al., 1980. Characterization of the heat-stable polypeptide of the ATP-dependent proteolytic system from reticulocytes. *The Journal of biological chemistry*, 255(16), pp.7525–7528.

Ciechanover, A., Heller, H., et al., 1980. ATP-dependent conjugation of reticulocyte proteins with the polypeptide required for protein degradation. *Proceedings of the National Academy of Sciences*, 77(3), pp.1365–1368.

Cimini, D., 2007. Detection and correction of merotelic kinetochore orientation by Aurora B and its partners. *Cell cycle (Georgetown, Tex.)*, 6(13), pp.1558–1564.

Ciosk, R. et al., 1998. An ESP1/PDS1 complex regulates loss of sister chromatid cohesion at the metaphase to anaphase transition in yeast. *Cell*, 93(6), pp.1067–1076.

Clarke, L. & Carbon, J., 1983. Genomic substitutions of centromeres in Saccharomyces cerevisiae. *Nature*, 305(5929), pp.23–28.

Clarke, L. & Carbon, J., 1980. Isolation of a yeast centromere and construction of functional small circular chromosomes. *Nature*, 287(5782), pp.504–509.

Clift, D. et al., 2018. Acute and rapid degradation of endogenous proteins by Trim-Away. *Nature protocols*, 13(10), pp.2149–2175.

Collin, P. et al., 2013. The spindle assembly checkpoint works like a rheostat rather than a toggle switch. *Nature Cell Biology*, 15(11), pp.1378–1385.

Conduit, P.T., Feng, Z., et al., 2014. The centrosome-specific phosphorylation of Cnn by Polo/Plk1 drives Cnn scaffold assembly and centrosome maturation. *Developmental Cell*, 28(6), pp.659–669.

Conduit, P.T., Richens, J.H., et al., 2014. A molecular mechanism of mitotic centrosome assembly in Drosophila. *eLife*, 3, p.e03399.

Conduit, P.T., Wainman, A. & Raff, J.W., 2015. Centrosome function and assembly in animal cells. *Nature reviews. Molecular cell biology*, 16(10), pp.611–624.

Cooke, C.A. et al., 1997. Localization of CENP-E in the fibrous corona and outer plate of mammalian kinetochores from prometaphase through anaphase. *Chromosoma*, 106(7), pp.446–455.

Coudreuse, D. & Nurse, P., 2010. Driving the cell cycle with a minimal CDK control network. *Nature*, 468(7327), pp.1074–1079.

Currie, C.E. et al., 2018. Bub1 is not essential for the checkpoint response to unattached kinetochores in diploid human cells. *Current biology : CB*, 28(17), pp.R929–R930.

D'Assoro, A.B. et al., 2002. Amplified centrosomes in breast cancer: a potential indicator of tumor aggressiveness. *Breast cancer research and treatment*, 75(1), pp.25–34.

da Fonseca, P.C.A. et al., 2011. Structures of APC/C(Cdh1) with substrates identify Cdh1 and Apc10 as the D-box co-receptor. *Nature*, 470(7333), pp.274–278.

Daniel, K. et al., 2018. Conditional control of fluorescent protein degradation by an auxin-dependent nanobody. *Nature communications*, 9(1), pp.3297–13.

David, Y. et al., 2010. The E2 ubiquitin-conjugating enzymes direct polyubiquitination to preferred lysines. *The Journal of biological chemistry*, 285(12), pp.8595–8604.

De Antoni, A. et al., 2005. The Mad1/Mad2 complex as a template for Mad2 activation in the spindle assembly checkpoint. *Current biology : CB*, 15(3), pp.214–225.

de Wolf, B. et al., Chromosomal instability by mutations in a novel specificity factor of the minor spliceosome. *biorvix*.

De Wulf, P., McAinsh, A.D. & Sorger, P.K., 2003. Hierarchical assembly of the budding yeast kinetochore from multiple subcomplexes. *Genes & development*, 17(23), pp.2902–2921.

Debec, A. & Abbadie, C., 1989. The acentriolar state of the Drosophila cell lines 1182. *Biology of the cell*, 67(3), pp.307–311.

Demeter, J. et al., 2000. The DNA damage checkpoint signal in budding yeast is nuclear limited. *Molecular Cell*, 6(2), pp.487–492.

Dery, T. et al., 2020. Follow-up of two adult brothers with homozygous CEP57 pathogenic variants expands the phenotype of Mosaic Variegated Aneuploidy Syndrome. *European journal of medical genetics*, 63(11), p.104044.

Di Fiore, B. & Pines, J., 2007. Emi1 is needed to couple DNA replication with mitosis but does not regulate activation of the mitotic APC/C. *The Journal of Cell Biology*, 177(3), pp.425–437.

Di Fiore, B. et al., 2015. The ABBA Motif Binds APC/C Activators and Is Shared by APC/C Substrates and Regulators. *Developmental Cell*, 32(3), pp.358–372.

Di Fiore, B. et al., 2016. The Mitotic Checkpoint Complex Requires an Evolutionary Conserved Cassette to Bind and Inhibit Active APC/C. *Molecular Cell*, 64(6), pp.1144–1153.

Dick, A.E. & Gerlich, D.W., 2013. Kinetic framework of spindle assembly checkpoint signalling. *Nature Cell Biology*, 15(11), pp.1370–1377.

Ditchfield, C. et al., 2003. Aurora B couples chromosome alignment with anaphase by targeting BubR1, Mad2, and Cenp-E to kinetochores. *The Journal of Cell Biology*, 161(2), pp.267–280.

Dobbelaere, J. et al., 2008. A genome-wide RNAi screen to dissect centriole duplication and centrosome maturation in Drosophila. M. Schliwa, ed. *PLoS Biology*, 6(9), p.e224.

Dou, Z. et al., 2019. Recent Progress on the Localization of the Spindle Assembly Checkpoint Machinery to Kinetochores. *Cells*, 8(3), p.278.

Doxsey, S., McCollum, D. & Theurkauf, W., 2005. Centrosomes in cellular regulation. *Annual review of cell and developmental biology*, 21(1), pp.411–434.

Doxsey, S.J. et al., 1994. Pericentrin, a highly conserved centrosome protein involved in microtubule organization. *Cell*, 76(4), pp.639–650.

Draetta, G. & Beach, D., 1989. The mammalian cdc2 protein kinase: mechanisms of regulation during the cell cycle. *Journal of cell science. Supplement*, 12(Supplement 12), pp.21–27.

Drinnenberg, I.A. et al., 2014. Recurrent loss of CenH3 is associated with independent transitions to holocentricity in insects. *eLife*, 3, p.2104.

Dube, P. et al., 2005. Localization of the coactivator Cdh1 and the cullin subunit Apc2 in a cryo-electron microscopy model of vertebrate APC/C. *Molecular Cell*, 20(6), pp.867–879.

Duro, J., & Nilsson, J. (2020). SAC during early cell divisions: Sacrificing fidelity over timely division, regulated differently across organisms. *BioEssays*, e2000174.

Duronio, R.J. & Xiong, Y., 2013. Signaling pathways that control cell proliferation. *Cold Spring Harbor perspectives in biology*, 5(3), pp.a008904–a008904.

Earnshaw, W.C. & Rothfield, N., 1985. Identification of a family of human centromere proteins using autoimmune sera from patients with scleroderma. *Chromosoma*, 91(3-4), pp.313–321.

El-Brolosy, M.A. et al., 2019. Genetic compensation triggered by mutant mRNA degradation. *Nature*, 568(7751), pp.193–197.

Elia, A.E.H., Cantley, L.C. & Yaffe, M.B., 2003. Proteomic screen finds pSer/pThr-binding domain localizing Plk1 to mitotic substrates. *Science*, 299(5610), pp.1228–1231.

Elia, A.E.H., Rellos, P., et al., 2003. The molecular basis for phosphodependent substrate targeting and regulation of Plks by the Polo-box domain. *Cell*, 115(1), pp.83–95.

Emanuele, M.J. & Stukenberg, P.T., 2007. Xenopus CEP57 is a novel kinetochore component involved in microtubule attachment. *Cell*, 130(5), pp.893–905.

Evans, T. et al., 1983. Cyclin: a protein specified by maternal mRNA in sea urchin eggs that is destroyed at each cleavage division. *Cell*, 33(2), pp.389–396.

Eytan, E. et al., 2014. Disassembly of mitotic checkpoint complexes by the joint action of the AAA-ATPase TRIP13 and p31(comet). *Proceedings of the National Academy of Sciences of the United States of America*, 111(33), pp.12019–12024.

Fachinetti, D. et al., 2013. A two-step mechanism for epigenetic specification of centromere identity and function. *Nature Cell Biology*, 15(9), pp.1056–1066.

Faesen, A.C. et al., 2017. Basis of catalytic assembly of the mitotic checkpoint complex. *Nature*, 542(7642), pp.498–502.

Fang, Guoliang et al., 2014. Centlein mediates an interaction between C-Nap1 and Cep68 to maintain centrosome cohesion. *Journal of cell science*, 127(Pt 8), pp.1631–1639.

Fang, Guowei, 2002. Checkpoint protein BubR1 acts synergistically with Mad2 to inhibit anaphase-promoting complex. M. J. Solomon, ed. *Molecular biology of the cell*, 13(3), pp.755–766.

Feng, Z. et al., 2017. Structural Basis for Mitotic Centrosome Assembly in Flies. *Cell*, 169(6), pp.1078–1089.e13.

Ferguson, R.L. & Maller, J.L., 2008. Cyclin E-dependent localization of MCM5 regulates centrosome duplication. *Journal of cell science*, 121(Pt 19), pp.3224–3232.

Fitzgerald-Hayes, M., Clarke, L. & Carbon, J., 1982. Nucleotide sequence comparisons and functional analysis of yeast centromere DNAs. *Cell*, 29(1), pp.235–244.

Foley, E.A. & Kapoor, T.M., 2013. Microtubule attachment and spindle assembly checkpoint signalling at the kinetochore. *Nature reviews. Molecular cell biology*, 14(1), pp.25–37.

Foley, E.A., Maldonado, M. & Kapoor, T.M., 2011. Formation of stable attachments between kinetochores and microtubules depends on the B56-PP2A phosphatase. *Nature Cell Biology*, 13(10), pp.1265–1271.

Fong, C.S. et al., 2014. SAS-6 assembly templated by the lumen of cartwheel-less centrioles precedes centriole duplication. *Developmental Cell*, 30(2), pp.238–245.

Fong, C.S., Ozaki, K. & Tsou, M.-F.B., 2018. PPP1R35 ensures centriole homeostasis by promoting centriole-to-centrosome conversion. W. Marshall, ed. *Molecular biology of the cell*, 29(23), pp.2801–2808.

Fong, K.-W. et al., 2008. CDK5RAP2 is a pericentriolar protein that functions in centrosomal attachment of the gamma-tubulin ring complex. S. Doxsey, ed. *Molecular biology of the cell*, 19(1), pp.115–125.

Foster, S.A. & Morgan, D.O., 2012. The APC/C subunit Mnd2/Apc15 promotes Cdc20 autoubiquitination and spindle assembly checkpoint inactivation. *Molecular Cell*, 47(6), pp.921–932.

Franco, A., Meadows, J.C. & Millar, J.B.A., 2007. The Dam1/DASH complex is required for the retrieval of unclustered kinetochores in fission yeast. *Journal of cell science*, 120(Pt 19), pp.3345–3351.

Fry, A.M., Leaper, M.J. & Bayliss, R., 2014. The primary cilium: guardian of organ development and homeostasis. *Organogenesis*, 10(1), pp.62–68.

Fry, A.M., Mayor, T., et al., 1998. C-Nap1, a novel centrosomal coiled-coil protein and candidate substrate of the cell cycle-regulated protein kinase Nek2. *The Journal of Cell Biology*, 141(7), pp.1563–1574.

Fry, A.M., Meraldi, P. & Nigg, E.A., 1998. A centrosomal function for the human Nek2 protein kinase, a member of the NIMA family of cell cycle regulators. *The EMBO Journal*, 17(2), pp.470–481.

Fu, J. & Glover, D.M., 2012. Structured illumination of the interface between centriole and peri-centriolar material. *Open biology*, 2(8), p.120104.

Funabiki, H., 2019. Correcting aberrant kinetochore microtubule attachments: a hidden regulation of Aurora B on microtubules. *Current Opinion in Cell Biology*, 58, pp.34–41.

Ganem, N.J. et al., 2014. Cytokinesis failure triggers hippo tumor suppressor pathway activation. *Cell*, 158(4), pp.833–848.

Ganem, N.J., Godinho, S.A. & Pellman, D., 2009. A mechanism linking extra centrosomes to chromosomal instability. *Nature*, 460(7252), pp.278–282.

García-Castillo, H. et al., 2008. Clinical and genetic heterogeneity in patients with mosaic variegated aneuploidy: delineation of clinical subtypes. *American journal of medical genetics. Part A*, 146A(13), pp.1687–1695.

Garnett, M.J. et al., 2009. UBE2S elongates ubiquitin chains on APC/C substrates to promote mitotic exit. *Nature Cell Biology*, 11(11), pp.1363–1369.

Garvanska, D.H., Larsen, M.S.Y. & Nilsson, J., 2016. Synergistic inhibition of the APC/C by the removal of APC15 in HCT116 cells lacking UBE2C. *Biology Open*, 5(10), pp.1441–1448.

Gascoigne, K.E. et al., 2011. Induced ectopic kinetochore assembly bypasses the requirement for CENP-A nucleosomes. *Cell*, 145(3), pp.410–422.

Gassmann, R. et al., 2010. Removal of Spindly from microtubule-attached kinetochores controls spindle checkpoint silencing in human cells. *Genes & development*, 24(9), pp.957–971.

Gavet, O. & Pines, J., 2010. Activation of cyclin B1–Cdk1 synchronizes events in the nucleus and the cytoplasm at mitosis. *The Journal of Cell Biology*, 189(2), pp.247–259.

Ge, S., Skaar, J.R. & Pagano, M., 2009. APC/C- and Mad2-mediated degradation of Cdc20 during spindle checkpoint activation. *Cell cycle (Georgetown, Tex.)*, 8(1), pp.167–171.

Gheghiani, L. et al., 2017. PLK1 Activation in Late G2 Sets Up Commitment to Mitosis. *CellReports*, 19(10), pp.2060–2073.

Gieffers, C. et al., 2001. Three-dimensional structure of the anaphase-promoting complex. *Molecular Cell*, 7(4), pp.907–913.

Glotzer, M., Murray, A.W. & Kirschner, M.W., 1991. Cyclin is degraded by the ubiquitin pathway. *Nature*, 349(6305), pp.132–138.

Gorbsky, G.J., 1995. Kinetochores, microtubules and the metaphase checkpoint. *Trends in Cell Biology*, 5(4), pp.143–148.

Gorbsky, G.J., Chen, R.H. & Murray, A.W., 1998. Microinjection of antibody to Mad2 protein into mammalian cells in mitosis induces premature anaphase. *The Journal of Cell Biology*, 141(5), pp.1193–1205.

Goshima, G. et al., 2007. Genes required for mitotic spindle assembly in Drosophila S2 cells. *Science*, 316(5823), pp.417–421.

Gosti-Testu, F. et al., 1986. Identification of centrosomal proteins in a human lymphoblastic cell line. *The EMBO Journal*, 5(10), pp.2545–2550.

Gould, R.R. & Borisy, G.G., 1977. The pericentriolar material in Chinese hamster ovary cells nucleates microtubule formation. *The Journal of Cell Biology*, 73(3), pp.601–615.

Graser, S., Stierhof, Y.-D. & Nigg, E.A., 2007. Cep68 and Cep215 (Cdk5rap2) are required for centrosome cohesion. *Journal of cell science*, 120(Pt 24), pp.4321–4331.

Gräf, R., 2018. Comparative Biology of Centrosomal Structures in Eukaryotes. *Cells*, 7(11), p.202.

Gregan, J. et al., 2011. Merotelic kinetochore attachment: causes and effects. *Trends in Cell Biology*, 21(6), pp.374–381.

Gundersen, G.G. & Bulinski, J.C., 1986. Microtubule arrays in differentiated cells contain elevated levels of a post-translationally modified form of tubulin. *European journal of cell biology*, 42(2), pp.288–294.

Habedanck, R. et al., 2005. The Polo kinase Plk4 functions in centriole duplication. *Nature Cell Biology*, 7(11), pp.1140–1146.

Habu, T. et al., 2002. Identification of a MAD2-binding protein, CMT2, and its role in mitosis. *The EMBO Journal*, 21(23), pp.6419–6428.

Hagan, R.S. et al., 2011. p31(comet) acts to ensure timely spindle checkpoint silencing subsequent to kinetochore attachment. *Molecular biology of the cell*, 22(22), pp.4236–4246.

Haider, M. & Segal, H.L., 1972. Some characteristics of the alanine aminotransferase- and arginase-inactivating system of lysosomes. *Archives of biochemistry and biophysics*, 148(1), pp.228–237.

Hansen, D.V. et al., 2004. Plk1 regulates activation of the anaphase promoting complex by phosphorylating and triggering SCFbetaTrCP-dependent destruction of the APC Inhibitor Emi1. *Molecular biology of the cell*, 15(12), pp.5623–5634.

Hara, M. & Fukagawa, T., 2018. Kinetochore assembly and disassembly during mitotic entry and exit. *Current Opinion in Cell Biology*, 52, pp.73–81.

Hardwick, K.G. et al., 1996. Activation of the budding yeast spindle assembly checkpoint without mitotic spindle disruption. *Science*, 273(5277), pp.953–956.

Hardy, T. et al., 2014. Multisite phosphorylation of C-Nap1 releases it from Cep135 to trigger centrosome disjunction. *Journal of cell science*, 127(Pt 11), pp.2493–2506.

Haren, L. et al., 2006. NEDD1-dependent recruitment of the gamma-tubulin ring complex to the centrosome is necessary for centriole duplication and spindle assembly. *The Journal of Cell Biology*, 172(4), pp.505–515.

Hartwell, L.H., 1970. Periodic density fluctuation during the yeast cell cycle and the selection of synchronous cultures. *Journal of bacteriology*, 104(3), pp.1280–1285.

Hartwell, L.H. & Weinert, T.A., 1989. Checkpoints: controls that ensure the order of cell cycle events. *Science*, 246(4930), pp.629–634.

Hartwell, L.H. et al., 1973. Genetic Control of the Cell Division Cycle in Yeast: V. Genetic Analysis of cdc Mutants. *Genetics*, 74(2), pp.267–286.

Hauf, S. et al., 2003. The small molecule Hesperadin reveals a role for Aurora B in correcting kinetochore-microtubule attachment and in maintaining the spindle assembly checkpoint. *The Journal of Cell Biology*, 161(2), pp.281–294.

Hegarat, N. et al., 2020. Cyclin A triggers Mitosis either via the Greatwall kinase pathway or Cyclin B. *The EMBO Journal*, 39(11), p.e104419.

Heinrich, S. et al., 2014. Mad1 contribution to spindle assembly checkpoint signalling goes beyond presenting Mad2 at kinetochores. *EMBO reports*, 15(3), pp.291–298.

Heinrich, S. et al., 2012. Mph1 kinetochore localization is crucial and upstream in the hierarchy of spindle assembly checkpoint protein recruitment to kinetochores. *Journal of cell science*, 125(20), pp.4720–4727.

Hershko, A. & Ciechanover, A., 1992. The ubiquitin system for protein degradation. *Annual review of biochemistry*, 61(1), pp.761–807.

Hershko, A. et al., 1991. Methylated ubiquitin inhibits cyclin degradation in clam embryo extracts. *The Journal of biological chemistry*, 266(25), pp.16376–16379.

Hershko, A. et al., 1980. Proposed role of ATP in protein breakdown: conjugation of protein with multiple chains of the polypeptide of ATP-dependent proteolysis. *Proceedings of the National Academy of Sciences*, 77(4), pp.1783–1786.

Herzog, F. et al., 2009. Structure of the anaphase-promoting complex/cyclosome interacting with a mitotic checkpoint complex. *Science*, 323(5920), pp.1477–1481.

Heun, P. et al., 2006. Mislocalization of the Drosophila centromere-specific histone CID promotes formation of functional ectopic kinetochores. *Developmental Cell*, 10(3), pp.303–315.

Hewitt, L. et al., 2010. Sustained MPS1 activity is required in mitosis to recruit O-Mad2 to the Mad1-C-Mad2 core complex. *The Journal of Cell Biology*, 190(1), pp.25–34.

Hieter, P. et al., 1985. Functional selection and analysis of yeast centromeric DNA. *Cell*, 42(3), pp.913–921.

Hinchcliffe, E.H. et al., 1999. Requirement of Cdk2-cyclin E activity for repeated centrosome reproduction in Xenopus egg extracts. *Science*, 283(5403), pp.851–854.

Hinshaw, S.M. & Harrison, S.C., 2019. The structure of the Ctf19c/CCAN from budding yeast. *eLife*, 8, p.531.

Hiruma, Y. et al., 2015. CELL DIVISION CYCLE. Competition between MPS1 and microtubules at kinetochores regulates spindle checkpoint signaling. *Science*, 348(6240), pp.1264–1267.

Hochegger, H., Takeda, S. & Hunt, T., 2008. Cyclin-dependent kinases and cell-cycle transitions: does one fit all? *Nature reviews. Molecular cell biology*, 9(11), pp.910–916.

Holland, A.J. et al., 2015. Preventing farnesylation of the dynein adaptor Spindly contributes to the mitotic defects caused by farnesyltransferase inhibitors. E. Holzbaur, ed. *Molecular biology of the cell*, 26(10), pp.1845–1856.

Holmes, J.K. & Solomon, M.J., 1996. A predictive scale for evaluating cyclin-dependent kinase substrates. A comparison of p34cdc2 and p33cdk2. *The Journal of biological chemistry*, 271(41), pp.25240–25246.

Hori, T. et al., 2013. The CCAN recruits CENP-A to the centromere and forms the structural core for kinetochore assembly. *The Journal of Cell Biology*, 200(1), pp.45–60.

Howell, B.J. et al., 2004. Spindle Checkpoint Protein Dynamics at Kinetochores in Living Cells. *Current Biology*, 14(11), pp.953–964.

Howell, B.J. et al., 2000. Visualization of Mad2 dynamics at kinetochores, along spindle fibers, and at spindle poles in living cells. *The Journal of Cell Biology*, 150(6), pp.1233–1250.

Howman, E.V. et al., 2000. Early disruption of centromeric chromatin organization in centromere protein A (Cenpa) null mice. *Proceedings of the National Academy of Sciences*, 97(3), pp.1148–1153.

Hoyt, M.A., Totis, L. & Roberts, B.T., 1991. S. cerevisiae genes required for cell cycle arrest in response to loss of microtubule function. *Cell*, 66(3), pp.507–517.

Hsu, C.-C. et al., 2010. Targeted methylation of CMV and E1A viral promoters. *Biochemical and biophysical research communications*, 402(2), pp.228–234.

Hutchins, J.R.A. et al., 2010. Systematic analysis of human protein complexes identifies chromosome segregation proteins. *Science*, 328(5978), pp.593–599.

Irniger, S. et al., 1995. Genes involved in sister chromatid separation are needed for B-type cyclin proteolysis in budding yeast. *Cell*, 81(2), pp.269–278.

Ishikawa, H. et al., 2005. Odf2-deficient mother centrioles lack distal/subdistal appendages and the ability to generate primary cilia. *Nature Cell Biology*, 7(5), pp.517–524.

Ito, D., Saito, Y. & Matsumoto, T., 2012. Centromere-tethered MPS1 pombe homolog (Mph1) kinase is a sufficient marker for recruitment of the spindle checkpoint protein Bub1, but not Mad1. *Proceedings of the National Academy of Sciences of the United States of America*, 109(1), pp.209–214.

Izawa, D. & Pines, J., 2011. How APC/C–Cdc20 changes its substrate specificity in mitosis. *Nature Cell Biology*, 13(3), pp.223–233.

Izawa, D. & Pines, J., 2012. Mad2 and the APC/C compete for the same site on Cdc20 to ensure proper chromosome segregation. *The Journal of Cell Biology*, 199(1), pp.27–37.

Izawa, D. & Pines, J., 2015. The mitotic checkpoint complex binds a second CDC20 to inhibit active APC/C. *Nature*, 517(7536), pp.631–634.

Izquierdo, D. et al., 2014. Stabilization of cartwheel-less centrioles for duplication requires CEP295-mediated centriole-to-centrosome conversion. *CellReports*, 8(4), pp.957–965.

Jablonski, S.A. et al., 1998. The hBUB1 and hBUBR1 kinases sequentially assemble onto kinetochores during prophase with hBUBR1 concentrating at the kinetochore plates in mitosis. *Chromosoma*, 107(6-7), pp.386–396.

Jackman, M. et al., 2020. Cyclin B1-Cdk1 facilitates MAD1 release from the nuclear pore to ensure a robust spindle checkpoint. *The Journal of Cell Biology*, 219(6), p.ra42.

Jaspersen, S.L., Charles, J.F. & Morgan, D.O., 1999. Inhibitory phosphorylation of the APC regulator Hct1 is controlled by the kinase

Cdc28 and the phosphatase Cdc14. *Current Biology*, 9(5), pp.227–236.

Jelluma, N. et al., 2010. Release of MPS1 from kinetochores is crucial for timely anaphase onset. *The Journal of Cell Biology*, 191(2), pp.281–290.

Ji, Z. et al., 2017. A sequential multi-target MPS1 phosphorylation cascade promotes spindle checkpoint signaling. *eLife*, 6, p.431.

Johnson, V.L., 2004. Bub1 is required for kinetochore localization of BubR1, Cenp-E, Cenp-F and Mad2, and chromosome congression. *Journal of cell science*, 117(8), pp.1577–1589.

Jokelainen, P.T., 1967. The ultrastructure and spatial organization of the metaphase kinetochore in mitotic rat cells. *Journal of ultrastructure research*, 19(1), pp.19–44.

Kalay, E. et al., 2011. CEP152 is a genome maintenance protein disrupted in Seckel syndrome. *Nature genetics*, 43(1), pp.23–26.

Kaláb, P. et al., 2006. Analysis of a RanGTP-regulated gradient in mitotic somatic cells. *Nature*, 440(7084), pp.697–701.

Kapitein, L.C. et al., 2005. The bipolar mitotic kinesin Eg5 moves on both microtubules that it crosslinks. *Nature*, 435(7038), pp.114–118.

Karki, M., Keyhaninejad, N. & Shuster, C.B., 2017. Precocious centriole disengagement and centrosome fragmentation induced by mitotic delay. *Nature communications*, 8(1), pp.15803–12.

Kasbek, C. et al., 2007. Preventing the degradation of MPS1 at centrosomes is sufficient to cause centrosome reduplication in human cells. S. Doxsey, ed. *Molecular biology of the cell*, 18(11), pp.4457–4469.

Kaur, H. et al., 2007. Analysis of mitotic phosphorylation of borealin. *BMC cell biology*, 8(1), pp.5–17.

Kellogg, D.R., Moritz, M. & Alberts, B.M., 1994. The centrosome and cellular organization. *Annual review of biochemistry*, 63(1), pp.639–674.

Kelly, A. et al., 2014. Ubiquitin chain elongation requires E3-dependent tracking of the emerging conjugate. *Molecular Cell*, 56(2), pp.232–245.

Kepinski, S. & Leyser, O., 2005. The Arabidopsis F-box protein TIR1 is an auxin receptor. *Nature*, 435(7041), pp.446–451.

Khodjakov, A. & Pines, J., 2010. Centromere tension: a divisive issue. *Nature Cell Biology*, 12(10), pp.919–923.

Kim, D.H. et al., 2018. TRIP13 and APC15 drive mitotic exit by turnover of interphase- and unattached kinetochore-produced MCC. *Nature communications*, 9(1), p.4354.

Kim, J., Kim, J. & Rhee, K., 2019. PCNT is critical for the association and conversion of centrioles to centrosomes during mitosis. *Journal of cell science*, 132(6), p.jcs225789.

Kim, J., Lee, K. & Rhee, K., 2015. PLK1 regulation of PCNT cleavage ensures fidelity of centriole separation during mitotic exit. *Nature communications*, 6(1), pp.10076–12.

Kim, K. et al., 2008. A novel function of CEP135 as a platform protein of C-NAP1 for its centriolar localization. *Experimental cell research*, 314(20), pp.3692–3700.

Kim, S. & Rhee, K., 2014. Importance of the CEP215-pericentrin interaction for centrosome maturation during mitosis. T. Toda, ed. *PloS one*, 9(1), p.e87016.

Kim, T.-S. et al., 2013. Hierarchical recruitment of Plk4 and regulation of centriole biogenesis by two centrosomal scaffolds, Cep192 and Cep152. *Proceedings of the National Academy of Sciences of the United States of America*, 110(50), pp.E4849–57.

King, R.W. et al., 1995. A 20S complex containing CDC27 and CDC16 catalyzes the mitosis-specific conjugation of ubiquitin to cyclin B. *Cell*, 81(2), pp.279–288.

Kitagawa, D. et al., 2011. Structural basis of the 9-fold symmetry of centrioles. *Cell*, 144(3), pp.364–375.

Kleylein-Sohn, J. et al., 2007. Plk4-induced centriole biogenesis in human cells. *Developmental Cell*, 13(2), pp.190–202.

Kline, S.L. et al., 2006. The human Mis12 complex is required for kinetochore assembly and proper chromosome segregation. *The Journal of Cell Biology*, 173(1), pp.9–17.

Kobayashi, T. et al., 2011. Centriolar kinesin Kif24 interacts with CP110 to remodel microtubules and regulate ciliogenesis. *Cell*, 145(6), pp.914–925.

Koch, L.B. et al., 2019. Autophosphorylation is sufficient to release MPS1 kinase from native kinetochores. *Proceedings of the National Academy of Sciences of the United States of America*, 116(35), pp.17355–17360.

Kohlmaier, G. et al., 2009. Overly long centrioles and defective cell division upon excess of the SAS-4-related protein CPAP. *Current biology : CB*, 19(12), pp.1012–1018.

Kollman, J.M. et al., 2011. Microtubule nucleation by γ-tubulin complexes. *Nature reviews. Molecular cell biology*, 12(11), pp.709–721.

Kong, D. et al., 2020. Prolonged mitosis results in structurally aberrant and over-elongated centrioles. *The Journal of Cell Biology*, 219(6), p.1233.

Kops, G.J.P.L. & Gassmann, R., 2020. Crowning the Kinetochore: The Fibrous Corona in Chromosome Segregation. *Trends in Cell Biology*, 30(8), pp.653–667.

Kops, G.J.P.L., Kim, Y., et al., 2005. ZW10 links mitotic checkpoint signaling to the structural kinetochore. *The Journal of Cell Biology*, 169(1), pp.49–60.

Kops, G.J.P.L., Weaver, B.A.A. & Cleveland, D.W., 2005. On the road to cancer: aneuploidy and the mitotic checkpoint. *Nature reviews. Cancer*, 5(10), pp.773–785.

Kraft, C. et al., 2003. Mitotic regulation of the human anaphase-promoting complex by phosphorylation. *The EMBO Journal*, 22(24), pp.6598–6609.

Kraft, C. et al., 2005. The WD40 propeller domain of Cdh1 functions as a destruction box receptor for APC/C substrates. *Molecular Cell*, 18(5), pp.543–553.

Kramer, E.R. et al., 1998. Activation of the human anaphase-promoting complex by proteins of the CDC20/Fizzy family. *Current Biology*, 8(22), pp.1207–1210.

Kratz, A.-S. et al., 2015. Plk4-dependent phosphorylation of STIL is required for centriole duplication. *Biology Open*, 4(3), pp.370–377.

Krenn, V. et al., 2014. KI motifs of human Knl1 enhance assembly of comprehensive spindle checkpoint complexes around MELT repeats. *Current biology : CB*, 24(1), pp.29–39.

Krenn, V. et al., 2012. Structural analysis reveals features of the spindle checkpoint kinase Bub1-kinetochore subunit Knl1 interaction. *The Journal of Cell Biology*, 196(4), pp.451–467.

Kruse, T. et al., 2014. A direct role of Mad1 in the spindle assembly checkpoint beyond Mad2 kinetochore recruitment. *EMBO reports*, 15(3), pp.282–290.

Kruse, T. et al., 2013. Direct binding between BubR1 and B56-PP2A phosphatase complexes regulate mitotic progression. *Journal of cell science*, 126(Pt 5), pp.1086–1092.

Kubai, D.F., 1975. The evolution of the mitotic spindle. *International review of cytology*, 43, pp.167–227.

Kuijt, T.E.F. et al., 2014. Conditional targeting of MAD1 to kinetochores is sufficient to reactivate the spindle assembly checkpoint in metaphase. *Chromosoma*, 123(5), pp.471–480.

Kulukian, A., Han, J.S. & Cleveland, D.W., 2009. Unattached kinetochores catalyze production of an anaphase inhibitor that requires a Mad2 template to prime Cdc20 for BubR1 binding. *Developmental Cell*, 16(1), pp.105–117.

Kurkowiak, M., Ziętkiewicz, E. & Witt, M., 2015. Recent advances in primary ciliary dyskinesia genetics. *Journal of medical genetics*, 52(1), pp.1–9.

la Torre-García, De, O. et al., 2019. A homozygous CEP57 c.915_925dupCAATGTTCAGC mutation in a patient with mosaic variegated aneuploidy syndrome with rhizomelic shortening in the upper and lower limbs and a narrow thorax. *European journal of medical genetics*, 62(3), pp.195–197.

Lacey, K.R., Jackson, P.K. & Stearns, T., 1999. Cyclin-dependent kinase control of centrosome duplication. *Proceedings of the National Academy of Sciences*, 96(6), pp.2817–2822.

Lambrus, B.G. et al., 2015. p53 protects against genome instability following centriole duplication failure. *The Journal of Cell Biology*, 210(1), pp.63–77.

Lane, A.H. et al., 2002. Mosaic variegated aneuploidy with growth hormone deficiency and congenital heart defects. *American journal of medical genetics*, 110(3), pp.273–277.

Lara-Gonzalez, P. et al., 2011. BubR1 blocks substrate recruitment to the APC/C in a KEN-box-dependent manner. *Journal of cell science*, 124(Pt 24), pp.4332–4345.

Lara-Gonzalez, P., Westhorpe, F.G. & Taylor, S.S., 2012. The spindle assembly checkpoint. *Current biology : CB*, 22(22), pp.R966–80.

Lawo, S. et al., 2012. Subdiffraction imaging of centrosomes reveals higher-order organizational features of pericentriolar material. *Nature Cell Biology*, 14(11), pp.1148–1158.

Lechner, J. & Carbon, J., 1991. A 240 kd multisubunit protein complex, CBF3, is a major component of the budding yeast centromere. *Cell*, 64(4), pp.717–725.

Lee, K. & Rhee, K., 2011. PLK1 phosphorylation of pericentrin initiates centrosome maturation at the onset of mitosis. *The Journal of Cell Biology*, 195(7), pp.1093–1101.

Lee, K. & Rhee, K., 2012. Separase-dependent cleavage of pericentrin B is necessary and sufficient for centriole disengagement during mitosis. *Cell cycle (Georgetown, Tex.)*, 11(13), pp.2476–2485.

Lee, K.S. et al., 2020. A self-assembled cylindrical platform for Plk4-induced centriole biogenesis. *Open biology*, 10(8), p.200102.

Lee, K.S. et al., 1998. Mutation of the polo-box disrupts localization and mitotic functions of the mammalian polo kinase Plk. *Proceedings of the National Academy of Sciences*, 95(16), pp.9301–9306.

Lee, S. & Rhee, K., 2010. CEP215 is involved in the dynein-dependent accumulation of pericentriolar matrix proteins for spindle pole formation. *Cell cycle (Georgetown, Tex.)*, 9(4), pp.774–783.

Lemmens, B. et al., 2018. DNA Replication Determines Timing of Mitosis by Restricting CDK1 and PLK1 Activation. *Molecular Cell*, 71(1), pp.117–128.e3.

Li, Q. et al., 2016. WD40 domain of Apc1 is critical for the coactivator-induced allosteric transition that stimulates APC/C catalytic activity. *Proceedings of the National Academy of Sciences of the United States of America*, 113(38), pp.10547–10552.

Li, Y. et al., 2007. Kinetochore dynein generates a poleward pulling force to facilitate congression and full chromosome alignment. *Cell research*, 17(8), pp.701–712.

Lindon, C., Grant, R. & Min, M., 2015. Ubiquitin-Mediated Degradation of Aurora Kinases. *Frontiers in Oncology*, 5(24), p.307.

Lingle, W.L. et al., 2002. Centrosome amplification drives chromosomal instability in breast tumor development. *Proceedings of the National Academy of Sciences*, 99(4), pp.1978–1983.

Lingle, W.L. et al., 1998. Centrosome hypertrophy in human breast tumors: implications for genomic stability and cell polarity. *Proceedings of the National Academy of Sciences*, 95(6), pp.2950–2955.

Littlepage, L.E. et al., 2002. Identification of phosphorylated residues that affect the activity of the mitotic kinase Aurora-A. *Proceedings of the National Academy of Sciences*, 99(24), pp.15440–15445.

Logarinho, E. et al., 2004. Different spindle checkpoint proteins monitor microtubule attachment and tension at kinetochores in Drosophila cells. *Journal of cell science*, 117(Pt 9), pp.1757–1771.

Logsdon, G.A. et al., 2015. Both tails and the centromere targeting domain of CENP-A are required for centromere establishment. *The Journal of Cell Biology*, 208(5), pp.521–531.

London, N. & Biggins, S., 2014. Mad1 kinetochore recruitment by MPS1-mediated phosphorylation of Bub1 signals the spindle checkpoint. *Genes & development*, 28(2), pp.140–152.

London, N. et al., 2012. Phosphoregulation of Spc105 by MPS1 and PP1 regulates Bub1 localization to kinetochores. *Current biology : CB*, 22(10), pp.900–906.

Lucas, E.P. & Raff, J.W., 2007. Maintaining the proper connection between the centrioles and the pericentriolar matrix requires Drosophila centrosomin. *The Journal of Cell Biology*, 178(5), pp.725–732.

Lukinavičius, G. et al., 2013. Selective chemical crosslinking reveals a CEP57-Cep63-Cep152 centrosomal complex. *Current biology : CB*, 23(3), pp.265–270.

Luo, X. et al., 2000. Structure of the Mad2 spindle assembly checkpoint protein and its interaction with Cdc20. *Nature structural biology*, 7(3), pp.224–229.

Lüders, J., 2012. The amorphous pericentriolar cloud takes shape. *Nature Cell Biology*, 14(11), pp.1126–1128.

Lüders, J. & Stearns, T., 2007. Microtubule-organizing centres: a re-evaluation. *Nature reviews. Molecular cell biology*, 8(2), pp.161–167.

Ma, H.T. & Poon, R.Y.C., 2018. TRIP13 Functions in the Establishment of the Spindle Assembly Checkpoint by Replenishing O-MAD2. *Cell Reports*, 22(6), pp.1439–1450.

Ma, H.T. & Poon, R.Y.C., 2016. TRIP13 Regulates Both the Activation and Inactivation of the Spindle-Assembly Checkpoint. *CellReports*, 14(5), pp.1086–1099.

Ma, Z. et al., 2019. PTC-bearing mRNA elicits a genetic compensation response via Upf3a and COMPASS components. *Nature*, 568(7751), pp.259–263.

Magidson, V. et al., 2015. Adaptive changes in the kinetochore architecture facilitate proper spindle assembly. *Nature Cell Biology*, 17(9), pp.1134–1144.

Maldonado, M. & Kapoor, T.M., 2011. Constitutive Mad1 targeting to kinetochores uncouples checkpoint signalling from chromosome biorientation. *Nature Cell Biology*, 13(4), pp.475–482.

Mali, P., Esvelt, K.M. & Church, G.M., 2013. Cas9 as a versatile tool for engineering biology. *Nature methods*, 10(10), pp.957–963.

Man, X., Megraw, T.L. & Lim, Y.P., 2015. Cep68 can be regulated by Nek2 and SCF complex. *European journal of cell biology*, 94(3-4), pp.162–172.

Mansfeld, J. et al., 2011. APC15 drives the turnover of MCC-CDC20 to make the spindle assembly checkpoint responsive to kinetochore attachment. *Nature Cell Biology*, 13(10), pp.1234–1243.

Mapelli, M. et al., 2006. Determinants of conformational dimerization of Mad2 and its inhibition by p31comet. *The EMBO Journal*, 25(6), pp.1273–1284.

Mardin, B.R. & Schiebel, E., 2012. Breaking the ties that bind: new advances in centrosome biology. *The Journal of Cell Biology*, 197(1), pp.11–18.

Mardin, B.R. et al., 2011. Plk1 controls the Nek2A-PP1γ antagonism in centrosome disjunction. *Current biology : CB*, 21(13), pp.1145–1151.

Marjanović, M. et al., 2015. CEP63 deficiency promotes p53-dependent microcephaly and reveals a role for the centrosome in meiotic recombination. *Nature communications*, 6(1), pp.7676–14.

Marquardt, J.R. et al., 2016. Modular elements of the TPR domain in the MPS1 N terminus differentially target MPS1 to the centrosome and kinetochore. *Proceedings of the National Academy of Sciences of the United States of America*, 113(28), pp.7828–7833.

Martinez-Campos, M. et al., 2004. The Drosophila pericentrin-like protein is essential for cilia/flagella function, but appears to be dispensable for mitosis. *The Journal of Cell Biology*, 165(5), pp.673–683.

Matsuo, K. et al., 2010. Involvement of a centrosomal protein kendrin in the maintenance of centrosome cohesion by modulating Nek2A kinase activity. *Biochemical and biophysical research communications*, 398(2), pp.217–223.

Matsuo, K. et al., 2012. Kendrin is a novel substrate for Separase involved in the licensing of centriole duplication. *Current biology : CB*, 22(10), pp.915–921.

Matyskiela, M.E. & Morgan, D.O., 2009. Analysis of activator-binding sites on the APC/C supports a cooperative substrate-binding mechanism. *Molecular Cell*, 34(1), pp.68–80.

Maupin-Furlow, J., 2011. Proteasomes and protein conjugation across domains of life. *Nature reviews. Microbiology*, 10(2), pp.100–111.

Mayor, T. et al., 2000. The centrosomal protein C-Nap1 is required for cell cycle-regulated centrosome cohesion. *The Journal of Cell Biology*, 151(4), pp.837–846.

MAZIA, D., 1961. How cells divide. *Scientific American*, 205(3), pp.100–120.

McEwen, B.F. et al., 2001. CENP-E is essential for reliable bioriented spindle attachment, but chromosome alignment can be achieved via redundant mechanisms in mammalian cells. T. Salmon, ed. *Molecular biology of the cell*, 12(9), pp.2776–2789.

McIntosh, J.R., 1991. Structural and mechanical control of mitotic progression. *Cold Spring Harbor symposia on quantitative biology*, 56(0), pp.613–619.

McLean, J.R. et al., 2011. State of the APC/C: organization, function, and structure. *Critical reviews in biochemistry and molecular biology*, 46(2), pp.118–136.

Mennella, V. et al., 2012. Subdiffraction-resolution fluorescence microscopy reveals a domain of the centrosome critical for pericentriolar material organization. *Nature Cell Biology*, 14(11), pp.1159–1168.

Meraldi, P., Draviam, V.M. & Sorger, P.K., 2004. Timing and checkpoints in the regulation of mitotic progression. *Developmental Cell*, 7(1), pp.45–60.

Mertins, P. et al., 2016. Proteogenomics connects somatic mutations to signalling in breast cancer. *Nature*, 534(7605), pp.55–62.

Min, M. & Lindon, C., 2012. Substrate targeting by the ubiquitin-proteasome system in mitosis. *Seminars in cell & developmental biology*, 23(5), pp.482–491.

Miniowitz-Shemtov, S. et al., 2010. ATP is required for the release of the anaphase-promoting complex/cyclosome from inhibition by the mitotic checkpoint. *Proceedings of the National Academy of Sciences of the United States of America*, 107(12), pp.5351–5356.

Miniowitz-Shemtov, S. et al., 2015. Mode of interaction of TRIP13 AAA-ATPase with the Mad2-binding protein p31comet and with mitotic checkpoint complexes. *Proceedings of the National Academy of Sciences of the United States of America*, 112(37), pp.11536–11540.

Miniowitz-Shemtov, S. et al., 2012. Role of phosphorylation of Cdc20 in p31(comet)-stimulated disassembly of the mitotic checkpoint complex. *Proceedings of the National Academy of Sciences of the United States of America*, 109(21), pp.8056–8060.

Minshull, J., Blow, J.J. & Hunt, T., 1989. Translation of cyclin mRNA is necessary for extracts of activated xenopus eggs to enter mitosis. *Cell*, 56(6), pp.947–956.

Mishra, R.K. et al., 2010. The Nup107-160 complex and gamma-TuRC regulate microtubule polymerization at kinetochores. *Nature Cell Biology*, 12(2), pp.164–169.

Mitchison, T. & Kirschner, M., 1984. Dynamic instability of microtubule growth. *Nature*, 312(5991), pp.237–242.

Momotani, K. et al., 2008. CEP57, a multidomain protein with unique microtubule and centrosomal localization domains. *The Biochemical journal*, 412(2), pp.265–273.

Monda, J.K. & Cheeseman, I.M., 2018. The kinetochore-microtubule interface at a glance. *Journal of cell science*, 131(16), p.jcs214577.

Montefalcone, G. et al., 1999. Centromere repositioning. *Genome research*, 9(12), pp.1184–1188.

Moore, L.L. & Roth, M.B., 2001. HCP-4, a CENP-C-like protein in Caenorhabditis elegans, is required for resolution of sister centromeres. *The Journal of Cell Biology*, 153(6), pp.1199–1208.

Morgan, D.O., 1999. Regulation of the APC and the exit from mitosis. *Nature Cell Biology*, 1(2), pp.E47–53.

Morgan, D.O., 2007. *The cell cycle: principles of control*,

Moritz, B., Becker, P.B. & Göpfert, U., 2015. CMV promoter mutants with a reduced propensity to productivity loss in CHO cells. *Scientific reports*, 5(1), pp.16952–8.

Morrow, C.J. et al., 2005. Bub1 and aurora B cooperate to maintain BubR1-mediated inhibition of APC/CCdc20. *Journal of cell science*, 118(Pt 16), pp.3639–3652.

Mosalaganti, S. et al., 2017. Structure of the RZZ complex and molecular basis of its interaction with Spindly. *The Journal of Cell Biology*, 216(4), pp.961–981.

Moshe, Y. et al., 2004. Role of Polo-like kinase in the degradation of early mitotic inhibitor 1, a regulator of the anaphase promoting complex/cyclosome. *Proceedings of the National Academy of Sciences*, 101(21), pp.7937–7942.

Moudgil, D.K. et al., 2015. A novel role of farnesylation in targeting a mitotic checkpoint protein, human Spindly, to kinetochores. *The Journal of Cell Biology*, 208(7), pp.881–896.

Murphy, T.D. & Karpen, G.H., 1995. Localization of centromere function in a Drosophila minichromosome. *Cell*, 82(4), pp.599–609.

Musacchio, A. & Desai, A., 2017. A Molecular View of Kinetochore Assembly and Function. *Biology*, 6(1), p.5.

Musacchio, A. & Salmon, E.D., 2007. The spindle-assembly checkpoint in space and time. *Nature reviews. Molecular cell biology*, 8(5), pp.379–393.

Nakajima, H. et al., 2003. Identification of a consensus motif for Plk (Polo-like kinase) phosphorylation reveals Myt1 as a Plk1 substrate. *The Journal of biological chemistry*, 278(28), pp.25277–25280.

Nakamura, A., Arai, H. & Fujita, N., 2009. Centrosomal Aki1 and cohesin function in Separase-regulated centriole disengagement. *The Journal of Cell Biology*, 187(5), pp.607–614.

Natsume, T. et al., 2016. Rapid Protein Depletion in Human Cells by Auxin-Inducible Degron Tagging with Short Homology Donors. *Cell Reports*, 15(1), pp.210–218.

Neumann, B. et al., 2010. Phenotypic profiling of the human genome by time-lapse microscopy reveals cell division genes. *Nature*, 464(7289), pp.721–727.

Nigg, E.A., 2007. Centrosome duplication: of rules and licenses. *Trends in Cell Biology*, 17(5), pp.215–221.

Nigg, E.A., 1991. The substrates of the cdc2 kinase. *Seminars in cell biology*, 2(4), pp.261–270.

Nigg, E.A. & Raff, J.W., 2009. Centrioles, centrosomes, and cilia in health and disease. *Cell*, 139(4), pp.663–678.

Nigg, E.A. & Stearns, T., 2011. The centrosome cycle: Centriole biogenesis, duplication and inherent asymmetries. *Nature Cell Biology*, 13(10), pp.1154–1160.

Nijenhuis, W. et al., 2013. A TPR domain-containing N-terminal module of MPS1 is required for its kinetochore localization by Aurora B. *The Journal of Cell Biology*, 201(2), pp.217–231.

Nilsson, J. et al., 2008. The APC/C maintains the spindle assembly checkpoint by targeting Cdc20 for destruction. *Nature Cell Biology*, 10(12), pp.1411–1420.

Nishimura, K. et al., 2020. A super-sensitive auxin-inducible degron system with an engineered auxin-TIR1 pair. *Nucleic acids research*, 48(18), pp.e108–e108.

Nishimura, K., Fukagawa, T., Takisawa, H., Kakimoto, T. & Kanemaki, M., 2009a. An auxin-based degron system for the rapid depletion of proteins in nonplant cells. *Nature methods*, 6(12), pp.917–922.

Nishimura, K., Fukagawa, T., Takisawa, H., Kakimoto, T. & Kanemaki, M., 2009b. An auxin-based degron system for the rapid depletion of proteins in nonplant cells. *Nature methods*, 6(12), pp.917–922.

Nurse, P., Thuriaux, P. & Nasmyth, K., 1976. Genetic control of the cell division cycle in the fission yeast Schizosaccharomyces pombe. *Molecular & general genetics : MGG*, 146(2), pp.167–178.

O'Connor, A. et al., 2015. Requirement for PLK1 kinase activity in the maintenance of a robust spindle assembly checkpoint. *Biology Open*, 5(1), pp.11–19.

Oegema, K. et al., 2001. Functional analysis of kinetochore assembly in Caenorhabditis elegans. *The Journal of Cell Biology*, 153(6), pp.1209–1226.

Ohi, M.D. et al., 2007. Structural organization of the anaphase-promoting complex bound to the mitotic activator Slp1. *Molecular Cell*, 28(5), pp.871–885.

Ohta, M. et al., 2014. Direct interaction of Plk4 with STIL ensures formation of a single procentriole per parental centriole. *Nature communications*, 5(1), pp.5267–12.

Okuda, M. et al., 2000. Nucleophosmin/B23 is a target of CDK2/cyclin E in centrosome duplication. *Cell*, 103(1), pp.127–140.

Oliveira, R.A. & Nasmyth, K., 2013. Cohesin cleavage is insufficient for centriole disengagement in Drosophila. *Current biology : CB*, 23(14), pp.R601–3.

Overlack, K. et al., 2015. A molecular basis for the differential roles of Bub1 and BubR1 in the spindle assembly checkpoint. *eLife*, 4, p.e05269.

Pagliuca, F.W., Collins, M.O. & Choudhary, J.S., 2011. Coordinating cell cycle progression via cyclin specificity. *Cell cycle (Georgetown, Tex.)*, 10(24), pp.4195–4196.

Paintrand, M. et al., 1992. Centrosome organization and centriole architecture: their sensitivity to divalent cations. *Journal of structural biology*, 108(2), pp.107–128.

Palmer, D.K. et al., 1987. A 17-kD centromere protein (CENP-A) copurifies with nucleosome core particles and with histones. *The Journal of Cell Biology*, 104(4), pp.805–815.

Pan, J. & Chen, R.-H., 2004. Spindle checkpoint regulates Cdc20p stability in Saccharomyces cerevisiae. *Genes & development*, 18(12), pp.1439–1451.

Parrilla, A. et al., 2016. Mitotic entry: The interplay between Cdk1, Plk1 and Bora. *Cell cycle (Georgetown, Tex.)*, 15(23), pp.3177–3182.

Passmore, L.A. & Barford, D., 2004. Getting into position: the catalytic mechanisms of protein ubiquitylation. *The Biochemical journal*, 379(Pt 3), pp.513–525.

Passmore, L.A. et al., 2003. Doc1 mediates the activity of the anaphase-promoting complex by contributing to substrate recognition. *The EMBO Journal*, 22(4), pp.786–796.

Passmore, L.A. et al., 2005. Structural analysis of the anaphase-promoting complex reveals multiple active sites and insights into polyubiquitylation. *Molecular Cell*, 20(6), pp.855–866.

Pereira, C. et al., 2018. Self-Assembly of the RZZ Complex into Filaments Drives Kinetochore Expansion in the Absence of Microtubule Attachment. *Current biology : CB*, 28(21), pp.3408–3421.e8.

Pesenti, M.E. et al., 2018. Reconstitution of a 26-Subunit Human Kinetochore Reveals Cooperative Microtubule Binding by CENP-OPQUR and NDC80. *Molecular Cell*, 71(6), pp.923–939.e10.

Peters, J.M., 1998. SCF and APC: the Yin and Yang of cell cycle regulated proteolysis. *Current Opinion in Cell Biology*, 10(6), pp.759–768.

Peters, J.M. et al., 1996. Identification of BIME as a subunit of the anaphase-promoting complex. *Science*, 274(5290), pp.1199–1201.

Petrovic, A. et al., 2010. The MIS12 complex is a protein interaction hub for outer kinetochore assembly. *The Journal of Cell Biology*, 190(5), pp.835–852.

Pickart, C.M., 2001. Ubiquitin enters the new millennium. *Molecular Cell*, 8(3), pp.499–504.

Piel, M. et al., 2001. Centrosome-dependent exit of cytokinesis in animal cells. *Science*, 291(5508), pp.1550–1553.

Piel, M. et al., 2000. The respective contributions of the mother and daughter centrioles to centrosome activity and behavior in vertebrate cells. *The Journal of Cell Biology*, 149(2), pp.317–330.

Pihan, G.A. et al., 1998. Centrosome defects and genetic instability in malignant tumors. *Cancer research*, 58(17), pp.3974–3985.

Pines, J. & Hunt, T., 1987. Molecular cloning and characterization of the mRNA for cyclin from sea urchin eggs. *The EMBO Journal*, 6(10), pp.2987–2995.

Pines, J. & Hunter, T., 1990. p34cdc2: the S and M kinase? *The New biologist*, 2(5), pp.389–401.

Pinson, L. et al., 2014. CEP57 mutation in a girl with mosaic variegated aneuploidy syndrome. *American journal of medical genetics. Part A*, 164A(1), pp.177–181.

Plechanovová, A. et al., 2012. Structure of a RING E3 ligase and ubiquitin-loaded E2 primed for catalysis. *Nature*, 489(7414), pp.115–120.

Primorac, I. et al., 2013. Bub3 reads phosphorylated MELT repeats to promote spindle assembly checkpoint signaling. *eLife*, 2, pp.213–20.

Przewloka, M.R. et al., 2011. CENP-C is a structural platform for kinetochore assembly. *Current biology : CB*, 21(5), pp.399–405.

Puntoni, F. & Villa-Moruzzi, E., 1997. Protein phosphatase-1 alpha, gamma 1, and delta: changes in phosphorylation and activity in mitotic HeLa cells and in cells released from the mitotic block. *Archives of biochemistry and biophysics*, 340(2), pp.177–184.

Qian, J. et al., 2017. An Attachment-Independent Biochemical Timer of the Spindle Assembly Checkpoint. *Molecular Cell*, 68(4), pp.715–730.e5.

Quintyne, N.J. et al., 2005. Spindle multipolarity is prevented by centrosomal clustering. *Science*, 307(5706), pp.127–129.

Raaijmakers, J.A. & Medema, R.H., 2019. Killing a zombie: a full deletion of the BUB1 gene in HAP1 cells. *The EMBO Journal*, 38(22), p.e102423.

Raaijmakers, J.A. et al., 2018. BUB1 Is Essential for the Viability of Human Cells in which the Spindle Assembly Checkpoint Is Compromised. *CellReports*, 22(6), pp.1424–1438.

Raaijmakers, J.A. et al., 2012. Nuclear envelope-associated dynein drives prophase centrosome separation and enables Eg5-independent bipolar spindle formation. *The EMBO Journal*, 31(21), pp.4179–4190.

Raff, J.W. & Glover, D.M., 1988. Nuclear and cytoplasmic mitotic cycles continue in Drosophila embryos in which DNA synthesis is inhibited with aphidicolin. *The Journal of Cell Biology*, 107(6 Pt 1), pp.2009–2019.

Ran, F.A. et al., 2013. Genome engineering using the CRISPR-Cas9 system. *Nature protocols*, 8(11), pp.2281–2308.

Rattner, J.B. et al., 1993. CENP-F is a .ca 400 kDa kinetochore protein that exhibits a cell-cycle dependent localization. *Cell motility and the cytoskeleton*, 26(3), pp.214–226.

Reddy, S.K. et al., 2007. Ubiquitination by the anaphase-promoting complex drives spindle checkpoint inactivation. *Nature*, 446(7138), pp.921–925.

Reed, S.I., 1982. Preparation of product-specific antisera by gene fusion: antibodies specific for the product of the yeast cell-division-cycle gene CDC28. *Gene*, 20(2), pp.255–265.

Reimann, J.D. et al., 2001. Emi1 regulates the anaphase-promoting complex by a different mechanism than Mad2 proteins. *Genes & development*, 15(24), pp.3278–3285.

Reimann, J.D.R. & Jackson, P.K., 2002. Emi1 is required for cytostatic factor arrest in vertebrate eggs. *Nature*, 416(6883), pp.850–854.

Richens, J.H. et al., 2015. The Drosophila Pericentrin-like-protein (PLP) cooperates with Cnn to maintain the integrity of the outer PCM. *Biology Open*, 4(8), pp.1052–1061.

Rieder, C.L. & Alexander, S.P., 1990. Kinetochores are transported poleward along a single astral microtubule during chromosome attachment to the spindle in newt lung cells. *The Journal of Cell Biology*, 110(1), pp.81–95.

Rieder, C.L. & Khodjakov, A., 1997. Mitosis and checkpoints that control progression through mitosis in vertebrate somatic cells. *Progress in cell cycle research*, 3(sup 1), pp.301–312.

Rieder, C.L. et al., 1995. The checkpoint delaying anaphase in response to chromosome monoorientation is mediated by an inhibitory signal produced by unattached kinetochores. *The Journal of Cell Biology*, 130(4), pp.941–948.

Rieder, C.L., Faruki, S. & Khodjakov, A., 2001. The centrosome in vertebrates: more than a microtubule-organizing center. *Trends in Cell Biology*, 11(10), pp.413–419.

Rocchi, M. et al., 2012. Centromere repositioning in mammals. *Heredity*, 108(1), pp.59–67.

Rodriguez-Rodriguez, J.-A. et al., 2018. Distinct Roles of RZZ and Bub1-KNL1 in Mitotic Checkpoint Signaling and Kinetochore Expansion. *Current biology : CB*, 28(21), pp.3422–3429.e5.

Roque, H. et al., 2018. Drosophila PLP assembles pericentriolar clouds that promote centriole stability, cohesion and MT nucleation. S. K. Dutcher, ed. *PLoS Genetics*, 14(2), p.e1007198.

Rosenberg, J.A. et al., 2006. Ppc89 links multiple proteins, including the septation initiation network, to the core of the fission yeast spindle-pole body. S. Schmid, ed. *Molecular biology of the cell*, 17(9), pp.3793–3805.

Rosenblatt, J. et al., 2004. Myosin II-dependent cortical movement is required for centrosome separation and positioning during mitotic spindle assembly. *Cell*, 117(3), pp.361–372.

Sacristan, C. & Kops, G.J.P.L., 2015. Joined at the hip: kinetochores, microtubules, and spindle assembly checkpoint signaling. *Trends in Cell Biology*, 25(1), pp.21–28.

Sacristan, C. et al., 2018. Dynamic kinetochore size regulation promotes microtubule capture and chromosome biorientation in mitosis. *Nature Cell Biology*, 20(7), pp.800–810.

Sahabandu, N. et al., 2019. Expansion microscopy for the analysis of centrioles and cilia. *Journal of microscopy*, 276(3), pp.145–159.

Sanchez, A.D. & Feldman, J.L., 2017. Microtubule-organizing centers: from the centrosome to non-centrosomal sites. *Current Opinion in Cell Biology*, 44, pp.93–101.

Santaguida, S. et al., 2011. Evidence that Aurora B is implicated in spindle checkpoint signalling independently of error correction. *The EMBO Journal*, 30(8), pp.1508–1519.

Santamaria, A. et al., 2011. The Plk1-dependent phosphoproteome of the early mitotic spindle. *Molecular & cellular proteomics : MCP*, 10(1), p.M110.004457.

Sathyan, K.M., Scott, T.G. & Guertin, M.J., 2020. ARF-AID: A Rapidly Inducible Protein Degradation System That Preserves Basal Endogenous Protein Levels. *Current protocols in molecular biology*, 132(1), p.e124.

Saurin, A.T., 2018. Kinase and Phosphatase Cross-Talk at the Kinetochore. *Frontiers in Cell and Developmental Biology*, 6, p.2964.

Saurin, A.T. et al., 2011. Aurora B potentiates MPS1 activation to ensure rapid checkpoint establishment at the onset of mitosis. *Nature communications*, 2(1), pp.316–9.

Scaglione, K.M. et al., 2013. The ubiquitin-conjugating enzyme (E2) Ube2w ubiquitinates the N terminus of substrates. *The Journal of biological chemistry*, 288(26), pp.18784–18788.

Schimke, R.T. & Doyle, D., 1970. Control of enzyme levels in animal tissues. *Annual review of biochemistry*, 39(1), pp.929–976.

Schmidt, T.I. et al., 2009. Control of centriole length by CPAP and CP110. *Current biology : CB*, 19(12), pp.1005–1011.

Schnell, J.D. & Hicke, L., 2003. Non-traditional functions of ubiquitin and ubiquitin-binding proteins. *The Journal of biological chemistry*, 278(38), pp.35857–35860.

Schöckel, L. et al., 2011. Cleavage of cohesin rings coordinates the separation of centrioles and chromatids. *Nature Cell Biology*, 13(8), pp.966–972.

Schreiber, A. et al., 2011. Structural basis for the subunit assembly of the anaphase-promoting complex. *Nature*, 470(7333), pp.227–232.

Schubert, von, C. et al., 2015. Plk1 and MPS1 Cooperatively Regulate the Spindle Assembly Checkpoint in Human Cells. *CellReports*, 12(1), pp.66–78.

Schwab, M. et al., 2001. Yeast Hct1 recognizes the mitotic cyclin Clb2 and other substrates of the ubiquitin ligase APC. *The EMBO Journal*, 20(18), pp.5165–5175.

Screpanti, E. et al., 2010. A screen for kinetochore-microtubule interaction inhibitors identifies novel antitubulin compounds. D. Cimini, ed. *PloS one*, 5(7), p.e11603.

Shang, W.-H. et al., 2010. Chickens possess centromeres with both extended tandem repeats and short non-tandem-repetitive sequences. *Genome research*, 20(9), pp.1219–1228.

Shrestha, R.L. & Draviam, V.M., 2013. Lateral to end-on conversion of chromosome-microtubule attachment requires kinesins CENP-E and MCAK. *Current biology : CB*, 23(16), pp.1514–1526.

Shrestha, R.L. et al., 2017. Aurora-B kinase pathway controls the lateral to end-on conversion of kinetochore-microtubule attachments in human cells. *Nature communications*, 8(1), pp.150–13.

Shukla, A. et al., 2015. Plk1 relieves centriole block to reduplication by promoting daughter centriole maturation. *Nature communications*, 6(1), pp.8077–13.

Sieben, C.J. et al., 2020. BubR1 allelic effects drive phenotypic heterogeneity in mosaic-variegated aneuploidy progeria syndrome. *The Journal of clinical investigation*, 130(1), pp.171–188.

Silió, V., McAinsh, A.D. & Millar, J.B., 2015. KNL1-Bubs and RZZ Provide Two Separable Pathways for Checkpoint Activation at Human Kinetochores. *Developmental Cell*, 35(5), pp.600–613.

Silkworth, W.T. & Cimini, D., 2012. Transient defects of mitotic spindle geometry and chromosome segregation errors. *Cell division*, 7(1), pp.19–8.

Silkworth, W.T. et al., 2009. Multipolar spindle pole coalescence is a major source of kinetochore mis-attachment and chromosome mis-segregation in cancer cells. K. G. Hardwick, ed. *PloS one*, 4(8), p.e6564.

Simonetta, M. et al., 2009. The influence of catalysis on mad2 activation dynamics. D. Pellman, ed. *PLoS Biology*, 7(1), p.e10.

Sir, J.-H. et al., 2011. A primary microcephaly protein complex forms a ring around parental centrioles. *Nature genetics*, 43(11), pp.1147–1153.

Sironi, L. et al., 2001. Mad2 binding to Mad1 and Cdc20, rather than oligomerization, is required for the spindle checkpoint. *The EMBO Journal*, 20(22), pp.6371–6382.

Sivakumar, S. & Gorbsky, G.J., 2015. Spatiotemporal regulation of the anaphase-promoting complex in mitosis. *Nature reviews. Molecular cell biology*, 16(2), pp.82–94.

Skoufias, D.A. et al., 2001. Mammalian mad2 and bub1/bubR1 recognize distinct spindle-attachment and kinetochore-tension checkpoints. *Proceedings of the National Academy of Sciences*, 98(8), pp.4492–4497.

Smith, E. et al., 2011. Differential control of Eg5-dependent centrosome separation by Plk1 and Cdk1. *The EMBO Journal*, 30(11), pp.2233–2245.

Sonnen, K.F. et al., 2012. 3D-structured illumination microscopy provides novel insight into architecture of human centrosomes. *Biology Open*, 1(10), pp.965–976.

Sonnen, K.F. et al., 2013. Human Cep192 and Cep152 cooperate in Plk4 recruitment and centriole duplication. *Journal of cell science*, 126(Pt 14), pp.3223–3233.

Sönnichsen, B. et al., 2005. Full-genome RNAi profiling of early embryogenesis in Caenorhabditis elegans. *Nature*, 434(7032), pp.462–469.

Spektor, A. et al., 2007. Cep97 and CP110 suppress a cilia assembly program. *Cell*, 130(4), pp.678–690.

Stegmeier, F. et al., 2007. Anaphase initiation is regulated by antagonistic ubiquitination and deubiquitination activities. *Nature*, 446(7138), pp.876–881.

Stiff, T. et al., 2020. Prophase-Specific Perinuclear Actin Coordinates Centrosome Separation and Positioning to Ensure Accurate Chromosome Segregation. *CellReports*, 31(8), p.107681.

Stucke, V.M., Baumann, C. & Nigg, E.A., 2004. Kinetochore localization and microtubule interaction of the human spindle checkpoint kinase MPS1. *Chromosoma*, 113(1), pp.1–15.

Sudakin, V., Chan, G.K.T. & Yen, T.J., 2001. Checkpoint inhibition of the APC/C in HeLa cells is mediated by a complex of BUBR1, BUB3, CDC20, and MAD2. *The Journal of Cell Biology*, 154(5), pp.925–936.

Suijkerbuijk, S.J.E. et al., 2012. Integration of kinase and phosphatase activities by BUBR1 ensures formation of stable kinetochore-microtubule attachments. *Developmental Cell*, 23(4), pp.745–755.

Sullivan, K.F., Hechenberger, M. & Masri, K., 1994. Human CENP-A contains a histone H3 related histone fold domain that is required for targeting to the centromere. *The Journal of Cell Biology*, 127(3), pp.581–592.

Swenson, K.I., Farrell, K.M. & Ruderman, J.V., 1986. The clam embryo protein cyclin A induces entry into M phase and the resumption of meiosis in Xenopus oocytes. *Cell*, 47(6), pp.861–870.

Takumi Chinen., & Kitagawa, D., Centriole and PCM cooperatively recruit CEP192 to spindle poles to promote bipolar spindle assembly

. *biorvix*.

Tame, M.A. et al., 2014. Astral microtubules control redistribution of dynein at the cell cortex to facilitate spindle positioning. *Cell cycle (Georgetown, Tex.)*, 13(7), pp.1162–1170.

Tanaka, T.U. et al., 2002. Evidence that the Ipl1-Sli15 (Aurora kinase-INCENP) complex promotes chromosome bi-orientation by altering kinetochore-spindle pole connections. *Cell*, 108(3), pp.317–329.

Tanaka, T.U., Stark, M.J.R. & Tanaka, K., 2005. Kinetochore capture and bi-orientation on the mitotic spindle. *Nature reviews. Molecular cell biology*, 6(12), pp.929–942.

Tang, C.-J.C. et al., 2011. The human microcephaly protein STIL interacts with CPAP and is required for procentriole formation. *The EMBO Journal*, 30(23), pp.4790–4804.

Tang, Z. et al., 2001. Mad2-Independent inhibition of APCCdc20 by the mitotic checkpoint protein BubR1. *Developmental Cell*, 1(2), pp.227–237.

Taylor, S.S., Ha, E. & McKeon, F., 1998. The human homologue of Bub3 is required for kinetochore localization of Bub1 and a Mad3/Bub1-related protein kinase. *The Journal of Cell Biology*, 142(1), pp.1–11.

Teichner, A. et al., 2011. p31comet Promotes disassembly of the mitotic checkpoint complex in an ATP-dependent process. *Proceedings of the National Academy of Sciences of the United States of America*, 108(8), pp.3187–3192.

Thomas, Y. et al., 2016. Cdk1 Phosphorylates SPAT-1/Bora to Promote Plk1 Activation in C. elegans and Human Cells. *CellReports*, 15(3), pp.510–518.

Thornton, B.R. et al., 2006. An architectural map of the anaphase-promoting complex. *Genes & development*, 20(4), pp.449–460.

Thrower, J.S. et al., 2000. Recognition of the polyubiquitin proteolytic signal. *The EMBO Journal*, 19(1), pp.94–102.

Tighe, A., Staples, O. & Taylor, S., 2008. MPS1 kinase activity restrains anaphase during an unperturbed mitosis and targets Mad2 to kinetochores. *The Journal of Cell Biology*, 181(6), pp.893–901.

Tipton, A.R. et al., 2012. Identification of novel mitosis regulators through data mining with human centromere/kinetochore proteins as group queries. *BMC cell biology*, 13(1), pp.15–15.

Tipton, A.R. et al., 2013. Monopolar spindle 1 (MPS1) kinase promotes production of closed MAD2 (C-MAD2) conformer and assembly of the mitotic checkpoint complex. *The Journal of biological chemistry*, 288(49), pp.35149–35158.

Tsang, W.Y. & Dynlacht, B.D., 2008. sSgo1, a guardian of centriole cohesion. *Developmental Cell*, 14(3), pp.320–322.

Tsou, M.-F.B. & Stearns, T., 2006. Mechanism limiting centrosome duplication to once per cell cycle. *Nature*, 442(7105), pp.947–951.

Tsou, M.-F.B. et al., 2009. Polo kinase and Separase regulate the mitotic licensing of centriole duplication in human cells. *Developmental Cell*, 17(3), pp.344–354.

Tuffanelli, D.L. et al., 1983. Anticentromere and anticentriole antibodies in the scleroderma spectrum. *Archives of dermatology*, 119(7), pp.560–566.

Uchida, N. et al., 2018. Chemical hijacking of auxin signaling with an engineered auxin-TIR1 pair. *Nature Chemical Biology*, 14(3), pp.299–305.

Uhlmann, F., Lottspeich, F. & Nasmyth, K., 1999. Sister-chromatid separation at anaphase onset is promoted by cleavage of the cohesin subunit Scc1. *Nature*, 400(6739), pp.37–42.

Uzunova, K. et al., 2012. APC15 mediates CDC20 autoubiquitylation by APC/C(MCC) and disassembly of the mitotic checkpoint complex. *Nature structural & molecular biology*, 19(11), pp.1116–1123.

van Breugel, M. et al., 2011. Structures of SAS-6 suggest its organization in centrioles. *Science*, 331(6021), pp.1196–1199.

Varetti, G. et al., 2011. Homeostatic control of mitotic arrest. *Molecular Cell*, 44(5), pp.710–720.

Vodermaier, H.C., 2004. APC/C and SCF: controlling each other and the cell cycle. *Current Biology*, 14(18), pp.R787–96.

Vodermaier, H.C. et al., 2003. TPR subunits of the anaphase-promoting complex mediate binding to the activator protein CDH1. *Current Biology*, 13(17), pp.1459–1468.

Wang, F. et al., 2011. A positive feedback loop involving Haspin and Aurora B promotes CPC accumulation at centromeres in mitosis. *Current biology : CB*, 21(12), pp.1061–1069.

Wang, Xiaoxing et al., 2008. sSgo1, a major splice variant of Sgo1, functions in centriole cohesion where it is regulated by Plk1. *Developmental Cell*, 14(3), pp.331–341.

Wang, Xinghui et al., 2014. Dynamic autophosphorylation of MPS1 kinase is required for faithful mitotic progression. Y. Xue, ed. *PloS one*, 9(9), p.e104723.

Watanabe, K., Takao, D., Ito, K.K., Takahashi, M. & Kitagawa, D., 2019. The CEP57-pericentrin module organizes PCM expansion and centriole engagement. *Nature communications*, 10(1), pp.931–13.

Watanabe, R. et al., 2019. CDK1-mediated CENP-C phosphorylation modulates CENP-A binding and mitotic kinetochore localization. *The Journal of Cell Biology*, 218(12), pp.4042–4062.

Waters, J.C. et al., 1998. Localization of Mad2 to kinetochores depends on microtubule attachment, not tension. *The Journal of Cell Biology*, 141(5), pp.1181–1191.

Wei, Z. et al., 2020. Requirement of the CEP57-Cep63 Interaction for Proper Cep152 Recruitment and Centriole Duplication. *Molecular and Cellular Biology*, 40(10), p.20130459.

Weiss, E. & Winey, M., 1996. The Saccharomyces cerevisiae spindle pole body duplication gene MPS1 is part of a mitotic checkpoint. *The Journal of Cell Biology*, 132(1-2), pp.111–123.

Wendt, K.S. et al., 2001. Crystal structure of the APC10/DOC1 subunit of the human anaphase-promoting complex. *Nature structural biology*, 8(9), pp.784–788.

Westhorpe, F.G. et al., 2011. p31comet-mediated extraction of Mad2 from the MCC promotes efficient mitotic exit. *Journal of cell science*, 124(Pt 22), pp.3905–3916.

Wollman, R. et al., 2005. Efficient chromosome capture requires a bias in the “search-and-capture” process during mitotic-spindle assembly. *Current Biology*, 15(9), pp.828–832.

Wong, Y.L. et al., 2015. Cell biology. Reversible centriole depletion with an inhibitor of Polo-like kinase 4. *Science*, 348(6239), pp.1155–1160.

Woodruff, J.B. et al., 2015. Centrosomes. Regulated assembly of a supramolecular centrosome scaffold in vitro. *Science*, 348(6236), pp.808–812.

Woodruff, J.B. et al., 2017. The Centrosome Is a Selective Condensate that Nucleates Microtubules by Concentrating Tubulin. *Cell*, 169(6), pp.1066–1077.e10.

Wordeman, L. et al., 1991. Chemical subdomains within the kinetochore domain of isolated CHO mitotic chromosomes. *The Journal of Cell Biology*, 114(2), pp.285–294.

Wu, Q. et al., 2012. CEP57, a NEDD1-binding pericentriolar material component, is essential for spindle pole integrity. *Cell research*, 22(9), pp.1390–1401.

Wu, T. et al., 2010. UBE2S drives elongation of K11-linked ubiquitin chains by the anaphase-promoting complex. *Proceedings of the National Academy of Sciences of the United States of America*, 107(4), pp.1355–1360.

Wueseke, O. et al., 2016. Polo-like kinase phosphorylation determines Caenorhabditis elegans centrosome size and density by biasing SPD-5 toward an assembly-competent conformation. *Biology Open*, 5(10), pp.1431–1440.

Xia, G. et al., 2004. Conformation-specific binding of p31(comet) antagonizes the function of Mad2 in the spindle checkpoint. *The EMBO Journal*, 23(15), pp.3133–3143.

Xu, P. et al., 2013. BUBR1 recruits PP2A via the B56 family of targeting subunits to promote chromosome congression. *Biology Open*, 2(5), pp.479–486.

Yamada, H., Kumada, K. & Yanagida, M., 1997. Distinct subunit functions and cell cycle regulated phosphorylation of 20S APC/cyclosome required for anaphase in fission yeast. *Journal of cell science*, 110 (Pt 15), pp.1793–1804.

Yamagishi, Y. et al., 2012. MPS1/Mph1 phosphorylates the kinetochore protein KNL1/Spc7 to recruit SAC components. *Nature Cell Biology*, 14(7), pp.746–752.

Yamaguchi, M. et al., 2016. Cryo-EM of Mitotic Checkpoint Complex-Bound APC/C Reveals Reciprocal and Conformational Regulation of Ubiquitin Ligation. *Molecular Cell*, 63(4), pp.593–607.

Yamano, H., Gannon, J. & Hunt, T., 1996. The role of proteolysis in cell cycle progression in Schizosaccharomyces pombe. *The EMBO Journal*, 15(19), pp.5268–5279.

Yang, J., Adamian, M. & Li, T., 2006. Rootletin interacts with C-Nap1 and may function as a physical linker between the pair of centrioles/basal bodies in cells. *Molecular biology of the cell*, 17(2), pp.1033–1040.

Yang, M. et al., 2007. p31comet blocks Mad2 activation through structural mimicry. *Cell*, 131(4), pp.744–755.

Yang, Z. et al., 2009. Cells satisfy the mitotic checkpoint in Taxol, and do so faster in concentrations that stabilize syntelic attachments. *The Journal of Cell Biology*, 186(5), pp.675–684.

Ye, Q. et al., 2017. The AAA+ ATPase TRIP13 remodels HORMA domains through N-terminal engagement and unfolding. *The EMBO Journal*, 36(16), pp.2419–2434.

Ye, Q. et al., 2015. TRIP13 is a protein-remodeling AAA+ ATPase that catalyzes MAD2 conformation switching. *eLife*, 4, p.213.

Yesbolatova, A. et al., 2020. The auxin-inducible degron 2 technology provides sharp degradation control in yeast, mammalian cells, and mice. *Nature communications*, 11(1), pp.5701–13.

Yost, S. et al., 2017. Biallelic TRIP13 mutations predispose to Wilms tumor and chromosome missegregation. *Nature genetics*, 49(7), pp.1148–1151.

Yuan, J. et al., 2009. Astrin regulates meiotic spindle organization, spindle pole tethering and cell cycle progression in mouse oocytes. *Cell cycle (Georgetown, Tex.)*, 8(20), pp.3384–3395.

Zachariae, W. & Nasmyth, K., 1999. Whose end is destruction: cell division and the anaphase-promoting complex. *Genes & development*, 13(16), pp.2039–2058.

Zachariae, W. et al., 1998. Control of cyclin ubiquitination by CDK-regulated binding of Hct1 to the anaphase promoting complex. *Science*, 282(5394), pp.1721–1724.

Zhang, G. et al., 2015. Distinct domains in Bub1 localize RZZ and BubR1 to kinetochores to regulate the checkpoint. *Nature communications*, 6(1), pp.7162–14.

Zhang, G. et al., 2019. Efficient mitotic checkpoint signaling depends on integrated activities of Bub1 and the RZZ complex. *The EMBO Journal*, 38(7), p.4385.

Zhang, G. et al., 2016. Two functionally distinct kinetochore pools of BubR1 ensure accurate chromosome segregation. *Nature communications*, 7(1), pp.12256–12.

Zhang, G., Lischetti, T. & Nilsson, J., 2014. A minimal number of MELT repeats supports all the functions of KNL1 in chromosome segregation. *Journal of cell science*, 127(Pt 4), pp.871–884.

Zhang, S. et al., 2016. Molecular mechanism of APC/C activation by mitotic phosphorylation. *Nature*, 533(7602), pp.260–264.

Zhang, Y. & Lees, E., 2001. Identification of an overlapping binding domain on Cdc20 for Mad2 and anaphase-promoting complex: model for spindle checkpoint regulation. *Molecular and Cellular Biology*, 21(15), pp.5190–5199.

Zhang, Z., Chang, L., et al., 2013. The four canonical tpr subunits of human APC/C form related homo-dimeric structures and stack in parallel to form a TPR suprahelix. *Journal of molecular biology*, 425(22), pp.4236–4248.

Zhang, Z., Yang, J., et al., 2013. Recombinant expression, reconstitution and structure of human anaphase-promoting complex (APC/C). *The Biochemical journal*, 449(2), pp.365–371.

Zhao, H. et al., 2020. CEP57 and CEP57l1 function redundantly to recruit the Cep63-Cep152 complex for centriole biogenesis. *Journal of cell science*, 133(13), p.jcs241836.

Zhou, Haining et al., 2016. CEP57 is a Mis12-interacting kinetochore protein involved in kinetochore targeting of Mad1-Mad2. *Nature communications*, 7(1), pp.10151–13.

Zhou, Houjiang et al., 2013. Toward a comprehensive characterization of a human cancer cell phosphoproteome. *Journal of proteome research*, 12(1), pp.260–271.

Zhu, F. et al., 2008. The mammalian SPD-2 ortholog Cep192 regulates centrosome biogenesis. *Current Biology*, 18(2), pp.136–141.

Zhu, X. et al., 1995. The C terminus of mitosin is essential for its nuclear localization, centromere/kinetochore targeting, and dimerization. *The Journal of biological chemistry*, 270(33), pp.19545–19550.

Zirkle, R.E., 1970. Ultraviolet-microbeam irradiation of newt-cell cytoplasm: spindle destruction, false anaphase, and delay of true anaphase. *Radiation research*, 41(3), pp.516–537.

Appendix A – Behaviour of TRIP13 KO cell lines

A

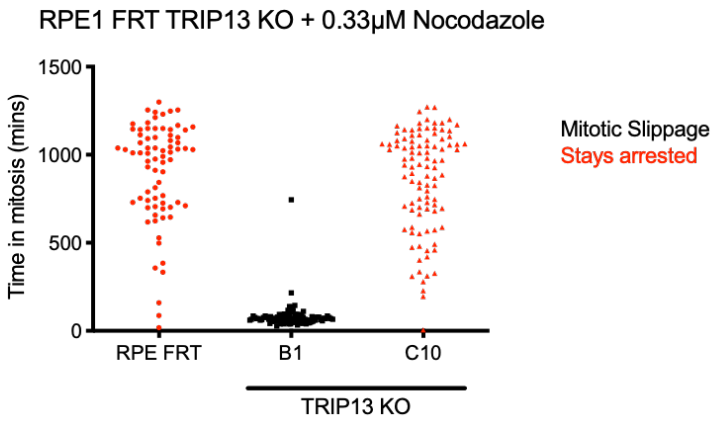

B

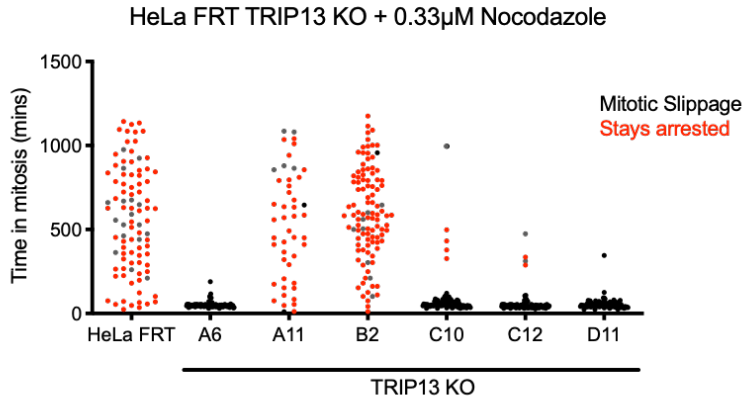

C

Q15645	180.6	13.3	52.5	30.2	17.8	19.4	21.7

Figure 8-1 Characterisation of TRIP13 KO clones

These data were collected by Chiara Marcozzi and Theo Roumeliotis. **A)** and **B)** show mitotic timing of KO clones arrested in 0.33μM nocodazole. Cells are coloured by phenotype of mitosis, black = mitotic slippage; red = stays arrested at end of film. Clones RPE C10 and HeLa A11 and B2 arrest like wildtype cells however, RPE B1 and HeLa A6, C10, C12, and D11 do not arrest and exit mitosis prematurely. **C)** Abundance levels for TRIP13 detected by LC MS/MS. HeLa clones that arrest have higher abundance than those that slip.

Appendix B – List of supplementary movies

Figure 6-5 CEP57 leads to premature centriole disengagement in mitosis but not in G2

1. 1B1-WT
2. 1F8-WT
3. 1H2-WT
4. 1B1-IAA
5. 1F8-IAA
6. 1H2-IAA

Figure 6-6 Centriole disengagement after DMA washout

7. 1B1-WT-DMA
8. 1F8-WT-DMA
9. 1H2-WT-DMA
10. 1B1-IAA-DMA
11. 1F8-IAA-DMA
12. 1H2-IAA-DMA

Figure 6-7 Inhibition of Plk1 partially rescues CEP57 mediated premature centriole disengagement

13. 1B1-IAA-BI2536-DMA
14. 1H2-IAA-BI2536-DMA

Appendix C – Single cell degradation

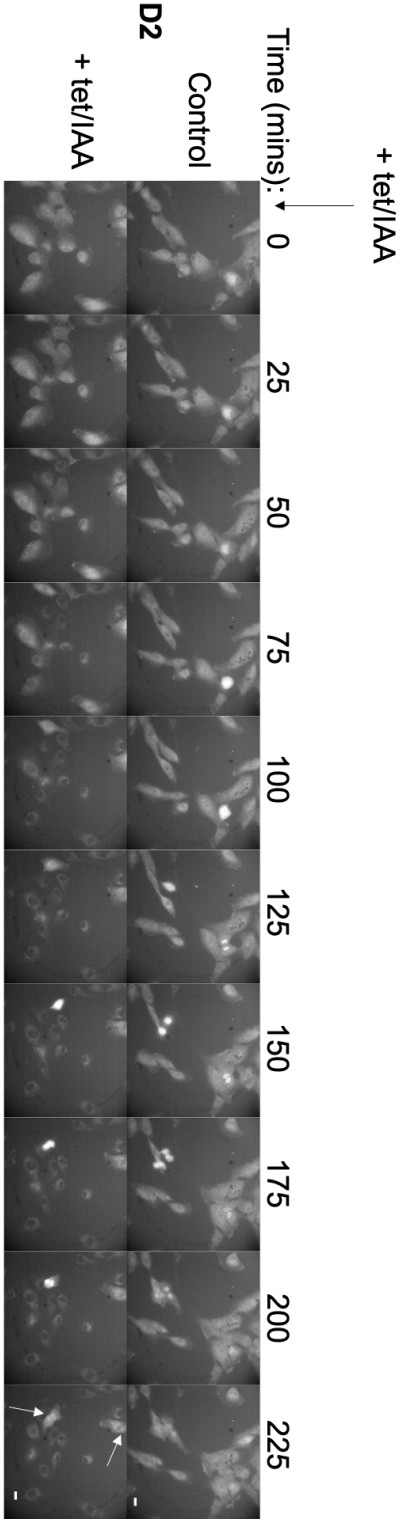

Figure 8-2 Enlargement of figure 3-12A For measuring TRIP13 intensity, the whole cell was drawn around manually in FIJI and normalised to background intensity and cell area

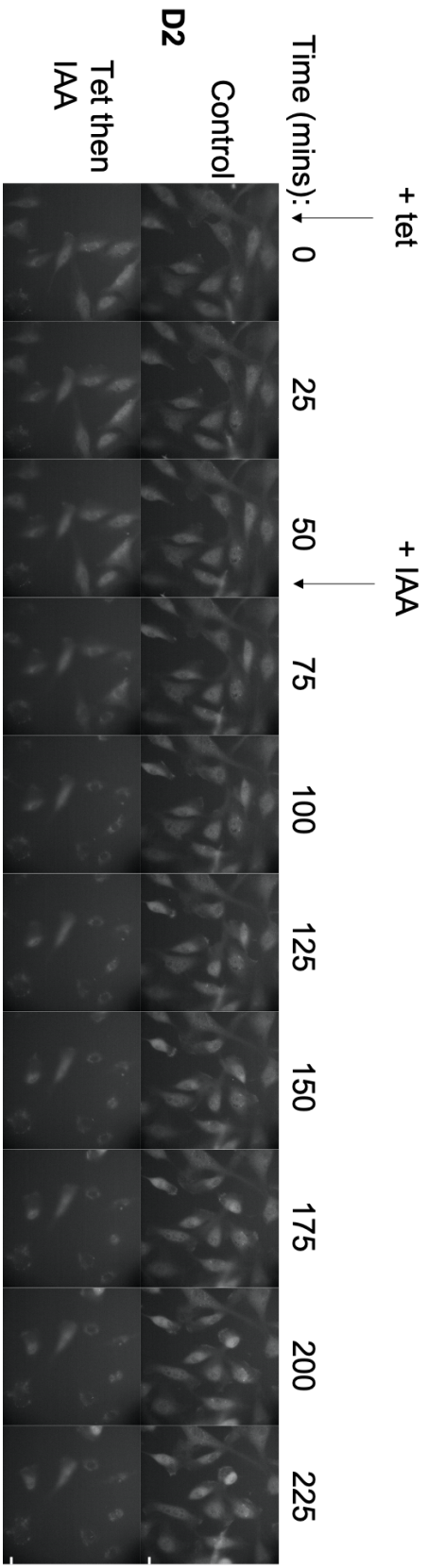

Figure 8-3 Enlargement of Figure 3-13A Measurements were taken as described in 8-2.

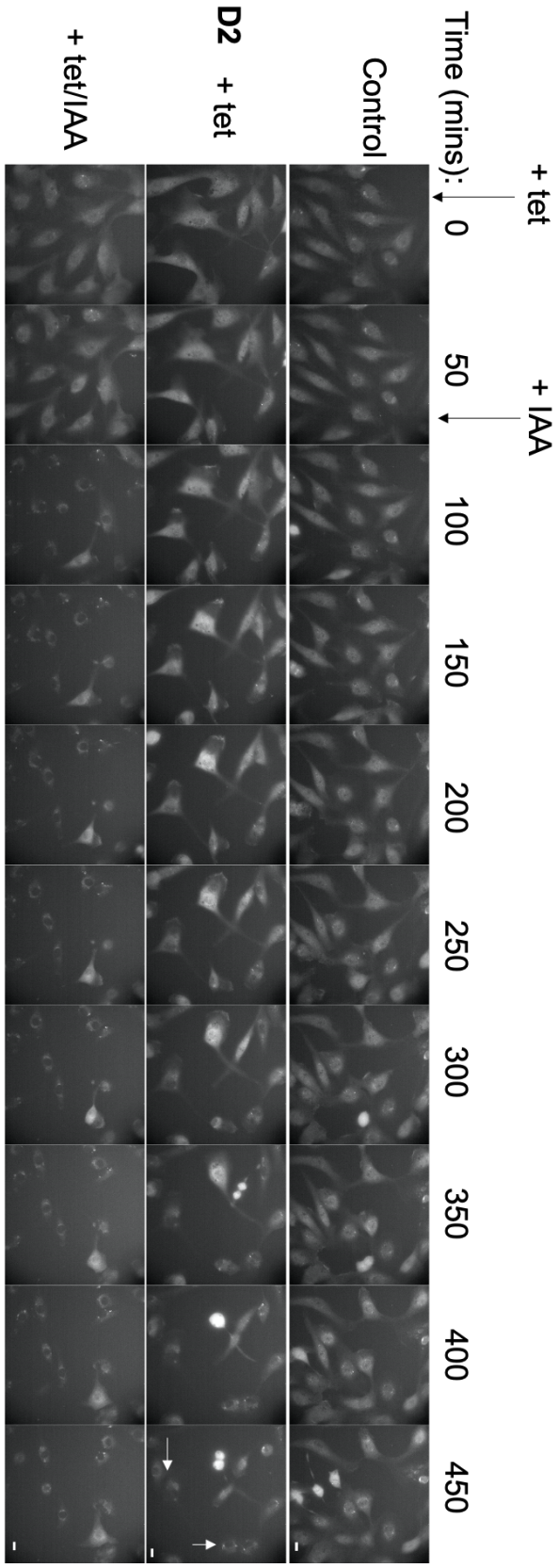

Figure 8-4 Enlargement of Figure 3-14A Measurements were taken as described in 8-2.

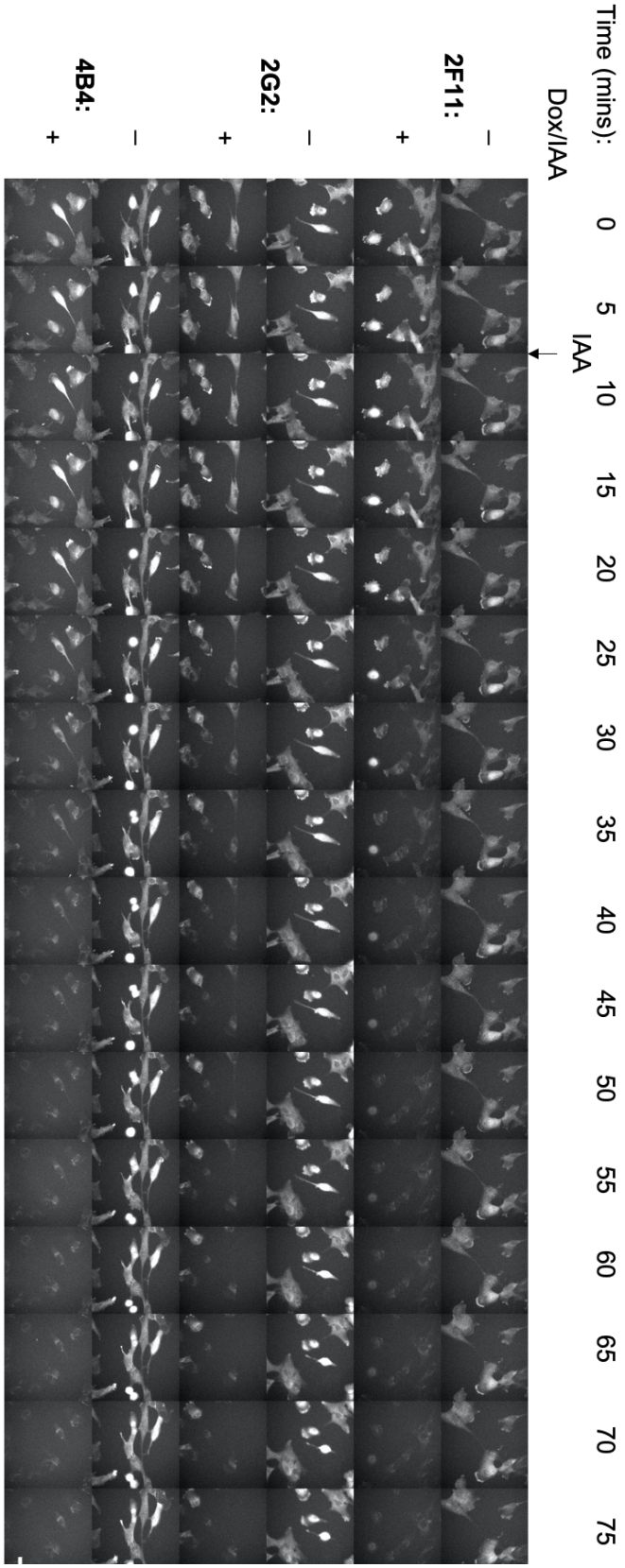

Figure 8-5 Enlargement of Figure 4-5A. Measurements were taken as described in 8-2.

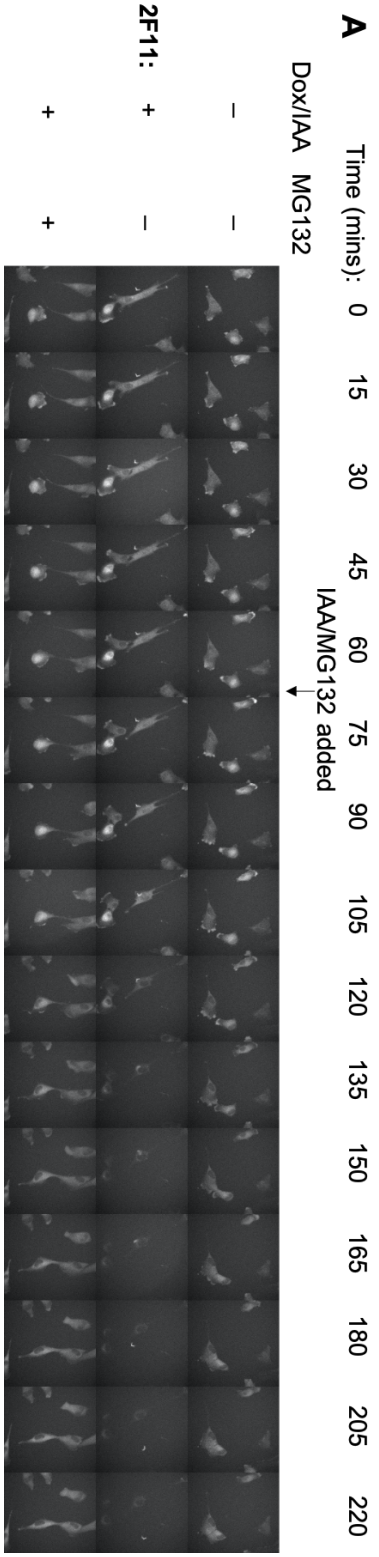

Figure 8-4 Enlargement of Figure 4-6A. Measurements were taken as described in 8-2.

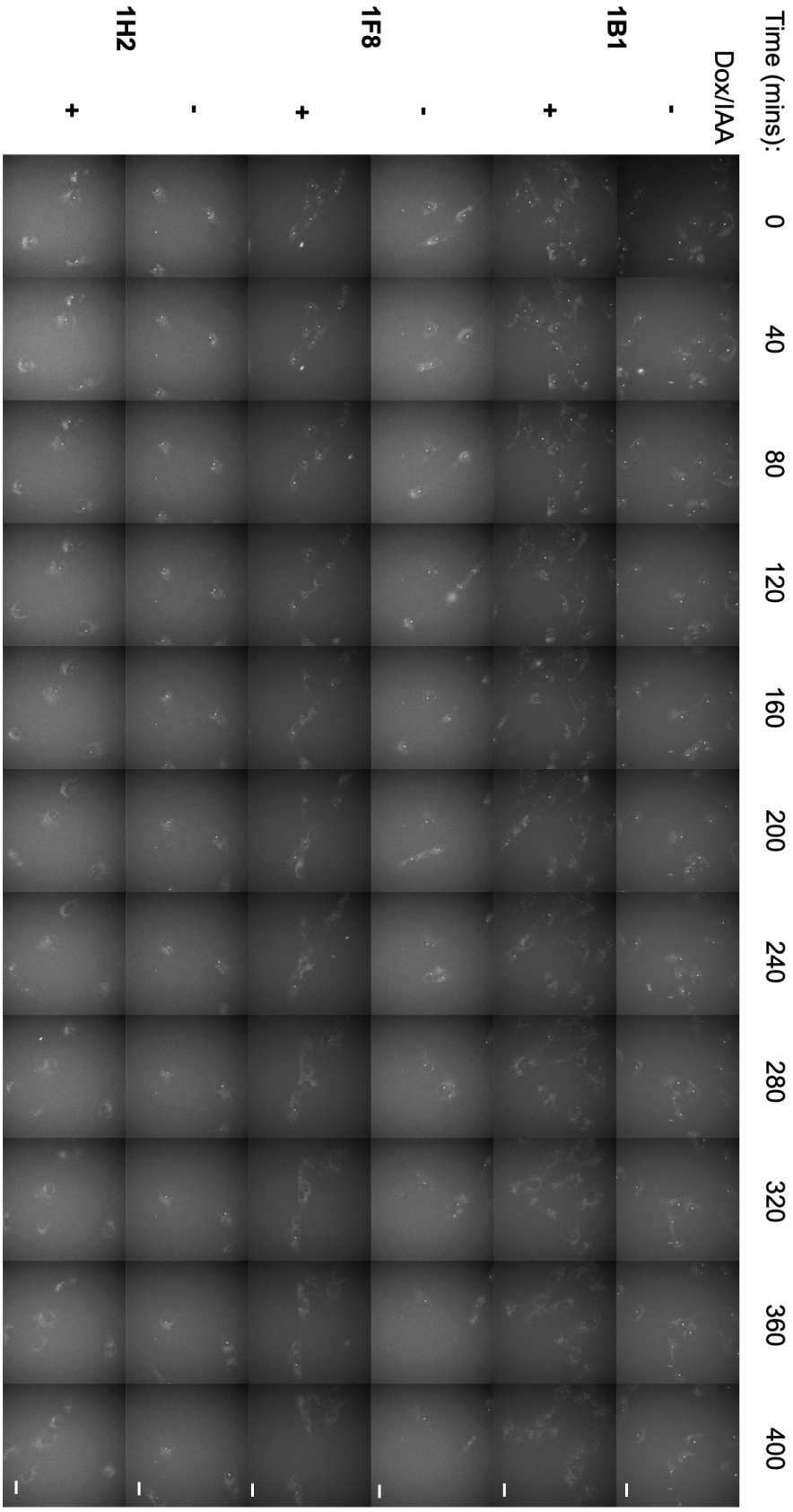

Figure 8-5 Enlargement of Figure 5-4A. For CEP57 intensity measurements, FIJI software was used to manually draw around individual foci in each cell and normalised as described before.